store

HIGH-RESOLUTION RECORDS OF CLIMATE CHANGE FROM LACUSTRINE STABLE ISOTOPES THROUGH THE LAST TWO MILLENNIA IN WESTERN TURKEY

M. D. JONES

PhD 2004

90 0587102 3

LIBRARY STORE

REFERENCE ONLY

This copy of the thesis has been supplied on condition that anyone who consults it is understood to recognise that its copyright rests with its author and that no quotation from the thesis and no information derived from it may be published without the author's prior consent.

HIGH-RESOLUTION RECORDS OF CLIMATE CHANGE FROM LACUSTRINE STABLE ISOTOPES THROUGH THE LAST TWO MILLENNIA IN WESTERN TURKEY

by

MATTHEW DAVID JONES

A thesis submitted to the University of Plymouth
in partial fulfilment for the degree of

DOCTOR OF PHILOSOPHY

School of Geography
Faculty of Social Science and Business

In collaboration with
NERC Isotope Geosciences Laboratory, Keyworth, UK
Maden Tetkik ve Arama Genel Müdürlüğü (MTA), Ankara, Turkey

2003

RY STORE

UNIVERSITY OF PLYMOUTH
Item No. 9005871023
Date - 1 APR 2004
Class No. THESIS 851.6 JON
Cont. No.
PLYMOUTH LIBRARY

REFERENCE ONLY

British Library Thesis No. DX235763

Matthew David Jones

High-resolution records of climate change from lacustrine stable isotopes through the last two millennia in western Turkey

Knowledge of past climate variability is vital if the causes of observed climate changes since instrumental records began are to be fully understood, particularly those, post-1850 AD, possibly due to anthropogenic activity. The past two millennia provide a long enough background with which to compare post-1850 AD change, whilst errors on proxy records remain relatively small. In the Eastern Mediterranean changes in water balance are of particular interest as water is an important resource. Oxygen isotope records from lakes in the region record changes in water balance and are therefore an important archive for observing natural, and anthropogenicaly forced, variability in hydrology.

Full understanding of climate proxies requires high-resolution analysis through the instrumental time period for comparison with measured climate variability. Varved lake sediments provide the possibility for obtaining annually-resolved archives of climate proxies, and strong chronological control through time. In this study geochemical climate proxies including oxygen and stable carbon isotope ratios were measured from two lakes in central Turkey with varved sediment archives. Lake Burdur's complex carbonate mineralogy and large catchment led to stable isotope data that is controlled by a variety of mechanisms and highlights the complex nature of some lake-isotope systems.

A 1725 year long record was obtained from Nar Gölü, with the top 900 years analysed at an annual resolution. Calibration of the top of this record with instrumental climate records suggests stable isotope variability at Nar is controlled by changes in evaporation, driven by changes in summer temperature and relative humidity. The proxy record from Nar shows summer evaporation at Nar to be enhanced at times of increased Indian and African monsoon rainfall, and reduced during drier monsoon periods. Major shifts in the climate system occur c. 500 and c. 1400 AD associated with times of change between relatively warm and cold periods of Northern Hemisphere temperatures. Cycles, with a frequency of 64 years, observed in the Nar isotope record and proxy records of solar activity suggest a solar forcing mechanism for decadal variability in the Eastern Mediterranean-Indian-African summer climate system.

List of Contents

Page

Abstract iii
List of contents iv
List of Tables viii
List of Figures xiii
Acknowledgements xxiii
Author's Declaration xxiv

Chapter 1 **Introduction** 1

1.1 Late Holocene climatic change 1
1.2 Near East hydrology 3
1.3 Lakes as palaeoarchives 4
1.4 Summary of thesis aims and objectives 8
1.5 Thesis outline 9

Chapter 2 **Stable isotope processes in lacustrine environments** 10

2.1 Notation and Standards 10
2.2 Isotope changes in the hydrological cycle 11
  2.2.1 Controls on isotopes in precipitation 14
  2.2.2 Controls on lake water $\delta^{18}O$ 18
2.3 Controls on stable isotopes in lake sediments 19
2.4 Controls on lake $\delta^{13}C$ 23
2.5 Summary 27

Chapter 3 **Turkish climate: past and present** 28

3.1 Contemporary climate 28
3.2 Recent climate trends 33
3.3 Controls on climate 36
3.4 Previous palaeoclimatic work in Turkey 39
3.5 Summary 46

Chapter 4 **Methodology** 47

4.1 Selection of study sites 47
4.2 Field methods 47
    4.2.1 Water Sampling 48
    4.2.2 Bathymetry 48
    4.2.3 Sediment Traps 49
    4.2.4 Lake coring 49
4.3 Laboratory methods 53
    4.3.1 Core preparation and sampling 53
    4.3.2 Dating 55
    4.3.3 Geochemistry 57
4.4 Numerical techniques 61

Chapter 5 **Nar Gölü – Contemporary limnology** **63**

5.1 Location and general site description 63
5.2 Catchment morphology and geology 63
5.3 Catchment vegetation 67
5.4 Climate 67
5.5 Lake chemistry 72
5.6 Hydrology 72
    5.6.1 Water balance model 75
    5.6.2 Isotope mass balance modelling 76
5.7 Lake sedimentation 83
    5.7.1 Carbonate chemistry 85
5.8 Summary 87

Chapter 6 **Nar Gölü – Palaeolimnology** **89**

6.1 Lithology 89
6.2 Chronology 92
6.3 Carbonate stable isotope results 100
    6.3.1 Interpretation of carbonate results 102
    6.3.2 Additional controls on $\delta^{13}C_{carbonate}$ 117

6.4 Organic laminae results 120
    6.4.1 Interpretation of organic results 120
6.5 Summary and comparison 127

Chapter 7 **Lake Burdur – Contemporary and palaeolimnology** **130**

7.1 Location and general site description 130
7.2 Catchment geology 130
7.3 Climate 133
7.4 Lake chemistry 133
7.5 Hydrology 137
    7.5.1 Water balance model 137
    7.5.2 Isotope mass balance modelling 138
    7.5.3 Summary of hydrological budget 142
7.6 Sediment Lithology 143
7.7 Chronology 147
7.8 Carbonate stable isotope results 152
    7.8.1 Interpretation of carbonate results 154
7.9 Summary 163

Chapter 8 **Quantifying climate change** **164**

8.1 Calibration with meteorological variables 165
8.2 Modelling 166
8.3 Reconstructions 184

Chapter 9 **Late Holocene climate trends** **189**

9.1 Comparison with other records 189
    9.1.1 Turkey and the Near East 189
    9.1.2 African Monsoon 200
    9.1.3 Indian Monsoon 203
9.2 Climate cycles 206
9.3 Controls on climate change 210
    9.3.1 Temperature change 210

9.3.2 Solar variability 214
9.4 Summary 217

Chapter 10 **Conclusions** 218

10.1 High resolution records of stable isotopes from authigenic carbonate 218
10.2 Controls on $\delta^{18}O$ values in Mediterranean lakes 219
10.3 Quantifying climate change 220
10.4 Late Holocene climate change 220
10.5 Future work 221

Appendix I XRD results I

Appendix II Other results (Data CD) VIII

References IX

LIST OF TABLES

Page

Table 5.1 Calculations of evaporation (from equation 5.1) and measured values of evaporation from 11 meteorological stations in Turkey (data from Meteoroloji Bolteni, 1974). See text for explanation. 70

Table 5.2 Lake water chemistry measurements from Nar Gölü. 73

Table 5.3 Nar Gölü lake water major ion chemistry. 73

Table 5.4 Summary of Nar Gölü hydrological budget. 88

Table 6.1 Carbonate mineralogy of Nar Gölü laminae analysed by XRD with grey scale and $d^{18}O$ ‰) values fro the laminae analysed. 93

Table 6.2 Fallout radionuclide concentrations in Nar Gölü lake sediments. 96

Table 6.3 Radiometric chronology for Nar Gölü from ^{210}Pb age-depth relationship corrected to ^{137}Cs ages. 97

Table 6.4 Comparison of laminae counts from cores NAR01, M2 and M3. 98

Table 6.5 Radiocarbon ages from Nar Gölü. 99

Table 6.6 Regression relationships between the Nar $\delta^{18}O$ record (corrected for mineralogy) and Ankara annually and seasonally averaged meteorological variables between 1926 and 2001 (Precipitation relationships are with Derinkuyu values between 1966 and 1990). Table shows p-value, the direction of the relationship, and the r^2 value. 109

Table 6.7 Regression relationships between the Nar $\delta^{18}O$ record (corrected for mineralogy) and smoothed (8 year weighted forward running mean) Ankara annually and seasonally averaged meteorological variables between 1933 and 2001 (Precipitation relationships are with Derinkuyu values between 1973 and 1990). Values as in Table 6.5. 109

Table 6.8 Regression relationships between the Nar $\delta^{18}O$ record (corrected for mineralogy) and Ankara annually and seasonally averaged meteorological variables between 1926 and 1986 (Precipitation relationships are with Derinkuyu values between 1966 and 1986). Values as in Table 6.5. 110

Table 6.9 Regression relationships between the Nar $\delta^{18}O$ record (corrected for mineralogy) and smoothed (8 year weighted forward running mean) Ankara annually and seasonally averaged meteorological variables between 1933 and 1986 (Precipitation relationships are with Derinkuyu values between 1973 and 1986). Values as in Table 6.5. 110

Table 6.10 Regression relationships between the Nar $\delta^{13}C$ record (corrected for mineralogy) and smoothed (8 year weighted forward running mean) Ankara annually and seasonally averaged meteorological variables between 1933 and 2001 (Precipitation relationships are with Derinkuyu values between 1973 and 1990). Values as in Table 6.5. 112

Table 6.11 Regression relationships between the Nar $\delta^{13}C$ record (corrected for mineralogy) and smoothed (8 year weighted forward running mean) Ankara annually and seasonally averaged meteorological variables between 1933 and 1986 (Precipitation relationships are with Derinkuyu values between 1973 and 1986). Values as in Table 6.5. 112

Table 6.12 Regression analyses with changing chronology for the Nar $\delta^{18}O$ data. Values as in Table 6.5. 115

Table 6.13 Regression analysis between 8 year weighted average summer meteorological variables and Nar $\delta^{18}O$ record between 1933 and 2001 with no ^{137}Cs correction to varve chronology. Values as in Table 6.5. 115

Table 6.14 Regression analyses with monthly meteorological values and the Nar $\delta^{18}O$ record. Values as in Table 6.5. 115

Table 6.15 Regression relationships between the Nar $\delta^{13}C_{organic}$ record and Ankara annually and seasonally averaged meteorological variables between 1926 and 2001 (Precipitation relationships are with Derinkuyu values between 1966 and 1990). Table shows p-value, the direction of the relationship, and the r^2 value. Significant relationships are highlighted. 125

Table 6.16 Regression relationships between the Nar $\delta^{13}C_{organic}$ record and smoothed (8 year weighted forward running mean) Ankara annually and seasonally averaged meteorological variables between 1933 and 2001 (Precipitation relationships are with Derinkuyu values between 1973 and 1990). Values as in Table 6.5. 125

Table 6.17 Regression relationships between the Nar C: N record and Ankara annually and seasonally averaged meteorological variables between 1926 and 1986 (Precipitation relationships are with Derinkuyu values between 1966 and 1986). Values as in Table 6.5. 126

Table 6.18 Regression relationships between the Nar C: N record and smoothed (8 year weighted forward running mean) Ankara annually and seasonally averaged meteorological variables between 1933 and 1986 (Precipitation relationships are with Derinkuyu values between 1973 and 1986). Values as in Table 6.5. 126

Table 6.19 Regression relationships between proxy data sets from the top 900 laminae from Nar Gölü. P-values, the direction of the relationship, and r^2 values are shown. 129

Table 7.1 Lake Burdur water chemistry measurements 135

Table 7.2 Burdur Gölü major ion water chemistry (mg/l) (Roberts, 1980). 135

Table 7.3 Summary of Lake Burdur hydrological budget 142

Table 7.4 Fallout radionuclide concentrations in Burdur Lake core BUR02MA1 148

Table 7.5 ^{210}Pb chronology for Burdur Gölü 149

Table 7.6 AMS Radiocarbon date from wood fragments in core BUR02MB2 (140cm depth). Calibration with INTCAL98 (Stuiver *et al.*, 1998). 149

Table 7.7 Strength of regression relationships between the amounts of calcium carbonate minerals and stable isotope values 155

Table 7.8 Regression relationships between the Burdur $\delta^{18}O$ record and averaged meteorological variables between 1941 and 2002. Table shows p-value, the direction of the relationship, and the r^2 value. 158

Table 7.9 Regression relationships between the Burdur $\delta^{18}O$ record and averaged meteorological variables between 1941 and 2002, with sample 8 removed. Values as in Table 7.3. 158

Table 8.1 Comparison of initial model values and recorded values from Nar Gölü. Values in LH column are described in chapter 5. 172

Table 8.2 Values of initial and maximum shifts and new equilibrium states for changes to Nar steady state models. 175

Table 8.3 Changes in initial and maximum shifts and equilibrium values from different initial states of Nar Model 1. 178

Table 8.4 Comparison of Model 1 relationships, for maximum shifts for a given climate change, and climate calibration relationships for the range of values in the Nar record. 178

Table 9.1 Comparison of Nar record sampled at different resolutions compared to the original $\delta^{18}O$ data set. 195

Table 9.2 Comparison of Nar record sampled at different resolutions compared to the annual part of the original $\delta^{18}O$ data set. 196

Table 9.3 Hypothetical radiocarbon ages for the Nar record. 198

Table 9.4 Dominant cycles observed in Nar Gölü proxy data from spectral analysis. 208

Table 9.5 Cycles found in Nar $\delta^{18}O$ records at different sampling resolutions. 208

Table 9.6 Cycles observed in Indian monsoon rainfall index and Indian monsoon proxy records from spectral analysis using the same techniques as the Nar data. 208

Table 9.7 Dominant decadal scale cycles, of approximately 60 years, from the Nar $\delta^{18}O$ record and the varved marine record of von Rad *et al.* (1998) during different time windows. 64 year cycles are highlighted in bold. 211

Table 9.8 Cycles observed in $\Delta^{14}C$ data sets from spectral analysis techniques used for the Nar data sets. 216

Table 9.9 Comparisons of the cycles discussed in this chapter. Bold cycles are those published but not found when using the same techniques as were used for the Nar data. 216

LIST OF FIGURES

Page

Fig. 1.1 Northern Hemisphere temperature reconstructions over the last 2 millennia, and instrumental data, relative to the 1961 – 1990 mean. Blue line (Jones *et al.,* 1998), green line (Briffa et al., 2001), black line (Mann and Jones, 2003) instrumental data are shown in red (from Mann and Jones, 2003). 2

Fig. 1.2 Late Holocene palaeolimnological studies from Africa. a) Lake level reconstruction from Lake Naivasha (Verschuren *et al.*, 2001), b) stable isotope record from Kajemarum Oasis (Street-Perrott *et al.*, 2000). 5

Fig. 1.3 δ^{18}O records for the last ~12 kyr from three Eastern Mediterranean lakes. The data are plotted on similar depth scales, with dates (boxed numbers) in calendar years BP. The horizontal line marks the Pleistocene-Holocene boundary (Roberts and Jones, 2002; data from Roberts *et al.* (2001), Lemcke and Sturm (1997) and Stevens *et al.* (2001)). 7

Fig. 2.1 Evaporated lake waters from Lake Gölhisar, Turkey, compared to precipitation isotope values (Jones *et al.*, 2002). GMWL = Global Meteoric Water Line, LEL = Local Evaporation Line. 12

Fig. 2.2 Controlling factors on δ^{18}O and δD in the hydrological cycle including lake systems (inset). Values given (δ) are for δ^{18}O and are general values to illustrate changes in the system. (After Gat (1996) and Rozanski *et al.*, (2001), with additional data from IAEA/WMO (2001), A. Dirican (pers. com.), Stuiver *et al.* (1995)). 13

Fig. 2.3 δ^{18}O v. temperature relationship for Ankara (GNIP, 2001). 15

Fig. 2.4 Comparisons of δ^{18}O values in precipitation from three sites in northern Europe demonstrating more negative values and increasing ranges of δ^{18}O with increasing continentality from coastal (Valentia) to continental (Moscow) stations (IAEA/WMO, 2001). 15

Fig. 2.5 Rainfall isotope values from three different source areas recorded at Gaaton, Israel (Rindsberger *et al.*, 1983). Group I rains from air masses arriving via the western Mediterranean and the north African coast, group II from air masses entering the eastern Mediterranean from continental Europe. Group III rains approach Israel from the south after travelling through central Europe and Africa. 17

Fig. 2.6 Possible range of $\delta^{18}O$ and δD values from volcanic lake waters (after Varekamp and Kreulen, 2000). With no influence of geothermal waters lake water will fall on the LEL, increasing influence of volcanic waters (shaded square) will move lake waters towards the local mixing line. 20

Fig. 2.7 Major sources, with associated stable carbon isotope values, and fluxes in lake carbon budgets (after Leng and Marshall, in press). 24

Fig. 2.8 Typical $\delta^{13}C$ and C/N values of organic fractions in lake sediments (after Meyers and Teranes, 2001; additional data from Leng and Marshall, in press). 26

Fig. 3.1a Wind climatologies at 850 hPa showing differences between winter (JFM) and summer (JAS) conditions over the Mediterranean basin (Raicich, *et al.*, 2003). 29

Fig. 3.1b Streamlines (averaged between 15 and 35E) showing differences between winter (JFM) and summer (JAS) conditions over the Mediterranean basin (Raicich, *et al.*, 2003). 30

Fig. 3.2 Mean total precipitation across Turkey (Türkeş, 2003). Red circles mark sites in this study (see chapters 5 and 7 for details). 32

Fig. 3.3 Dominant storm tracks affecting Turkey (Karaca *et al.*, 2000). 32

Fig. 3.4 Turkish rainfall regimes (Türkeş, 1995). See text for description. 32

Fig. 3.5 Mean temperatures across Turkey (after Türkeş *et al.*, 1995). 34

Fig. 3.6 Mean values of aridity index across Turkey (Türkeş, 2003). Red circles mark sites in this study (see chapters 5 and 7 for details). 34

Fig. 3.7 Recent trends in Turkish temperatures (data from Turkish State Meteorological Service); black lines show ten year running means. 35

Fig. 3.8 Extreme phases of the North Sea-Caspian Pattern (Kutiel and Benaroch, 2002). Showing areas of relative high (+) and low (-) pressure and dominant wind directions for negative (a) and positive (b) phases of the NCP. 38

Fig. 3.9 Sites of palaeoclimatic studies in Turkey discussed in the text. (Lake sites, black circles; 1. Gölhisar, 2. Beyşehir, 3. Pınarbası, 4. Suleymanhacı, 5. Akgöl, 6. Eski Acıgöl, 7. Van. Tree ring sites for Touchan *et al.* (2003) reconstruction (8, 9, 10), D'Arrigo and Cullen (2001) precipitation reconstruction for Sivas (11.)). Red circles mark sites in this study (see chapters 5 and 7 for details). 40

Fig. 3.10 Climate proxy records from Turkey through the last glacial interglacial transition and the Holocene from Eski Acıgöl (Roberts *et al.*, 2001), Akgöl (Leng *et al.*, 1999) and Gölhisar (Jones *et al.*, 2002). The right hand chart describes general climatic shifts described by these records. Bold lines tie pollen depth stratigraphy to Eski Acıgöl age model as analyses from different cores (Roberts *et al.*, 2001). 42

Fig. 3.11 Precipitation reconstructions from tree rings through the last 700 years from Turkey (a, D'Arrigo and Cullen, 2001; b, Touchan *et al.*, 2003). 45

Fig. 4.1 Sketch showing location of sediment traps in the water column in Nar Gölü (A), with a photograph (B) and cross section (C) of one of the traps. 50

Fig. 4.2 Glew coring at Nar Gölü. 51

Fig. 4.3 The 3m Mackereth corer. 51

Fig. 4.4 Method for greyscale analysis of the Nar Sediments. The final data set is made up of the mean value of three point measurements for each pale lamina (5). 54

Fig. 4.5 Typical processes for core samples from Nar taken during this study. Cores from Lake Burdur underwent a similar process. 56

Fig. 4.6 Comparison of $\delta^{18}O$ and $\delta^{13}C$ from equivalent laminae in overlapping cores from Nar Gölü. 60

Fig. 5.1 Photograph of Nar Gölü looking north from high on the southern edge of the catchment (Photo: A. Mather). 64

Fig. 5.2 Location and local geology (after Sassan, 1964) of Nar Gölü (34°27'30''E; 38°22'30''N; 1363 masl). 65

Fig. 5.3 Detail of Nar catchment (shaded grey) showing location of sediment traps (yellow circles), water sampling locations (blue circles; including springs (Sp1 and Sp2)) and coring sites from 2001 (Grey circle) and 2002 (Red circles). The details of the cores are discussed in chapter 6. 66

Fig. 5.4 Average monthly temperatures (minimum, average and maximum temperatures) between 1965 and 1990 (a) and average monthly precipitation between 1966 and 1990 (b) at Derinkuyu (data from Turkish state Meteorological Service). Error bars show 1 standard deviation of variability through this time period. 68

Fig. 5.5 Relationship between recorded and calculated amounts of evaporation for 11 meteorological stations across Turkey (from table 5.1). 71

Fig. 5.6 Lake chemistry depth profiles from July 2001 and August 2002. 74

Fig 5.7 δD v. $\delta^{18}O$ plot of contemporary water from Nar Gölü. 78

Fig 5.8 Relationship between monthly average temperatures in Derinkuyu and Ankara between 1965 and 1990. Data from Turkish State Meteorological Service. 78

Fig. 5.9 Calculated values of δ_E from equation 5.9 for all values of f_{ad}. 82

Fig. 5.10 Organic (black diamonds) and inorganic (grey squares) carbon stratigraphy of sediment traps from Nar Gölü. Upper trap is pictured. 84

Fig. 5.11 Calculation of $\delta^{18}O$ of equilibrium precipitated calcite for each month at Nar Gölü with mean, minimum and maximum air temperatures. 86

Fig. 6.1 Photograph of the 376 cm Master sequence from Nar Gölü against depth (black figures in cm) and number of laminae from the top of the core (red numbers). 90

Fig. 6.2 Composition of Nar laminae. A: with aragonite lamina, B: with calcite lamina, C: with both aragonite and calcite lamina. 91

Fig. 6.3 Grey-scale values from carbonate laminae through the Nar sequence. 94

Fig 6.4 ^{137}Cs profile from the top of the Nar sequence. 96

Fig 6.5 Comparison of ^{137}Cs (red squares) corrected ^{210}Pb chronology (yellow line) to varve chronology (grey line) from Nar Gölü. The varve chronology has been shifted by 5 years to younger values. 97

Fig. 6.6 Age-depth relationship for varve chronology from Nar Gölü. 98

Fig. 6.7 $\delta^{18}O$ and $\delta^{13}C$ results from carbonate laminae through the Nar core sequence. 101

Fig 6.8a $\delta^{13}C$ values through major changes in mineralogy, showing the raw isotope data (black lines) and values corrected to calcite values (grey lines). 103

Fig 6.8b δ^{18}O values through major changes in mineralogy, showing the raw isotope data (black lines) and values corrected to calcite values (grey lines). 104

Fig.6.9 δ^{18}O v. δ^{13}C for all the Nar carbonate results. 106

Fig 6.10 Cumulative sum of the square difference for carbonate δ^{18}O and δ^{13}C from the Nar sequence (thick line). The thin line represents a gradient of two, below which the cumulative sum will fall if the two data sets are positively correlated. Gradient of the Nar data; 0.36; r2 = 0.82; p=0.000. 106

Fig. 6.11 The corrected Nar δ^{18}O record plotted with summer maximum temperature, summer average temperature and summer relative humidity (both raw (points) and 8 year smoothed (line) meteorological variables are plotted). 113

Fig. 6.12 Comparison of Nar waters to other lakes in the region (within the same rainfall regime as described by Türkeş, 1995, Fig. 3.4). There is no evidence of extreme deviation from the Local Evaporation Line of the Nar waters due to geothermal heating. 118

Fig. 6.13 δ^{13}C$_{organic}$ and C/N results for the top 900 laminae from Nar Gölü. 121

Fig. 6.14 δ^{13}C$_{organic}$ against C: N ratios from Nar, compared to ranges of plant types from previous studies (Meyers and Teranes, 2001; Leng and Marshall, in press; Fig. 2.8). Values from Nar lie above the normal ranges for algae and C3 plants due to the ^{13}C enriched DIC pool at Nar. Samples between algal or terrestrial plant values are a mix of these two sources, or possibly from lake macrophytes. 123

Fig. 6.15 Comparison of 5 proxy records from the top 900 laminae from Nar Gölü. 128

Fig. 7.1 a) Location of Burdur Gölü and other locations mentioned in the text. b) Burdur lake area in 1970 and 2002. 131

Fig. 7.2 Geology map of the region around Lake Burdur showing major geological units and major faults (after Price and Scott, 1994; Şenel, 1997). 132

Fig. 7.3 Average monthly temperatures at Burdur between 1980 and 2001. Error bars show standard deviations from the mean through this time period (data from Turkish State Meteorological Service). 134

Fig. 7.4 Average monthly values of precipitation at Burdur between 1980 and 2001. Error bars show standard deviations from the mean through this time period (data from Turkish State Meteorological Service). 134

Fig. 7.5 Lake chemistry depth profiles for Burdur Gölü. 136

Fig. 7.6 Position of Burdur Gölü (grey squares) on the local evaporation line (LEL), of other lakes (black diamonds) within the same precipitation regime of Türkeş (1996), compared to the Isparta meteoric water line (IMWL). 140

Fig. 7.7 Location of core sites in Lake Burdur. 144

Fig. 7.8 Photograph of laminated clays from Lake Burdur. 145

Fig. 7.9 Core BUR02MA1 lithology, LOI and carbonate mineralogy. 146

Fig. 7.10 SEM photograph of Lake Burdur sediments. 145

Fig. 7.11 ^{137}Cs profile through core BUR02MAI. 148

Fig. 7.12 Comparison of magnetic susceptibility profiles from core BUR02MB2 and BUR02MAI. Tie points from magnetic susceptibility (squares) and visual inspection of the cores (diamonds) are shown in inset. 150

Fig. 7.13 Comparison of ^{137}Cs and radiocarbon dates with laminae counts. a) Detail of recent sediments with ^{210}Pb chronology and ^{137}Cs ages. 151

Fig. 7.14 $\delta^{18}O$ and $\delta^{13}C$ results from BUR02MAI. Lithology key is the same as in Fig. 7.9. 153

Fig. 7.15 $\delta^{18}O$ v. $\delta^{13}C$ for BUR02MA1 (with sample 8 removed). 155

Fig. 7.16 Sediment $\delta^{18}O$ (a) and spring and autumn minimum temperatures (b) (the two strongest relationships for $\delta^{18}O$ v. climate data) between 1940 and 2000 AD. 159

Fig. 7.17 Burdur lake levels between 1940 and 2001. 161

Fig. 7.18 Lake level and maximum summer temperature curves from Lake Burdur. Temperature curve, smoothed with a ten-year running mean, is inverted as higher temperatures (increased evaporation) would lead to lower lake levels. 161

Fig. 7.19. Comparison of normalised P-E (normalised precipitation – normalised temperature) and lake level curves from Lake Burdur. 162

Fig. 7.20 Comparison of oxygen isotope values and lake level curve from Lake Burdur 162

Fig. 8.1 Reconstructed summer relative humidity through the instrumental time period with 1 σ (dark grey lines) and 2 σ (light grey lines) errors from relationships with 8 year (a) and 13 year (b) smoothed meteorological variables. Grey squares show recorded summer relative humidity. 167

Fig. 8.2 Reconstructed summer average temperature through the instrumental time period with 1 σ (dark grey lines) and 2 σ (light grey lines) errors from relationships with 8 year (a) and 13 year (b) smoothed meteorological variables. Grey squares show recorded summer average temperature. 168

Fig. 8.3 Relationships between lake volume and lake area (a) and lake volume and lake bed surface area (b) from Nar. 170

Fig. 8.4 Change in lake water isotope value with a change in average temperature from 8.85 to 9.85 °C in Model 1. 173

Fig. 8.5 Equilibrium δ_l values with changing values of precipitation in Model 1. 177

Fig. 8.6 Shifts from annual steady state model to monthly steady state model using average precipitation and temperature values from Derinkuyu. 180

Fig. 8.7 Modelled and recorded annual variability in lake water isotope values. Compared to estimated values from recorded isotope values (*). 180

Fig. 8.8 Modelled and recorded carbonate isotope values between 1966 and 1990 with constant precipitation. 182

Fig. 8.9 Modelled and recorded carbonate isotope values between 1926 and 2001 with constant precipitation, models run with varying residence times compared to carbonate isotope values (black line). 182

Fig. 8.10 Temperature reconstruction between 1410 and 1986 AD. 184

Fig. 8.11 Relative humidity reconstruction between 276 and 2001 AD 184

Fig. 9.1 Comparison of Nar $\delta^{18}O$ record with other Turkish and Near East lake isotope records (all y-axis values are $\delta^{18}O$ ‰), with possible correlations shown with dashed lines. 191

Fig. 9.2 Range and mean value relationship for $\delta^{18}O$ values from lakes in Fig. 9.1. 192

Fig. 9.3 Comparison of Nar $\delta^{18}O$ record with $\delta^{18}O$ records from the Eastern Mediterranean Sea and Soreq cave, Israel, with possible correlations shown by dashed lines. 193

Fig. 9.4 Comparison of Nar record with theoretical record at 16cm sampling resolution. 198

Fig. 9.5 Hypothetical age-depth model for Nar. 199

Fig. 9.6 Comparison of $\delta^{18}O$ record from Nar plotted with varve chronology and hypothetical radiocarbon chronology. 199

Fig. 9.7 Relationship between the Nar $\delta^{18}O$ record and Sahel rainfall (Hulme, 2003) through the instrumental time period. 201

Fig. 9.8 Comparison of Nar $\delta^{18}O$ record with African late Holocene lake records from Naivasha (Verschuren *et al.*, 2001) and Kajemarum Oasis (Street-Perrott *et al.*, 2002). 202

Fig. 9.9 Comparison of Nar record with Indian monsoon rainfall index (Parthasarathy *et al.*, 1995) through the instrumental time period (1820-1998). 204

Fig. 9.10 Record of varve thickness from offshore Pakistan as a proxy record of the Indian monsoon (von Rad *et al.*, 1999) compared to $\delta^{18}O$ record from Nar Gölü. 205

Fig. 9.11 Raw periodograms (Fourier Transform) from Nar Gölü $\delta^{18}O$ data for annual record (a) and 5 year mean record (b), major peaks are labelled with length of cycle in years. From cycles observed in 1000 perturbations of the data cycles below ~60 years are not significant. 207

Fig. 9.12 60 year cycles in Nar and Indian monsoon (von Rad *et al.*, 1999) proxy records. 211

Fig. 9.13 Nar $\delta^{18}O$ record compared to temperature reconstruction through the past 2000 years (Mann and Jones, 2003). 212

Fig. 9.14 Nar $\delta^{18}O$ record compared to $\Delta^{14}C$ residual plot (Stuiver and Braziunas, 1995), showing sine curve with a 512 year periodicity. 215

ACKNOWLEDGMENTS

I would like to thank my supervisors, Neil Roberts, Melanie Leng and Greg Price for all their help, advice and support during all stages of this thesis. In addition I am grateful to Rana Moyeed for help and advice on statistical matters, Murat Türkeş for discussions regarding Turkish climate and John Gibson for useful e-mail correspondence regarding lake isotope mass balance models.

My grateful thanks go to Mustafa Karabiyikoğlu and Abdullah Dirican for their hospitality and generous assistance during my trips to Turkey. Thanks also to my fieldwork colleagues; Neil, Mustafa, Warren Eastwood, Jane Reed, Anne Mather, Ann England, Catherine Kuzucuoğlu, Damase Mouralis, Sevinç Kapan, Hakan Yiğitbaşıoğlu, Şükran Şahbudak. The work in Turkey would not have been possible without the logistical and financial support of MTA and the British Institute of Archaeology in Ankara (BIAA). I would like to thank all the staff at the BIAA, in particular Hugh and Krista Elton and Gülgün Girdivan.

I am indebted to Ann Kelly, Kevin Solman, Richard Hartley and Andy Elmes for all there help in the Lab and preparing equipment for our field seasons. Hilary Sloane, Carol Arrowsmith and Jo Green all provided help and assistance in the NIGL laboratories. I would also like to thank Tim Absalom, Brian Rogers, Gareth Johnston and Jamie Quinn for cartographic support.

The University of Plymouth, the Natural Environmental Research Council, the Quaternary Research Association and the Dudley Stamp memorial fund provided funds in support of the project and I am grateful to them. The fieldwork would not have been possible without additional grants from the BIAA and National Geographic to Neil Roberts. I would like to thanks all the staff and students of the Quaternary Research Group in Plymouth for their support and advice along the way.

On a more personal note I would like to take this opportunity to thank David Fox, Nick Dorey, and Chris Turney who guided me through various stages of my academic career and kept my interest in the Earth Sciences bubbling away. In particular I would like to thank David Bell for his support during my time at Oxford and encouraging me to keep going afterwards. I would not have got through the thesis without the great number of friends and fellow postgraduates who I have met along the way. In particular thanks to Pasquale Tiano and Gavin Stewart for getting trainers back on my feet and dragging me round the roads of Plymouth and through the Dartmoor fog, also to Marcus Vandergoes and Zoë Hazell who were always there to share a good laugh. I would also like to thank Rhiannon Stevens for sticking with me through it all.

Finally, a big thank you to Mum and Dad for 27 years of selfless support.

AUTHOR'S DECLARATION

At no time during the registration for the degree of Doctor of Philosophy has the author been registered for any other University award.

This study was financed with the aid of a studentship from the University of Plymouth and carried out in collaboration with the NERC Isotope Geosciences Laboratory as part of a three year co-project between the School of Geography, University of Plymouth and Maden Tetkik ve Arama Genel Müdürlüğü (General Directorate of Mineral Research and Exploration), Ankara, Turkey.

As part of the programme of study a course in Stable Isotopes in the Lacustrine and Marine Environment was undertaken at University College London. An ESF-HOLIVAR training course, Quantitative climate reconstructions and data-model comparisons, was attended, also at the Environmental Change Research Centre, University College London.

During the programme of study the work was presented in publications, at conferences and seminars.

Publications:

Roberts, C.N. and Jones, M.D. for the ISOMED working group, 2002. Towards a regional synthesis of Mediterranean climatic change using lake stable isotope records. *PAGES newsletter* 10(2), 13-15.

Jones, M.D., 2002 The Holocene stable isotope limnology of Western Anatolia. A preliminary report. *Quaternary Newsletter* No. 97, 50-52.

Oral conference presentations:

Jones, M.D., Roberts, C.N. and Leng, M.J. High-resolution stable isotope record of climate change in central Turkey during the last two millennia. *9th International Paleolimnology Symposium* August 2003, Espoo, Finland.

Jones, M.D., Roberts, C.N. and Leng, M.J. Stable Isotope Hydrology of Western Turkish Lakes: the Key to Understanding Holocene Climate Change in the Eastern Mediterranean? *ISOMED workshop,* Aix-en-Provence, August 2001.

Progress reports were given during each year of the study at the *QRA Postgraduate Symposium.*

Poster conference presentations:

Jones, M.D., Roberts, C.N. (presenting author) and Leng, M.J. High-resolution stable isotope record of climate change in central Turkey during the last two millennia. *XVI INQUA Congress,* July 2003, Reno, USA.

Jones, M.D., Roberts, C.N., Leng, M.J. and Moyeed, R. Annual record of lake stable isotope response to the last 900 years of climate change in Central Turkey. *EGS – AGU – EUG Joint assembly,* April 2003, Nice, France

Jones, M.D., Roberts, C.N. (presenting author), Leng, M.J. and Moyeed, R. Annual record of lake stable isotope response to the last 900 years of climate change in Central Turkey. *3rd International Limnogeology Congress*, April 2003, Tucson, USA.

Jones, M.D., Roberts, C.N. and Leng M.J. Stable Isotope Hydrology of Western Turkish Lakes: the Key to Understanding Holocene Climate Change in the Eastern Mediterranean? *Past climate variability through Europe and Africa,* August 2001, Aix-en-Provence, France.

Co-authored presentations and additional conferences attended:

Achieving climate predictability using paleoclimate data. EuroConference on abrupt climate change dynamics. November 2001, Pascoli, Italy.

Roberts, C.N., Jones M.D. and ISOMED members. Stable isotope records of Late Quaternary palaeoclimate from Mediterranean lakes: background to an emerging thesis. *6th ELDP workshop,* May 2001, Potsdam, Germany.

Further to the collaborating institutions the following were visited for consultation processes:

Abdullah Dirican at the Turkish Atomic Energy Authority, Ankara Nuclear Research and Training Centre. Part of the IAEA global network for isotopes in precipitation.

Dr. Murat Türkeş at the Turkish State Meteorological Service, Ankara.

Signed:

Date: 10/02/2004

Chapter 1

INTRODUCTION

1.1 Late Holocene climatic change

Warming trends observed in instrumental temperature data since records began in the late 18th century have led to questions as to the anthropogenic influence on global climate, particularly as a result of industrialisation over the last 200 years. Instrumental data do not extend back far enough, into pre-industrial times, for answers to these questions to be obtained. Proxy records of climate change are therefore required to give a background picture of late Holocene climate variability to which the observed recent warming can be compared (Mann and Jones, 2003; Jones *et al.*, 1998).

The last two millennia have become a key focus for recording this background variability, as they represent a sufficient amount of time with which to compare the recent observed warming. Additionally, as proxy records go back further in time the degree of certainty in the interpretation decreases. Even through the last two millennia comparisons between the 5th or 6th century AD with the 20th century, for example, may be difficult, although comparisons between the 5th and 6th centuries may be more valid (Jones *et al.*, 1998).

To put the recent warming into context climate proxies must be quantified. Proxy records sampled at a high temporal resolution can be directly correlated to recent instrumental data (e.g. Esper *et al.*, 2002 using tree rings) or proxy assemblages (e.g. of pollen, diatoms) can be compared to modern day assemblages and climatic tolerances through transfer functions (Birks, 1998) or mutual climatic range models (Atkinson *et al.*, 1987). Resulting relationships can then be used to quantify past climates through changes in the proxy record. Palaeotemperature proxies have received particular focus and a range of temperature reconstructions for all or part of the last 2000 years now exist (Fig. 1.1) from tree rings (e.g. Briffa *et al.*, 2001; Esper *et al.*, 2002), and combinations of ice core, tree ring and coral data (e.g. Mann *et al.*, 1998; Jones *et al.*, 1998). These quantified records of past climate are also important for the testing of climate models attempting to predict future climate change.

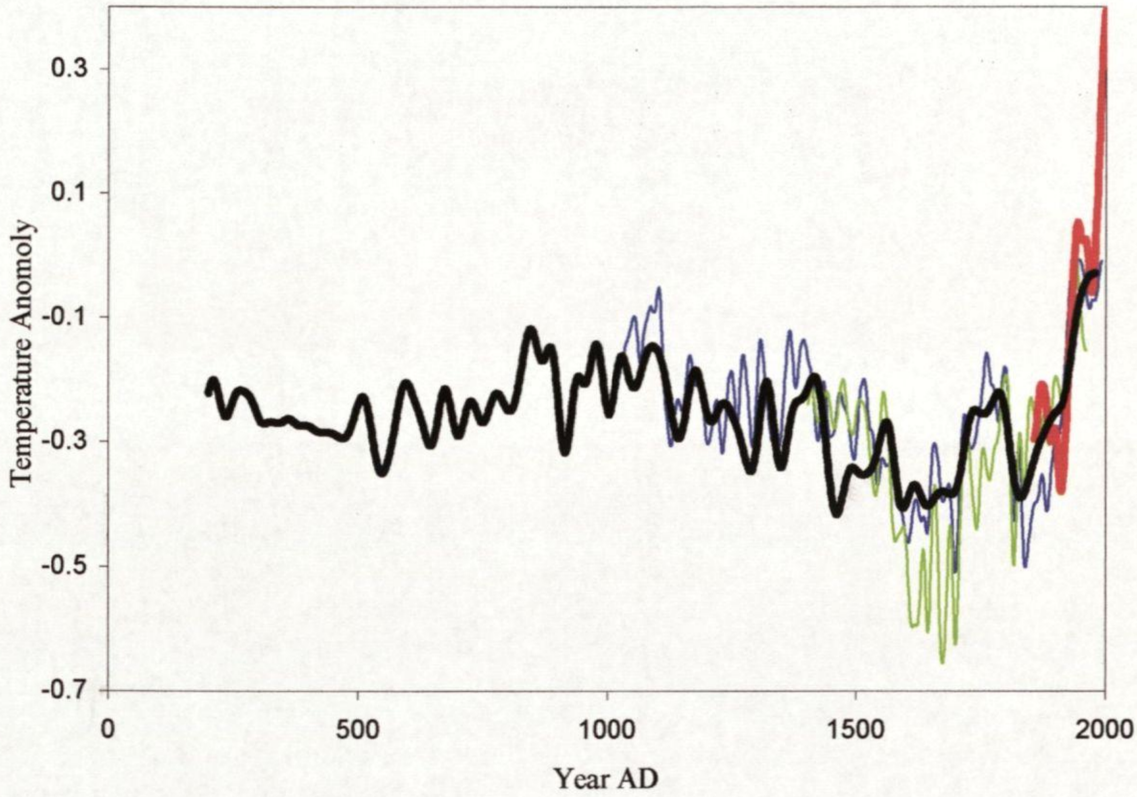

Fig. 1.1 Northern Hemisphere temperature reconstructions over the last 2 millennia, and instrumental data, relative to the 1961 – 1990 mean. Blue line (Jones *et al* ., 1998), green line (Briffa *et al.* , 2001), black line (Mann and Jones, 2003) instrumental data is shown in red (from Mann and Jones, 2003).

These temperature reconstructions all show similar long-term trends, with a long-term cooling from 1000 AD to 1800 AD followed by a relatively rapid warming to the present day (Fig. 1.1). They all suggest that the temperatures recorded at the present day are unprecedented through the last two millennia. The periods of coldest temperatures, during the 17th and 19th centuries, lie within what is commonly know as the Little Ice Age (LIA), dated to between 1550 and 1900 in most studies, although with some variability (Jones *et al.*, 2001). The longer reconstruction of Mann and Jones (2003) identifies a period between 800 and 1400 AD that is warmer than the preceding and following centennial –scale periods. This relatively warm, pre-LIA, period is often referred to as the Medieval Warm Period (MWP; Jones *et al.*, 2001).

This study aims to obtain high-resolution records of climate variability through the last two millennia in the Eastern Mediterranean. The region has very few published high resolution records through this time period (see discussion later in this chapter and in chapter 3) and is of climatic interest as it is influenced by Northern European, African, and Asian climate systems (Bolle, 2003; Chapter 3).

1.2 Near East hydrology

In the countries bordering the eastern Mediterranean Sea water is an important resource, and changes in hydrology, associated with the recent observed warming discussed above, may have social and political implications (Mann, 2002). Population in the region is increasing by 3.5 % each year and irrigation practices consume at least 80 % of the available water supply (Cullen and deMenocal, 2000). Changes in hydrology in better-watered countries such as Turkey not only affect water availability in those countries but also that of neighbouring countries. Syria and Iraq, for example, rely on water from the Tigris and Euphrates rivers which rise in eastern Turkey.

The Mediterranean basin is a region with an exceptionally long and rich history of human occupation, stretching back to the advent of Neolithic farming in southwest Asia around 10,000 years ago (Roberts, 2002). Changes in hydrology are therefore also potentially important for understanding past changes in human occupation. The rich archaeological archive is one of the major factors leading to interest in the environmental history of the region, especially through the last glacial-interglacial transition and the Holocene (chapter 3 reviews previous palaeoenvironmental work in Turkey).

Stable isotope values from lakes in the region tend to be a record of past hydrological balance (see discussion in chapters 2 and 3). They are therefore an important resource for recording past changes in hydrology and obtaining knowledge of natural variability that may be needed to plan for future change, as well as understanding past changes in hydrology that may have impacted on former civilisations.

This study aims to obtain high-resolution records of stable isotopes from lake sediments from sites in western Turkey. These sites were chosen to provide the high temporal resolution required to compare with other detailed studies of the past 2000 years as discussed above (chapter 4 discusses in detail the reasons for site selection).

1.3 Lakes as palaeoarchives

Lake sediments have been widely used as an archive for proxies of past environmental and climate change, and provide one of the few continuous archives from continental settings. They allow the recording of numerous proxies from the same core leading to more robust palaeoenvironmental reconstructions. Compared to tree rings and ice cores lakes have been underused as archives of environmental variability through the last two millennia, largely because they rarely have the detailed, annual chronological control through the entire record required for comparison with these high resolution records. Sampling of lake sediments is also rarely carried out on a resolution that nears the annual variability measured in tree rings and ice cores, although in most lakes it is possible to achieve records with at least decadal resolution (Battarbee, 2000). However, lakes are widespread and therefore have the potential to fill in some of the spatial gaps left by the ice core records, which are concentrated at the poles and tropical mountains (e.g. Thompson *et al.*, 2002), and tree rings, where the current temperature records are largely from higher latitude sites (e.g. Esper *et al.*, 2002; Briffa *et al.*, 2002). This wide spatial distribution leads to the potential for lakes to provide a network of sites to assess regional climate variations on continental scales (Battarbee, 2000).

There are limited numbers of lake records previously published for the late Holocene, at decadal or sub-centennial resolution. From Africa (Fig. 1.2) lake-level reconstructions from Lake Naivasha, Kenya, (Verschuren *et al.*, 2000) and stable isotope records from Kajemarum Oasis, Nigeria, (Street-Perrott *et al.*, 2000) suggest that climate was relatively

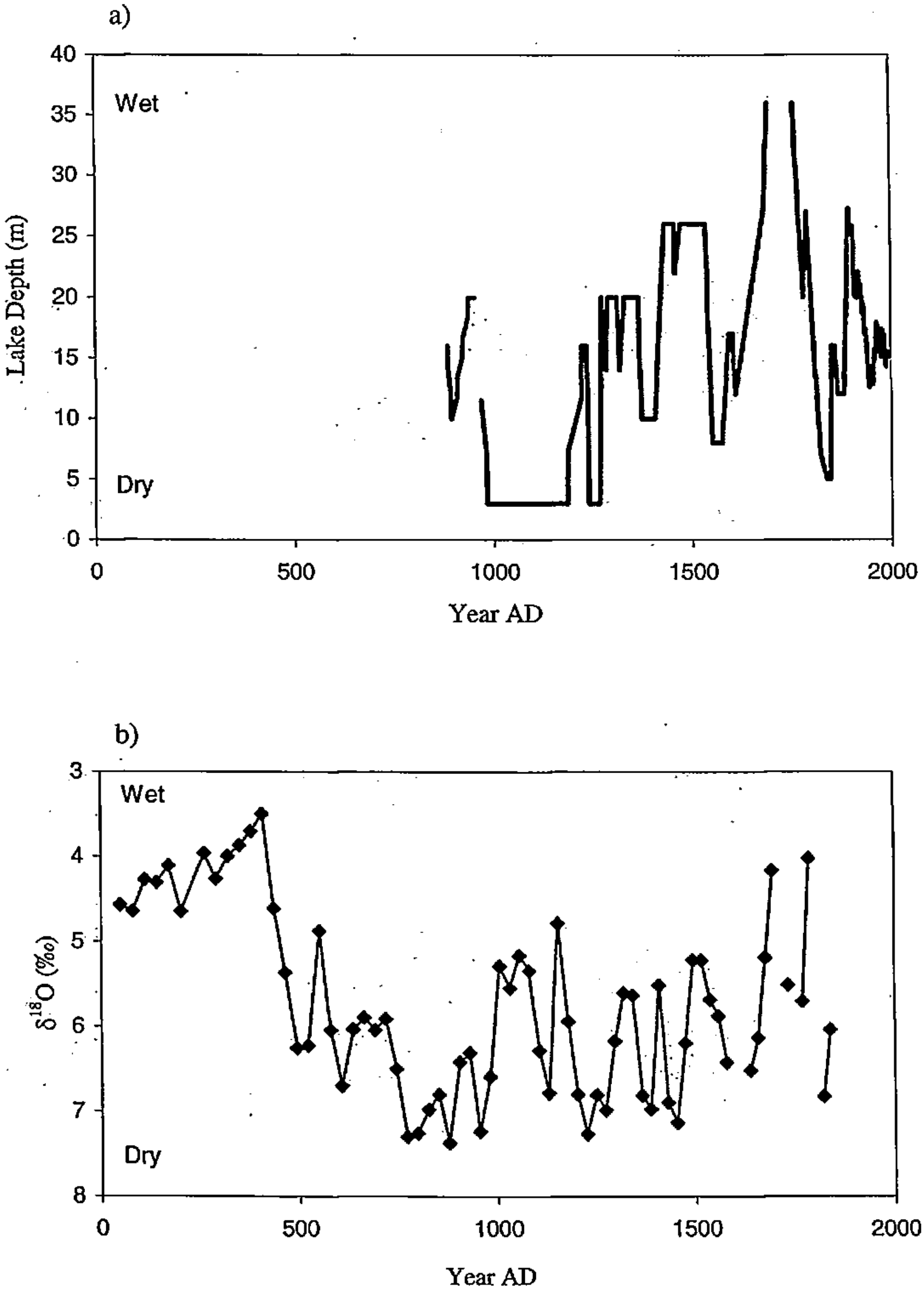

Fig. 1.2 Late Holocene palaeolimnological studies from Africa. a) Lake level reconstruction from Lake Naivasha (Verschuren *et al.,* 2000), b) stable isotope record from Kajemarum Oasis (Street-Perrott *et al.,* 2000).

dry during the MWP and relatively wet during the LIA, although the largest shift in the Kajemarum record, from wet to dry conditions, occurs between 400 and 500 AD. In North America changes between a warm and dry MWP and cold and wet LIA were noted from changes in grain size in Pine Lake, Canada (Campbell *et al.*, 1998) and Fritz *et al.* (2000) show drought periods in North Dakota, USA, throughout the last two millennia from diatom salinity reconstructions and ostracod trace-element chemistry. Moore *et al.* (2001) produced a palaeotemperature from Baffin Island, Canada, for the last 1250 years from a varve thickness record calibrated against instrumental temperature records from the recent past. The record shows the onset of a cold LIA around 1375 AD.

Most of the early palaeolimnological studies in Turkey, as elsewhere (Schnurrenberger *et al.*, 2003), were pollen reconstructions of past environments (e.g. van Zeist *et al.*, 1975). However, more recently many additional proxies have been used for palaeoclimatic reconstructions (discussed in chapter 3), in particular diatoms (e.g. Reed *et al.*, 1999; Eastwood *et al.*, 1999) and stable isotopes (e.g. Leng *et al.*, 1999; Roberts *et al.*, 2001). The advantage of these other proxies over pollen is they record changes local to the lake catchment, rather than regional vegetation changes, and may be less influenced by human disturbance of the environment. In some cases changes in catchment vegetation will significantly affect the hydrology (Rosenmeier *et al.*, 2002) and therefore also change stable oxygen isotope values or lake salinity, recorded by diatoms. However stable isotopes, in particular, are less likely to be affected by land-use changes than regional pollen records.

A number of stable isotope studies from continental archives in the region are now available, in particular from lake records (e.g. Leng *et al.*, 1999; Tzedakis *et al.*, 2002) but also from speleothems (Bar-Matthews *et al.*, 1997) and land snails (Goodfriend, 1990). These isotope records have the potential to allow comparison of environmental change across the Mediterranean basin. However, which specific climatic and environmental factors drive the changes in stable isotope ratios remains under debate. Further understanding of climate-lake isotope interactions are needed for these records to be fully understood.

Figure 1.3 shows the $\delta^{18}O$ records from three Eastern Mediterranean lakes lying in comparable climatic settings, but the generally similar trends in isotope values have been

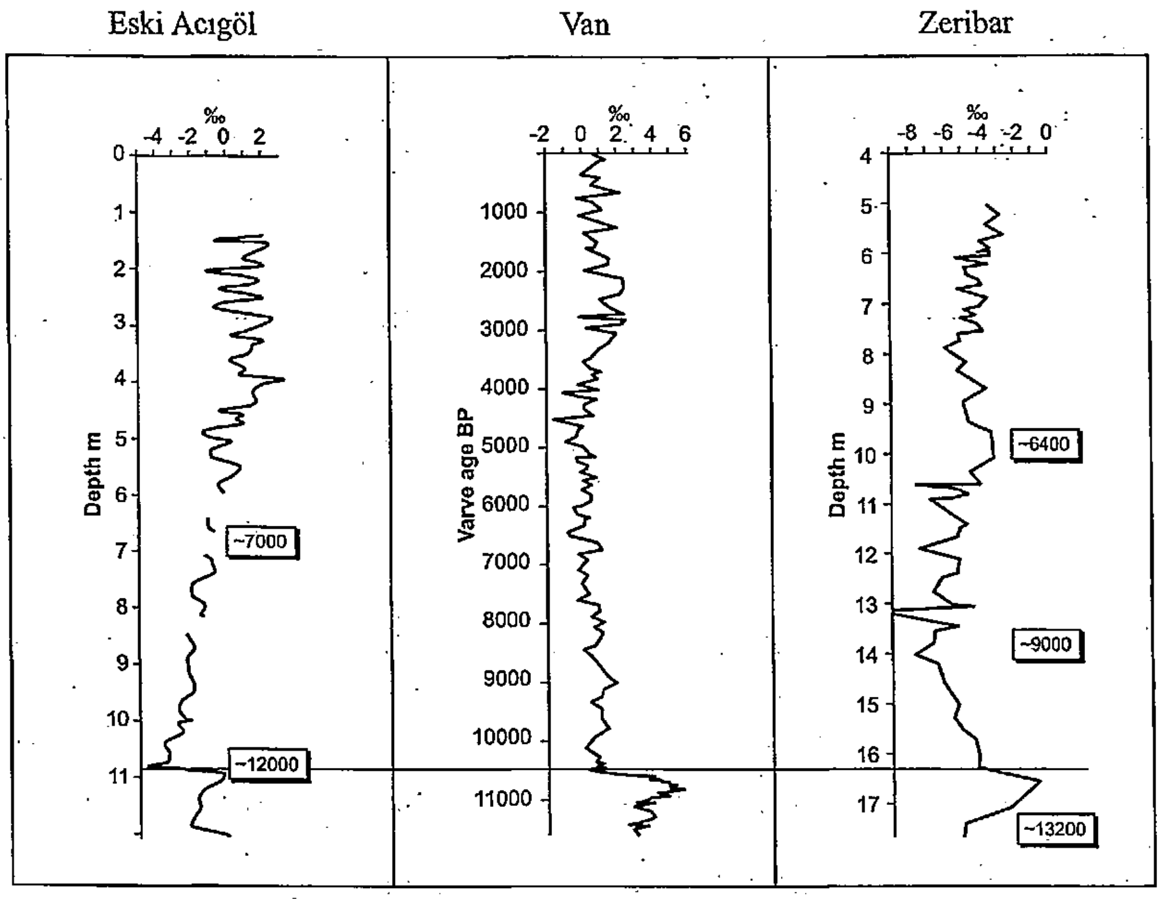

Fig. 1.3 δ^{18}O records for the last ~12 kyr from three Eastern Mediterranean lakes. The data are plotted on similar depth scales, with dates (boxed numbers) in calendar years BP. The horizontal line marks the Pleistocene-Holocene boundary (Roberts and Jones, 2002; data from Roberts *et al.* (2001), Lemcke and Sturm (1997) and Stevens *et al.* (2001)).

interpreted differently from site to site. The record from Eski Acıgöl has been interpreted as following changes in the precipitation: evaporation ratio at the lake site (Roberts *et al.*, 2001), the lake Van record (Lemcke and Sturm, 1997) as recording evaporation changes due to changes in relative humidity and the oxygen isotope record from Zeribar (Stevens *et al.*, 2001) has been interpreted as recording changes in the seasonality of rainfall. It is likely that all these, and other factors such as temperature, will affect the isotope values of lake waters and the resulting values of the carbonate preserved in the sedimentary record.

The dominant control on the lake-isotope system may vary from lake to lake and over different time scales. However, although the three records shown here have all been interpreted differently they display common trends. Firstly, a clear shift to more negative $\delta^{18}O$ values during the late Pleistocene to early Holocene climatic transition and secondly a common trend towards more positive oxygen isotope values during the second half of the Holocene, although the precise timing of this shift appears to vary between sites. These common trends suggest large scale isotope trends in the lake records may ultimately be driven by the same controlling mechanism and this study aims to further understanding of Mediterranean lake isotope systems response to climate change.

1.4 Summary of thesis aims and objectives

This study aims to obtain high-resolution proxy records of climate change through the last 2,000 years from the Eastern Mediterranean region via records of lacustrine chemical variability, particularly changes in oxygen-isotope values, by:

- obtaining lake cores with precise temporal control i.e. varves.
- high-resolution sampling and analysis of these lake sediments.

To further interpretation of the stable isotope records other geochemical proxies, including mineralogy and colour analysis, will also be measured from the lake sediments.

Additionally the thesis aims to calibrate high-resolution lacustrine stable isotope records with instrumental climate data, and study contemporary lake isotope systems, to increase understanding of the controls on lake isotope dynamics in the Mediterranean region.

Through the climate calibration and from modelling lake oxygen isotope variability the thesis will aim to quantify proxy records of past climate variability. The data obtained during this study will be compared to previous work from the Eastern Mediterranean region and beyond to understand better changes in climate through the last two millennia.

1.5 Thesis Outline

The thesis first discusses the controls on lake stable isotope values, the primary technique used in this study (chapter 2), and climate patterns in the Eastern Mediterranean and Turkey today, and through the Late Quaternary (chapter 3), to understand what the results from this study may mean in terms of climate change through the last two millennia. The methods used during fieldwork and in the laboratory are explained (chapter 4) prior to presenting the results of analyses from the contemporary lake environment (chapters 5 and 7) and for core samples from two sites in central Turkey (chapters 6 and 7). Quantification of the proxy archives is attempted through calibration of stable isotope records against instrumental climate records and modelling of the lake stable isotope system (chapter 8). The results are then discussed in terms of global patterns of Late Holocene climate change (chapter 9) as well as critically reviewing the methods used.

Chapter 2

STABLE ISOTOPE PROCESSES IN LACUSTRINE ENVIRONMENTS

Stable isotopes of oxygen and carbon have become widely used proxies for terrestrial environmental and climatic change, with records produced from speleothems (e.g. Bar-Matthews *et al.*, 1997), land snails (e.g. Goodfriend, 1990), and soil profiles (e.g. Zanchetta *et al.*, 2000) as well as lake sediment sequences (e.g. von Grafenstein *et al.*, 1999; Wei and Gasse, 1999). The high sensitivity of the freshwater isotopic system, relative to its marine counterpart (Stuiver, 1970), allows detailed records to be obtained for periods of relatively stable climate, such as the Holocene (e.g. Lamb *et al.*, 2000).

However, lake chemistry systems are complex with many possible controlling mechanisms and an understanding of these is important before palaeoclimatic or palaeoenvironmental inferences can be drawn from geological records. This chapter will therefore review the processes controlling oxygen and stable carbon isotope ratios in the lacustrine system. Firstly, the processes controlling oxygen isotope values in the hydrological cycle are outlined (section 2.2), and the processes by which oxygen isotope values in lake waters may change as they are recorded by sedimentary proxies are then discussed (section 2.3). Controls on the lake carbon budget and the possible resulting changes in $\delta^{13}C$ values are also discussed (section 2.4). Examples of how these processes have been used to interpret previous records of lacustrine stable isotope variability will be discussed in chapter 3 and in the interpretation of results from this study (chapters 5-7).

2.1 Notation and standards.

Stable isotope values are expressed in the delta notation e.g. δD, $\delta^{18}O$, $\delta^{13}C$ (for the ratios $^{2}H/^{1}H$ [D/H], $^{18}O/^{16}O$, $^{13}C/^{12}C$ respectively), as relative values compared to a laboratory standard such that

$$\delta X = [R\ (\text{sample}) - R\ (\text{standard}) / R\ (\text{standard})] \times 1000 \qquad (2.1)$$

where R is the ratio $^{heavy}X/\,^{light}X$ (e.g. $^{18}O/\,^{16}O$).

Conventional standards are Standard Mean Ocean Water (SMOW), for isotope ratios from waters, and PDB [from a Cretaceous belemnite used in the first stable isotope experiments (Craig, 1957)] for carbonate materials.

δ^{18}O *and* δD

Oxygen and hydrogen isotope records are often discussed together, as the controls on them are the same, although they respond at different rates to these changes. Waters are often therefore plotted in δD v. δ^{18}O space in which precipitation isotope values describe the Meteoric Water Line (MWL);

$$\delta D = s\delta^{18}O + d \qquad (2.2)$$

s is the gradient of the line and d the intercept of the line on the δD axis, known as the Deuterium excess. d is initially fixed by the conditions of evaporation from the source water body, particularly by the initial relative humidity of the air mass (Merlivat and Jouzel, 1979). The controlling factors on the slope of the line are poorly understood although maybe related to relative humidity (see discussion below). Mean global precipitation values lie along a line (Global Meteoric Water Line; GMWL) where $s = 8.1 \pm 0.1$ and $d = 11 \pm 1$ (Dansgaard, 1964). More regional relationships have also been observed e.g. in the Eastern Mediterranean where $s = 8$ and $d = 22$ (Gat and Carmi, 1970).

Other waters, such as those from rivers or lakes, can therefore be compared to meteoric waters by their δ^{18}O and δD values (Fig. 2.1). Waters that plot away from the MWL have undergone additional fractionation, often as a result of evaporation where waters become increasingly enriched in ^{18}O as ^{16}O is preferentially evaporated. The slope of this Local Evaporation Line (LEL), between the evaporated waters and their initial composition on the meteoric water line, depends on relative humidity, temperature and wind strength. The slope approaches s with increasing relative humidity (Leng, 2003).

2.2 Isotope changes in the hydrological cycle

Throughout the hydrological cycle processes occur which change the oxygen isotope values of water (Fig. 2.2). Here discussion will focus on changes in isotope values of precipitation (2.2.1) and during in-lake processes (2.2.2).

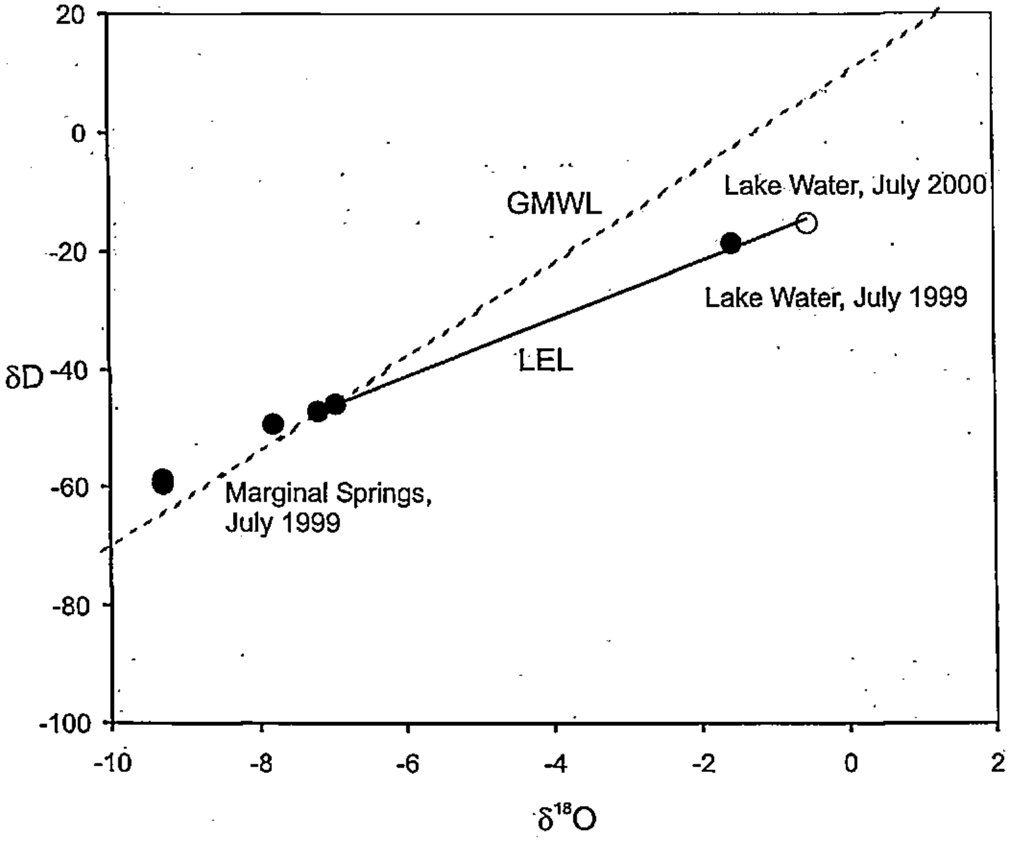

Fig. 2.1 Evaporated lake waters from Lake Gölhisar, Turkey, compared to precipitation isotope values (Jones *et al.*, 2002). GMWL = Global Meteoric Water Line, LEL = Local Evaporation Line.

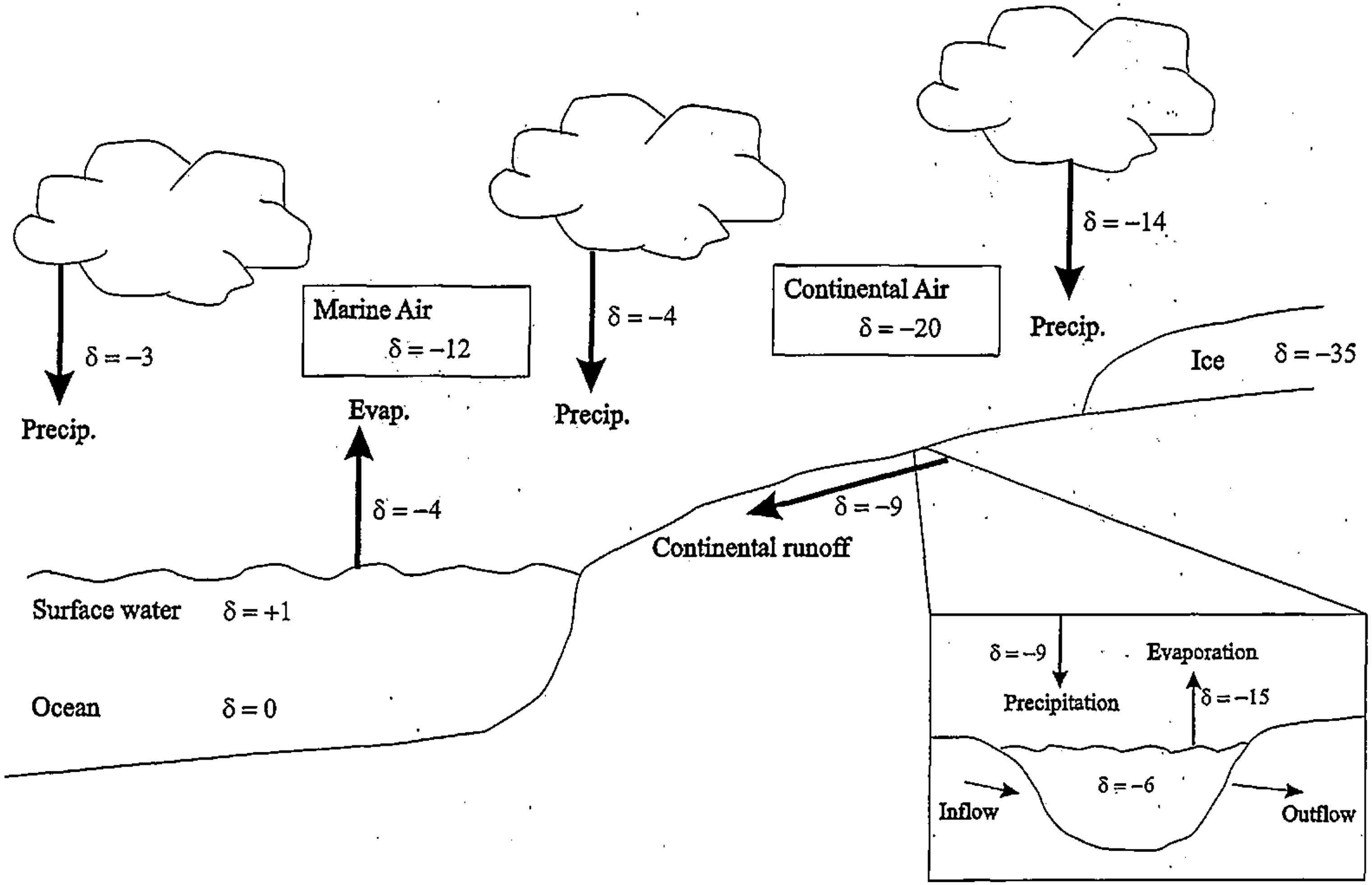
δ = −3
Precip.
Marine Air
δ = −12
Evap.
δ = −4
δ = −4
Precip.
Continental Air
δ = −20
δ = −14
Precip.
Ice
δ = −35
δ = −9
Continental runoff
Surface water
δ = +1
Ocean
δ = 0
δ = −9
Precipitation
Evaporation
δ = −15
δ = −6
Inflow
Outflow

Fig. 2.2 Controlling factors on $\delta^{18}O$ and δD in the hydrological cycle including lake systems (inset). Values given (δ) are for $\delta^{18}O$ and are general values to illustrate changes in the system. (After Gat (1996) and Rozanski *et al.*, (2001), with additional data from IAEA/WMO (2001), A. Dirican (pers. com.), Stuiver *et al.*(1995)).

2.2.1 Controls on isotopes in precipitation.

Following the early reviews (Craig, 1961; Dansgaard, 1964) which accompanied the formation of the IAEA global network for isotopes in precipitation (GNIP) a number of trends have been recognised between the oxygen and hydrogen isotope values of precipitation ($\delta^{18}O_{precip}$, δD_{precip}) and physical and climatic factors. These include temperature (Rozanski *et al.*, 1992), seasonality, altitude, continentality (Rozanski, 1985), the amount of precipitation, and precipitation source area (Rindsberger *et al.*, 1983).

Temperature

The temperature – precipitation isotope relationship is due to two factors (Cole *et al.*, 1999). Firstly, as an air mass cools vapour is lost through condensation, the air mass is consequently depleted in the heavier isotopes as these are preferentially condensed. Secondly, the isotope fractionation factor α, which determines the partitioning of the isotopes during phase transitions (e.g. evaporation and condensation), is also temperature dependent.

$$\alpha = Ra / Rb \qquad (2.3)$$

where R is the ratio $^{18}O/^{16}O$ or D/H and *a* and *b* are the two phases (e.g. water and water vapour). For example, values for the water to vapour transition are 1.0098 at 20°C and 1.0117 at 0°C for oxygen (Gat, 1996).

The result of these factors is that increases in temperature are reflected by precipitation isotope values enhanced in ^{18}O (Fig. 2.3). This relationship has been shown to hold for long-term trends in temperature and precipitation isotope composition for European stations (Rozanski *et al.*, 1992) between 1960 and 1990, with an average shift of 0.6‰$°C^{-1}$. Stuiver (1970) suggests a 0.7‰ shift in $\delta^{18}O$ for each 1°C change in ΔT, where ΔT represents the difference between the temperature during the evaporation of the air mass and the temperature at the time of precipitation.

Seasonality

There are also seasonal changes in the isotope values of precipitation although the degree of change is dependent on latitude and continentality. Over continental areas, there is an enhancement of the seasonal variations with increasing distance from the coast (Fig. 2.4).

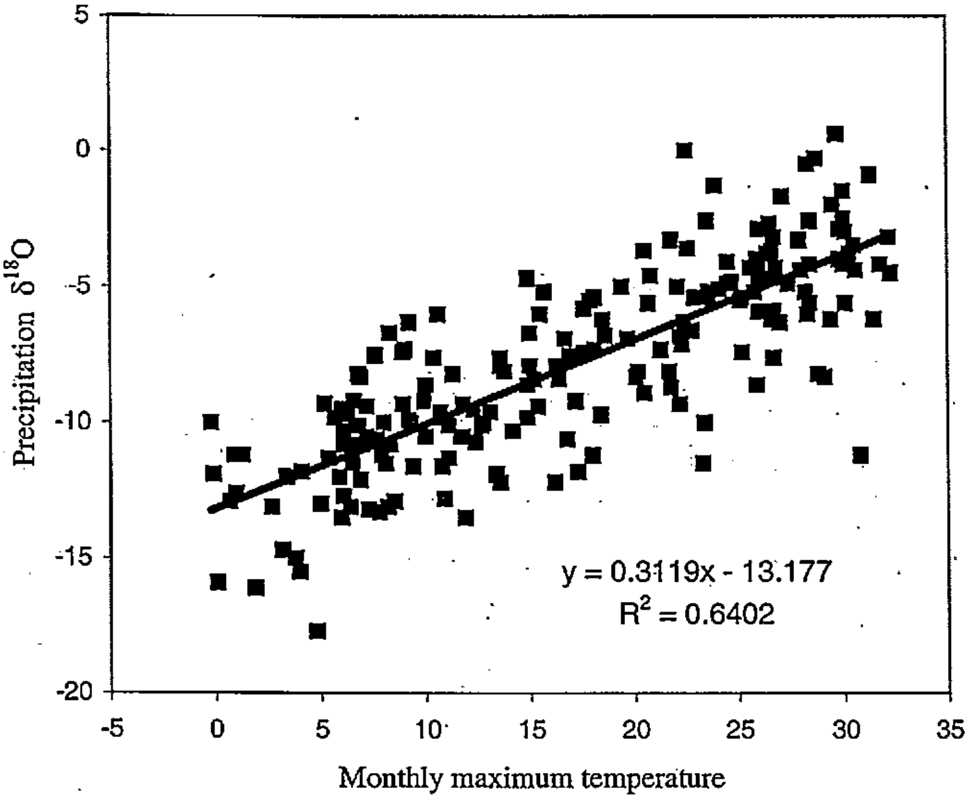

Fig. 2.3 δ^{18}O v. temperature relationship for Ankara (IAEA/WMO, 2001).

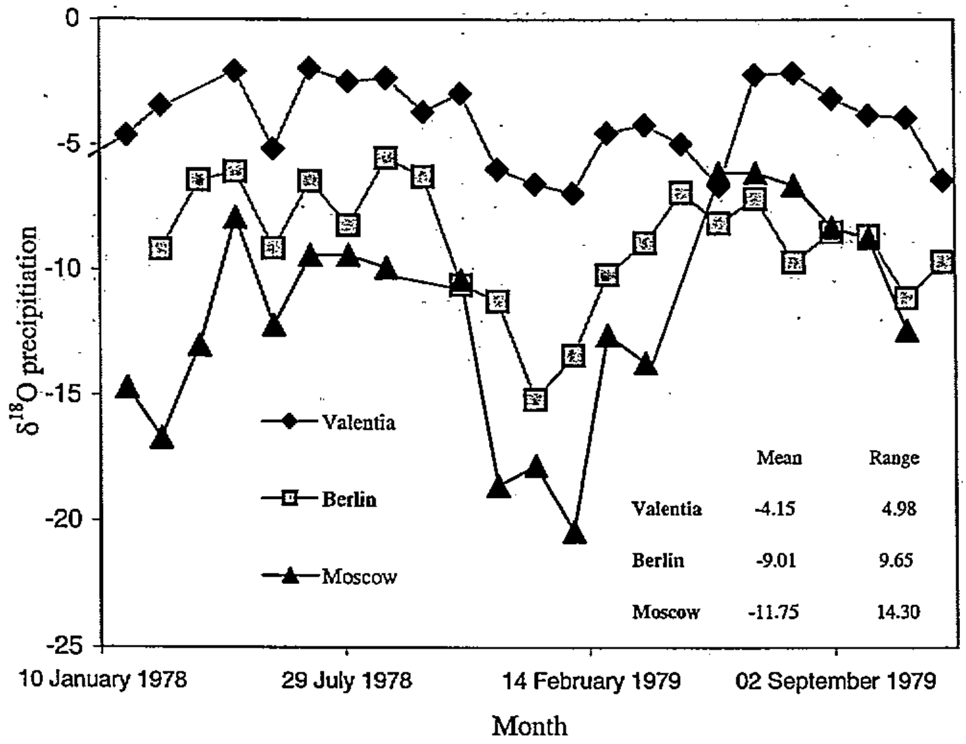

Fig. 2.4 Comparisons of δ^{18}O values in precipitation from three sites in northern Europe demonstrating more negative values and increasing ranges of δ^{18}O with increasing continentality from coastal (Valentia) to continental (Moscow) stations (IAEA/WMO, 2001).

These seasonal variations are due to larger seasonal temperature differences at mid and high latitudes (or more continental settings) compared to the tropics (or coastal areas), differences in the evaporation flux over the continents inducing seasonal differences in atmospheric water balance, and seasonally changing source areas or different storm trajectories (Jouzel, *et al.*, 1997).

Altitude

From observations of the GNIP data a relationship has been observed between altitude and precipitation isotope values, a large part of which is due to the corresponding change in temperature. The observed relationships show changes of between -0.1‰ and -0.6‰/100m for $\delta^{18}O$, with smaller changes at higher altitudes (Gat *et al.*, 2001).

Continentality

As air masses lose moisture due to precipitation, the isotope values become lighter due to the preferential rain out of the heavier isotopes. Consequently precipitation further along a given storm track, for example, will be more depleted in ^{18}O than the first rains that fell from it. This pattern is illustrated by the comparison of waters from Northern Europe (Fig. 2.4), where more easterly stations have considerably lighter precipitation $\delta^{18}O$ values. The continental effect varies considerably from area to area and from season to season (Gat *et al.*, 2001), in the example shown here (Fig. 2.4) the difference in mean values between Valentia, on the Irish Atlantic coast, and Moscow, Russia, is 7.6 ‰, although the difference is much larger in winter compared to summer.

Amount of precipitation

Relationships have been observed between the amount of precipitation and $\delta^{18}O$ (Dansgaard, 1964). For example, very heavy tropical rainfall may be extremely depleted in $\delta^{18}O$. Rainfall values from convective storms in northwest Europe have changed by –7 ‰ within the space of one hour (Gat *et al.*, 2001). Small amounts of rain, especially in more arid regions, can be more enriched in the heavy isotopes due to the evaporation of rain droplets as they fall to the ground.

Source area

Rindsberger *et al.* (1983) clearly demonstrate the effect of source area on precipitation isotope values (Fig. 2.5) in Gaaton (Israel), where precipitation isotope values fall into three distinct groups in δD v $\delta^{18}O$ space. These three groups correspond to the three main

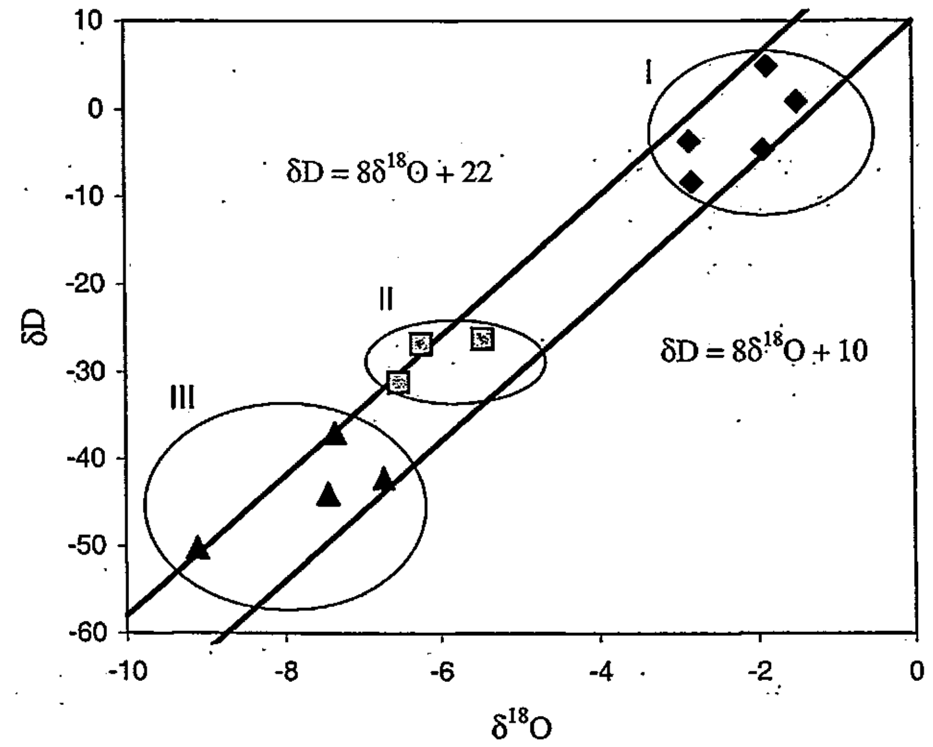

Fig. 2.5 Rainfall isotope values from three different source areas recorded at Gaaton, Israel (Rindsberger *et al.*, 1983). Group I rains from air masses arriving via the western Mediterranean and the north African coast, group II from air masses entering the eastern Mediterranean from continental Europe. Group III rains approach Israel from the south after travelling through central Europe and Africa.

trajectories for rain bearing air masses on the Israeli coast. These differences may be amplified by, or largely due to, differences in rain out history (see *Continentality*).

2.2.2 Controls on lake water $\delta^{18}O$

Changes in the isotopic composition of water entering a lake are largely due to changes in the isotope composition of the rainfall as described above. Some change may occur during transport through the catchment, e.g. due to evaporation, however the major controls on lake water values depend on the hydrological setting of the lake.

Open lakes

Open lakes, with a permanent input and output and a short residence time, are controlled predominantly by isotopic changes external to the lake basin as discussed above (2.2.1).

Closed lakes

In closed lakes, where residence times are long, lake waters have the potential to become enriched in ^{18}O due to the preferential removal of the lighter isotope during evaporation. This relationship can be demonstrated by comparing lake waters from closed lake basins, or in areas with negative water balance (evaporation > precipitation), with the MWL (Fig. 2.1).

A series of water masses from the same region may plot along a LEL. The interception of the LEL with the MWL is taken to be the weighted average value of the annual precipitation for the region (Leng and Anderson, 2003); i.e. the value lake waters would be if there was no significant evaporation.

The residence time of the lake is therefore important in the control of lake water isotope values. Closed systems may show greater variability in isotope values during a given climate change (Leng and Marshall, in press) as isotope shifts due to changes in hydrological budget are larger than those caused by changes due to precipitation and temperature in open systems. However, due to the long residence times, changes in $\delta^{18}O_w$ may be damped, especially in large lakes with residence times on century time scales, as the waters are an average of many years flux through the system (Leng and Marshall, in press.).

Non-climatic processes

Although the residence time of lakes is important in controlling the isotope values of the lake waters, changes in hydrology may not always be due to changes in climate. Changes in groundwater inflow may change the amount of water entering the lake, with the potential to result in rapid shifts to more negative isotope values if there is a sudden influx of meteoric water. This may particularly occur in crater lakes where changes in groundwater hydrology may occur due to tectonic or volcanic processes (e.g. Roberts *et al.*, 2001).

Crater lakes have further possible influences on the stable isotope chemistry of their lake waters. The input of volcanic waters into the system and the heating of the lake water in a hydrothermal regime both effect stable isotope values. Varekamp and Kreulen (2000) studied a series of volcanic lakes from Indonesia. A range of lake types was found ranging from those composed almost entirely of meteoric water to those including waters that had mixed with volcanic waters with a specific $\delta^{18}O$ and δD composition. As a result of the differences, volcanic lakes were found to describe a concave band on a $\delta^{18}O$ *v.* δD plot, compared to the normal straight evaporation line observed from non-volcanic lakes as waters from the hottest lakes, which therefore evaporate the most, also have most mixing with volcanic waters. In general terms, volcanic lakes therefore lie between the local evaporation line and the local mixing line for volcanic waters (Fig. 2.6). Additionally, lakes that are warm with respect to the atmosphere have a flatter evaporation line than cool lakes because of the stronger decrease in αD relative to $\alpha^{18}O$ with temperature.

2.3 Controls on stable isotopes in lake sediments

Isotope values are measured from a number of proxies found in lake sediments. As well as the hydrological controls discussed above specific controlling factors are associated with each proxy.

Sedimentary carbonate

Carbonate in lake sediments comes from one or more of three main sources (Kelts and Hsu, 1978). Calcareous skeletons and shell material from organisms living within the lake may make up some of the sediment and can be used independently for measurements of

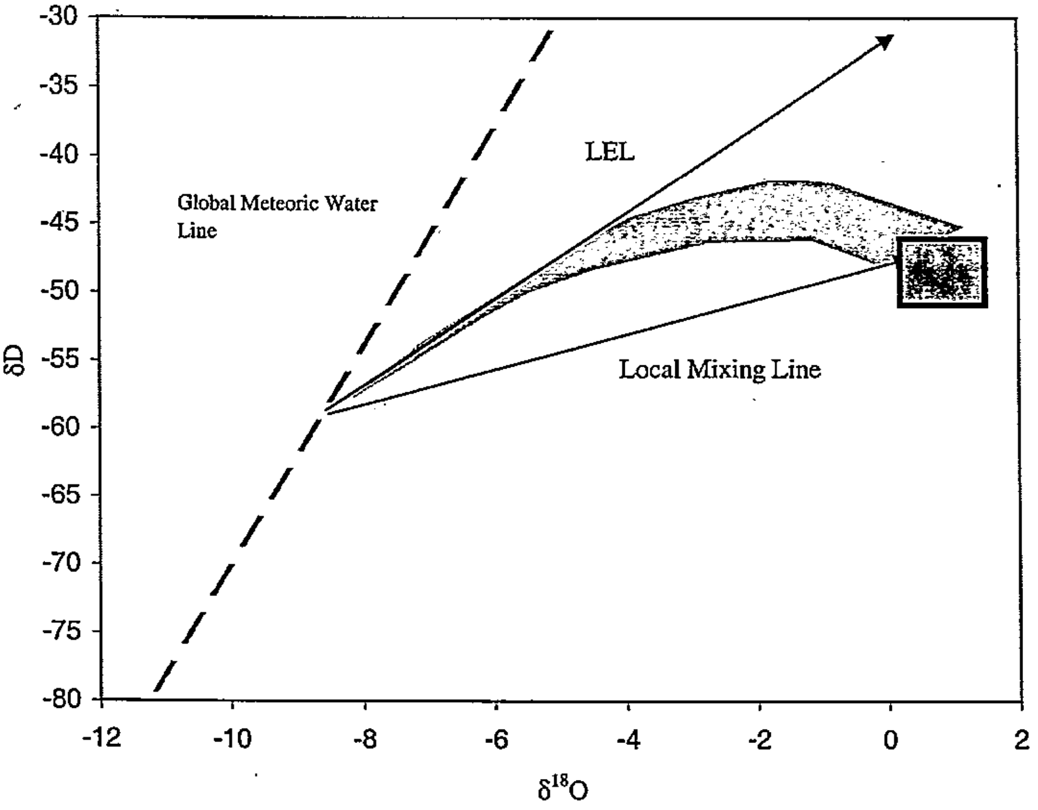

Fig. 2.6 Possible range of $\delta^{18}O$ and δD values from volcanic lake waters (light grey shaded area; after Varekamp and Kreulen, 2000). With no influence of volcanic waters lake water will fall on the LEL, increasing influence of volcanic waters (shaded square) will move lake waters towards the local mixing line.

$\delta^{18}O$ and $\delta^{13}C$ (see discussion below). Clastic input may bring allochtonous carbonates eroded and transported from the catchment into the lake and thirdly, carbonate may be precipitated directly from the water column.

Carbonate is precipitated in lakes as bicarbonate is utilised, to cope with the depletion of CO_2 in the lake waters, during the photosynthesis of aquatic plants and algae (Siegenthaler and Eicher, 1986), where

$$Ca^{++} + 2HCO_3^- = CO_2 + CaCO_3 + H_2O \qquad (2.4)$$

There is a temperature dependent carbonate-water fractionation of the oxygen isotopes. The values measured from the precipitated $CaCO_3$ ($\delta^{18}O_{carbonate}$) are therefore dependent on the temperature of the lake waters. $\delta^{18}O$ values decrease at 0.24‰°C^{-1} (Stuiver, 1970) as a result of this fractionation, although any changes in $\delta^{18}O_{carbonate}$ will also be due to changes in the lake waters.

From experimental data the relationship between temperature, lake water isotope values and the isotope values of the precipitated carbonate can be expressed as:

$$1000\ln\alpha_{(calcite/water)} = 18.03(10^3T^{-1})-32.42 \qquad \text{(Kim and O'Neil, 1997)} \qquad (2.5)$$

where T is the lake temperature in Kelvin. Using the relationship between calcite values on the SMOW and PDB scales (Coplen *et al.*, 1983) and the approximation that:

$$1000\ln\alpha_{(calcite/water)} \sim = \delta^{18}O_{calcite\ (SMOW)} - \delta^{18}O_{water\ (SMOW)} \qquad (2.6)$$

equation 2.5 was re-expressed by Leng and Marshall (in press) as

$$T\ (^\circ C) = 13.8 - 4.58(\delta_c - \delta_w) + 0.08(\delta_c - \delta_w)^2 \qquad (2.7)$$

where δ_c is $\delta^{18}O$ carbonate (PDB) and δ_w is $\delta^{18}O$ water (SMOW).

It has been suggested (Mook *et al.*, 1974) that there is a small temperature fractionation effect on $\delta^{13}C$, with values becoming lighter with increasing temperature. However, the effect is small, c. 0.08‰°C $^{-1}$, and will therefore usually be lost in the overall isotope signal.

In open lakes, where lake waters are controlled by changes in precipitation isotope values there are therefore two temperature controls on the recorded stable isotope values, firstly due to changes in precipitation values (section 2.2.1), e.g. at + 0.6‰/°C in northern Europe, and secondly due to the fractionation as carbonate is precipitated at -0.24‰/°C. Using these figures there is therefore an overall relationship of + 0.36 ‰/°C, which may be used to quantify past temperature changes from isotope records if lake water values can be shown only to be controlled by precipitation isotope values in turn only controlled by temperature.

Allochthonous carbonates from local bedrock will influence stable isotope values measured from lake sediments. The degree of influence is difficult to quantify, although where this is possible the amount of allochthonous carbonate can be used as a proxy for inwash and any isotope values corrected to leave only the effect of authigenic carbonates (Hammarlund *et al.*, 1999).

Biogenic carbonate

Carbonate shells of freshwater organisms such as ostracods and molluscs can also be measured for $\delta^{18}O$ and $\delta^{13}C$ values. Generally the carbonate used by these organisms to make their shells will form in equilibrium with the lake waters however there may be additional species-specific fractionation factors, or "vital effects", especially in ostracod shells (Holmes, 1996) that will shift isotope values away from equilibrium values. As long as the same species can be analysed throughout a sedimentary sequence this effect should be constant and trends observed therefore dependent on temperature and isotope values of the lake waters. Mollusc shells are usually made of unstable aragonite and can often be replaced by calcite following deposition; this process may reset the isotope signature of the shell.

It has been demonstrated, for both molluscs and ostrocods, that different species living at the same time in the same lake yield different $\delta^{18}O$ and $\delta^{13}C$ values (Jones *et al.*, 2002; Heaton *et al.*, 1995), probably due to differences in microhabitat water isotope values and differences in predominant periods of shell growth.

Ostracods and small molluscs represent only a short period of time, from a few hours to a year, and therefore a number of individuals need to be analysed from any sample level to show variation in $\delta^{18}O$ during the time represented by that sample. Larger freshwater snails live for a number of years and have the potential to record seasonal changes in lake water $\delta^{18}O$ over a period of time (Leng *et al.*, 1999).

Biogenic Silica

$\delta^{18}O$ values can be measured from silica deposited by freshwater diatoms and sponges. This is a particularly useful technique in lakes where there is little carbonate to exploit. Biogenic silica has been used as a proxy for temperature change (e.g. Rosquist *et al.*, 1999; Leng *et al.*, 2001), although the exact temperature $\delta^{18}O$ relationship has yet to be fully explained (Leng and Marshall, in press). As well as temperature shifts in silica $\delta^{18}O$ records have also been interpreted as changes in the moisture balance regime (Barker *et al.*, 2001) or changes in the source of precipitation (Shemesh *et al.*, 2001) reflected in changes in lake water $\delta^{18}O$.

2.4 Controls on lake $\delta^{13}C$

Dissolved inorganic carbon (DIC) in lake waters is incorporated into carbonates and the $\delta^{13}C$ values of DIC reflect environmental changes in the lake carbon pool. Groundwater and river water entering the lake typically have $\delta^{13}C$ values between -10 and -15 ‰ (Leng and Marshall, in press). Exchange of CO_2 with the atmosphere, biological productivity, and changes in catchment vegetation types, may all then contribute to changes in the carbon isotope ratio (Fig. 2.7).

Closed lakes have sufficient time for exchange with atmospheric CO_2 ($\delta^{13}C = -7.8$ ‰; Boutton, 1991) to have a significant impact on DIC $\delta^{13}C$ values. Due to fractionation processes carbonates from lakes in equilibrium with atmospheric CO_2 may have carbonate $\delta^{18}O$ values of up to +2‰ (Valero-Garces, 1999). Within lake productivity of aquatic algae will also influence DIC. Increased productivity leads to more positive $\delta^{13}C$ values as ^{12}C is preferentially incorporated into plant materials and therefore removed from the system as the plants are sedimented out. This effect will be cancelled out if the organic matter is then oxidised at the lake bed, releasing ^{12}C back into the carbon pool. If additional terrestrial carbon occurs in the lake sediment the amount of released ^{12}C will be greater than that

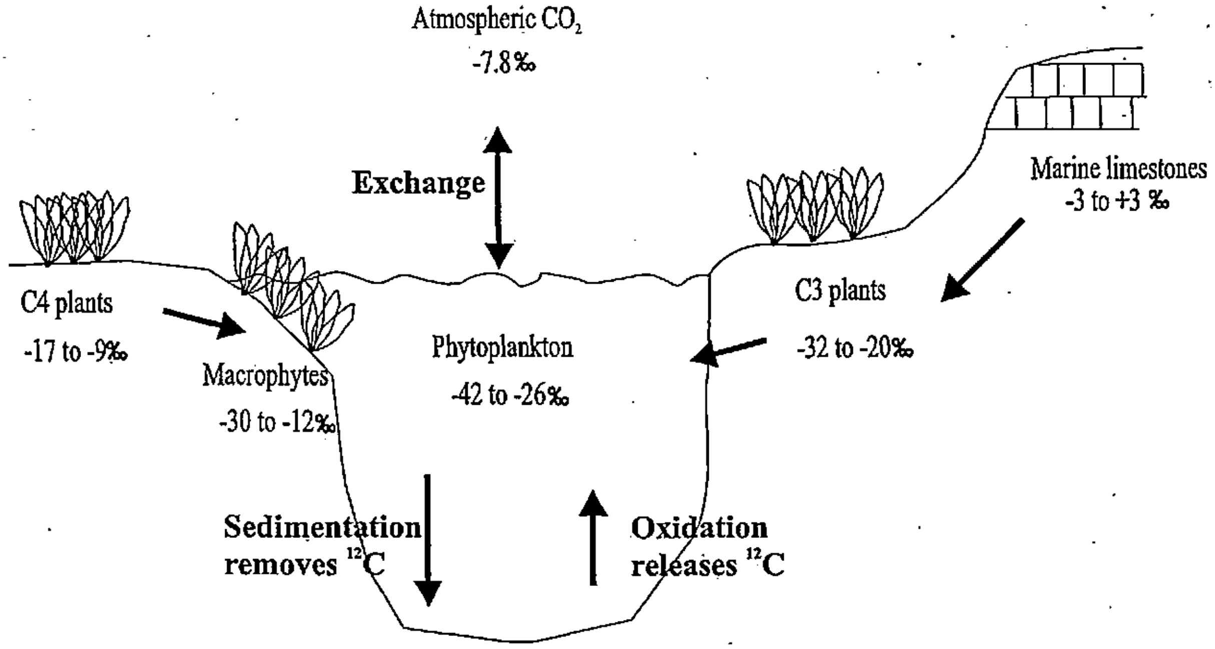
Atmospheric CO_2
-7.8‰
Exchange
Marine limestones
-3 to +3 ‰
C4 plants
-17 to -9‰
C3 plants
-32 to -20‰
Macrophytes
-30 to -12‰
Phytoplankton
-42 to -26‰
Sedimentation removes ^{12}C
Oxidation releases ^{12}C

Fig. 2.7 Major sources, with associated stable carbon isotope values, and fluxes in lake carbon budgets (after Leng and Marshall, in press).

removed by plants in the lake waters resulting in a decrease in $\delta^{13}C$ values (Meyers and Teranes, 2001).

Outside the lake, the stability of the catchment slopes is an important control on the carbon entering the lake. As soils develop in a catchment, land plants become established and ^{12}C enriched carbon ($\delta^{13}C$ = -25‰ for C3 plants) may enter the lake through soils and organic matter dissolved in groundwaters (Wassenaar *et al.*, 1990). A significant change in the plant types within the lake catchment may therefore affect the values of DIC; C4 plants have $\delta^{13}C$ values significantly more positive (~ -15‰) than the C3 value. Inwash of carbonate from rocks within the catchment with a set $\delta^{13}C$ value (usually more positive than DIC values) will also effect the $\delta^{13}C$ of the total DIC (TDIC).

Organic matter

The $\delta^{13}C$ of organic matter is dependent on the influences on DIC, from which submergent aquatic plants fix their carbon (Turney, 1999) as described above, and also on differences in $\delta^{13}C$ between different sources of organic matter (Fig. 2.7).

Commonly $\delta^{13}C$ values are obtained from bulk samples of lake sediment. Without some secondary indicator of the source of the organic matter records are difficult to interpret, as lake algae and terrestrial C3 plants have a similar range in $\delta^{13}C$ (Meyers and Teranes, 2001). C:N ratios can be used to identify the dominant source of the organic matter as lake algae have values between 7 and 9 and C3 plant values are generally above 17 (Fig. 2.8). If the organic material is predominantly lake algae, $\delta^{13}C_{organic}$ records are largely controlled by productivity, whereas $\delta^{13}C$ values for terrestrial organic matter will depend on the type of source vegetation (see more detailed discussion above).

Both $\delta^{18}O$ and $\delta^{13}C$ can be measured from lake organic matter cellulose (e.g. Abbot *et al*, 2000). Interpretation of these records is based on the assumption that the fine-grained cellulose fraction analysed from lake sediments is derived solely from aquatic plants and algae and that the oxygen isotope fractionation between water and aquatic cellulose in known (Wolfe *et al.*, 2001).

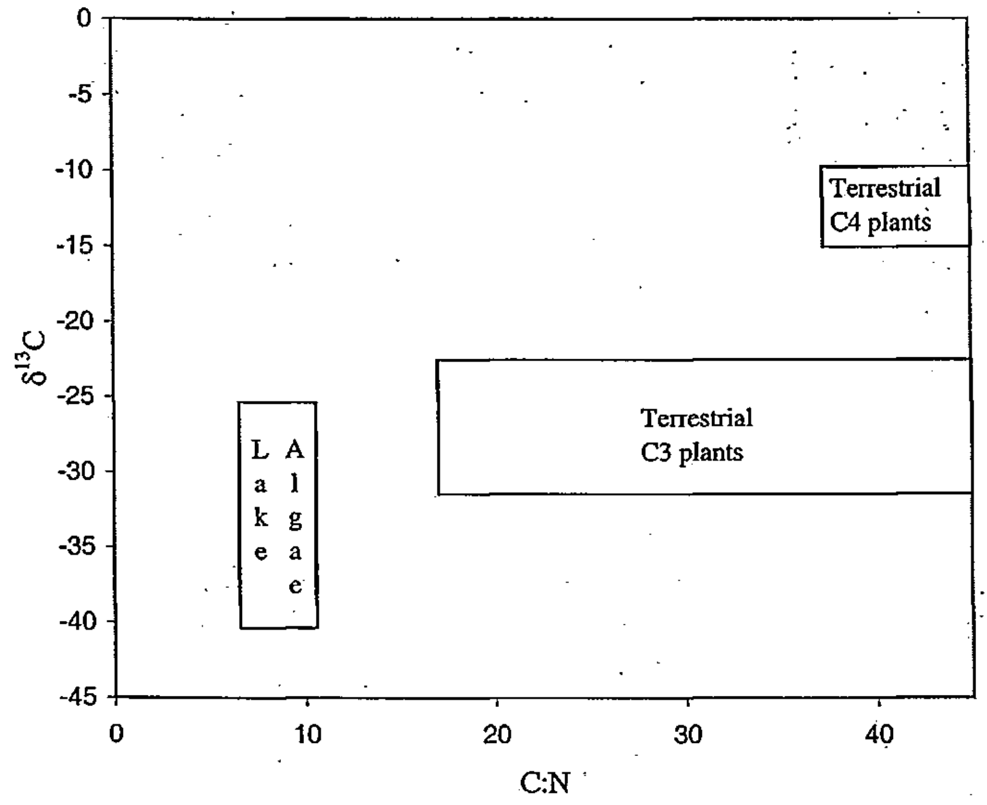

Fig. 2.8 Typical δ^{13}C and C/N values of organic fractions in lake sediments (after Meyers and Teranes, 2001; additional data from Leng and Marshall, in press).

2. 5 Summary

There are a large number of factors controlling lake stable isotope values, all of which must be taken into account when interpreting palaeorecords. In general open lakes with short residence times will have lake water $\delta^{18}O$ values controlled by changes in precipitation, and sedimentary carbonate $\delta^{18}O$ will be additionally dependent on temperature at the time of carbonate precipitation. In closed lake systems $\delta^{18}O$ values of the lake waters will be additionally controlled by evaporation.

$\delta^{13}C$ values also have many controlling mechanisms; primarily the degree of equilibration with atmospheric CO_2, particularly in lakes with longer residence times, and changes in lake productivity. Changes in catchment vegetation and inwash may also be important.

Chapter 3

TURKISH CLIMATE: PAST AND PRESENT

As well as understanding the controls that may affect lake chemistry, as discussed in the previous chapter, an understanding of the regional climate regime, which may lead to changes in these conditions, is also important before correct inferences can be drawn from proxy records. This chapter will therefore review current knowledge regarding climate in Turkey and the atmospheric processes controlling it. Previous studies of past climatic climate change will be also be reviewed to understand how the region responds to large scale climatic events and over long time periods.

3.1 Contemporary Climate

The Mediterranean climate zone is characterized by wet, mild winters and hot, dry, cloudless summers (Kendrew, 1961) with autumn tending to be warmer than spring. In general, summer conditions are similar to North Africa with winter climates more comparable to northern Europe. During the winter the Mediterranean basin is under the influence of the westerlies (Bolle, 2003) and the descending branch of the Hadley circulation during the summer (Fig. 3.1).

The climate of Turkey is more complex than this simple Mediterranean picture, and only the southern Mediterranean coast can be described as having a truly Mediterranean climate. Three major physical factors contribute to this more complex climate regime (Türkeş, 1996):

1) High mountain ranges run west to east along both the northern and southern edge of the Anatolian Peninsula.
2) Turkey sits between three major water bodies, the Mediterranean, the Aegean and the Black seas.
3) The Anatolian Plateau has a mean elevation of over 1100m.

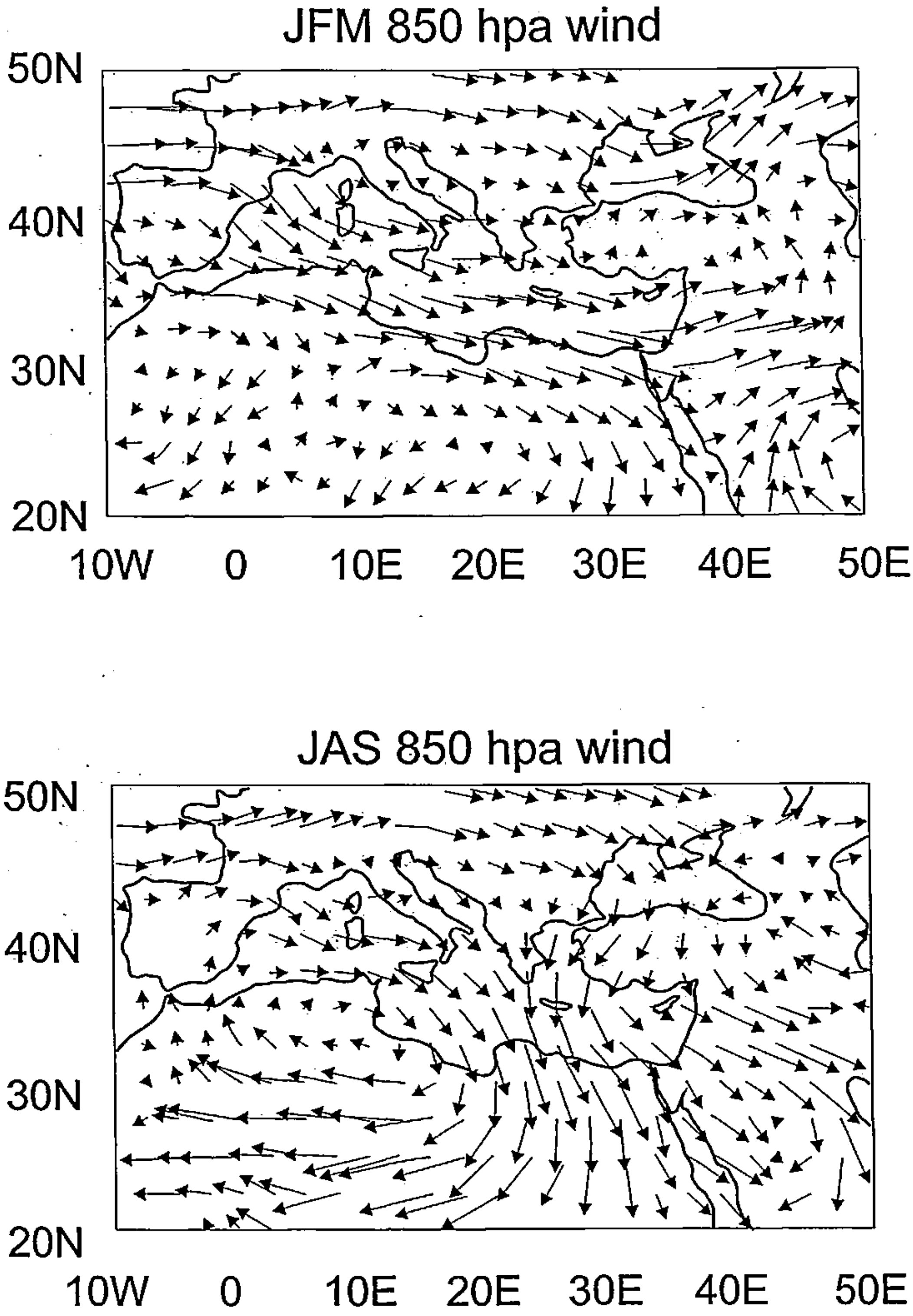
JFM 850 hpa wind
50N
40N
30N
20N
10W
0
10E
20E
30E
40E
50E
JAS 850 hpa wind
50N
40N
30N
20N
10W
0
10E
20E
30E
40E
50E

Fig. 3.1a Wind climatologies at 850 hPa showing differences between winter (JFM) and summer (JAS) conditions over the Mediterranean basin (Raicich *et al.*, 2003).

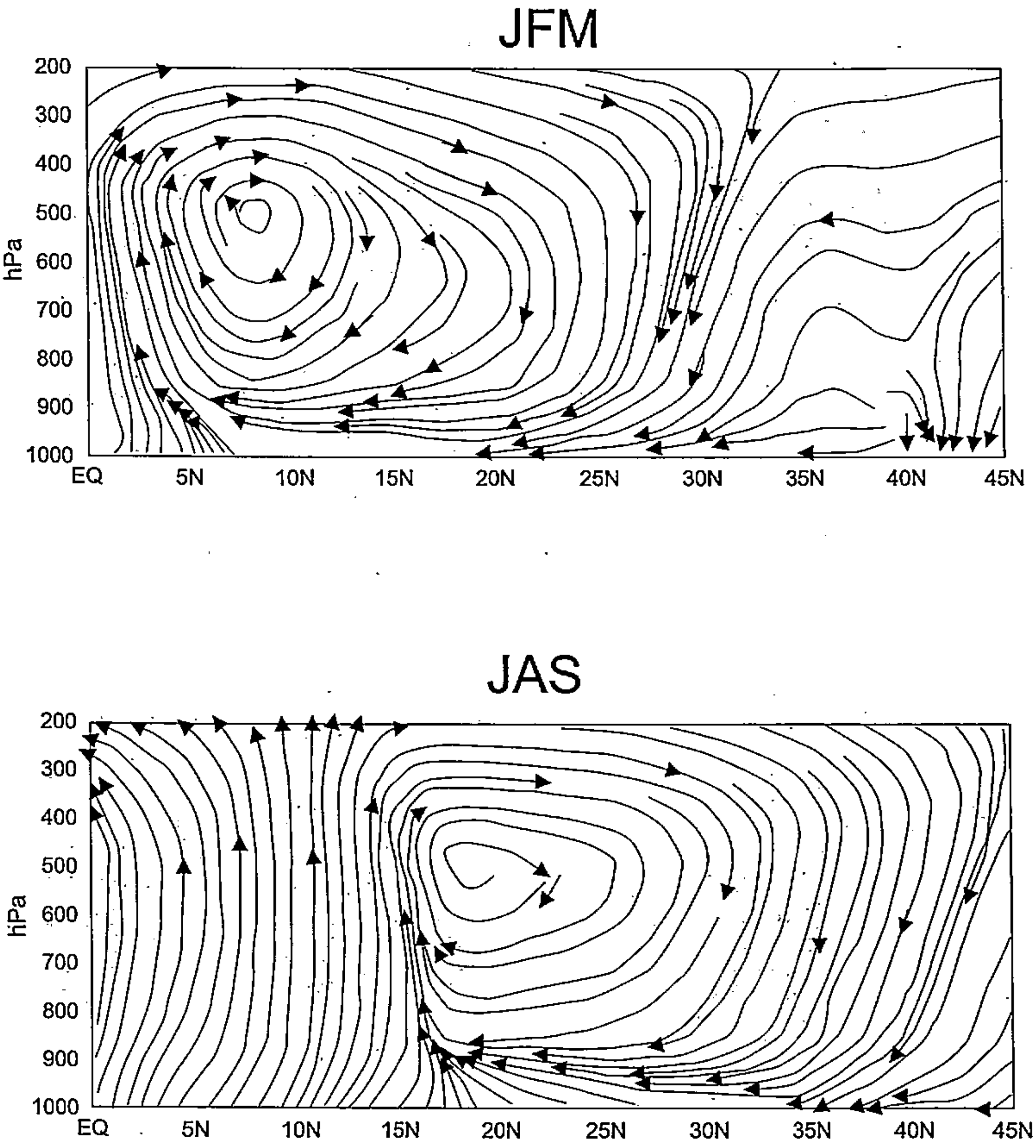

Fig. 3.1b Streamlines (averaged between 15 and 35E) showing differences between winter (JFM) and summer (JAS) conditions over the Mediterranean basin (Raicich *et al.*, 2003).

Precipitation

The mountain ranges provide a barrier to maritime polar (from the Atlantic) and Mediterranean air masses moving on to the northern and southern coasts of Turkey, respectively. This leads to varying amounts of rainfall across the country (Fig. 3.2). Precipitation from the maritime polar air masses on the Black Sea coast is heavy through autumn, winter and spring, although rain also falls through the summer. Air masses that reach the south coast from the Mediterranean bring heavy rains through the winter, although summers are very dry.

The three basins that surround Turkey act as natural passages for frontal cyclones, moving east across the Mediterranean, around the higher-pressure systems that usually sit over the Turkish peninsula. The highest numbers of depressions reach Turkey in the winter months, over half of which follow track IIIb (Fig. 3.3), across Italy and Greece, and reach Turkey via the west coast. These depressions may be sourced in the Western Mediterranean or modified there after forming in the mid-latitude Atlantic. Tracks I and II are typically summer time trajectories bringing summer storms to the north of the country, tracks III and IV are the dominant winter storm paths, affecting the south (Karaca *et al.*, 2000).

The height of the Anatolian plateau, particularly the high mountains in the east of the country, means that winters are cold and snowy across most of Turkey.

A number of rainfall regimes were assigned by Türkeş (1996) to account for the changes in rainfall patterns across Turkey (Fig. 3.4). The **Black Sea** region is temperate with rainfall throughout the year; maximum precipitation is in the autumn. The **Mamara** region, a transition between the Mediterranean and the Black Sea on the western coast, again has precipitation throughout the year but with lighter rains through the warm summer. The **Mediterranean** region is markedly seasonal with heavy rains in the cool winters and warm dry summers. In the **Continental Mediterranean** rain falls in the winter and spring but summers are severely hot and dry. **Continental Central Anatolia** has cool, wet springs and winters with some light precipitation during the warm summers. The transition between central Anatolia and the Mediterranean region has only moderate rains through winter and spring.

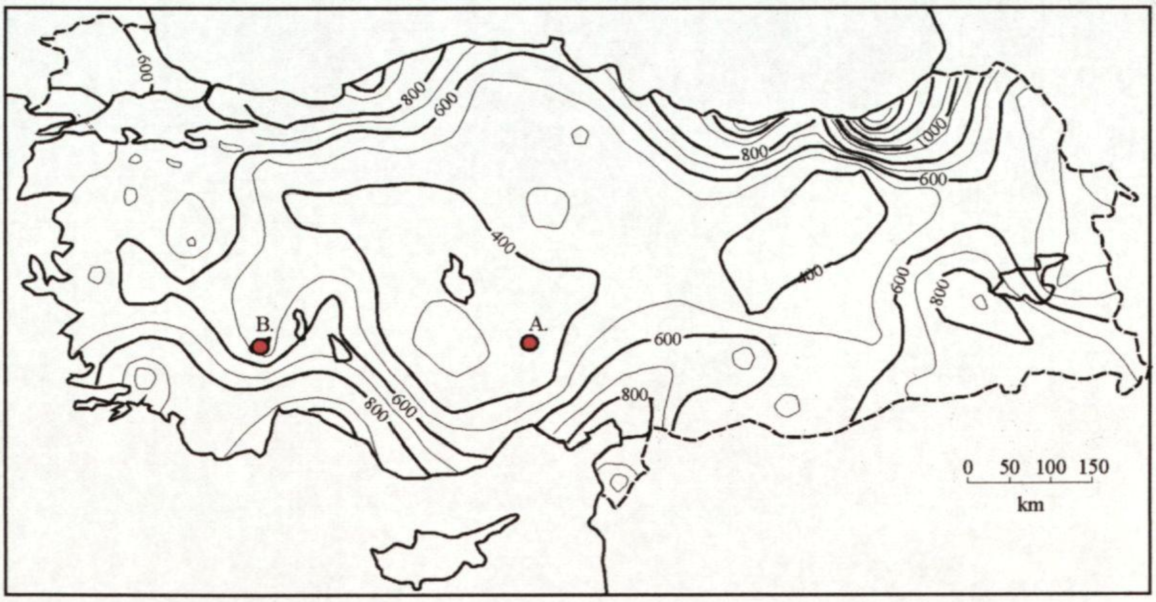
600
800
600
800
1000
600
400
400
600
800
B.
A.
600
800
600
800
800
0 50 100 150
km

Fig. 3.2 Mean total precipitation across Turkey (Türkeş, 2003). Red circles mark sites in this study A. Nar Gölü ; B. Burdur Gölü (see chapters 5 and 7 for details).

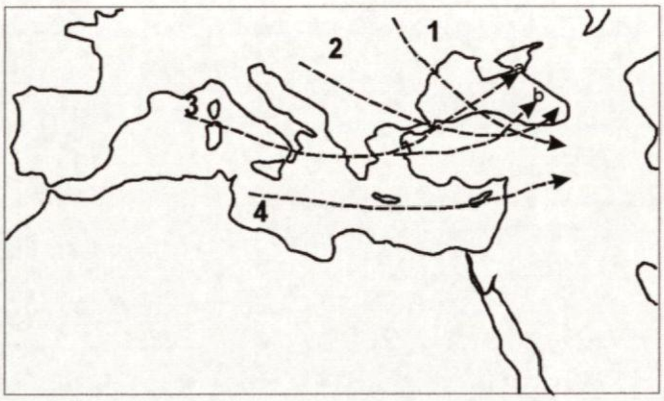

Fig. 3.3 Dominant storm tracks affecting Turkey (Karaca *et al.*, 2000).

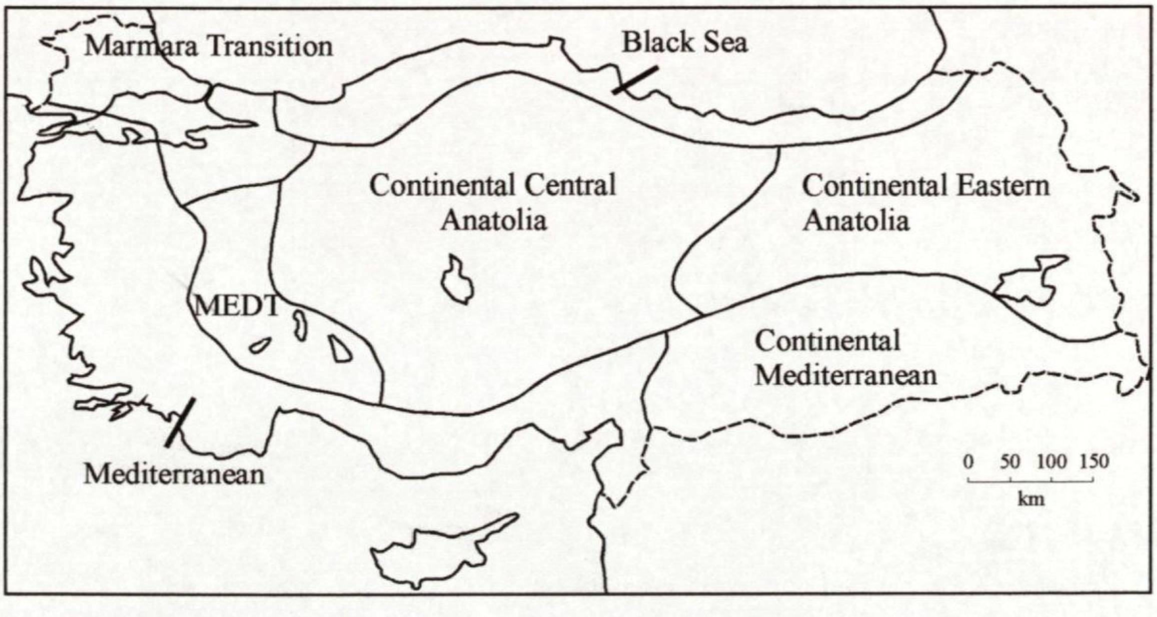
Marmara Transition
Black Sea
Continental Central Anatolia
Continental Eastern Anatolia
MEDT
Continental Mediterranean
Mediterranean
0 50 100 150
km

Fig. 3.4 Turkish rainfall regimes (Türkeş, 1996). See text for description.

Continental Eastern Anatolia has very cold and snowy winters with cool springs and early summers accompanied by light rains.

Temperature

The complexity of Turkish climate is also evident in the temperature patterns (Fig. 3.5). Major controls on temperature include topography and proximity to the sea. In general annual mean temperature decreases away from the coastal region and to the eastern part of the country where the topography is considerably higher. The highest mean temperatures are found along the Mediterranean coast (20°C). Along the Black Sea coast annual mean temperatures are around 12°C, compared to averages between 8°C and 12°C in the interior of the country (Türkeş *et al.*, 1995).

Aridity

Large parts of Turkey have an annual moisture deficit, where potential evapotranspiration (PE) > precipitation (P). Fig. 3.6 shows the spatial distribution of an Aridity Index (AI = P/PE) for Turkey. Large parts of continental Anatolia are dry sub-humid regions (0.50 < AI < 0.65) with certain areas, especially in south central Turkey between Tuz Gölü and the Taurus Mountains, semi-arid (0.20 < AI < 0.50) (Türkeş, 2003).

3.2 Recent Climate trends

Meteorological records are available at some sites in Turkey from 1926. However many of these stations have been moved from time to time during this time period, and the longest records are found in the largest centers of population some of which have undergone periods of severe atmospheric pollution in the latter half of the twentieth century, which may affect meteorological observations (Türkeş *et al.*, 1996).

Looking at average temperatures between 1930 and 1992, for the whole of Turkey, Türkeş *et al.* (1995) found a general warming trend from 1930 to the late 1960's followed by an overall cooling trend, interrupted by a brief warming from about 1972 to 1980 (Fig. 3.7). A more detailed study of the data between 1940 and 1993 (Türkeş *et al*, 1996) showed a general trend

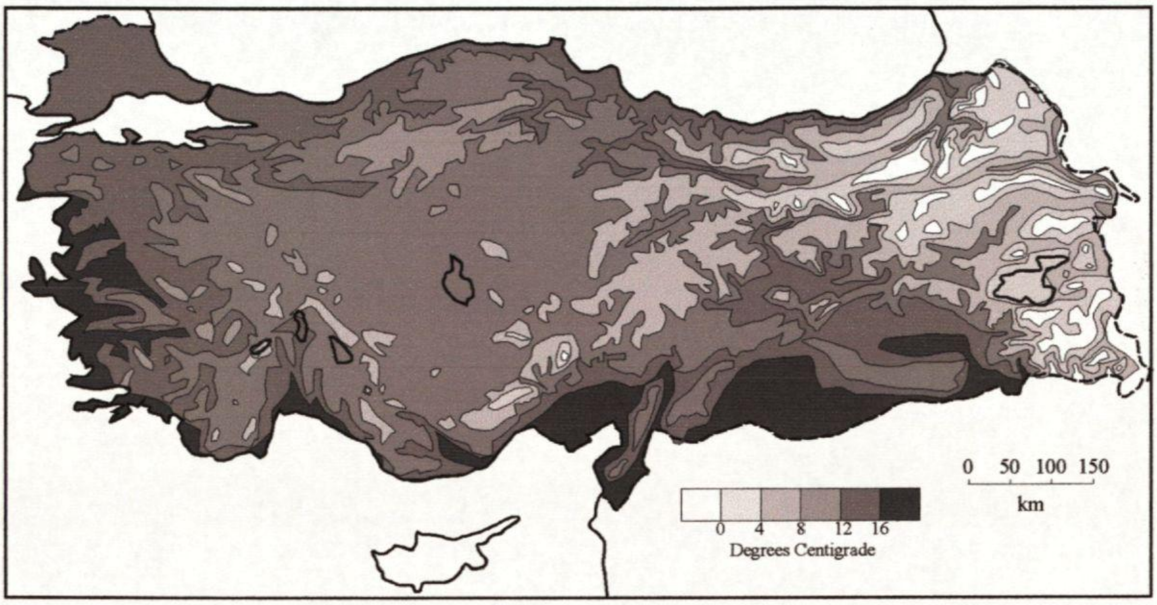
0 50 100 150
km
0 4 8 12 16
Degrees Centigrade

Fig. 3.5 Mean temperatures across Turkey (after Türkeş *et al.*, 1995).

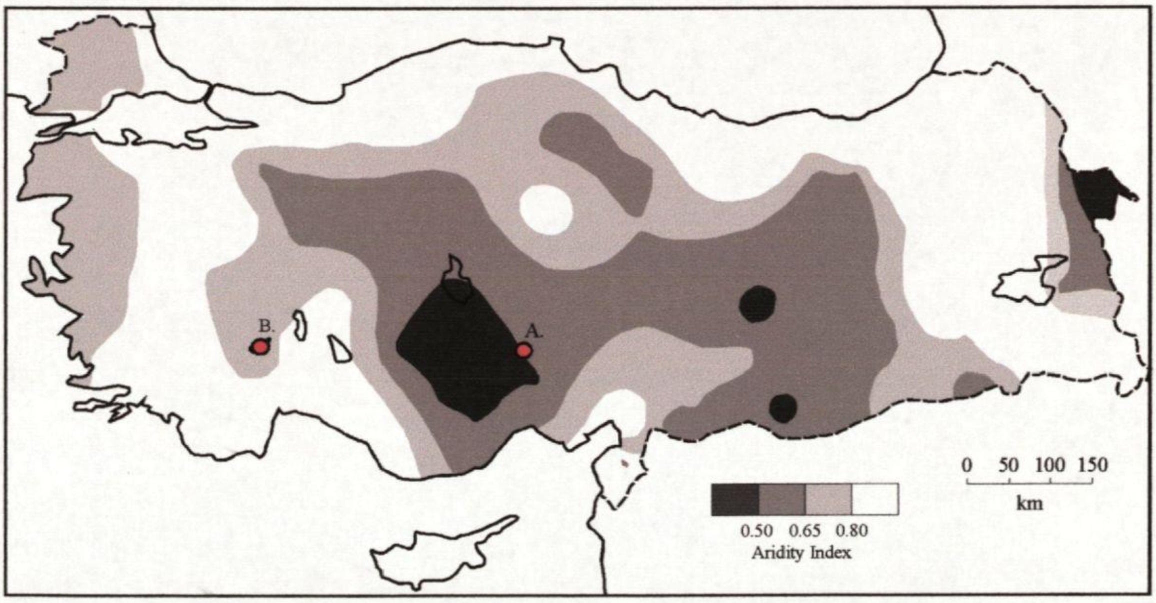
B.
A.
0 50 100 150
km
0.50 0.65 0.80
Aridity Index

Fig. 3.6 Mean values of aridity index across Turkey (Türkes, 2003). Red circles mark sites in this study A. Nar Gölü ; B. Burdur Gölü (see chapters 5 and 7 for details).

Fig. 3.5 Mean temperatures across Turkey (after Turkes *et al.*, 1995)

Fig. 3.6 Mean values of aridity index across Turkey (Turkes, 2003). Red circles mark sites in this study A: Nar Gölü, B: Burdur Gölü (see chapters 5 and 7 for details).

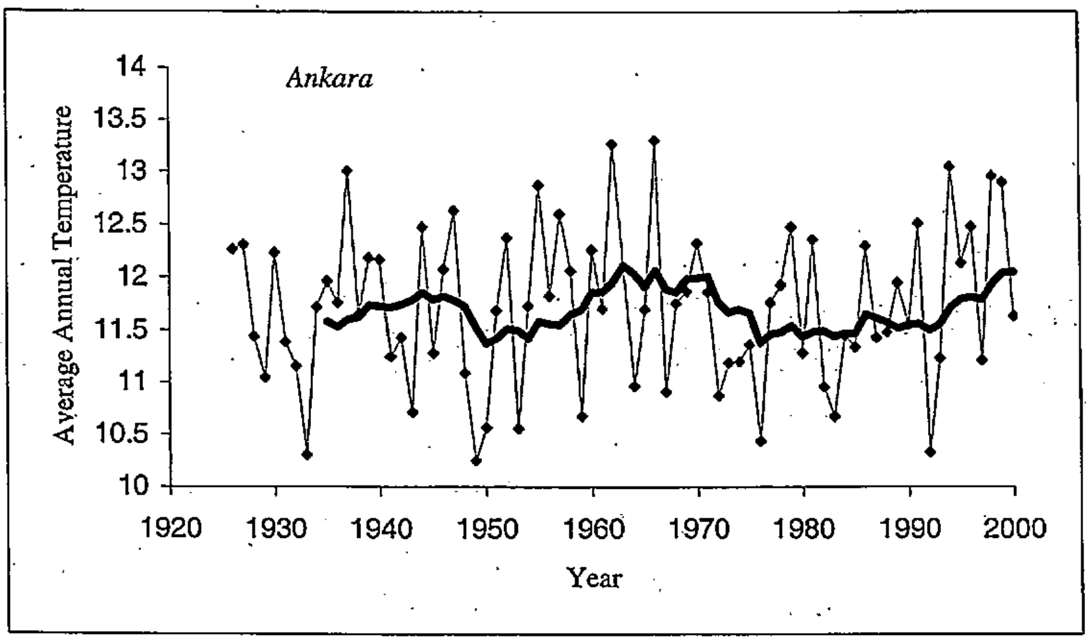

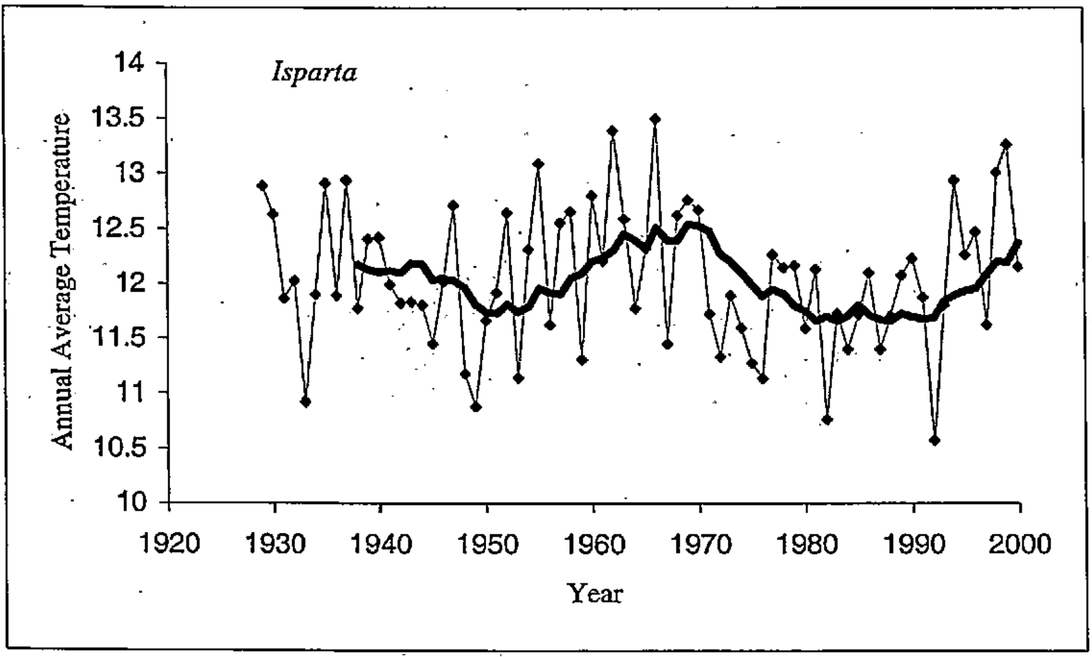

Fig. 3.7 Recent trends in Turkish temperatures (data from Turkish State Meteorological Service), black lines show ten year running means.

of cooling in the seasonal maximum temperatures and warming in the seasonal minimum temperatures resulting in an overall decrease in the temperature range across Turkey.

There are few trends in the amount of rainfall through the time period covered by meteorological observations across Turkey. Those individual stations which do show a statistically significant trend, mostly in the Mediterranean rainfall regime, show a downward trend mostly during the last 25 – 30 years (Türkeş, 1996).

3.3 Controls on climate

Some of the shifts in precipitation and temperature across Turkey can be linked to hemispheric and global climate phenomena.

North Atlantic Oscillation (NAO)

The NAO describes pressure differences between the Azores High and the Icelandic low. Numerical indices describing this relationship are based on locations representative of these pressure systems e.g. between Lisbon, Portugal and Stykkisholmur, Iceland (Hurrell, 1995). The negative NAO state, where the Icelandic low is relatively high, results in an increase in storm tracks that enter the Mediterranean basin. Eastern Mediterranean climates are linked to this North Atlantic activity via the secondary genesis of cyclonic storms near Crete, Cyprus and the Black Sea, following the storm tracks entering the Western Mediterranean (Cullen and deMenocal, 2000). The NAO index is more pronounced during winter months due to an increased sea-air temperature contrast.

Tan and Unal (2003) show that the result of this teleconnection is that Turkey experiences drier winters during positive NAO index years. During NAO negative years southern Turkey experiences wetter conditions although the northeastern region is relatively dry. Mann (2002) shows that during positive NAO phases the eastern Mediterranean would experience cooler than normal temperatures.

North Sea-Caspian Pattern (NCP)

Kutiel and Benaroch (2002) have described a teleconnection between the Eastern Mediterranean and the North Atlantic climate systems. The NCP index defines the difference in the 500-hPa geopotential height between the North Sea and the North Caspian Sea. The index is defined such that a negative NCP phase relates to higher pressure over the Caspian Sea. Teleconections are more frequent and stronger in the winter months compared to summer.

Kutiel *et al.* (2002) showed that this index was associated with changes in temperatures and precipitation in Turkey. The positive phase of the NCP is associated with below normal temperatures due to increased northeasterly winds over Turkey. Higher temperatures due to increased southerly winds are associated with negative phases of the NCP (Fig. 3.8).

The impact on rainfall variability is more complex. In regions dominated by southern maritime fluxes, such as the Mediterranean and Mediterranean to Central Anatolian transition rainfall regimes, there is increased rainfall during negative phases of the NCP. In regions dominated by northerly maritime fluxes, such as the Black Sea rainfall regime, rainfall is higher during the positive NCP phases (Kutiel *et al.*, 2002).

Southern Oscillation (SO)

The SO describes a shift in surface air pressure between Darwin, Australia and Tahiti in the South Pacific. When the pressure is high at Darwin it is low at Tahiti and vice versa (NOAA, 2003). Global climate events are often associated with El Niño and its sister event La Niña, the extreme phases of the SO. El Niño refers to a warming of the eastern tropical Pacific, and La Niña a cooling.

Kahya and Karabork (2001) describe a connection between Turkish streamflow and SO extreme events. During El Niño events Turkey experiences extreme wet seasonal streamflow, and it is drier in Eastern Anatolia during La Niña phases. Mann (2002) also finds a connection between temperatures in the Middle/Near East region and SO suggesting cold anomalies in the region during La Niña events. However the relationships are not as strong as those with the NAO.

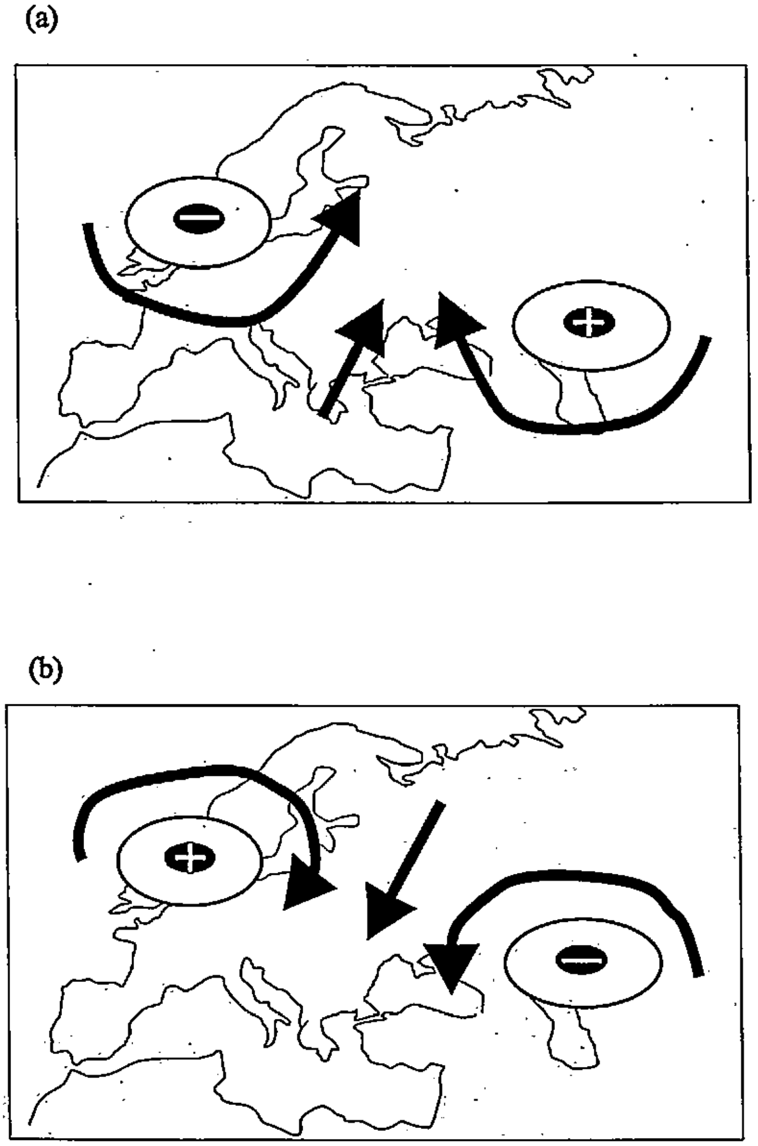

Fig. 3.8 Extreme phases of the North Sea-Caspian Pattern (Kutiel and Benaroch, 2002). Showing areas of relative high (+) and low (-) pressure and dominant wind directions for negative (a) and positive (b) phases of the NCP.

Although the relationships are statistically significantly between the SO and Eastern Mediterranean climate patterns there is as yet no simple causative explanation for such a teleconnection (Kutiel *et al.*, 2002).

Indian Monsoon

During the summer Turkish climate is linked to the Indian Monsoon via the zonal tropical circulation which is coupled to the Hadley cell (Bolle, 2003). Raicich *et al.* (2003) show that increased Indian monsoon precipitation occurs during times of lower atmospheric pressure over the Eastern Mediterranean. There is a similar correlation with rainfall in the Sahel region of northern Africa. Although the exact mechanism for the connection between these weather systems is unclear (Raicich *et al.*, 2003) it appears that the Eastern Mediterranean is connected to northern African and Indian Monsoon systems during the summer.

3.4 Previous palaeoclimatic work in Turkey

Turkey has been the focus of a significant amount of palaeoenvironmental work, driven by questions related to climatic changes in the Mediterranean compared to other regions, and of past human occupation. The majority of this work has come from lake cores although tree rings have also been used for reconstructions of more recent climate changes. The sites discussed here, describing climate variability in Turkey from the late Pleistocene through to the last millenium, are shown in Fig. 3.9.

Late Pleistocene

Pre-Holocene lake sediments have been recovered from a few Turkish lakes, although dating control on these records is limited they do show changes in Pleistocene climate. A record between 27 and 58 ka BP from Lake Pınarbaşı shows enriched $\delta^{18}O$ from carbonate material around 58 ka and between 30 and 35 Ka BP, interpreted as periods of relatively warm summers (Leng *et al.*, 1999). These warm summers correspond to periods of increased spring snowmelt inferred from $\delta^{18}O$ records from diatom silica in the same core. Diatom inferred salinity remains constant throughout the record (Reed *et al.*, 1999). A $\delta^{18}O$ and diatom inferred salinity record from the nearby Lake Suleymanhacı suggest that prior to 23 ka BP the region

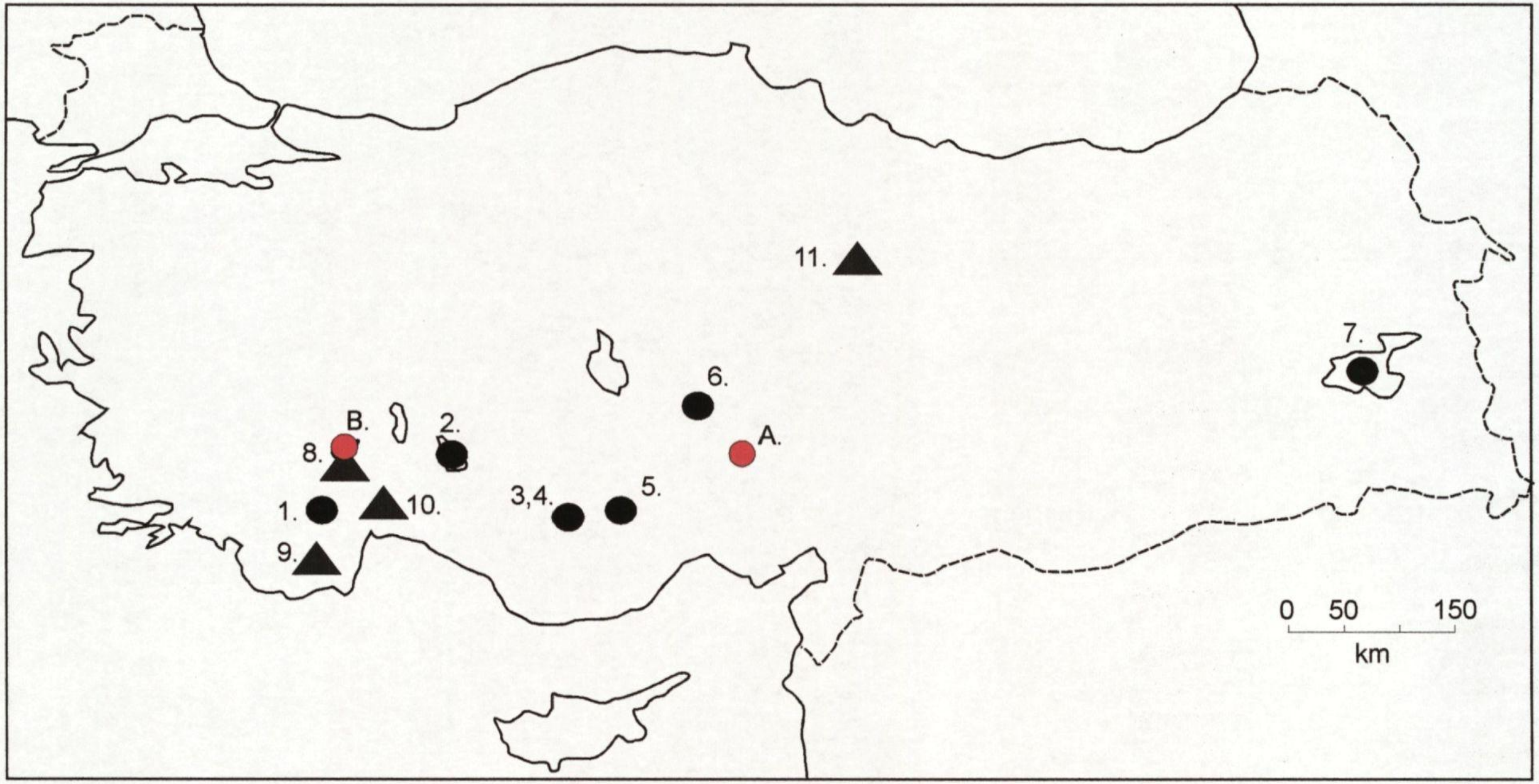

Fig. 3.9 Sites of palaeoclimatic studies in Turkey discussed in the text. (Lake sites, black circles; 1. Gölhisar, 2. Beyşehir, 3. Pinarbası, 4. Suleymanhacı, 5. Akgöl, 6. Eski Acıgöl, 7. Van. Tree ring sites for Touchan *et al.* (2003) reconstruction (8,9,10), D'Arrigo and Cullen (2001) precipitation reconstruction for Sivas (11.)). Red circles mark sites in this study A. Nar Gölü ; B. Burdur Gölü (see chapters 5 and 7 for details).

was arid relative to the Holocene, due to the more positive $\delta^{18}O$ values and higher conductivity in this closed lake basin.

Last glacial-interglacial transition

On the basis of the pollen stratigraphy Landmann *et al.* (1996) and Wick *et al.* (2003) describe an arid or semi-arid climate around 13,600 yr BP recorded in Lake Van. There is a decrease in the number of trees and increase in *Artemisia* between c. 11,500 yr BP and 10,500 yr BP suggesting drier conditions and a decline in vegetation at the time of the Younger Dryas event in northern Europe. The number of trees begins to increase slowly, as climate becomes warmer and wetter from 10,500 yr BP.

From the same lake Lemcke and Sturm (1997) describe a rapid and large (5.6‰) shift to more negative $\delta^{18}O$ values between 10,950 and 10,460 varve years BP. This follows a steady trend to more positive values between 12,600 and 10,950 varve years BP. This isotope trend is interpreted as a proxy for relative humidity with a trend to more arid conditions during the Younger Dryas type event followed by a rapid shift to more humid conditions at the beginning of the Holocene. Values prior to 13,000 yr BP are similar to those of the early Holocene, and may correlate with the Bolling-Alerod stage of northern Europe.

A similar trend in $\delta^{18}O$ values is shown at Eski Acıgöl (Roberts *et al.*, 2001). Here there is a shift to more negative values around ~ 16, 000 yr BP (Fig. 3.10) prior to a trend to more positive values and the rapid shift to negative values at the beginning of the Holocene (~12,000 yr BP). The changes in $\delta^{18}O$ are interpreted as changes in the precipitation: evaporation ratio, with the shifts to more negative values at 16, 000 and 12, 000 yr BP due to increases in precipitation as climate warms. A dramatic shift in vegetation is observed at 12,000 yr BP as well as the rapid and large shift in $\delta^{18}O$ (Fig. 3.10). There is a dramatic reduction in steppic herbs and an increase in grasses again suggesting a more favorable water balance. Tree pollen, as at Van, increases more slowly.

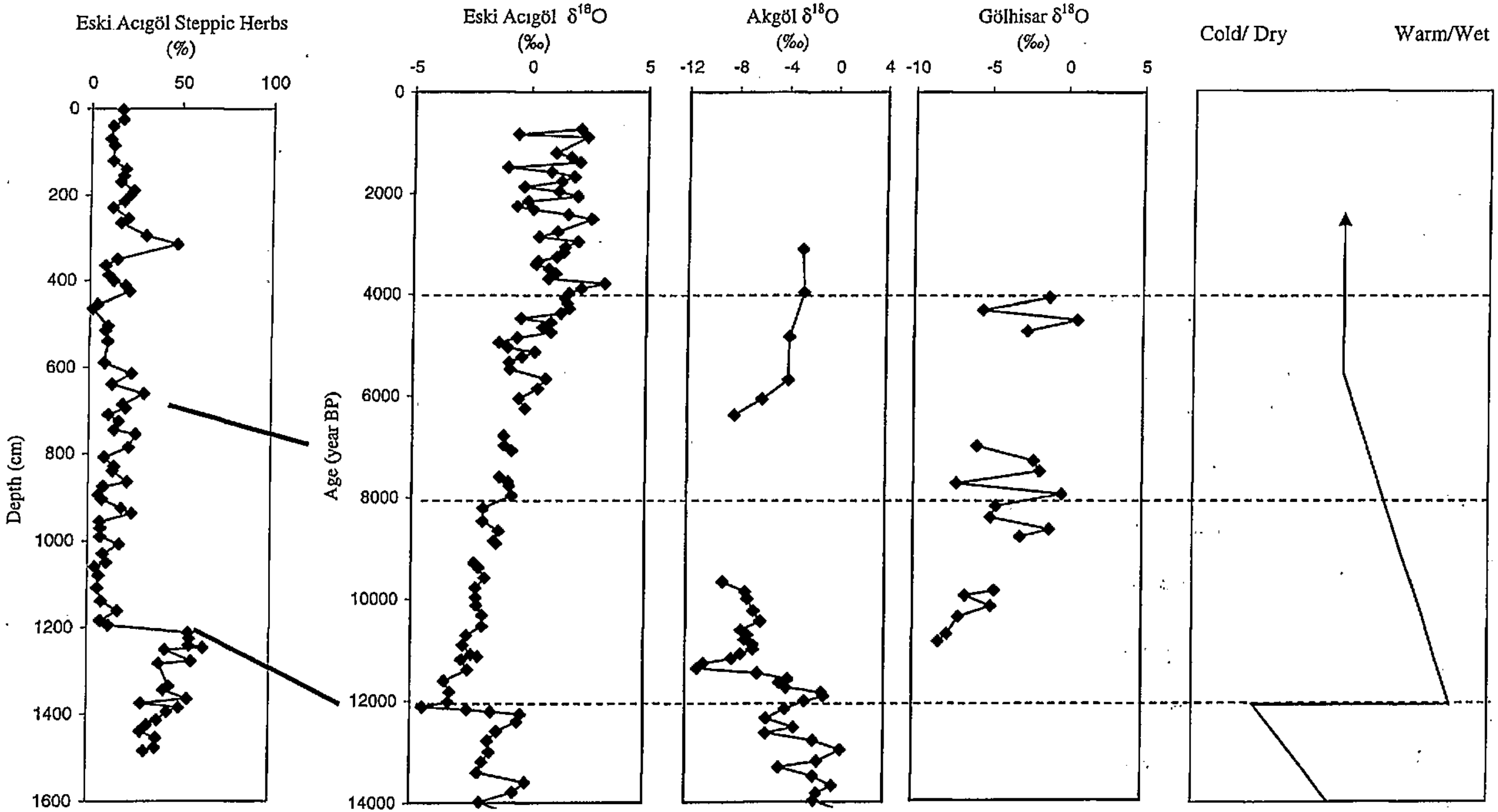

Fig. 3.10 Climate proxy records from Turkey through the last glacial-interglacial transition and the Holocene from Eski Acıgöl (Roberts *et al*., 2001), Akgöl (Leng *et al*., 1999) and Gölhisar (Jones *et al.,* 2002). The right hand chart describes general climatic shifts described by these records. Bold lines tie pollen depth stratigraphy to Eski Acıgöl age model as analyses from different cores (Roberts *et al*., 2001).

At Akgöl (Leng *et al.*, 1999) there is also a negative shift in $\delta^{18}O$ at the start of the Holocene (Fig. 3.10). This shift is interpreted as being due to an increase in precipitation or by increased amounts of snowmelt with waters depleted in ^{18}O entering the lake system as the climate warms.

Pollen and stable isotope records both suggest that in Turkey climate changed from cold and dry to warm and wet from the last glacial into the Holocene.

The Holocene

The slow increase in arboreal pollen has been observed elsewhere in the region as well as at Van and Eski Acıgöl (Eastwood *et al.*, 1999). At Van, Holocene tree pollen reached a maximum between 6200 and 4000 yr BP, interpreted as the Holocene climatic optimum for the region (Wick *et al.*, 2003). However, it has been suggested (Roberts, 2002) that this slow increase, compared to the rapid change in smaller vegetation at Eski Acıgöl and the rapid shift in $\delta^{18}O$ values from many records across the region (Roberts and Jones, 2002), is due to anthropogenic influences on the landscape. Early Neolithic settlers and trees would be competing for the same space as climate became more hospitable for both and even limited land management may have lead to the slow rate of tree advance following the climatic amelioration.

Certain pollen types can be used to show previous periods of human occupation. For example, cores from a number of lakes in south-west Turkey, including Beyşehir and Gölhisar (Bottema and Woldring, 1984; Eastwood *et al.*, 1999), show a period of human occupation between ~3200 BP and ~1500BP marked by the reduction of arboreal pollen due to forest clearance and the appearance of cereal and other crops such as olives in the pollen record.

Stable isotope records from Eski Acıgöl and Van show a trend to more positive values through the Holocene, both suggesting that conditions have become more arid. At Eski Acıgöl, $\delta^{18}O$ records stabilise at these more positive values around 6000 yr BP. The $\delta^{18}O$ record at Van shows a period between 4,190 and 2,000 varve years BP of more arid conditions. The trend to more arid conditions has also been observed in other isotope records from Gölhisar (Jones *et* *al.*, 2002) and Suleymanhacı, where diatom inferred conductivity also increases into the late Holocene again suggesting more arid conditions (Reed *et al.*, 1999).

As all the stable isotope records through the Holocene come from closed lakes, where changes in climatic proxies are driven by changes in water balance, it is difficult to know how temperatures have changed in association with the observed shift to more arid conditions from the beginning of the Holocene.

The last millennium

Touchan *et al.* (2003) reconstructed May-June precipitation between 1339 and 1998 AD (Fig. 3.11a) in southwest Turkey from the composite record of three tree ring records. The reconstruction was based on the correlation between the first and third principle components of these data sets and gridded precipitation records between 1931 and 1998. In total 139 drought events, with a mean interval of 4.8 years between them, were observed in the record, with the single driest spring in 1746 and the longest period of drought between 1476 and 1479. Extended wet periods were most prominent between 1532 to 1535 and 1688 to 1690.

A shorter, 350 year (1628 to 1980 AD), reconstruction of precipitation at Sivas (Fig. 3.11b) has also been obtained from a composite record of 5 tree ring records from across Turkey (D'Arrigo and Cullen, 2001). The most extreme drought years in this record are in 1660, 1746 and 1887. The wettest years were found in 1689, 1709 and 1960.

The most extreme dry event in 1746 and the wet event of 1689 are common to both reconstructions.

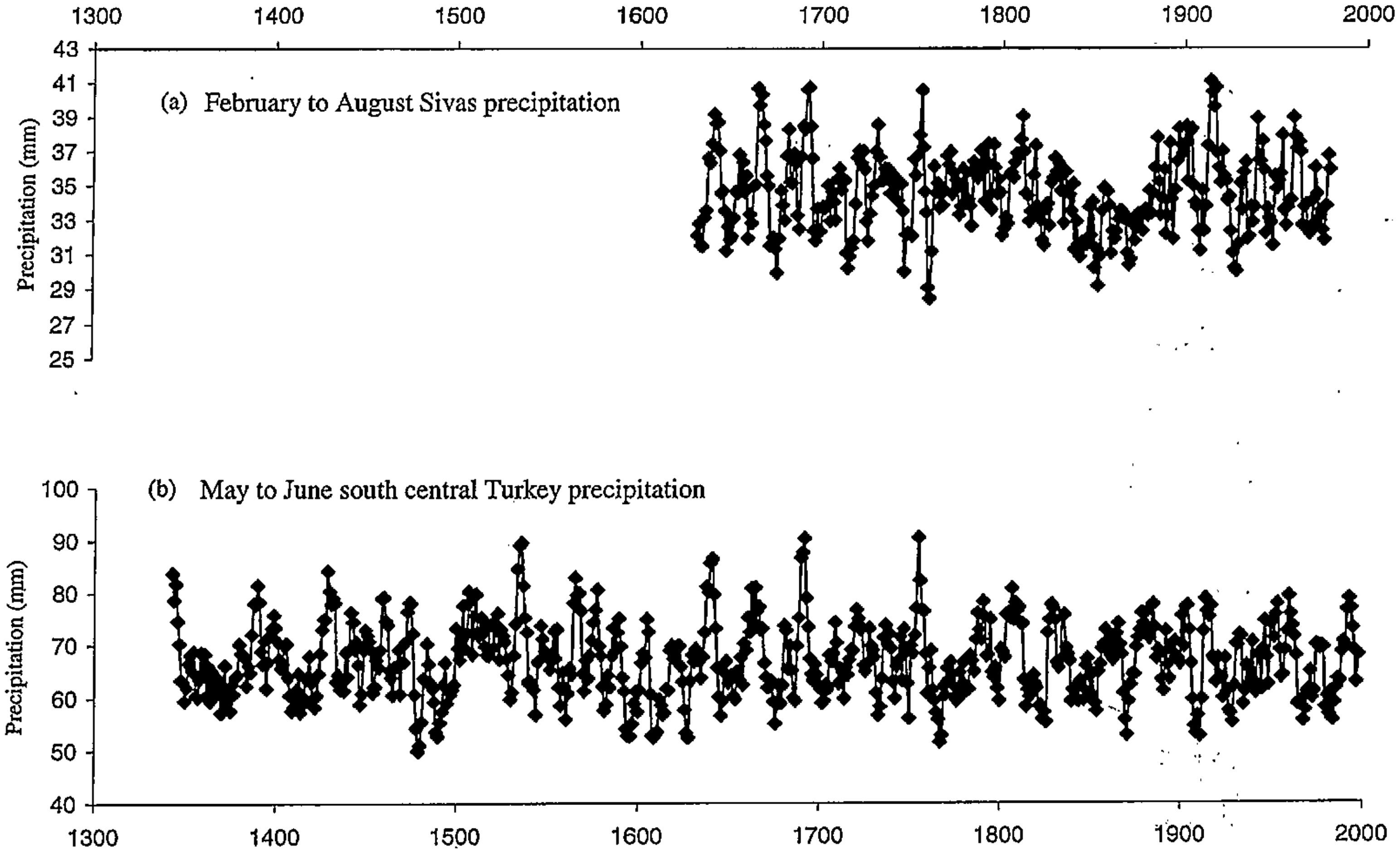

Fig. 3.11 Precipitation reconstructions from tree rings through the last 700 years from Turkey (a, D'Arrigo and Cullen, 2001; b, Touchan *et al.*, 2003).

3.5 Summary

Climate in Turkey has changed on different scales through the past 50,000 years. Some of these changes have affected the whole country e.g. most records display a rapid shift to wet conditions at the beginning of the Holocene followed by a trend to more arid conditions. Dry events have been recorded in tree rings from across the country in 1746 with a wet event in 1689. Other trends appear in individual records and probably describe more local climatic variations.

Studies of climate variations through the last 80 years have shown that shifts in Turkish climate are related to changes in atmospheric circulation as described by indices such as the NAO and the NCP during the winter, and to the Indian Monsoon and Hadley circulation during the summer.

Chapter 4

METHODOLOGY

4.1 Selection of Study Sites

The aims of this study were to produce high-resolution, well-dated records of climate change through the late Holocene, and to calibrate lacustrine stable isotope variability with meteorological data. The sites chosen for the study therefore needed a high degree of chronological control, preferably annual e.g. from laminated sediments.

Preliminary investigations by Prof. Neil Roberts and co-workers in 1999 had identified Nar Gölü, a crater lake in the Cappadocian region of central Turkey (see chapter 5 for location and full site description), as having laminated sediments similar in nature to the non-glacial varves described by Kelts and Hsu (1978) from Lake Zurich. Nar is also a small, hydrologically closed system and therefore would likely be isotopically sensitive to the relatively subtle climate variations of the late Holocene. The volcanic catchment also contains no carbonate rocks, so all carbonates in the lake sediments would be authigenic. There is a small possibility of influx of soil carbonates into the lake but soil formation in the catchment is very limited and is unlikely to have a significant impact.

A number of other lakes (Golcük (Isparta), Lake Salda, and Lake Burdur) were investigated to look for a second site to compare with the record from Nar. Lake Burdur (see chapter 7) was the only other site found to have laminated sediments and was therefore chosen. The lake lies within a slightly different climatic region of Turkey and is much larger in size, although also a closed system, and therefore makes an interesting comparison to Nar.

4.2 Field Methods

Fieldwork consisted of investigations of the contemporary lakes being studied, to better understand controls on the lake stable isotope systems, and sampling of core sequences for studies of past changes in lake stable isotope values.

4.2.1 Water Sampling

Lake waters were sampled for pH, conductivity, temperature and stable isotopes during summer field seasons in 2000, 2001 and 2002 and water samples were also collected in April 2002. As well as surface waters, depth profiles were taken to observe any stratification of the lake waters. Temperature and pH were measured by a Hanna instruments HI 9025 pH Meter and conductivity with a Hanna HI 9033 Conductivity Meter.

Water samples for stable isotope analysis of oxygen, hydrogen and carbon were collected to understand the present day stable isotope hydrology of the lake, thereby allowing better interpretation of palaeorecords of stable isotope change. Water samples were taken in leak proof plastic bottles that had been washed 3 times in the sample and additionally sealed with plastic insulating tape to reduce the risk of contamination. Lake surface samples were taken at 0.5 m depth to remove any direct effects of exchange with the atmosphere, which may change on a daily or hourly basis. Bottles were filled completely to prevent isotopic exchange with any air bubbles. Total dissolved inorganic carbon (TDIC) was precipitated from the water on site with the addition of $BaCl_2.NaOH$ solution. This prevents exchange within the sample's carbon budget due to photosynthesis by any remaining organic matter before the sample can be analysed. The samples were refrigerated at the earliest opportunity, until analysis could be undertaken.

4.2.2 Bathymetry

A picture of lake bed morphology is required before coring can take place. Cores were taken from the deepest and flattest part of the lake basin where sediment is most likely to accumulate horizontally and have least disturbance from catchment inwash. A calculation of lake volume, requiring bathymetry, was also required for accurate hydrological modelling of the lake systems.

Lake depth was measured using a Garmin Fish Finder across a number of north-south and east-west transects across Nar Gölü. The depths measured by the fish finder were calibrated and confirmed using a weighted tape measure at the full range of depths across the lake.

The depths recorded electronically were found to be correct to within 10 cm. Lake volume was calculated from these transects using *RockWorks* computer software.

4.2.3 Sediment traps

The primary use of sediment traps in lacustrine environments has been to give an estimate of the sedimentation rate and to understand the composition of the sediment (e.g. Dillon *et al.*, 1990; Nuhfer *et al.*, 1993). In this study sediment traps were used for the collection of sediment falling through the water column at Nar Gölü, for comparison of sediment chemistry with the isotope values from the lake waters and those of the surface sediments, as well as to observe the type of sedimentation during one year in the lake. Sedimentation rate was not the aim of the study and therefore the primary design requirement for the traps was that they could be easily transported and constructed.

Traps (Fig. 4.1) were secured at two depths in the water column, at two separate locations in the deepest part of the basin, in July 2001 and collected in August 2002.

4.2.4 Lake coring

With advances in palaeolimnology over the last 50 years a number of methods have been developed for sampling sediment archives from the bottom of lakes (e.g. Lotter *et al.* 1997). The choice of coring system depends on the length of record required and the physical properties, most significantly water depth, of the lake under investigation.

In this study undisturbed cores were required covering the last 100 - 200 years for comparison of proxy records with meteorological records and to obtain ^{210}Pb dating profiles. It was also important to recover the sediment water interface, to be confident that the top of the core represented the most recent sediments. At both Nar Gölü and Lake Burdur (July 2001) a Glew corer (Glew, 1991) was used to sample the surface sediments (Fig. 4.2).

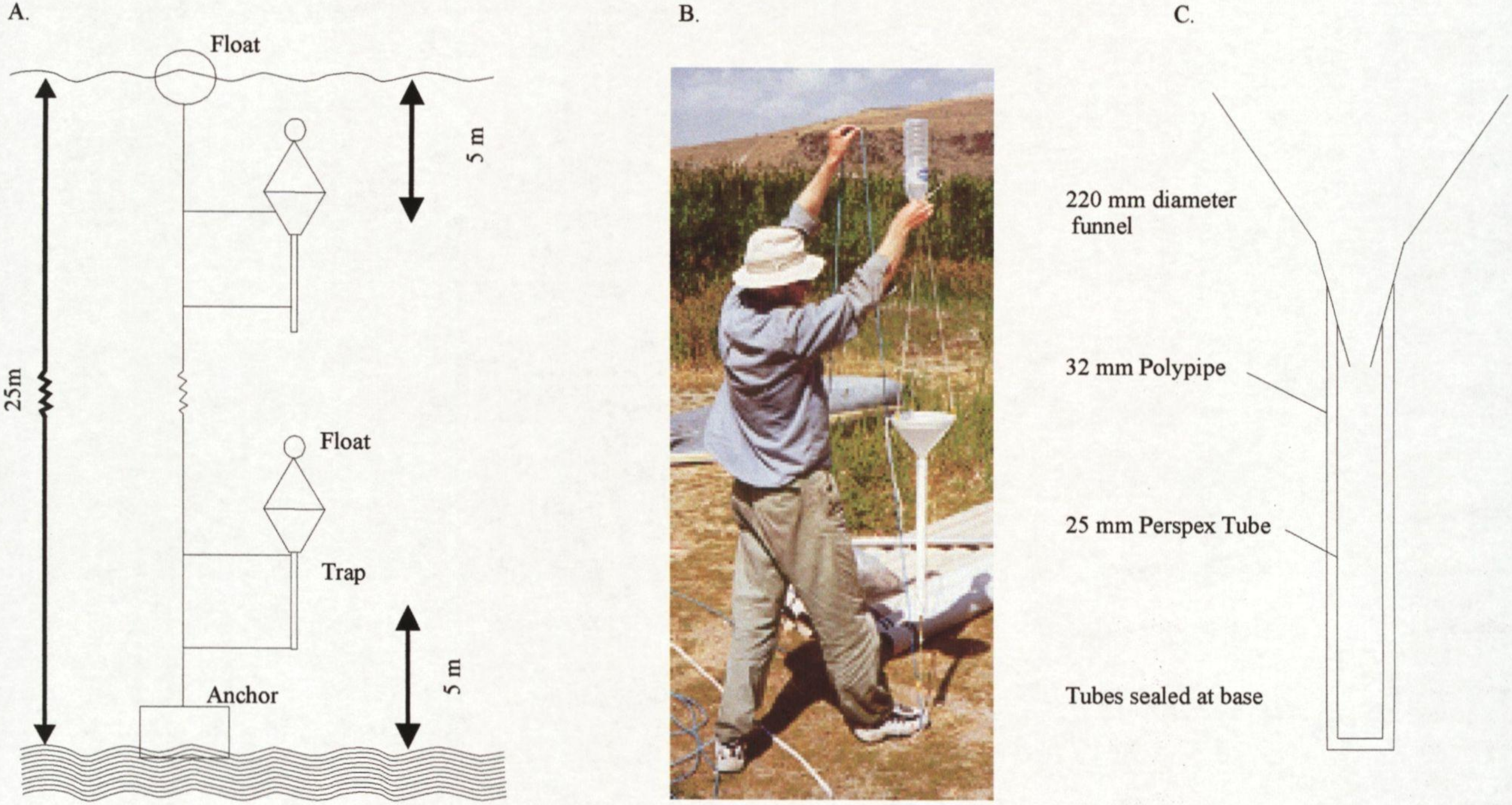
A.
Float
5 m
25m
Float
Trap
Anchor
5 m
B.
C.
220 mm diameter funnel
32 mm Polypipe
25 mm Perspex Tube
Tubes sealed at base

Fig. 4.1 Sketch showing location of sediment traps in the water column in Nar Gölü (A), with a photograph (B) and cross section (C) of one of the traps.

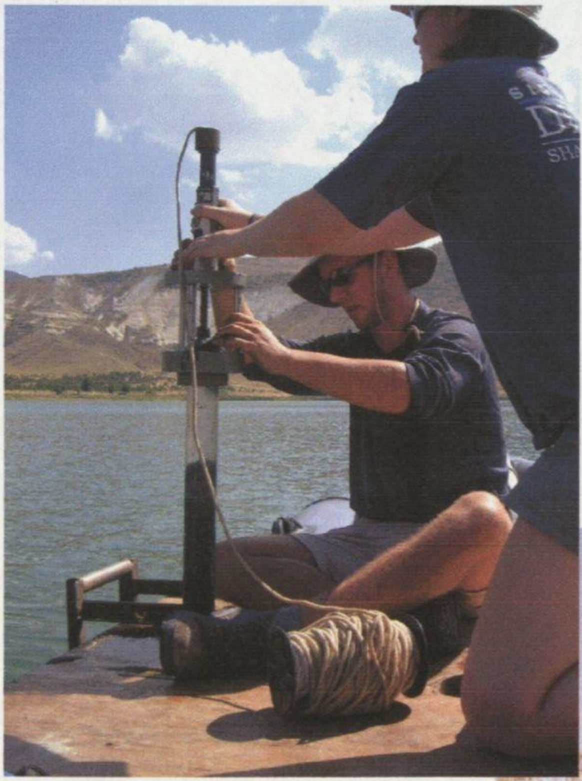

Fig. 4.2 Glew coring at Nar Gölü.

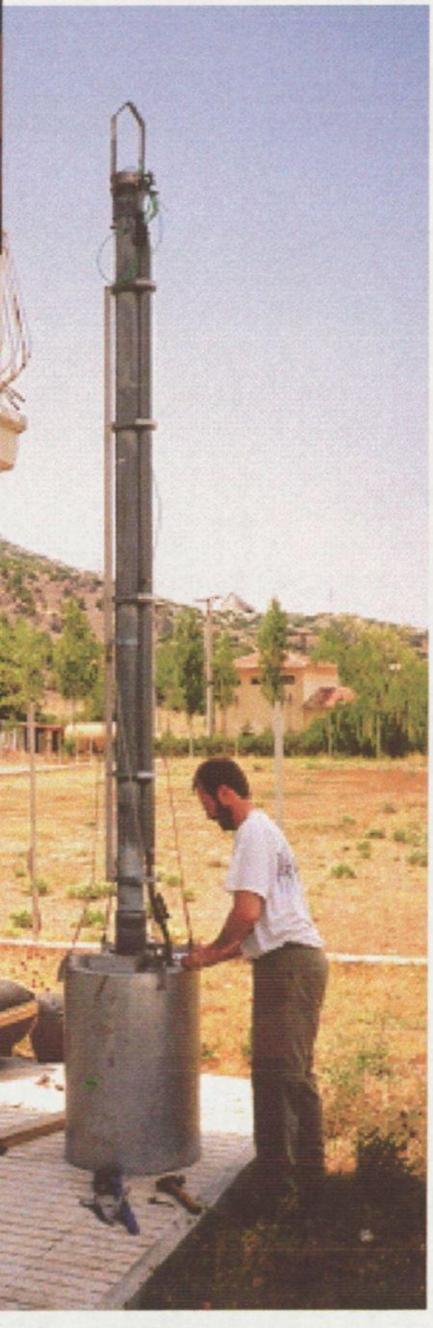

Fig. 4.3 The 3m Mackereth corer.

It was found that with a 50 cm core tube, 30 – 50 cm of sediment was regularly recovered including an undisturbed sediment water interface. However, the soft surface sediments at Nar Gölü led other coring systems (used for obtaining longer cores) to penetrate beyond 50 cm sediment depth. Longer tubes were therefore added to the Glew corer resulting in the retrieval of 60–65 cm of sediment. This was sufficient to overlap with the longer core sequences.

Due to the laminated nature of the sediments at Nar and Burdur it was important that the sediments were as undisturbed as possible so sampling could be carried out at an inter-laminae resolution. To achieve this Glew cores were returned to the laboratory within the core tubes, packed at either end with Oasis, after all bottom waters had been removed, and heavily taped. In some cases drying and shrinking of the sediment occurred, however no stratigraphic integrity was lost.

Preliminary investigations at Nar (September 1999) had used a 1m Mackereth corer (Mackereth, 1969) but investigations for this study required a longer sequence. A Livingstone coring system was used initially (Livingstone, 1955, Wright, 1967) resulting in a 5m sediment sequence being recovered (July 2001).

The Livingstone corer only produces cores of 1m length and the top and bottom of the core sections are often disturbed. To gain a continuous sequence it was therefore necessary to take two overlapping cores in close proximity to each other. Due to the depth of the water at Nar a core liner, constructed from plastic down-piping, was first lowered into the sediment to guide the corer and rods and to keep them from drifting or bending in the water column. Similar piston systems have been used where one drive, with core tubes 3.5 m or 7.5 m long, produce much longer cores (Wright, 1980). This technique would have been unsuitable for use at Nar Gölü due to difficulties with handling the weight of rods and sediment through 25m of water. Further, continuous cores from Nar were taken in summer 2002 using a 3m Mackereth coring system (Mackereth, 1958; Fig. 4.3).

Both 1m and 3m Mackereth samplers were used to obtain cores from Lake Burdur during the summer 2002 field season.

On retrieval, the core sections were extruded into lengths of half guttering, and covered in non – PVC cling film to prevent the sediments reacting with the plastic. The two halves of guttering were then taped and sealed within lay-flat plastic tubing after being carefully labelled with the top and bottom of the core and the depths from the water surface. At the earliest opportunity the core sections were refrigerated at 4°C.

4.3 Laboratory methods

4.3.1 Core preparation and sampling

On return from the field both Glew and Livingstone core sections were cut in half lengthways with cheese wire and rewrapped in clean non-PVC cling-film. The core sections were then kept refrigerated. The half core sections were cleaned to remove smearing caused during the cutting and then described and photographed.

Once all cores had been described a master sequence was constructed from the Livingstone core sections. Correlation between the cores was possible due to the detailed stratigraphic variation of the laminated sediments.

Laminae counting

Cores were pinned at equivalent laminae, at approximately 6 cm intervals, and the numbers of laminae in each section were counted independently by two counters. If the difference between two counts for any given section was greater than 3 laminae both counters recounted the section until agreement was reached.

Colour measurement

As the entire sequence from Nar comprises laminated sediments, changes in the core were best described by changes in colour. Grey scale changes, on a scale from 0 (white) to 255 (black), were measured quantitatively from digital (Tiff) images of the core sequence in the *analySIS* image analysis software (Fig. 4.4).

This method also provides a further numerical data-set of change in the lake system. Grey scale values recorded from laminated sediments elsewhere, from both lake (e.g. Schaaf and Thurow, 1997) and marine sediments (e.g. von Rad *et al.*, 1997), have shown that colour

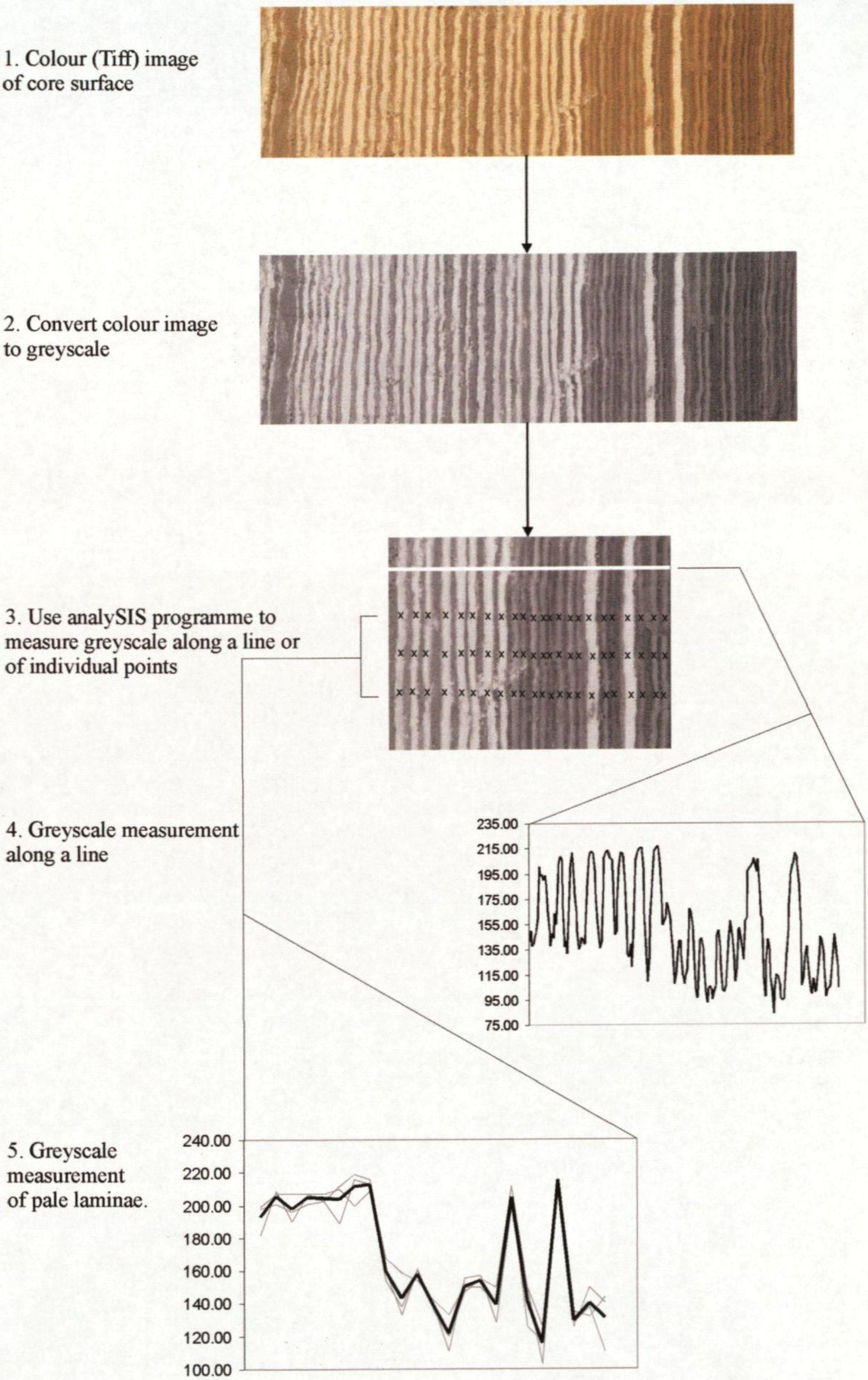
1. Colour (Tiff) image of core surface
2. Convert colour image to greyscale
3. Use analySIS programme to measure greyscale along a line or of individual points
4. Greyscale measurement along a line
235.00
215.00
195.00
175.00
155.00
135.00
115.00
95.00
75.00
5. Greyscale measurement of pale laminae.
240.00
220.00
200.00
180.00
160.00
140.00
120.00
100.00

Fig. 4.4 Method for greyscale analysis of the Nar Sediments. The final data set is made up of the mean value of three point measurements for each pale lamina (5).

analysis is not a stand alone technique and requires high-resolution analysis of other proxies to establish any link between colour and climate (Shaaf and Thurow, 1997).

Sampling

Samples could then be taken from the cores for palaeoenvironmental proxy analysis. Individual laminations were sampled by scraping successive laminae from the top of the core, and prepared for geochemical analysis (Fig. 4.5).

4.3.2 Dating

^{210}Pb

Dried sediment samples were analysed for ^{210}Pb, ^{226}Ra and ^{137}Cs by direct gamma assay in the Liverpool University Environmental Radioactivity Laboratory, using Ortec HPGe GWL series well-type coaxial low background intrinsic germanium detectors (Appleby *et al.* 1986). ^{210}Pb was determined via its gamma emissions at 46.5keV, and ^{226}Ra by the 295keV and 352keV γ-rays emitted by its daughter isotope ^{214}Pb, following 3 weeks storage in sealed containers to allow radioactive equilibration. ^{137}Cs was measured by its emissions at 662keV. The absolute efficiencies of the detectors were determined using calibrated sources and sediment samples of known activity. Corrections were made for the effect of self-absorption of low energy γ-rays within the sample (Appleby *et al.* 1992).

^{14}C

Samples were dated by ^{14}C detection in an accelerator-mass-spectrometer (AMS) by Beta Analytic Inc.

From the Nar sediments, bulk organic sediments were first washed in acid to remove any carbonates. Carbonate sediments were dated without undergoing any pre-treatments.

Wood fragments were picked from the Burdur sediments under a binocular microscope after the very fine clay fraction had been decanted following settling of agitated samples in beakers for 24 hours. Prior to dating the sample was washed in hot HCl to remove carbonates and then in NaOH to remove secondary organic acids. The alkali washes were followed by a final acid rinse to neutralise the solution prior to drying.

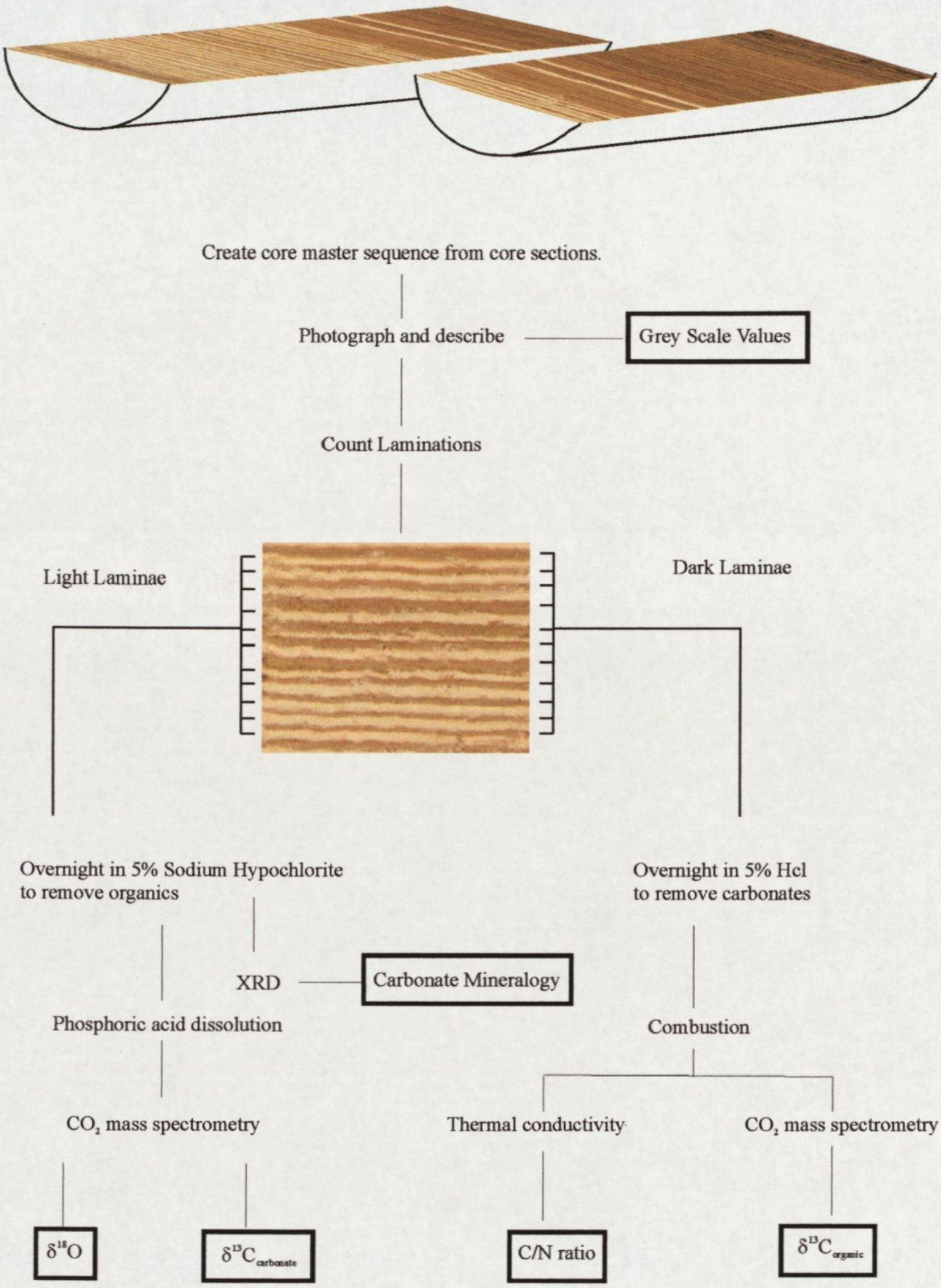
Create core master sequence from core sections.
Photograph and describe
Grey Scale Values
Count Laminations
Light Laminae
Dark Laminae
Overnight in 5% Sodium Hypochlorite to remove organics
Overnight in 5% Hcl to remove carbonates
XRD
Carbonate Mineralogy
Phosphoric acid dissolution
Combustion
CO_2 mass spectrometry
Thermal conductivity
CO_2 mass spectrometry
$\delta^{18}O$
$\delta^{13}C_{carbonate}$
C/N ratio
$\delta^{13}C_{organic}$

Fig. 4.5 Typical processes for core samples from Nar taken during this study. Cores from Lake Burdur underwent a similar process.

4.3.3 Geochemistry

Water analysis

Analysis of water samples, for isotope ratios of oxygen and hydrogen, were undertaken at the NERC Isotope Geosciences Laboratory, using the equilibration method for oxygen (Epstein & Mayeda, 1953), and Zn-reduction method for hydrogen (Coleman *et al.*, 1982; Heaton & Chenery, 1990), using a VG SIRA mass spectrometer. Isotopic ratios are defined in relation to the international standard, V-SMOW (Vienna Standard Mean Ocean Water). Analytical precision is typically +/-0.05‰ for $\delta^{18}O$ and +/-2.0‰ for δD.

The $BaCO_3$ precipitated on site from the TDIC was filtered from the water and washed three times with deionised water. The precipitated carbonate was then reacted in vacuo overnight in phosphoric acid and the liberated CO_2 measured for $\delta^{13}C$ on a dual inlet mass spectrometer (see more detailed discussion below).

Sediment Analysis

Carbon content

Prior to stable isotope analysis the carbonate and organic content of the sample must be known, as the mass spectrometer requires an optimal amount of CO_2 and the initial sample size must be adjusted accordingly. Changes in carbonate or organic content through the core also provide palaeoenvironmental information.

An estimate of organic and carbonate content was gained by loss on ignition. Dried sediment samples of a known weight were combusted at 550°C and then reweighed to give a value for organic carbon content. The same samples were then combusted at 950°C to remove carbonate material and reweighed (Dean, 1974).

Where little sample material was available total carbon (TC) and inorganic carbon (IC) content were measured on the Shimadzu TOC-5000 carbon analyser in the School of Geography, University of Plymouth. Samples were combusted at 950°C and the amount of CO_2 released measured. Organic carbon was removed from the samples by combusting at 575°C for 10 minutes. The percentage of organic carbon present in the samples was then estimated from the TC and IC values.

Carbonate mineralogy

Before $\delta^{18}O$ records from lacustrine carbonates can be fully interpreted the type of carbonate being analysed must be known.

Carbonate mineralogy was measured by X-ray diffraction in the Department of Geological Sciences at the University of Plymouth. Where sufficient material was available cavity mounts were prepared (Hardy and Tucker, 1988); smaller samples were smeared on a silicon slide. Carbonate mineralogy was found qualitatively by comparison of the sample diffractometer trace with standard carbonate traces (Appendix 1).

If more than one form of calcium carbonate is present e.g. calcite and aragonite, the percentage of each can be estimated from the XRD trace. The area of the primary aragonite and calcite peaks is estimated, assuming that the peaks are regular triangles, the ratio of the aragonite peak, as a percentage of the sum of the two peak areas is then used to estimate the percentage of aragonite from experimentally calibrated conversion curves (Hardy and Tucker, 1998). Calibration curves are also established for estimates of the percentage of dolomite compared to calcite (Hardy and Tucker, 1998).

Carbonate stable-isotope analysis

Carbonate samples were disaggregated in sodium hypochlorite solution overnight to remove any organic material (Lamb *et al.*, 2000). Organic impurities in the sample may lead to errors in the final stable isotope measurement as organic materials can produce molecular fragments in the same mass range as the CO_2 measured by the mass spectrometers. Organic material can also be removed by combusting the samples at 250°C (combustion at 450°C may cause fractionation of the carbonate isotopes) although it has been shown that pre-treatment by chemical oxidation yields smaller deviations than through heating (Siegenthaler and Eicher, 1986).

Samples were then sieved at 75µm to remove any shell fragments. The <75µm fraction was filtered through quartz micro fibre filter paper (Whatman 41) and washed three times with deionised water to remove any remaining sodium hypochlorite solution and oxidised organic matter before drying at 40°C. The dried sediment was crushed in an agate pestle and mortar to homogenise the sample and create a fine powder to aid reaction with the acid (Lamb *et al.*, 2000).

Samples containing ~10mg of calcium carbonate were weighed into glass vials and placed in a reaction vessel with anhydrous phosphoric acid. The samples were then reacted with the acid under vacuum and left at 25°C overnight (Craig, 1957). The liberated CO_2 was collected through a cold trap that removed any remaining water and organic fractions from the CO_2 sample. The CO_2 was frozen in collection vessel with liquid N_2 allowing any other fractions that had reached the vessel to be pumped away.

Stable isotope measurements were then made from the CO_2 on a dual inlet (VG Optima) mass spectrometer. The CO_2 from the lake sediment samples was compared to a standard CO_2 gas. Three mass fractions are measured (44, 45 and 46), leading to values for oxygen and carbon stable isotope ratios. It is assumed that the 45/44 mass ratio comprises $^{13}C^{16}O_2/^{12}C^{16}O_2$, and the 46/44 mass ratio comprises $^{12}C^{16}O^{18}O/^{12}C^{16}O_2$. These ratios lead, respectively, to the values for $\delta^{13}C$ and $\delta^{18}O$ where the δ notation refers to the measured ratios relative to an international standard (for carbonates, Vienna Pee Dee Belemnite (VPDB)).

Errors calculated from the standard deviation of laboratory standards used throughout the analyses, and repeats of individual samples, show that analytical error is ± 0.1 ‰ for $\delta^{18}O$ and $\delta^{13}C$. Where overlapping cores were used in the Nar record equivalent laminae were analysed in both cores and errors were of the same magnitude (Fig. 4.6).

Organic samples

Organic samples were left overnight in 5% HCL to remove any carbonate. Samples were then filtered (Whatman 4 filter papers) and washed three times with deionised water. After drying at <40°C the samples were homogenised in an agate pestle and mortar.

Samples containing 1 to 2 mg of Carbon, weighed into tin cups, were analysed for $^{13}C/^{12}C$ and C/N ratios by combustion in a Carlo Erba 1500 on-line to a VG TripleTrap and Optima dual-inlet mass spectrometer. Samples are dropped, in a continuous flow of helium carrier gas, into a 1020°C furnace. A pulse of oxygen causes an exothermal flash oxidation of the tin, ensuring full combustion of the sample, and the product gases are further oxidised by chromium and cobaltous oxides. Excess oxygen and water are removed by passage through hot copper and magnesium perchlorate.

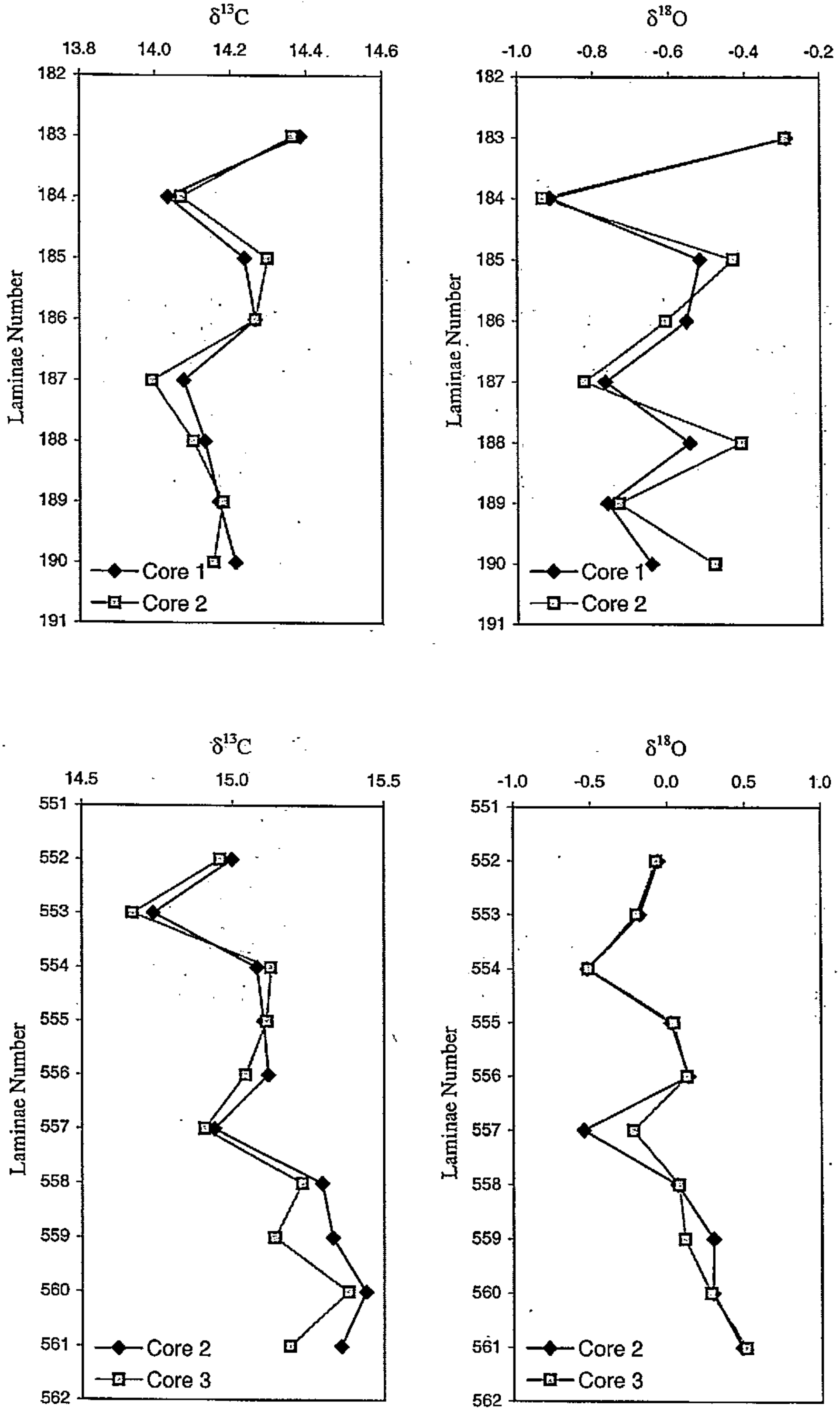

Fig. 4.6 Comparison of $\delta^{18}O$ and $\delta^{13}C$ from equivalent laminae in overlapping cores from Nar Gölü.

The remaining N_2 and CO_2 then pass through a GC column and by a thermal conductivity detector, which generates an electrical signal proportional to the concentrations of N_2 and CO_2 present in the helium stream. C/N ratios are quantified by calibration against a laboratory standard.

The CO_2 is frozen in the Triple Trap, held at –166°C, allowing the N_2 and helium to vent to atmosphere. The TripleTrap is then evacuated before warming the CO_2 trap and expanding the sample CO_2 into the mass spectrometer. $\delta^{13}C$ values are calculated to the VPDB scale by comparison with a laboratory standard calibrated against NBS-19 and NBS-22.

Errors from the standard deviation of standards used throughout the analyses show that analytical errors for $\delta^{13}C_{organic}$ were ± 0.1 ‰ and ± 0.2‰ for C:N ratios.

4.4 Numerical Techniques

Once collected, a number of techniques, as well as standard statistical analyses, are used to analyse the data.

Normalising

Two series can be plotted on the same scale if they are normalised, such that if they co-vary ($r^2 = 1$) they will fall on the same points through the whole series in normalised space. Data is normalised by subtracting the mean of the full data set from each value, and dividing by the standard deviation, the resulting normalised series will therefore have a mean of 0 and a standard deviation of 1.

Co-variation

An idea of how two series co-vary can be gained from the R^2 values form the two series, which also suggests how much of the variance in series y can be explained by series x. Here each equivalent point in the two series is taken to be independent. However in geological series each set of points is also dependent on the previous values; there is a temporal dependence in the relationship.

The relationship between two variables can be expressed as the cumulative sum of the square of the difference between two normalised data sets and this provides a test of whether any relationship is constant with time (Taylor *et al.*, 2002). When the series are strongly correlated the slope of the graph, cumulative sum against time, will be close to 0. If the variables are uncorrelated the slope will be 2. How well the two series are correlated can be measured from where the gradient lies between 0 and 2, equivalent to an r^2 value, where a paired series resulting in a gradient of 0 would have and "r^2" value of 1 and a gradient of 2 would have an "r^2" of 0. The probability that any relationship has arisen by chance can be estimated by comparing the slope with slopes generated from random distribution of the data sets (Moyeed, pers. com., 2003). The probability can be expressed as a fraction *p*. Analyses of *p* values from 1000 perturbations of the data sets were run using S-Plus 6.1 computer software.

Spectral analysis

Geological data sets may contain cycles, which may be related to natural variability in the climate system. These cycles can be observed in data series using spectral analysis techniques, where curves of different wavelengths are fitted to the data to observe if there are any wavelengths that closely match the variability in the dataset.

Spectral analysis was performed using AnalySeries 1.1 (Paillard *et al.*, 1996) and S-Plus 6.1. Standard Fourier transforms of the data and analyses using the Blackman-Tukey method, where the data sets are smoothed prior to Fourier transformation, were carried out using AnalySeries. S-Plus 6.1 was used to observe which cycles in the data were significant, as with the cumulative sum of the squared difference technique above, the data can be randomly arranged in 1000 perturbations and spectral analyses performed, from which it is possible to observe which cycles in the data set are significant, rather than just noise.

Chapter 5

NAR GÖLÜ – CONTEMPORARY LİMNOLOGY

For robust interpretations of lacustrine palaeoenvironmental records to be made the lake system, particularly the hydrology and sedimentation regime, must be understood. This chapter describes the physical and chemical characteristics of contemporary Nar Gölü.

5.1 Location and general site description

Nar Gölü (Fig. 5.1) is a small crater lake located 25 km west of Derinkuyu in the Cappadocian region of central Anatolia (Fig. 5.2). The lake has an area of 556,500 m^2 and is 26 m deep at the deepest point. The north, east and west sides dip steeply to this depth with a more gradual slope on the southern shore where an alluvial fan is present, lake volume is 7,692,360 m^3 (July 2001). The crater is steep sided creating a small catchment with an area of 2,408,000 m^2 (Fig. 5.3).

5.2 Catchment morphology and geology

The north, east and west sides of the crater are steep with a faulted basalt intrusion visible on the eastern and western sides. The southern side of the crater is less steep, and is made largely of volcanic ash. At the southern end of the crater is an alluvial fan which extends into the lake. There is no stream activity in this fan system at present, either during the summer or during April, the wettest part of the year. It is possible that the fan was formed during times of permanent stream flow during the past, or by a series of extreme events, e.g. heavy rainfall, which lead to sediment transport into the crater.

The Nar crater lies within the Göllüdağ volcanic complex (Fig. 5.2) and the first volcanic activity in the region occurred south of Nar Gölü, where basaltic to andesitic lavas are K/Ar dated to around 1.6 Ma. Above these lavas, tephras, geochemically similar to Göllüdağ products, are reworked in fluvio-lacustrine sediments. Overlying these sediments two lava flow units sandwich a pumice fall Ar/Ar dated around to 1.3 Ma (D. Mouralis, pers. com.).

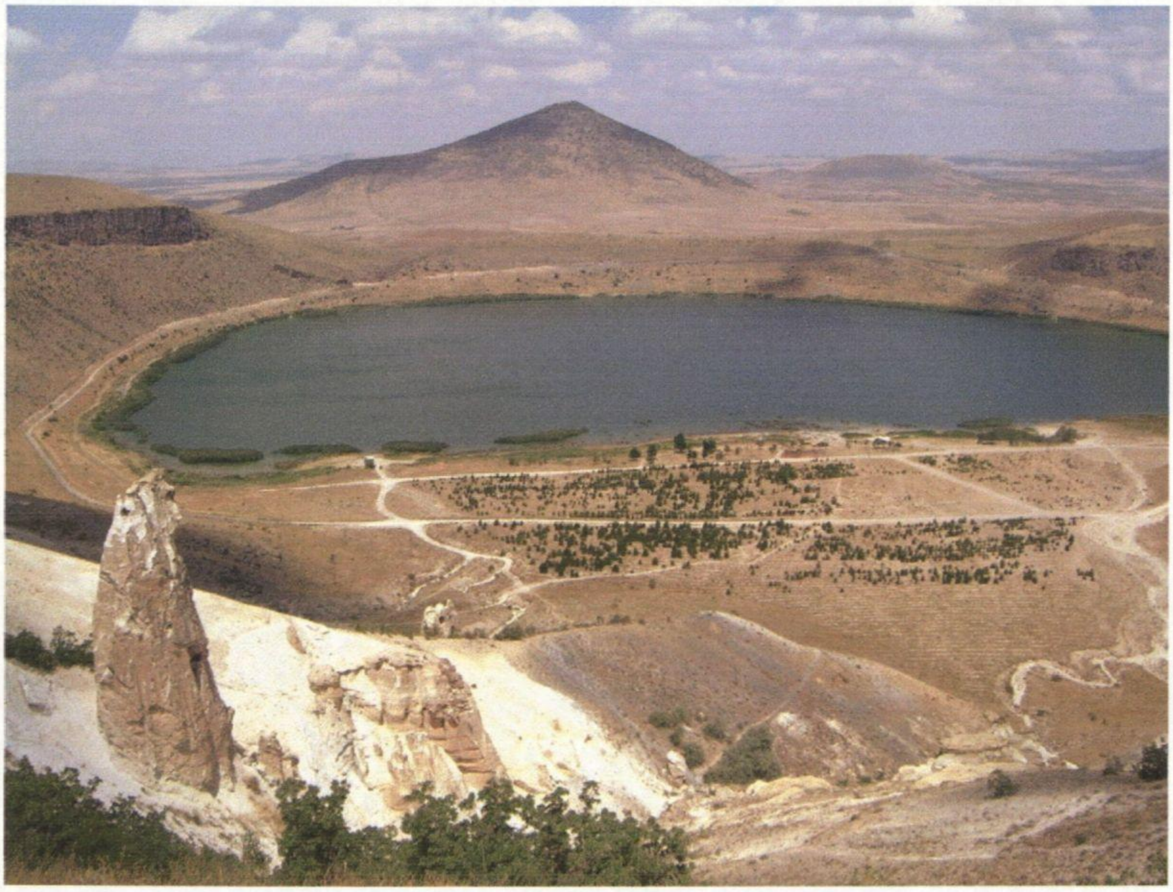

Fig. 5.1 Photograph of Nar Gölü looking north from high on the southern edge of the catchment (Photo: A. Mather).

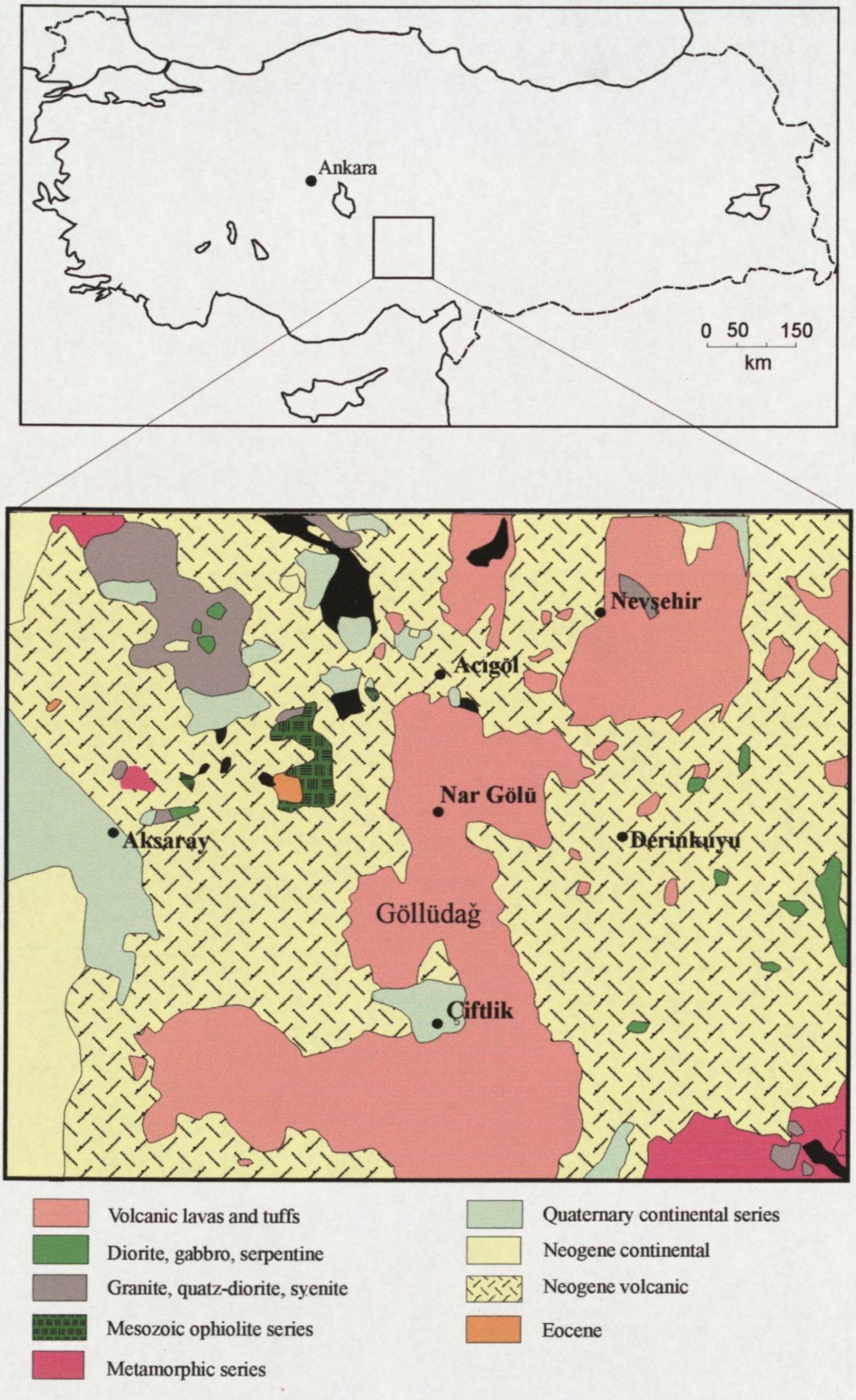
Ankara
0 50 150
km
Nevşehir
Acıgöl
Nar Gölü
Derinkuyu
Aksaray
Göllüdağ
Çiftlik
Volcanic lavas and tuffs
Diorite, gabbro, serpentine
Granite, quatz-diorite, syenite
Mesozoic ophiolite series
Metamorphic series
Quaternary continental series
Neogene continental
Neogene volcanic
Eocene

Fig. 5.2 Location and local geology (after Sassan, 1964) of Nar Gölü (34°27'30"E; 38°22'30"N; 1363 masl).

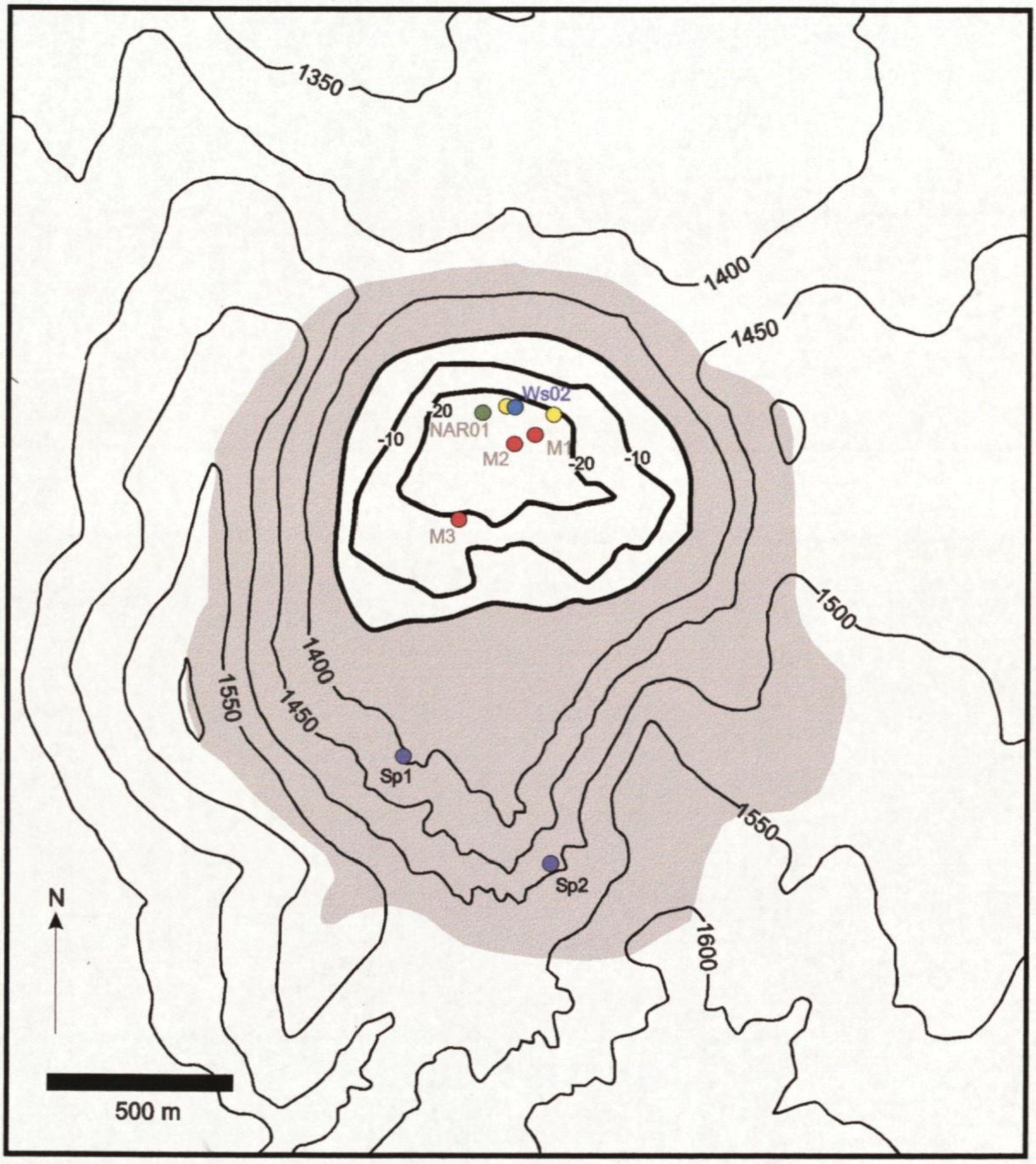
1350
1400
1450
1500
1550
1600
1400
1450
1550
-10
-20
-20
-10
Ws02
NAR01
M1
M2
M3
Sp1
Sp2
N
500 m

Fig. 5.3 Detail of Nar catchment (shaded grey) showing location of sediment traps (yellow circles), water sampling locations (blue circles; including springs (Sp1 and Sp2)) and coring sites from 2001 (Grey circle) and 2002 (Red circles). The details of the cores are discussed in chapter 6.

Nar Gölü is younger than the 1.6 Ma basalt and the volcanic ash layers at the south of the Nar crater are typical of those associated with the activity around 1.3 Ma. There is no evidence of any more locally derived volcanic product overlying this ash, implying the Nar Gölü crater may be older than 1.3 Ma. However magmatic products from Nar are rare suggesting some erosion may have taken place. It is therfore impossible to give a definitive youngest age for the Nar crater (D. Mouralis, pers. com.).

5.3 Catchment vegetation

On the steep north, east, and western slopes there is relatively little vegetation as the slopes are mostly scree, the vegetation present consists of deciduous oak (*Quercus cerris* type) which is also found at higher elevations in the south of the catchment. A few small fields around the edge of the lake have been cultivated with a variety of crop plants (including lentils and chickpeas). In the summer months much of this vegetation had been harvested leaving empty fields.

Lines of pine trees have been planted in the crater on the alluvial fan complex. There are also limited pine trees higher on the southern slopes of the catchment along with some Plane trees (*Platanus orientalis*) planted near the springs to give shade. Grasses around the high edge of the crater are grazed by sheep and goats.

A fringe of *Phragmites* sp and other macrophytes (including *Scirpus maritimus*) surrounds the lake and there is little vegetation on the lakebed beyond this fringe. (Species names courtesy of Dr. Warren Eastwood).

5.4 Climate

The nearest meteorological station to Nar Gölü was at Derinkuyu, although data were only recorded there between 1965 and 1990. The warmest months of the year are July and August, with January and February the coldest (Fig. 5.4). Through the 26 years of recording there was greater variability in winter temperatures compared with summer values. The standard deviation of the average monthly temperatures for January and February are 3.3°C and 3.2°C respectively compared to 1.0°C and 1.3°C for June and July.

(a)

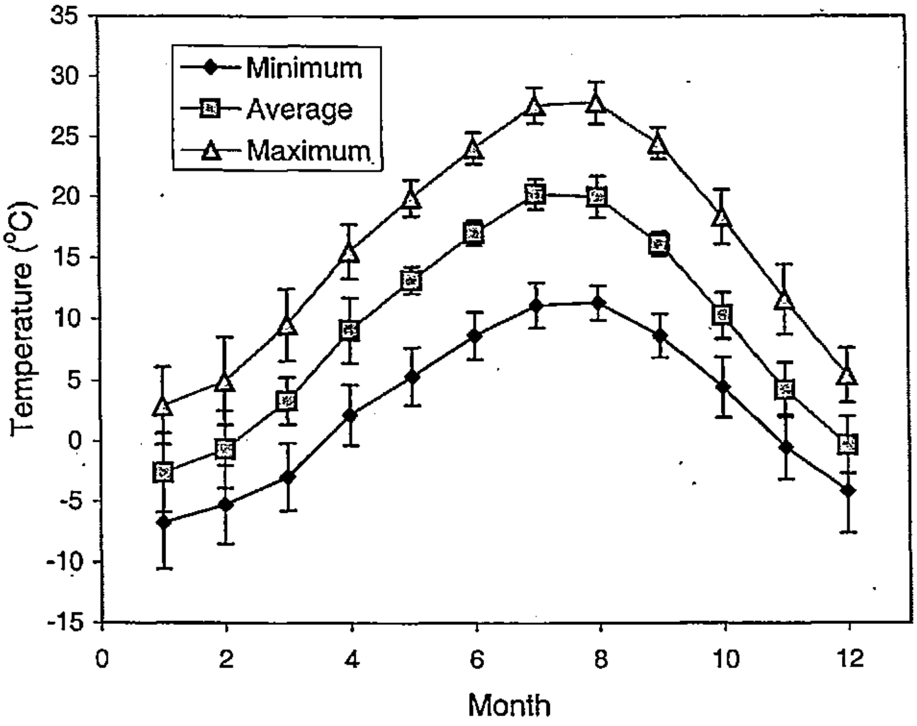

(b)

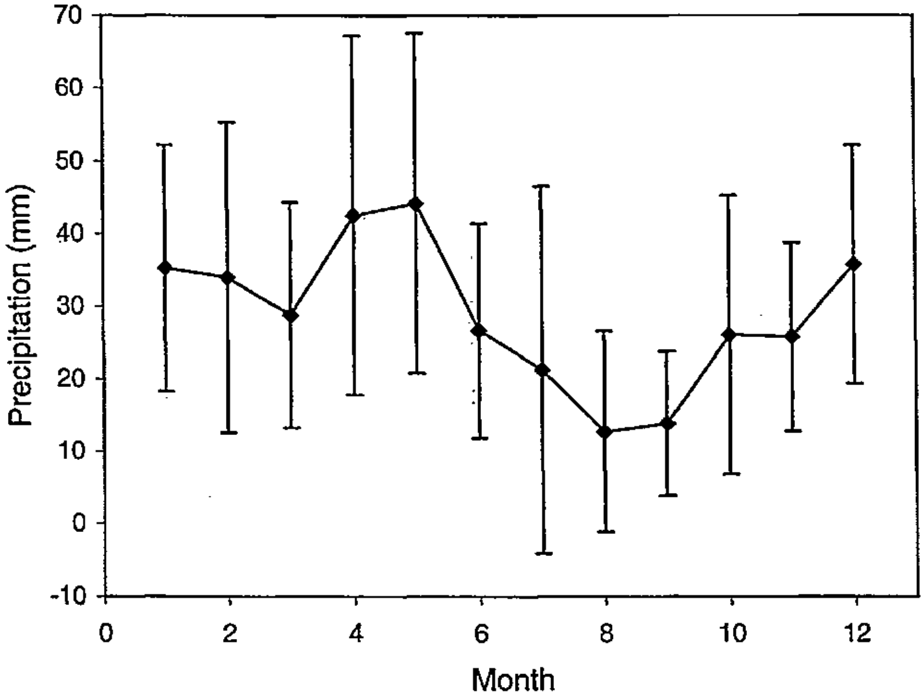

Fig. 5.4 Average monthly temperatures (minimum, average and maximum temperatures) between 1965 and 1990 (a) and average monthly precipitation between 1966 and 1990 (b) at Derinkuyu (data from Turkish state Meteorological Service). Error bars show 1 standard deviation of variability through this time period.

Total annual precipitation averaged 320 ± 68 mm (mean value ± 1 S.D.) between 1966 and 1990 (1965 data are only available from June – December). April and May are the wettest months, accounting for 27 % of the total annual precipitation, with the driest two months, August and September, accounting for only 2 % of the annual total. Fig. 5.4 shows a summary of the average precipitation amounts for each month. There is considerable variability in the monthly values through the 25 years recorded.

Values of evaporation are measured at only a few of the meteorological stations in Turkey, with the nearest station to Nar at Niğde (1208 masl; 37 59' N, 34 40' E), where the average value between 1935 and 1970 was 1547.6 mm yr^{-1} (Meteoroloji Bulteni, 1974). Ankara (894 masl; 37 57' N, 32 53' E) had an average value of 1307.6 mm yr^{-1}. However, it is also possible to calculate the amount of evaporation, for example Penman (1948) simplified by Linacre (1992):

$$E = [0.015 + 4 \times 10^{-4} T + 10^{-6} z] \times [480 (T + 0.006z)/(84 - A) - 40 + 2.3 u (T - T_d)] \quad (5.1)$$

E = evaporation (mm/day), T = air temperature (°C), z = altitude (m), A = latitude, u = wind speed, and T_d = dew point temperature which is defined as (Linacre, 1992),

$$T_d = 0.52\, T_{min} + 0.60\, T_{max} - 0.009\, (T_{max})^2 - 2\ °C \quad (5.2)$$

Using annual average values from Derinkuyu for temperature, and Nevşehir (1260 masl; 38 35'N, 34 40'E) for wind speed (the nearest station with available data) evaporation at Nar Gölü is calculated at 1140 mm yr^{-1}.

However values from the same equation for Ankara and Niğde (1209 and 1315 mm yr^{-1} respectively) are below the recorded values. There is a systematic difference between recorded E (Meteoroloji Bulteni, 1974) and calculated E using equation 5.1. Using 11 stations across Turkey for which there are data (Table 5.1) the relationship between the measured and calculated evaporation loss is (Fig. 5.5):

$$E_{recorded} = 1.35\, E_{calculated} - 512.22 \ \text{mm yr}^{-1} \quad (5.3)$$

Table 5.1 Calculations of evaporation (from equation 5.1) and measured values of evaporation from 11 meteorological stations in Turkey (data from Meteoroloji Bulteni, 1974). See text for explanation.

	T (°C)	Z (m)	A (°)	u (ms^{-1})	T_d (°C)	T_{min} (°C)	T_{max} (°C)	Calculated E ($mmyr^{-1}$)	Recorded E ($mmyr^{-1}$)
Niğde	11.1	1208	38.0	3.4	8.2	4.7	17.4	1314.8	1547.6
Ankara	11.8	894	38.0	3.2	8.9	5.9	17.7	1209.0	1307.6
Burdur	13.2	967	37.5	2.1	10.1	7.6	19.0	1327.0	1072.2
Bolu	10.2	742	40.5	1.6	7.7	4.0	17.0	947.5	677.2
Konya	11.5	1131	38.0	2.1	8.5	5.0	17.9	1252.4	1186.7
Sivas	8.6	1285	39.5	2.0	6.1	2.2	14.9	1061.9	1043.9
Afyon	11.2	1034	38.5	2.6	8.0	4.4	17.3	1219.7	1054.8
Antalya	18.7	42	37.0	3.1	14.4	13.9	23.9	1512.7	1445.8
Beyşehir	11.3	1129	37.5	1.6	8.2	4.9	17.3	1189.7	987.5
Erzurum	6	1869	40.0	2.6	4.0	0.5	11.5	1124.8	1059.0
Golcük(Kocaeli)	14.4	16	40.5	2.7	11.4	9.9	19.4	1050.9	798.2

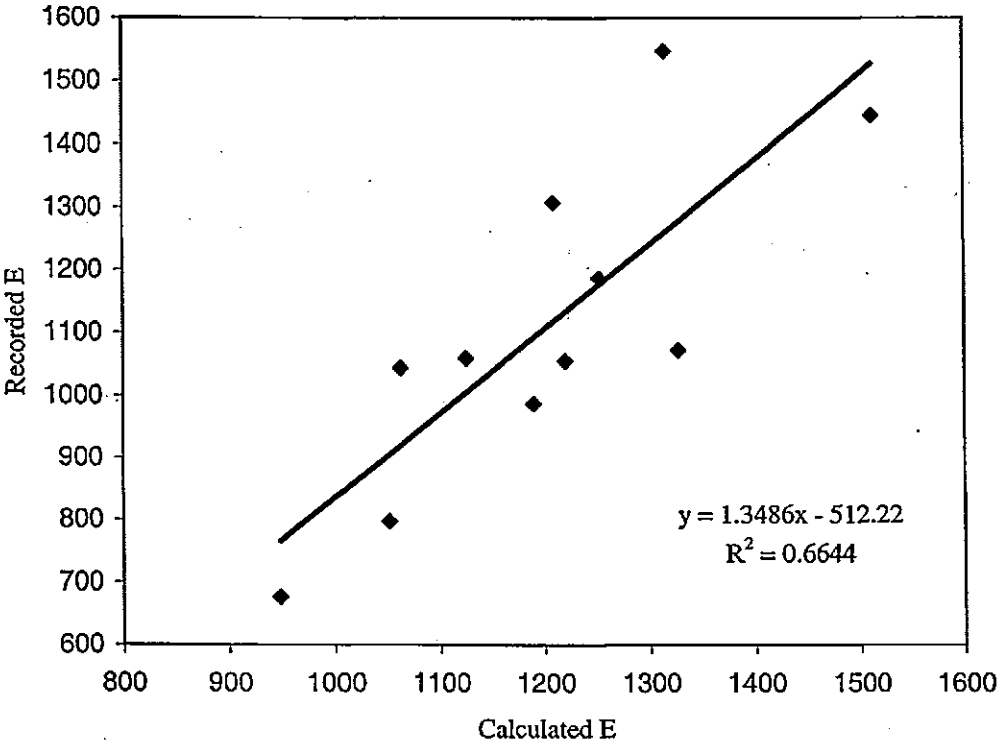

Fig. 5.5 Relationship between recorded and calculated amounts of evaporation for 11 meteorological stations across Turkey (from table 5.1).

Using this relationship, evaporation at Nar Gölü is the equivalent of a recorded value of 1025 ± 121 mm yr^{-1} (errors from residuals of equation 5.3).

This value would leave to an Aridity Index of 0.31 (P/E) which compares well to that shown by Türkeş (2003) for the Cappadocian region (Fig. 3.6).

5.5 Lake chemistry

The pH and conductivity values suggest the lake is alkaline and oligosaline, becoming slightly more alkaline and more saline between August 1999 and August 2002 (Table 5.2). $\delta^{18}O$ values have become more positive at the same time (from -3.0 ‰ to -2.4 ‰) suggesting that evaporation is currently exceeding precipitation which accounts for the increase in salinity (3.1 mS in August 1999 to 4.0 mS in August 2002). The major ion water chemistry in the summer of 1999 (Table 5.3) was dominated by Na^+ (380 mg/l), Mg^{2+} (103.4 mg/l) and Cl^- (970 mg/l) (Jane Reed, pers. com.).

The waters show stratification in all the measured variables (Fig. 5.6). There are significant differences in the scale of stratification between July 2001 and August 2002 and the difference in depth of the thermocline between the two sample dates. Lake depth had not changed measurably over the year and chemistry measurements were made at the deepest part of the lake in both years. From the data available it is not possible to explain these differences in stratification between the two sample dates. Nor is it known if the lake is stratified all year or if it is mixed at any time.

The lake bottom waters are anoxic. There is no evidence of benthic life in any of the surface sediment cores taken, sediments change colour from black to green and yellow on contact with the air due to oxidation, and waters below the thermocline smell anoxic.

5.6 Hydrology

The hydrological budget of a lake can be explained by the sum of the inflows and outflows from the system (e.g. Ricketts and Johnson, 1996; Gibson *et al.*, 1999), for example

$$dV/dt = P + S_i + G_i - E - S_o - G_o. \quad (5.4)$$

Table 5.2 Lake water chemistry measurements from Nar Gölü.

Sample		Temperature (°C)	Conductivity (mS)	pH	$\delta^{18}O$	δD	$\delta^{13}C$
Location	Depth (m)						
Lake Waters (08/1999)							
Lake Edge		22.0	3.1	7.1			
Lake Centre		21.0	2.5	7.4	-3.0	-37.3	9.3
Lake Waters (07/2000)							
Lake Edge	0	26.8	2.9	6.4	-3.2	-36.8	10.8
Lake Waters (07/2001)							
Lake Centre	0	24.2	3.3	7.9	-2.6	-34.6	11.3
	4	24.1	3.4	7.2			
	9	22.0	3.4	7.2	-2.8	-36.1	11.2
	12	20.7	3.2	6.6			
	14	17.2	3.2	6.2	-2.9	-35.8	10.6
	19	16.7	3.1	6.6			
	24	15.7	3.0	6.5	-3.2	-38.9	9.1
Lake Waters (04/2002)							
Lake Edge		8.9			-3.1	-37.3	9.3
Lake Waters (08/2002)							
Lake Centre	0	23.2	4.0	8.0	-2.4	-33.3	11.6
	5	22.8	4.2	7.9	-2.4	-33.1	11.6
	7.5	20.3	4.2	7.6	-2.8	-35.5	7.6
	10	14.3	4.0	7.1	-3.3	-39.0	8.6
	12.5	10.7	4.0	7.1	-3.3	-39.3	7.8
	15	9.9	4.0	6.9	-3.3	-39.0	10.4
	20	10.1	4.0	6.8	-3.3	-38.2	7.2
Hot Springs (2000)					-10.6	-73.7	-13.7
Springs (07/2001)							
Spring 1		15.7	0.1	6.0	-9.3	-64.7	-14.3
Spring 2		12.6	0.2	7.1	-10.5	-73.7	-10.7
Springs (04/2002)							
Spring 2					-10.6	-75.0	-11.2
Springs (08/2002)							
Spring 2					-10.7	-75.0	-13.7

Table 5.3 Nar Gölü major ion water chemistry (mg/l), summer 1999.

	Cl^-	SO_4^{2-}	Mg^{2+}	Ca^{2+}	Sr^{2+}	Na^+	K^+
Lake Centre	970.0	154.0	103.4	59.8	31.3	380.0	144.4
Lake Edge	970.0	154.0	103.4	59.8	31.3	380.0	144.4
Hot Spring	830.0	155.0	106.0	72.4	28.9	374.8	145.1

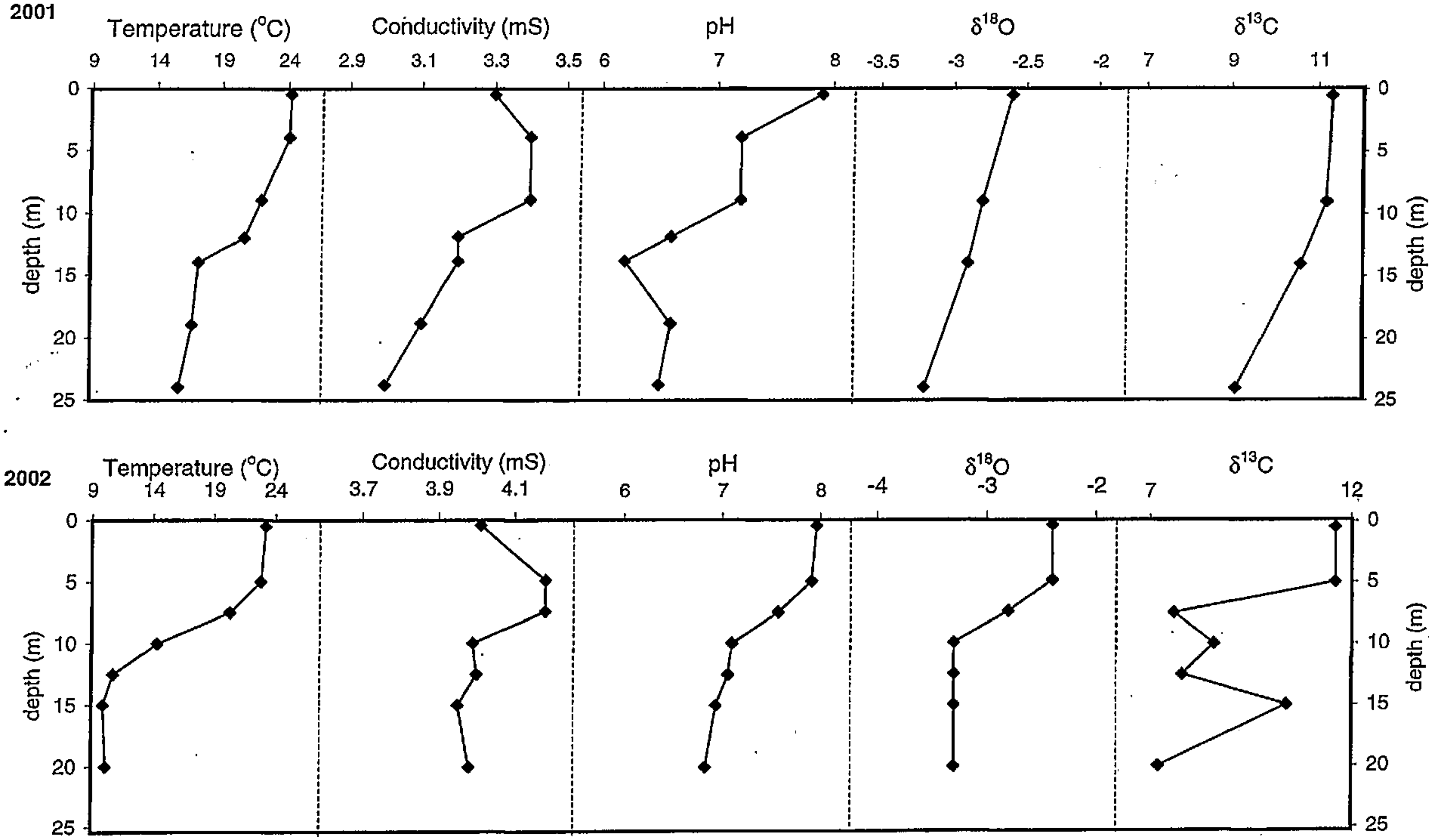

Fig. 5.6 Lake chemistry depth profiles from July 2001 and August 2002.

where V is lake volume; t, time (dV/dt = change in volume per unit time); P, precipitation; S_i, surface inflow; G_i, groundwater inflow; E, evaporation; S_o, surface outflow; G_o, groundwater outflow. V, P, S_i, G_i, E, S_o and G_o are measured in the same units.

Some of these values can be measured directly e.g. P, S_i, others have to be calculated e.g. E or estimated e.g. G_o. Here two methods, a water balance model and an isotope mass balance model, will be used to estimate all unknown values in equation 5.4.

5.6.1 Water balance model

For a given period of time it can be assumed that the lake volume is constant so that

$$P + S_i + Gi = E + S_o + G_o. \qquad (5.5)$$

The following values are known:

P: 178,080 m^3 of rainfall enters the lake directly from precipitation each year (lake area x mean annual rainfall).

E: 570,412 m^3 of water is lost from the lake each year through evaporation (annual evaporation x lake area).

S_o: there is no surface runoff from the lake.

S_i: runoff from the catchment is the only factor to take into account as there are no rivers or permanent streams that currently enter the lake. A runoff coefficient (k) of 0.25 ± 0.07 will be assumed. Although k is unknown, if it is assumed that $G_i > G_o$ (see further discussion below), then $k < 0.4$, from the extreme values of P and E. (Si = k x precipitation x (catchment area – lake area)). A value of 0.25 has been used elsewhere for crater lakes in evaporatively dominated regions (Telford and Lamb, 1999).

Using these values it can be calculated that

$$G_i - G_o = 244{,}212 \text{ m}^3 \qquad (5.6)$$

Gi and Go are both unknown and difficult to estimate. Go is assumed to be low, relative to E as the lake has been shown to be isotopically enriched and saline. This would not be the case if Go was high and the residence time of the lake was therefore low.

5.6.2 Isotope mass balance modelling.

As well as the water balance model discussed above the stable isotope values of the lake must also balance such that

$$dV\delta_l/dt = P\delta_P + S_i\delta_{Si} + G_i\delta_{Gi} - E\delta_E - S_o\delta_{So} - G_o\delta_{Go} \qquad (5.7)$$

where the values δ_l, δ_p, δ_{Si}, δ_{Gi}, δ_E, δ_{So}, δ_{Go} are the isotope values, either $\delta^{18}O$ or δD, of the lake waters, precipitation, surface inflow, groundwater inflow, evaporation, surface outflow and groundwater outflow respectively.

At Nar there is no surface outflow, lake waters leaving the lake through ground water are assumed to be the same value as all other waters within the lake such that $\delta_{Go} = \delta_l$. As the only surface input into the lake is from runoff directly from precipitation $\delta_{Si} = \delta_P$.

Therefore for Nar

$$dV\delta_l/dt = P\delta_P + S_i\delta_P + G_i\delta_{Gi} - E\delta_E - G_o\delta_l \qquad (5.8)$$

As in 5.4 it is assumed that the lake is in a steady state such that $dV\delta_l/dt = 0$. This relationship also assumes that the lake is well mixed although in reality it is stratified for at least part of the year (Fig. 5.6).

Taking these assumptions into account

$$P\delta_P + S_i\delta_P + G_i\delta_{Gi} = E\delta_E + G_o\delta_l \qquad (5.9)$$

P, S_i, and E are already known from measurements and the discussion above.

δ_l : lake surface waters between 2000 and 2002 have $\delta^{18}O$ values of -2.8 ± 0.4 ‰ (Table 5.2; Fig. 5.7)

δ_{GI}: spring waters from both the catchment and the hot springs in the lake lie at approximately $\delta^{18}O = -10.6 \pm 0.1$, $\delta D = -74.4 \pm 0.7$. Spring waters have given more or less consistent values through 3 years (2000-2002), compared to varying lake water values. All groundwaters lie on the Ankara meteoric water line (AMWL) suggesting they have not been affected by evaporation or geothermal effects.

δ_P: in a given year the average isotope ratio of rainwaters entering the lake will be a weighted average of the values for each month. The weighted average of annual rainfall at Ankara is (-8.8, -58.6) from 1996, 1997, 2000 and 2001 monthly values (IAEA/WMO, 2002; A. Dirican, pers. com., 2002).

It is unlikely that isotope values of precipitation are the same at Nar. Various relationships are known for differences in precipitation isotope values between locations (e.g. Dansgaard, 1964; Rozanski *et al.*, 1993; see full discussion in Chapter 2) and these relationships can be used to estimate values for Nar Gölü based on those recorded in Ankara. Temperatures in Derenkuyu are consistently colder than those in Ankara (Fig 5.8). Using the relationship between precipitation isotope values and temperature from Ankara (Fig. 2.3) $\delta^{18}O$ values would be 0.89‰ lower at Derinkuyu and δD values 6.38‰ lower. These values would be even more depleted if the relationships described by Dansgaard (1964) were used. However these are calculations based on northern European stations and the Ankara relationship is probably more suitable for use here.

There is also a standard relationship for changes in isotope values due to height, a large part of which is due to the corresponding change in temperature (Gat *et al.*, 2001). Nar lake lies 460 m above the recording station in Ankara and this corresponds to a change of –0.92 ‰ in oxygen isotope values (-0.2‰/100m) and – 6.9‰ in δD (-1.5‰/100m).

Nar lies further along given rain tracks than Ankara (Fig 3.3) and δ_p values are likely to be more negative due to the rain out effect. This effect is difficult to quantify with the data currently available.

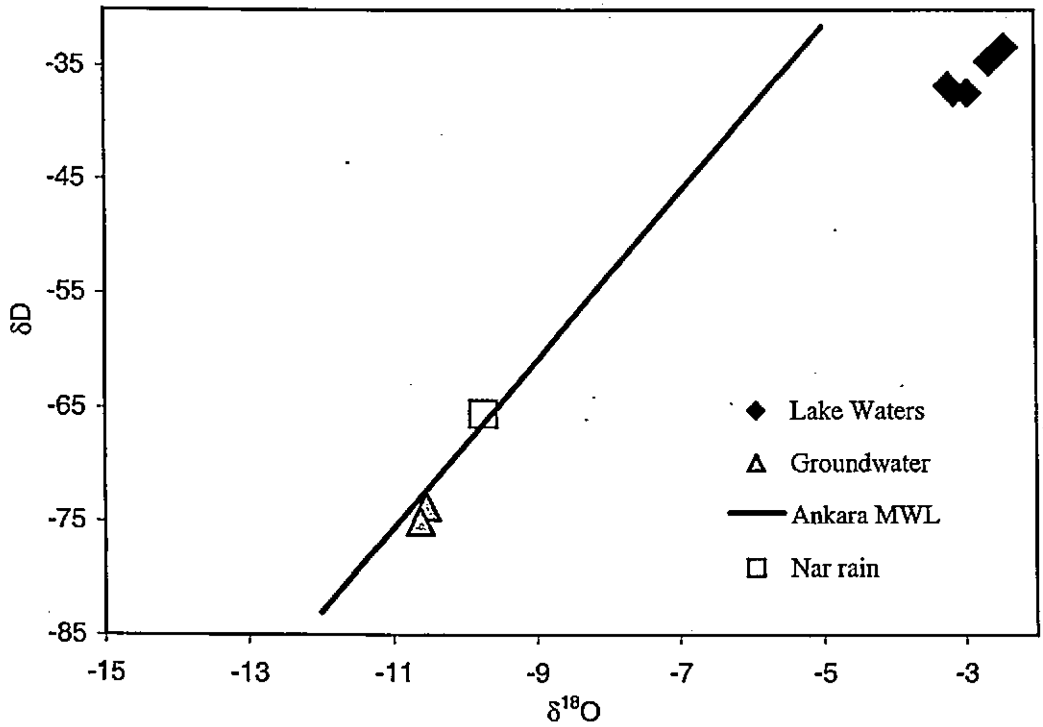

Fig 5.7 δD v. $\delta^{18}O$ plot of contemporary water from Nar Gölü.

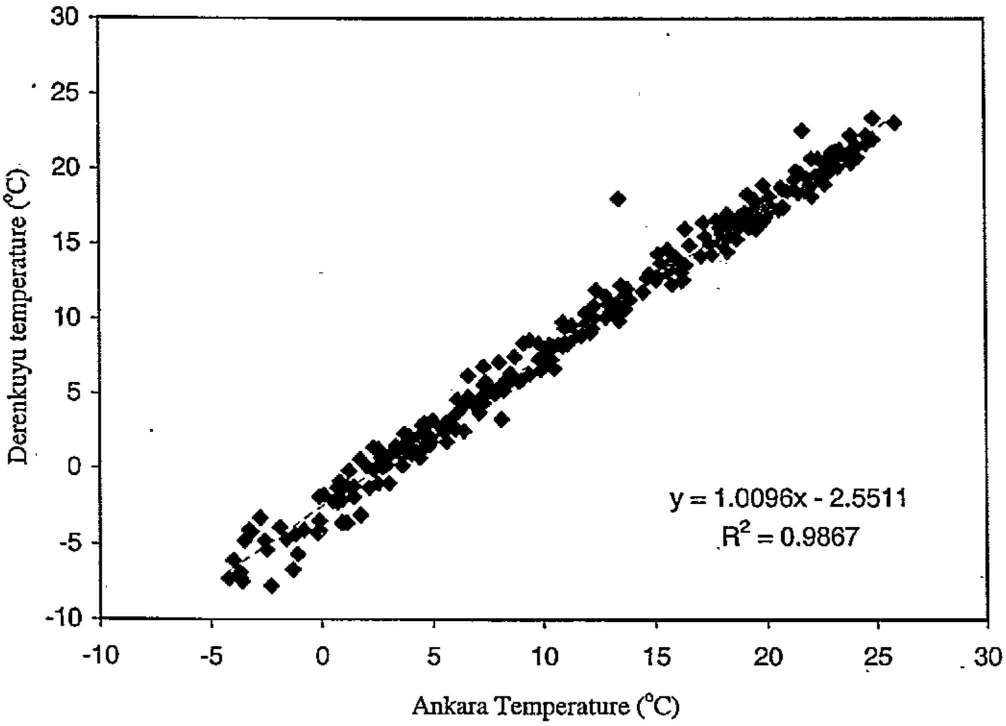

Fig 5.8 Relationship between monthly average temperatures in Derinkuyu and Ankara between 1965 and 1990. Data from Turkish State Meteorological Service.

As the altitude effect is largely due to changes in temperature, the altitude correction will be used to give values for rainfall at Nar Gölü, by adding this effect to the weighted values of precipitation from Ankara.

This gives weighted values of oxygen and hydrogen isotope ratios in precipitation over Nar as –9.74 ± 0.1 ‰ and – 65.53 ± 0.6 ‰ respectively. δ_P has also been estimated from the intercept of local evaporation lines with meteoric water lines, i.e. the value of the waters from which lakes in a given region evaporate from (e.g. Ricketts and Johnson, 1996). Nar waters evaporation line intercepts the Ankara meteoric water line at $\delta^{18}O = -11.0$ ‰. Groundwater values may also represent the weighted average value of mean annual rainfall and lie close to the intercept value at -10.6 ‰.

δ_E: is very difficult to measure directly and is usually calculated.

Many authors (e.g. Gonfiantini, 1986, Gibson *et al.*, 1999) use equations based on the Craig-Gordon model of evaporation (Craig and Gordan, 1965) such as:

$$\delta_E = ((\alpha^*\delta_l) - h\delta_A - \epsilon)/(1 - h + \epsilon_k) \qquad \text{(Kebede } et\ al.\text{, 2002)} \qquad (5.10)$$

where α^* is the equilibrium isotopic fractionation factor dependent on the temperature at the evaporating surface, h is the relative humidity normalised to the saturation vapour pressure at the temperature of the air water interface (lake surface temperature); $\epsilon = \epsilon^* + \epsilon_k$; $\epsilon^* = 1000\ (1- \alpha^*)$ and ϵ_k is the kinetic fraction factor. δ_A is the isotopic value of the air vapour over the lake.

α^*: the equilibrium fractionation factor, can be calculated

$$1/\alpha^* = \alpha_{eq} = \exp(1137\ T^{-2} - 0.4156\ T^{-1} - 2.0667 \times 10^{-3}) \qquad (5.11)$$

where T is the temperature of the lake surface water in degrees Kelvin (Majoube, 1971).

T: lake surface temperatures measured over a number of field seasons lie between the average and maximum monthly temperatures from Derinkuyu. Lake surface temperatures will therefore be taken to be the mean of the average and maximum air temperatures. This gives a value of 12.6°C for the mean annual lake surface temperature.

h: for a relative humidity of 0.57 at an average air temperature of 9.2°C, the normalised value of h at 12.6°C is 0.45.

ϵ^*: can be calculated from α^*.

ϵ_k: for $\delta^{18}O$ has been shown to approximate 14.2(1-h) (Gonfiantini, 1986).

δ_A: the isotope value of atmospheric moisture is difficult to quantify unless measured at the site, although is usually assumed to be proportional to δ_P. From the relationship between the isotope values of atmospheric moisture and precipitation recorded at Ankara (A. Dirican, pers. com., 2002) a value of -21 ‰ for $\delta_{atmosphere}$ over Nar Gölü is used. δ_A has often been calculated as $\delta_P - \epsilon^*$, and been shown experimentally to be a correct approximation to with in 5% (Gibson *et al.*, 1999). For the Nar data this method gives a δ_a value of –20.2‰, close to that calculated from the moisture precipitation relationship in Ankara.

An alternative equation for calculating δ_E was obtained from observations at Pyramid Lake, Nevada (Benson and White, 1994), and has been used by other authors (e.g. Ricketts and Johnson, 1996) such that:

$$\mathbf{R}_{evap} = [(\mathbf{R}_{lake}/\alpha_{eq})-(RHf_{ad}\mathbf{R}_{ad})]/[(1-RH)/\alpha_{kin})+RH(1-f_{ad})] \qquad (5.12)$$

where $\delta_i = (\mathbf{R}_i - 1)10^3$, $\mathbf{R}_{ad}$ is the isotope ratio of the free atmospheric water vapour, f_{ad} is the fraction of atmospheric water vapour in the boundary layer over the lake (if all the atmospheric water overlying the lake is derived from evaporation then $f_{ad} = 0$), RH is the relative humidity, and α_{eq} and α_{kin} are fractionation factors.

$\mathbf{R}_{lake}$ is known.

α_{eq}: can be calculated as shown above (equation 5.11).

RH: The average relative humidity at Derinkuyu through the recording period (1965-1990) was 57%. This is expressed as a fraction for this calculation.

f_{ad}: is unknown and lies between 0 (if all the water above the lake is derived from evaporation) and 1.

R_{ad}: is discussed above.

α_{kin}: the kinetic fractionation factor, is dependent on wind speed and for wind speeds less than 6.8 ms^{-1}, $\alpha_{kin} = 0.994$. This value is appropriate for Nar as average wind speeds in the region are 3.2 ms^{-1}.

From equation 5.10 δ_E is shown to equal –20.58 ‰.

Values of δ_E from equation 5.12 can be calculated for all values of f_{ad} (Fig. 5.9) showing that δ_E will lie between –8.66 ‰ and –15.68 ‰.

Benson and White (1994) suggest that f_{ad} should always be taken as 0 as the water vapour immediately overlying the liquid surface will be the dominant control on δ_E and will be almost entirely made up of evaporated water. δ_E must also lie to the left of the AMWL in δ^{18}O:δD space. As –15.68 ‰ lies closest to the value calculated from equation 5.10 this will be taken as the value from equation 5.12 to be used in the hydrological balance model.

Using the known values in equation 5.8 it can then be shown that, if δ_E = - 20.58‰, then

$$10.6G_i - 2.8G_o = 8{,}561{,}891 \qquad (5.13)$$

alternatively, if δ_E = - 15.68 ‰, then

$$10.6G_i - 2.8G_o = 5{,}766{,}872 \qquad (5.14)$$

Simultaneously solving equations 5.6 and 5.13 or 5.14 therefore gives values for G_i and G_o (see table 5.4 in chapter summary for values).

G_i will be a combination of shallow groundwaters, predominantly from rainfall seeping from higher ground outside the catchment, and deep groundwaters brought into the lake via the hot springs. Chloride is a conservative ion that is not involved in any significant chemical or biological reactions within the lake and can be considered negligible in both

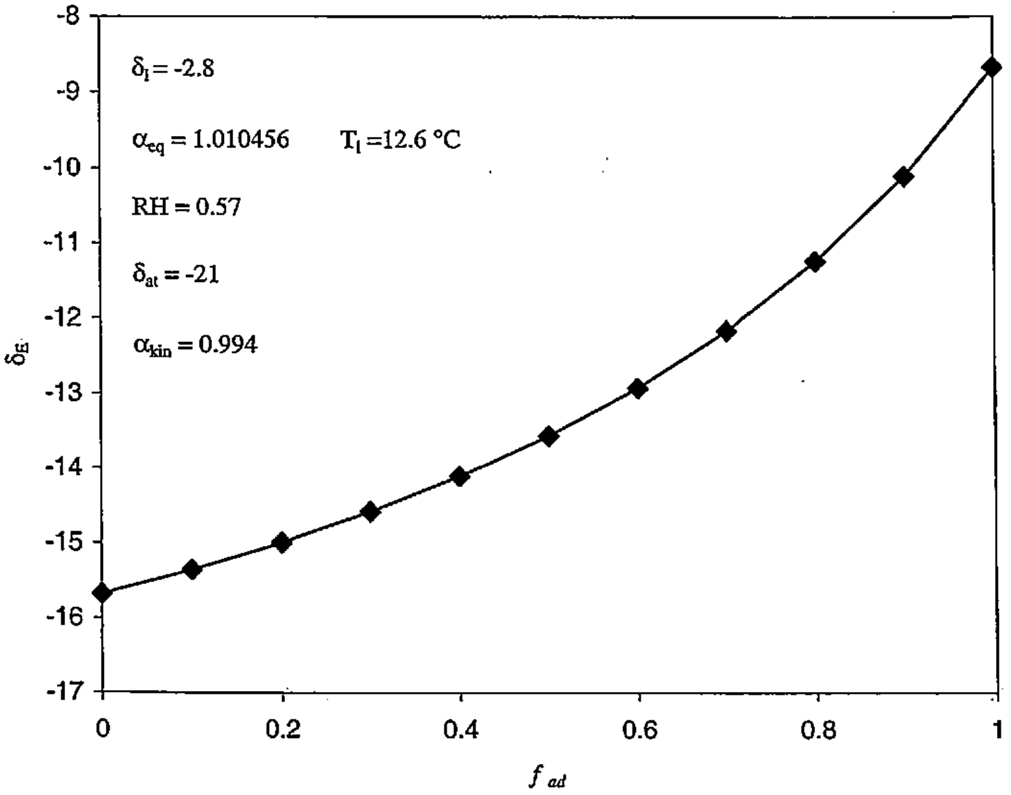

Fig. 5.9 Calculated values of δ_E from equation 5.9 for all values of f_{ad} .

precipitation and evaporation (Telford and Lamb, 1999). If the shallow groundwaters are considered to be predominantly precipitation, having little time to be altered on route to the lake, a chloride balance, $G_iC_{Gi} = G_oC_{Go}$ (where C_{Gi} and C_{Go} are the chloride concentrations of the groundwater inflow and outflow respectively), will describe the relationship between the lake waters, assumed to be the same as C_{Go}, and the deep groundwaters. From this relationship it can be shown, from the values is tables 5.3 and 5.4, that the groundwater outflow from the lake is 83% of the deep groundwater inflow.

5.7 Lake Sedimentation

Lake sediments were collected in sediment traps between July 2001 and August 2002. The upper trap from the eastern mooring was lost during the year. The carbon stratigraphy of the two western traps is shown in Fig. 5.10. The top trap, at 5m water depth, comprises largely inorganic carbon. If it assumed that all the inorganic carbon comes from calcium carbonate (see below for discussion of carbonate chemistry) where all the carbon has a mass of 12 then between 0 and 25 cm of the top trap the sediments comprise between 80 and 90 % calcium carbonate with values of around 2 to 3 % of organic carbon. At around 30 cm there is a shift to increased amounts of organic carbon, to around 6 %, with inorganic carbon suggesting approximately 50% of the sediment is calcium carbonate.

In the lower trap, at ~ 20m water depth, the same pattern is repeated with more organic rich sediments overlain by more calcium carbonate rich sediments. Organic carbon only accounts for 10 to 13 % of the sediment mass at the base of the trap, with approximately 30 to 40 % due to calcium carbonate. The majority of the rest of the mass will be diatom silica.

It appears that sedimentation in Nar Gölü comprises a period of sedimentation dominated by diatoms, with some carbonate deposition, followed by a period dominated by calcium carbonate deposition. The sediment trap at 5m water depth was covered in carbonate precipitate whereas the two traps from the deep water were clean, suggesting that carbonate precipitates in the surface waters, probably within the photic zone. Planktonic diatoms seem only to appear in the lake for part of the year, whereas carbonate is precipitated throughout the year. Diatom blooms may be caused by increased nutrient supply during periods of mixing (Lamb *et al.*, 2002), and this is possible in Nar although it is not known if or when mixing occurs (see further discussion in chapter 6).

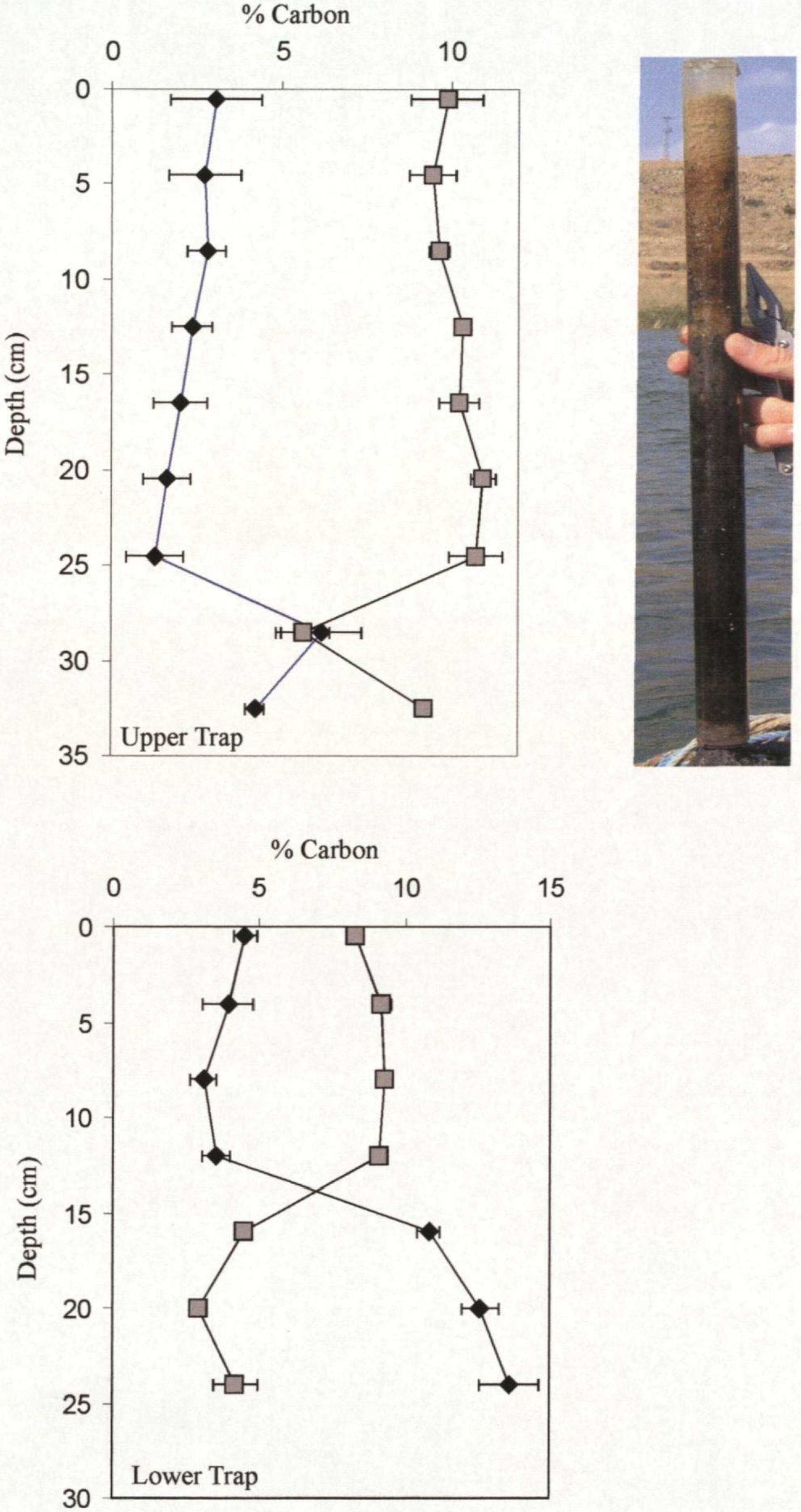

Fig. 5.10 Organic (black diamonds) and inorganic (grey squares) carbon stratigraphy of sediment traps from Nar Gölü. Upper trap is pictured.

The top trap contains relatively little organic matter, compared to the bottom trap. It is likely that some of the organic matter in the upper trap will have oxidised during the year, and preserved in the anoxic waters of the bottom trap, accounting for this difference in preservation.

5.7.1 Carbonate chemistry

From XRD analysis contemporary precipitated carbonates are shown to be calcite. Kelts and Hsu (1978) state that carbonates precipitating from waters with Mg/Ca <2 will be calcite so this would be expected (from the Nar lake water chemistry Mg/Ca = 1.7).

It has been shown, from Leng and Marshall (in press), that

$$\delta^{18}O_{calcite(SMOW)} - \delta^{18}O_{water(SMOW)} = 18.03(10^3T^{-1})-32.42 \qquad (5.15)$$

for carbonates precipitated in equilibrium with lake waters, where T is given in Kelvin.

Using the water data from 2002 and measured $\delta^{18}O$ values of carbonate precipitates from the 2001 – 2002 sediment trap it is possible to check that these carbonates are precipitating in equilibrium by using equation 5.14. Note that both carbonate and water values must be given against the same standard i.e. SMOW and so carbonate values measured against PDB must be corrected to SMOW such that (Coplen *et al.*, 1983)

$$\delta^{18}O_{calcite(SMOW)} = 1.03091\delta^{18}O_{calcite(PDB)} + 30.91 \qquad (5.16)$$

With lake water values from 2002 of –2.4‰ in the top 5m of water, where the carbonate is precipitated, and lake temperatures of 23°C, a value of –4.7‰ is calculated from equation 5.14 for $\delta^{18}O_{carbonate(PDB)}$. This compares to measured values of –3.3‰ and –3.5‰ for precipitated carbonate and lake surface sediments respectively. However the water isotope and temperature values are from August 2002 and this may not have been the time of carbonate precipitation. Using the values for lake temperatures as discussed above (i.e. the mean of the average and maximum temperatures for each month), and by estimating monthly lake water values by fitting a sine curve to the lake water values from April and August 2002, calculations of $\delta^{18}O_{carbonate(PDB)}$ can be made for each month (Fig. 5.11).

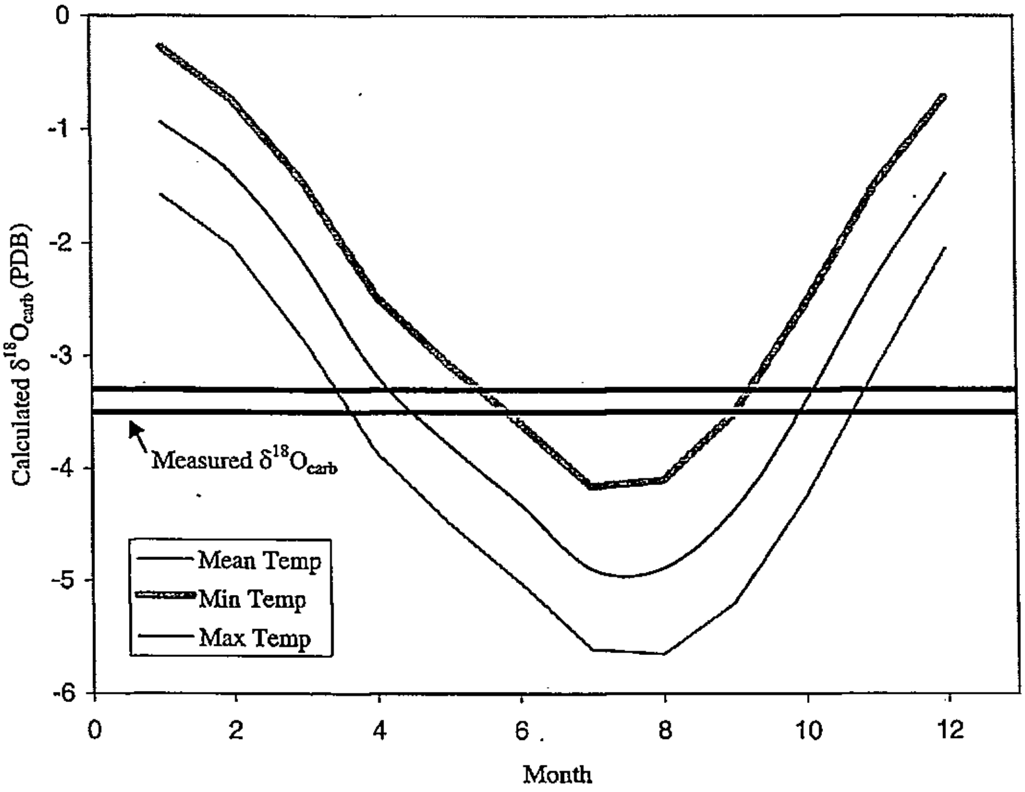

Fig. 5.11 Calculation of $\delta^{18}O$ of equilibrium precipitated calcite for each month at Nar Gölü with mean, minimum and maximum air temperatures.

Compared to the measured values of carbonate from 2002 this suggests that carbonate was precipitated between April and June, most likely during May, or between September and November. The latter scenario is unlikely as the carbonate deposition was on top of the sediment trap and was therefore the most recent sediment precipitated in the lake. It therefore seems most likely that carbonate sedimentation at Nar takes place in late spring and early summer, if the carbonates here follow relationships found elsewhere and are precipitating in equilibrium with the lake waters.

5.8 Summary

Nar Gölü is a relatively small lake with no surface inflow or outflow, although there is probably a significant amount of groundwater throughflow in the system. Calculations of the hydrological budget (Table 5.4) show that only 24 to 33 % of the water entering the lake comes from direct precipitation or surface runoff, although the latter is generally unknown, with an estimated value of *k*. The remainder of the water entering the lake is therefore from groundwaters. Both deep, from the hot springs, and shallow groundwaters lie on the meteoric water line, and are therefore rain-waters. Influx of lake waters is therfore probably controlled by the amount of precipitation.

Depending on the δ_E calculation used, evaporation from the lake accounts for between 43 and 58 % of the water leaving the lake. The result of the calculated hydrological flux is that lake-water residence time, based on the lake volume divided by the flux (Lamb *et al.*, 2002), is between 6 and 8 years (Table 5.4). Changing the isotope values for precipitation to -10.6 or -11.0‰, due to estimates based on the local groundwaters and intercept of the LEL with the Ankara MWL rather than the calculated value of -9.6‰, make no significant difference to the lake residence times calculated (maximum change is ~ 5%).

Lake sedimentation largely comprises calcite precipitated, in the surface waters of the lake, during the early summer. There is also a period of increased organic sedimentation, probably associated with an algal bloom in spring or autumn.

Table 5.4 Summary of Nar Gölü hydrology.

Lake Area	556,500 m^2	**Lake Volume**	7,692,360 m^3
Catchment Area	2,408,000 m^2	**Precipitation**	0.320 myr^{-1}
Evaporation	1.025 myr^{-1}	δ_P	- 9.74 ‰
Run off coefficient (k)	0.25	δ_{Gi}	- 10.6 ‰

Hydrological Budget

	Value (m^3 yr^{-1})			**Percentage**	
		δ_E = -20.58	δ_E = -15.68	δ_E = -20.58	δ_E = -15.68
Inputs					
Precipitation	178,080			13	18
Runoff	148,120			11	15
Deep Groundwater		922,650	490,922	69	50
Shallow Groundwater		87,392	160,755	7	17
Outputs					
Evaporation	570,412			43	58
Groundwater		765,800	407,465	57	42
Total Flux		1,336,212	977,877		
Residence Time		5.76 yrs	7.87 yrs		

Chapter 6

NAR GÖLÜ - PALAEOLIMNOLOGY

A 218 cm continuous core sequence from Nar Gölü (NAR01) was obtained in 2001 from Glew and Livingstone core samples (core locations in Fig. 5.3). Further sediments, up to a depth of 5m were also recovered but there were significant gaps, of unknown length, in the stratigraphy below 218 cm. From this sequence the top 900 individual carbonate laminae were sampled consecutively and analysed for $\delta^{18}O$ and $\delta^{13}C$, with the intermediate organic laminae analysed for $\delta^{13}C$ and C/N ratios, and changes in colour were measured using image analysis techniques. Mackereth coring in 2002 (Fig. 5.3) allowed the continuous core sequence to be extended to 376 cm. A further 825 carbonate laminae were analysed for $\delta^{18}O$ and $\delta^{13}C$, from continuous bulk samples of 5 laminae, and for changes in colour.

6.1 Lithology

The 376 cm core sequence is laminated throughout (Fig. 6.1), with occasional 0.1-5.0 cm thick grey clastic layers, which often show a fining upwards sequence. Laminations are formed of couplets comprising light, often white, largely carbonate layers and dark layers, made up of largely organic material and diatoms.

The composition of the dark laminae remains more or less constant through the sequence. However there are marked changes in the carbonate laminae. In some case the carbonate laminae comprise fine grained aragonite crystals (< 5 μm in size; Fig. 6.2a) whereas other laminae are made up of a fining upwards sequence of calcite polyhedra (10-40 μm in size; Fig. 6.2b). In some laminae both aragonite and calcite layers appear in the carbonate part of the couplet, with the aragonite layer overlying calcite polyhedra (Fig. 6.2c).

Laminated sediments composed of alternating carbonate and organic laminae with fining upwards calcite crystals have been described elsewhere (e.g. Anderson, 1993; Kelts and Hsu, 1978). In general the light calcium carbonate layer is precipitated in warm waters during the spring and summer and the dark organic layer represents the autumn and winter periods (Saarnisto, 1986).

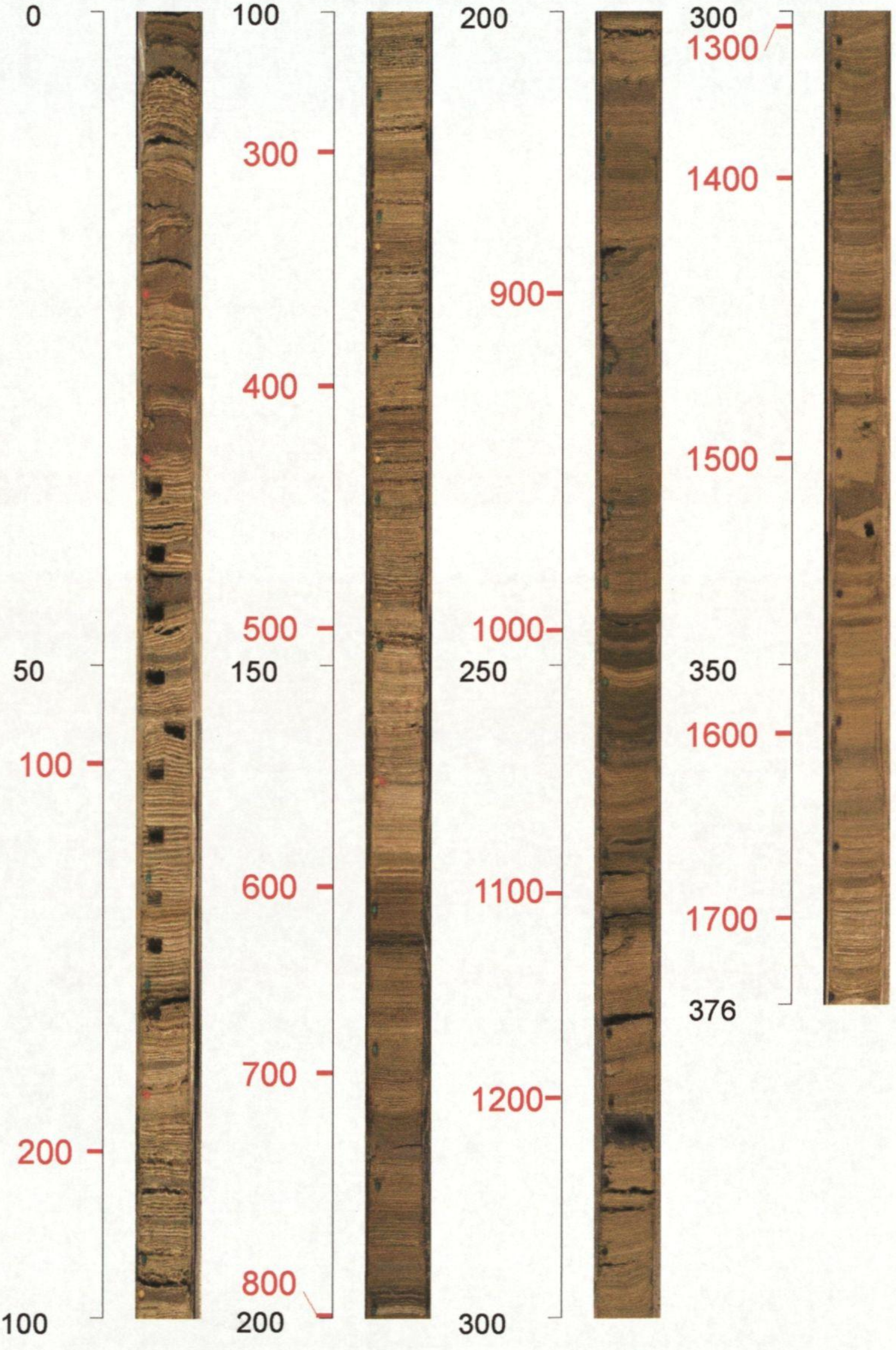
0
50
100
100
200
100
300
400
500
150
600
700
800
200
200
900
1000
250
1100
1200
300
300
1300
1400
1500
350
1600
1700
376

Fig. 6.1 Photograph of the 376 cm Master sequence from Nar Gölü against depth (black figures in cm) and number of laminae from the top of the core (red numbers).

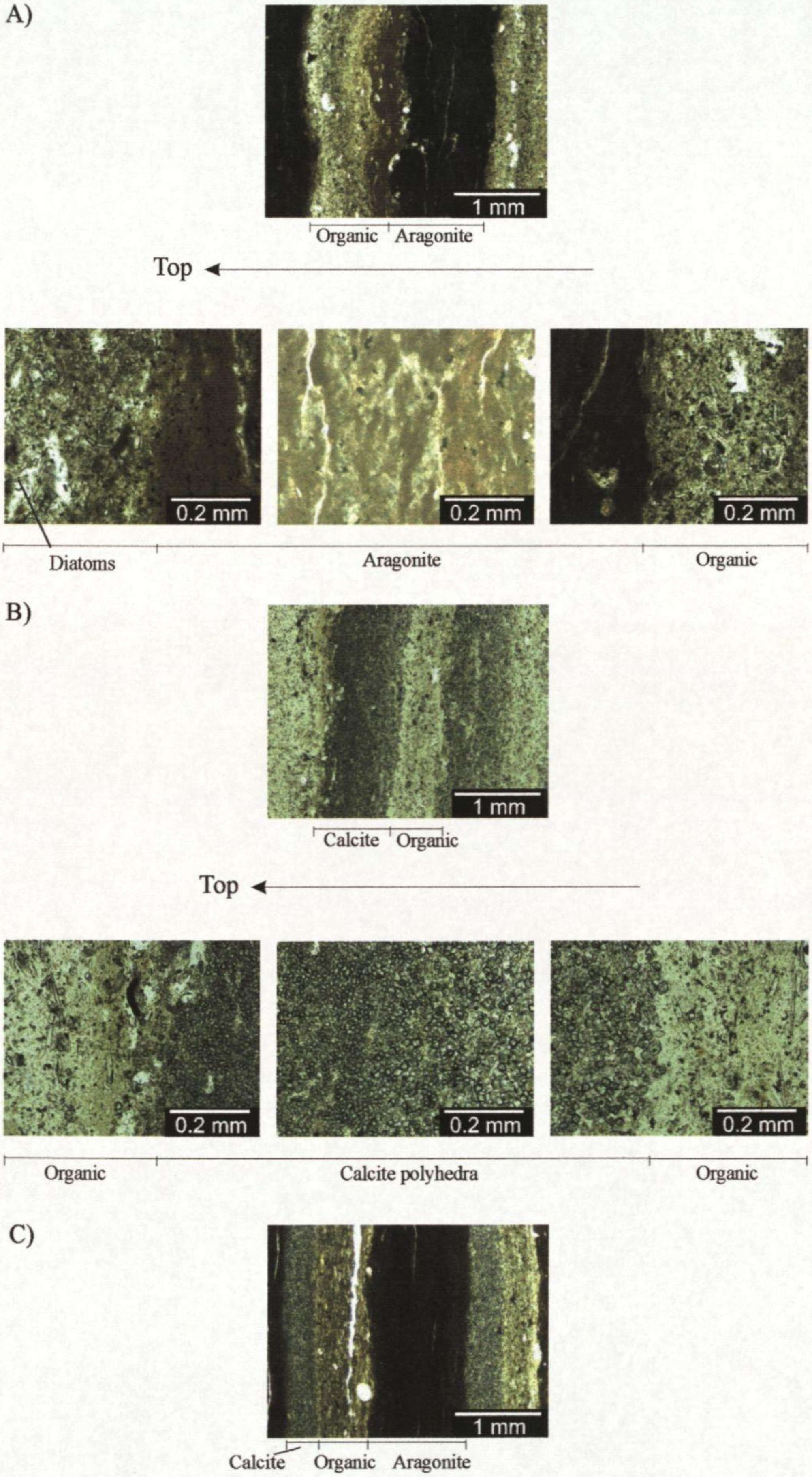
A)
1 mm
Organic
Aragonite
Top
0.2 mm
0.2 mm
0.2 mm
Diatoms
Aragonite
Organic
B)
1 mm
Calcite
Organic
Top
0.2 mm
0.2 mm
0.2 mm
Organic
Calcite polyhedra
Organic
C)
1 mm
Calcite
Organic
Aragonite

Fig. 6.2 Composition of Nar laminae. A: with aragonite lamina, B: with calcite lamina, C: with both aragonaite and calcite lamina.

Contemporary sedimentation at Nar would support this (Chapter 5) and further suggest that most of the calcium carbonate is formed before July, the time the sediment trap was placed in the lake, as the first sediments in the trap are more organic rich followed by more carbonate rich sediments. The isotope values of the carbonate also suggest that they are precipitated in the late spring or early summer. It is possible that the calcium carbonate deposition is associated with times of increased photosynthesis caused by increased productivity during times of mixing of the water column (Lamb *et al.*, 2002) although it is not known if the Nar waters mix at any time during the year, or are permanently stratified..

Changes in carbonate mineralogy occur from one year to the next e.g. between laminae 10 and 11, and between 587 and 588 (Table 6.1). These changes in mineralogy are accompanied by a change in colour. The fine-grained aragonite laminae are much whiter than the calcite laminae. These changes can be observed in the greyscale values through the core sequence (Fig. 6.3). From the samples analysed grey scale values explain ~60% of the percentage of calcite in the samples, however most of laminae are nearly 100% calcite or aragonite, there are few samples in between, suggesting there are further controls on the colour of the carbonate sediments.

Changes in the mineralogy of calcium carbonate precipitated are due to changes in the Mg/Ca ratio within the lake. With Mg/Ca < 2 calcite is precipitated, as in the current lake (Chapter 5). With increased evaporation the lake becomes enriched in Mg and the Mg/Ca ratio increases such that aragonite may precipitate (Kelts and Hsu, 1978). For the laminae containing both forms of calcium carbonate aragonite overlies the calcite suggesting the lake became more enriched through the year resulting in the Mg/Ca ratio passing the threshold needed for aragonite to form.

6.2 Chronology

Contemporary sedimentation (see 5.7) suggests that each lamina couplet represents 1 year of sedimentation. Samples from the top 50 cm of the NAR01 sequence were dated to validate this assumption for the whole core.

The ^{137}Cs activity profile (Table 6.2; Fig. 6.4) has two well resolved peaks, at 6 cm and 30.5 cm that probably record fallout from the 1986 Chernobyl reactor accident and the 1963 fallout maximum from the atmospheric testing of nuclear weapons. The 1963 date is

Table 6.1 Carbonate mineralogy of laminae analysed by XRD with corresponding grey scale and $\delta^{18}O$ (‰) values.

Laminae No	**Carbonate Mineralogy**		**Grey Scale**	**$\delta^{18}O$**
	% Calcite	**% Aragonite**		
3	100	0	131.7	-4.3
5	100	0	125.7	-3.4
10	90	10	120.3	-4.8
11	5	95	191.7	-2.8
12	2	98	173.0	-2.5
13	0	100	181.0	-2.2
20	1	99	188.7	-1.3
30	0	100	175.7	-0.5
33	0	100	176.7	0.3
40	0	100	167.3	0.6
55	0	100	211.3	0.3
142	0	100	199.0	0.1
328	20	80	166.7	-1.7
584	10	90	211.0	0.3
585	30	70	210.3	-2.2
586	10	90	200.0	-0.2
596	10	90	184.0	-2.1
597	100	0	96.7	-1.6
598	20	80	212.0	-2.4
807	100	0	166.0	-1.8
896	100	0	112.3	-3.8
921-925	100	0	111.2	-3.3
1141-1145	65	35	152.6	0.2
1196-1200	100	0	122.1	-2.0
1441-1445	50	50	100.5	-4.8
1446-1450	1	99	156.8	-2.7
1631-1635	0	100	161.9	-0.5
1711-1715	1	99	194.3	-0.7

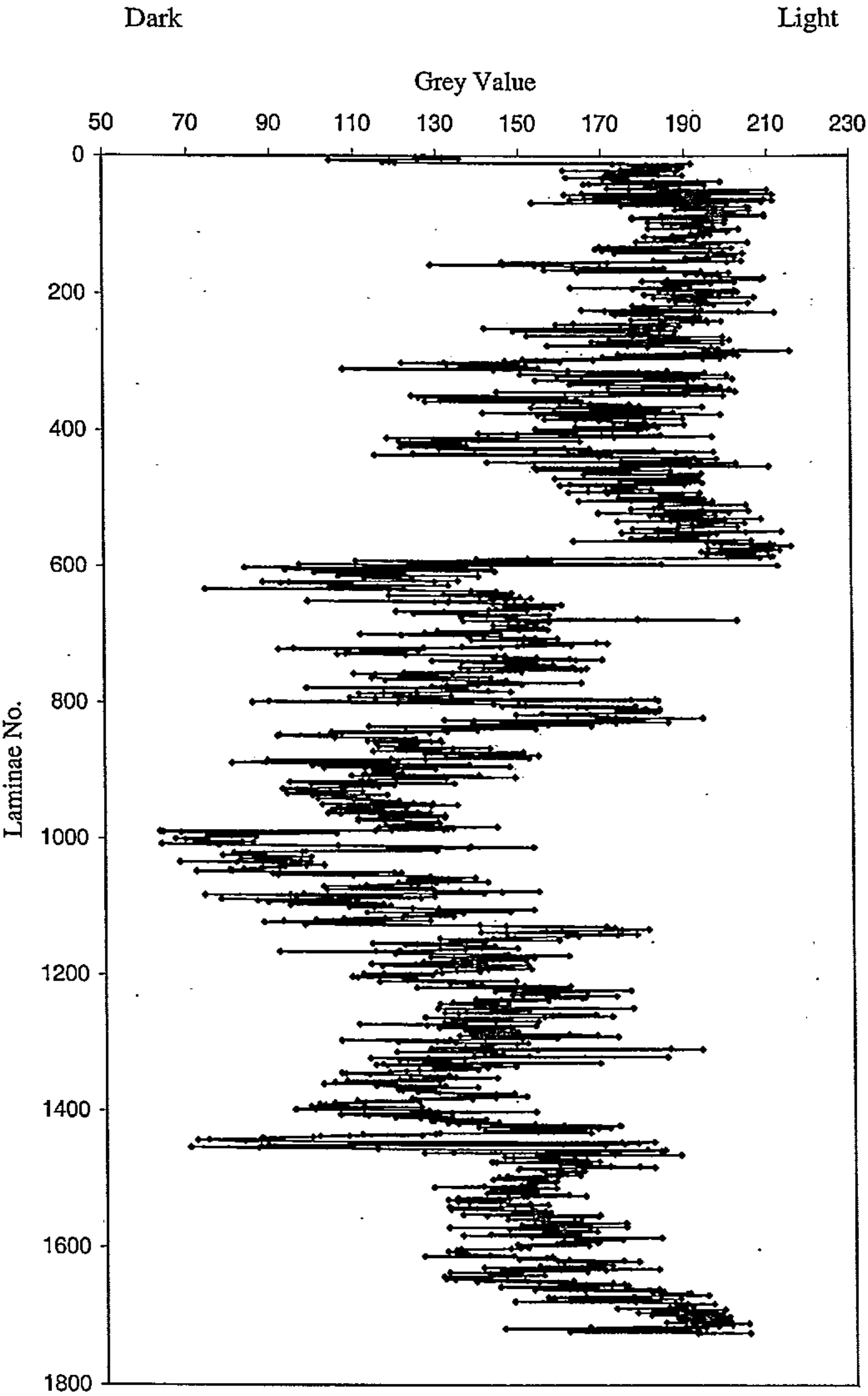

Fig. 6.3 Grey scale values from carbonate laminae through the Nar sequence (data in appendix 2).

supported by the detection of significant concentrations of ^{241}Am at that depth (Appleby *et al.*, 1991). ^{210}Pb dates calculated using the CRS dating model (Appleby and Oldfield, 1978) show different age-depth relationships compared to the ^{137}Cs peaks, placing 1986 at a depth of ~10.5 cm and 1963 at a depth of ~15.5 cm. The most likely causes of this discrepancy are incomplete recovery of the ^{210}Pb record in the older sections of the core, due to very low activities caused by rapid accumulation rates. There may have also been variations in the ^{210}Pb supply rate at the core site (Appleby, pers. com. 2003).

By fitting the ^{210}Pb age model to the ^{137}Cs dates, following methods outlined in Appleby (2001), a composite model has been used to construct a chronology that best fits all of the radiometric data (Table 6.3). The detailed values given in this table, other than the dates determined from the ^{137}Cs record, have some uncertainties due to the problems with the ^{210}Pb ages as discussed above.

The laminae count from the NAR01 sequence compared to the radiometric age model from Table 6.2 shows that at any given depth the laminae count is younger than the ^{210}Pb age. However, the laminae counts lie 5 years from both the ^{137}Cs dates and shifting all the laminae counts by 5 years results in the two chronologies fitting very well (Fig. 6.5).

Laminae in the very top of the core, where the two chronologies diverge, are unclear because the sedimentation regime changed above 7 cm depth. It appears from the age models that laminae number 6 represents 1991, and laminae 1 to 5 represent 2001 – 1992. Below laminae 6 each couplet represents one years' sedimentation and a chronology can, therefore, be obtained for the rest of the sequence by counting the number of laminae couplets (Fig. 6.6) where ages are given in varve years before 2001, converted to years AD. The loss of laminae in the very top of the core may be due to disturbance of the soft surface sediments during coring, or due to a change in sedimentation patterns in the lake, possibly associated with recent anthropogenic activity.

The laminae count from the NAR01 sequence was compared with laminae counts from two continuous cores (M2 and M3), taken in 2002 from different parts of the basin (Fig. 5.3), to show if there were any parts of the NAR01 sequence that significantly underrepresented the number of laminae through the stratigraphy (Table 6.3). Comparison of the three counts shows that the NAR01 core was a good representation of the number of

Table 6.2 Fallout radionuclide concentrations in Nar Gölü lake sediments.

		^{210}Pb							
Depth		Total		Unsupported		Supported		^{137}Cs	
cm	g cm^{-2}	Bq kg^{-1}	±	Bq kg^{-1}	±	Bq kg^{-1}	±	Bq kg^{-1}	±
0.25	0.1	112.4	11.3	55.8	11.7	56.6	3	4.1	1.7
4	1.7	78.2	9.3	25.6	9.6	52.6	2.7	6.6	1.56
6.5	2.9	102.1	8.4	13.7	8.8	88.4	2.5	48	1.99
9	4.2	98.4	10.2	36.2	10.6	62.2	3	20.1	2.08
11.5	5.6	107.6	13.2	65.2	13.4	42.5	2.5	5.9	1.75
17.5	9	80.6	12.1	28.3	12.3	52.4	2.4	11.9	1.75
23.5	12.5	75.2	8.8	10.8	8.3	63	2.4	26.8	1.78
26.5	14.5	71.7	8.7	-8.1	9	79.9	2.2	20.6	1.55
28.5	15.6	66	8.6	-3	8	66.4	2	41.5	1.73
30.5	16.8	87.8	9.9	28.8	10.3	59	2.8	56.8	2.51
32.5	18.1	82.9	8.3	20.3	8.6	62.6	2.5	20.6	1.83
36.5	20.5	59.1	6.1	4.4	6.4	54.7	1.8	6.3	1.32
40.5	23	51.9	6.7	-14.6	7	64.6	2.2	5.7	1.31
44.5	25.5	63.3	9.5	7.2	9.7	56.1	2	0	0
48.5	28.1	51.5	8	-11.9	8.3	63.4	2.3	1.3	1.21

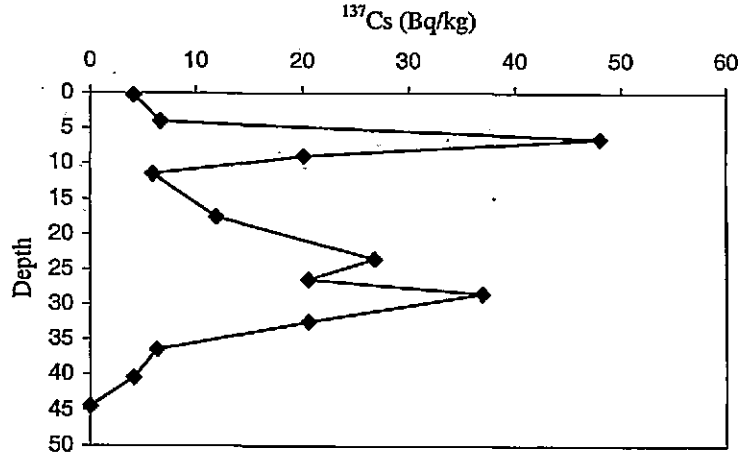

Fig 6.4 ^{137}Cs profile from the top of the Nar sequence.

Table 6.3 Radiometric chronology for Nar Gölü from ^{210}Pb age depth relationship corrected to ^{137}Cs ages.

Depth cm	Date AD	Age y	Error ±
0	2001	0	
2.5	1995	6	2
4.5	1990	11	2
6.5	1987	14	3
8.5	1984	17	3
12.5	1979	22	4
16.5	1973	28	4
20.5	1969	32	4
24.5	1966	35	4
28.5	1964	37	4
30.5	1963	38	4
32.5	1959	42	5
36.5	1956	45	5
40.5	1954	47	6
44.5	1952	49	6

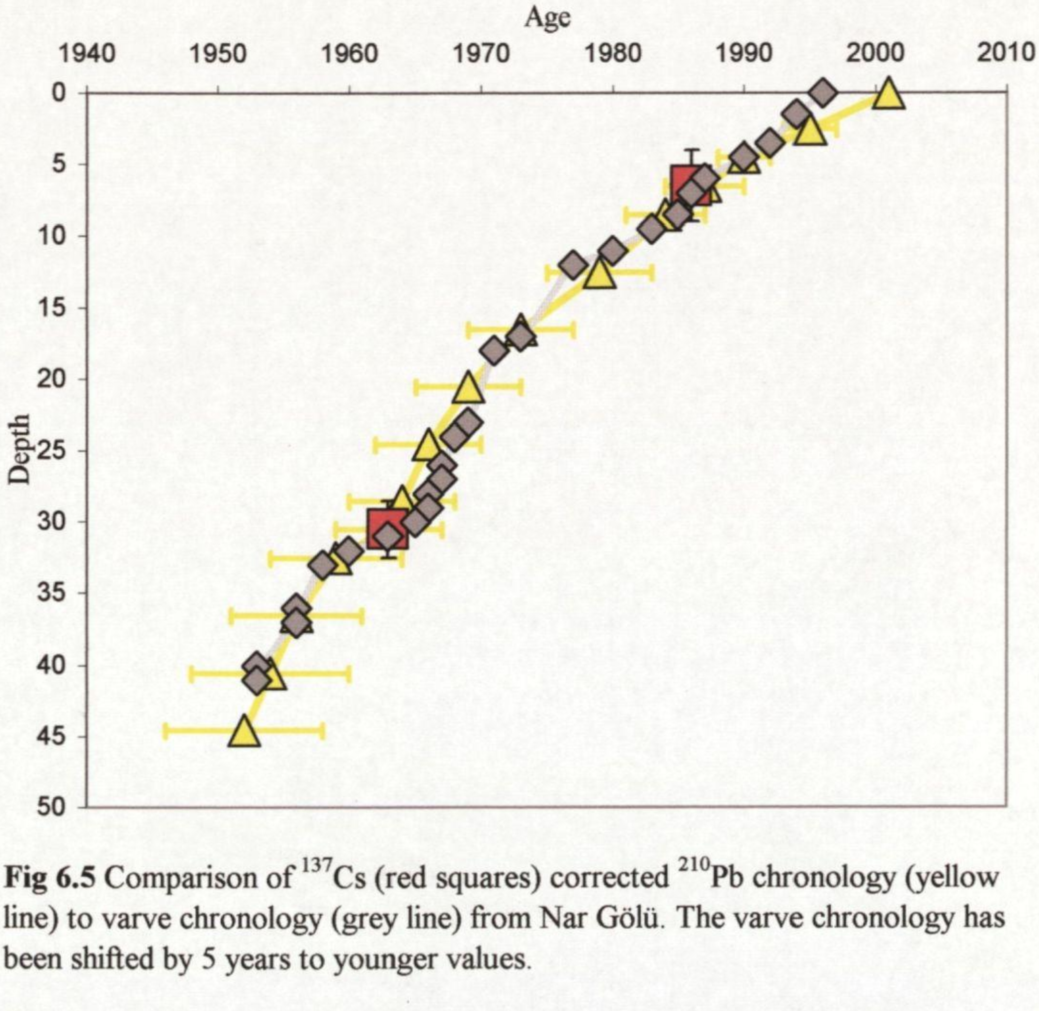

Fig 6.5 Comparison of ^{137}Cs (red squares) corrected ^{210}Pb chronology (yellow line) to varve chronology (grey line) from Nar Gölü. The varve chronology has been shifted by 5 years to younger values.

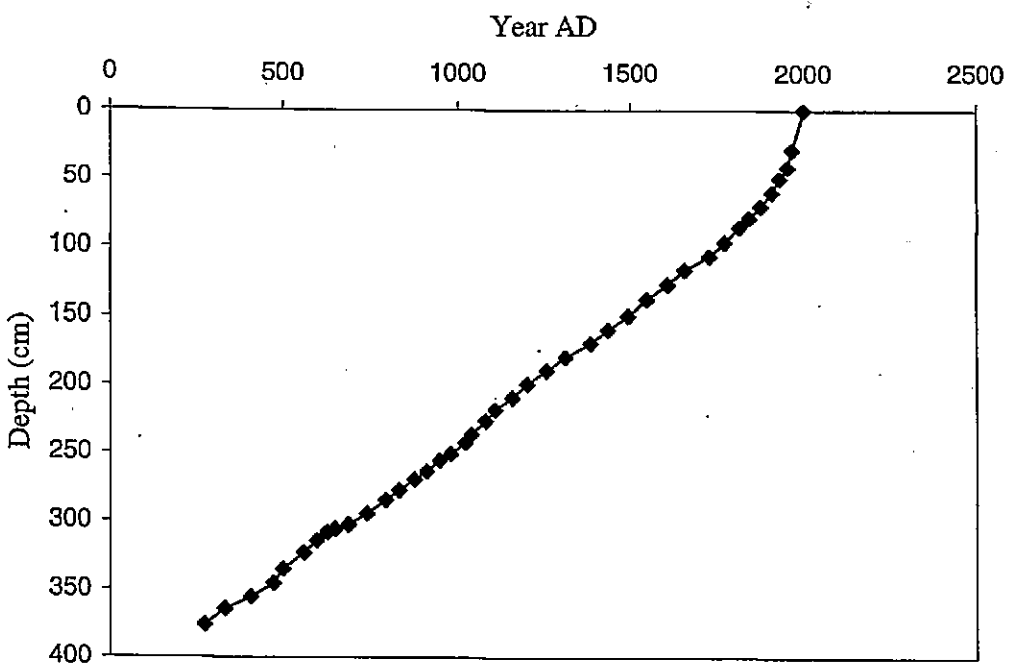

Fig. 6.6 Age depth relationship for varve chronology from Nar Gölü (data in appendix 2).

Table 6.4 Comparison of laminae counts from cores NAR01, M2 and M3.

NAR01 depth	Counts Nar 01	M2	M3	Max	Cumulative count Nar 01	M2	Max
29.5	31	33		33	31	33	33
42.5	13	13		13	44	46	46
50.5	23	23		23	67	69	69
60.5	22	26	26	26	89	95	95
70.5	33	33	30	33	122	128	128
79	32	32	33	33	154	160	161
85.5	27	27	27	27	181	187	188
96.5	43	44	44	44	224	231	232
106.5	45	48	47	48	269	279	280
116.5	70	70	68	70	339	349	350
127	50	51	53	53	389	400	403
138	60	60	55	60	449	460	463
149.5	55	55	56	56	504	515	519
159.5	58	57	57	58	562	572	577
169.5	51	53	/	53	613	625	630
179.5	73	76	70	76	686	701	706
189.5	56	55	58	58	742	756	764
199.5	56	56	53	56	798	812	820
209.5	42	39	39	42	840	851	862
218.5	50	45	52	52	890	896	914

laminae across the lake. The similarity of the three cores suggests the stratigraphy is constant across the lake basin.

Comparison of the NAR01 counts with the maximum number of laminae in the stratigraphy suggests that errors in the counting of NAR01 are up to 2.5% below (younger) the actual number of laminae, representing 43 years at the base of the sequence. The relationship between the maximum laminae count and the counts from the NAR01 cores can be used to give an error estimate at any point down the core.

Samples from further down the core were radiocarbon dated to try and tie the laminae chronology at depth. The resulting radiocarbon ages were very old in relation to the laminae age by approximately 14,000 years (Table 6.5). This indicates that there may be a source of old carbon feeding into the lake or that ^{14}C is being removed from the lake system prior to sediment formation. These issues will be discussed further in the interpretation of the $\delta^{13}C$ records from Nar later in this chapter.

Table 6.5 AMS Radiocarbon ages from Nar Sediments

Sample Depth (cm)	Laminae No.	Laminae Age (years BP)	Sample Dated	Lab Code	Pre-treatment	Radiocarbon Age (years BP)
162-164	555-575	508-528	Bulk Organic matter	Beta-168920	Acid washes	14320 ± 50
			Bulk carbonate	Beta-169096	none	23450 ±120

6.3 Carbonate Stable Isotope Results

$\delta^{18}O$

Over the whole record (Fig. 6.6) $\delta^{18}O$ values range between +2.4 ‰ and –5.7 ‰ with an average value of –1.4 ‰. There are three relatively large and rapid shifts, from positive to negative values between 486 and 561 AD (+2.4‰ to –5.7‰) and between 1949 and 1987 AD (+0.9‰ to –4.8‰), and from negative to positive values between 1393 and 1429 AD (-4.3‰ to +1.2‰).

From the base of the record, at 276 AD, to 486 AD there is a trend to more positive values with a mean value of +0.7‰.

Between 561 and 1393 AD $\delta^{18}O$ values have a mean of –2.7 ‰. There is a trend to more positive values between 731 (-4.8 ‰) and 861 AD (+0.3 ‰) and then a return to more negative values between 861 and 1036 AD (-4.8 ‰). There then follows a further trend to more positive values until 1186 AD (-0.6 ‰).

The mean value between 1429 and 1949 AD is –0.6 ‰. There is a long-term trend to more negative values between 1429 and 1687 AD (-2.4 ‰), with a short excursion to more positive values reaching 1.0 ‰ in 1600 AD. Between 1687 and 1860 AD the general trend is to more positive values.

Between 1987 and 2001 AD the mean value is –3.8 ‰, with a trend to more positive values.

$\delta^{13}C_{carbonate}$

$\delta^{13}C_{carbonate}$ values (Fig. 6.6) range between +16.3 ‰ and +11.3 ‰ with a mean value of +14.1‰. As in the $\delta^{18}O$ record there are relatively large and rapid shifts in $\delta^{13}C_{carbonate}$ values. These occur between 496 and 556 AD (+15.7 ‰ to +11.8 ‰), 796 to 816 AD (+12.8 ‰ to +14.6 ‰), 1412 to 1417 AD (+13.2 ‰ to +15.4 ‰), and 1971 to 1987 AD (+15.3 ‰ to +11.3 ‰).

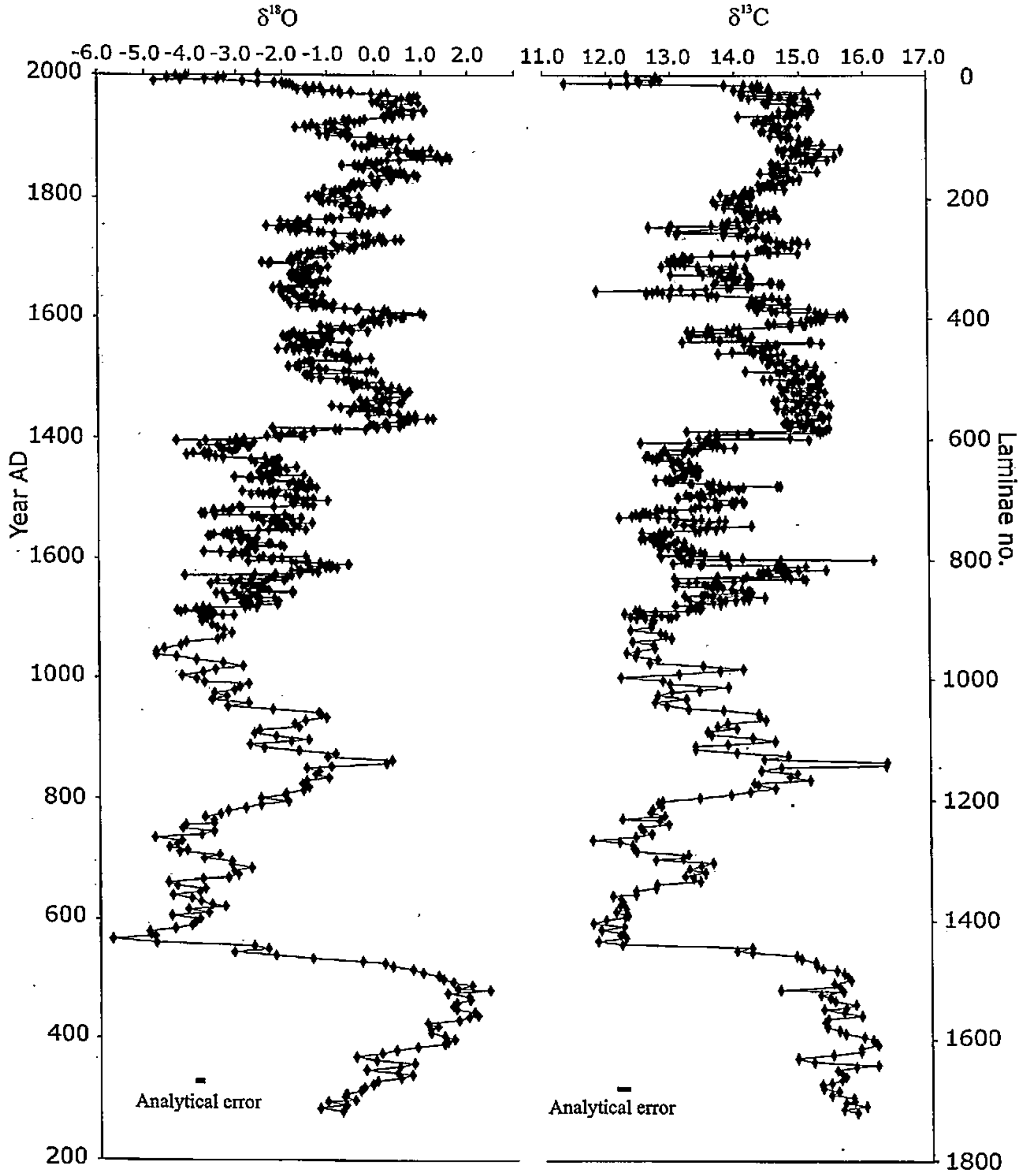

Fig. 6.6 $\delta^{18}O$ and $\delta^{13}C$ results from carbonate laminae through the Nar core sequence (data in appendix 2).

From the base of the record until 496 AD values are fairly constant with a mean value of 15.6 ‰.

Between 556 and 796 AD there is an excursion to more positive values (+13.6 ‰ in 691 AD) with a mean value through the whole section of +12.5‰.The mean value between 816 and 1412 AD is +13.5‰. Values become more negative between 816 and 1041 AD (+12.3 ‰) and then move towards more positive values again until 1180 AD (+15.4 ‰).

Between 1417 and 1971 AD there is a mean value of +14.5‰ with a general trend to more negative values between 1417 and 1686 AD (+12.8 ‰) and then a general trend to more positive values until 1971.

6.3.1 Interpretation of carbonate results

There is considerable variability in both the $\delta^{18}O$ and $\delta^{13}C_{carbonate}$ records and, because of the large number of possible controlling mechanisms on both data sets, as discussed in Chapter 2, it is important to look carefully at the possible driving mechanisms behind these changes.

Carbonate mineralogy

Both oxygen and carbon stable isotope ratios are affected by changes in carbonate mineralogy. For both oxygen and carbon isotopes aragonite has higher values (i.e. more enriched in the heavier isotopes) than calcite. The differences are due to different mineral-water fractionation effects and are thought to be constant at all temperatures so an off set can be applied (Kim and O'Neil, 1997; Grossman, 1984).

There are large changes in the isotope records at times of calcium carbonate mineralogy change in the Nar sequence. $\delta^{13}C$ values are enriched by approximately 1.89 ‰ in aragonite compared to calcite (Grossman, 1984). At Nar the rapid shifts in the $\delta^{13}C$ record are of this magnitude (Fig. 6.8a) so can be explained entirely as a mineralogy change. However, there are other long term trends and larger shifts in the $\delta^{13}C$ record that can not be explained by changes in mineralogy, as the full range in the $\delta^{13}C$ record is 5 ‰.

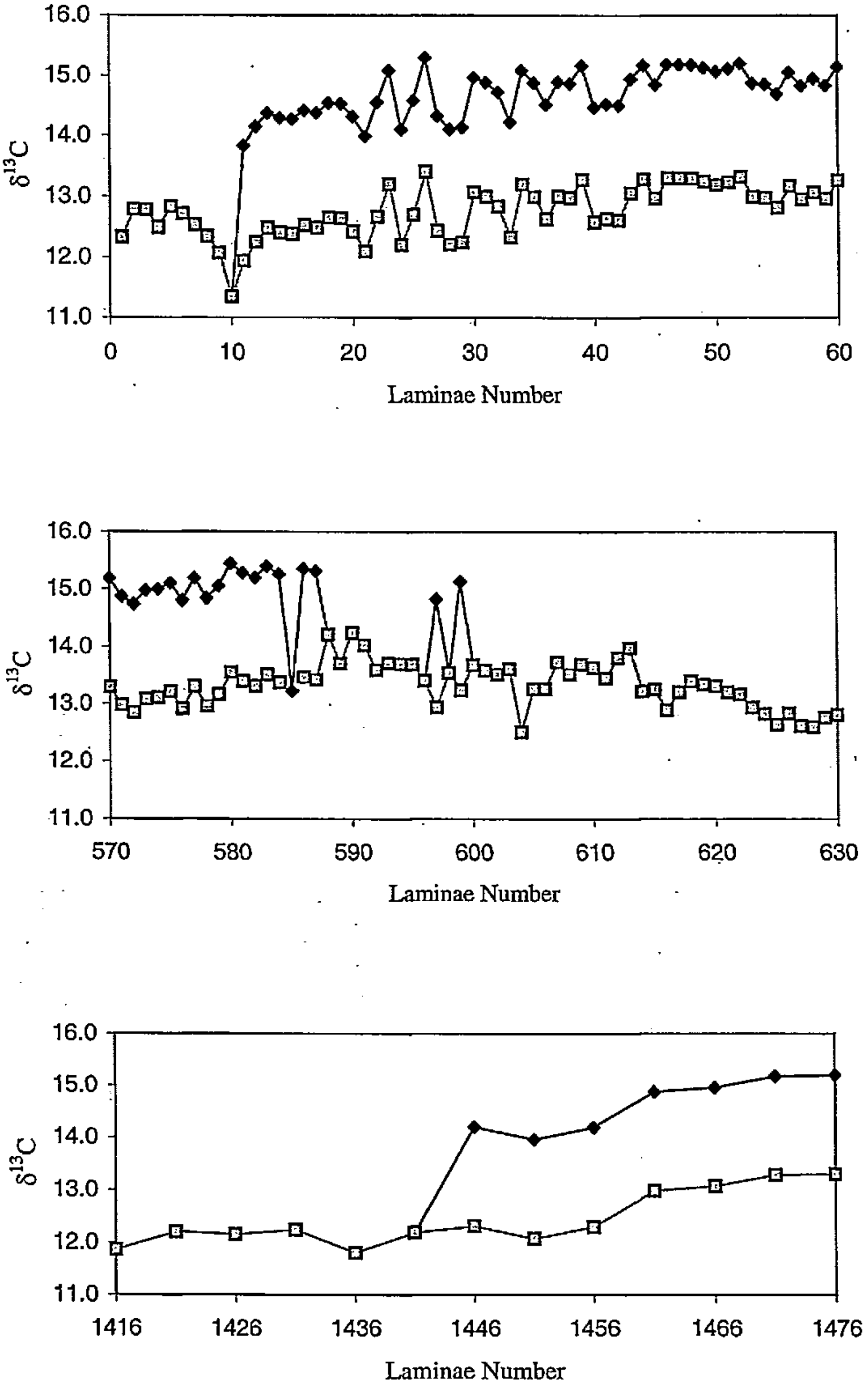

Fig 6.8a $\delta^{13}C$ values through major changes in mineralogy. Showing the raw isotope data (black lines) and values corrected to calcite values (grey lines).

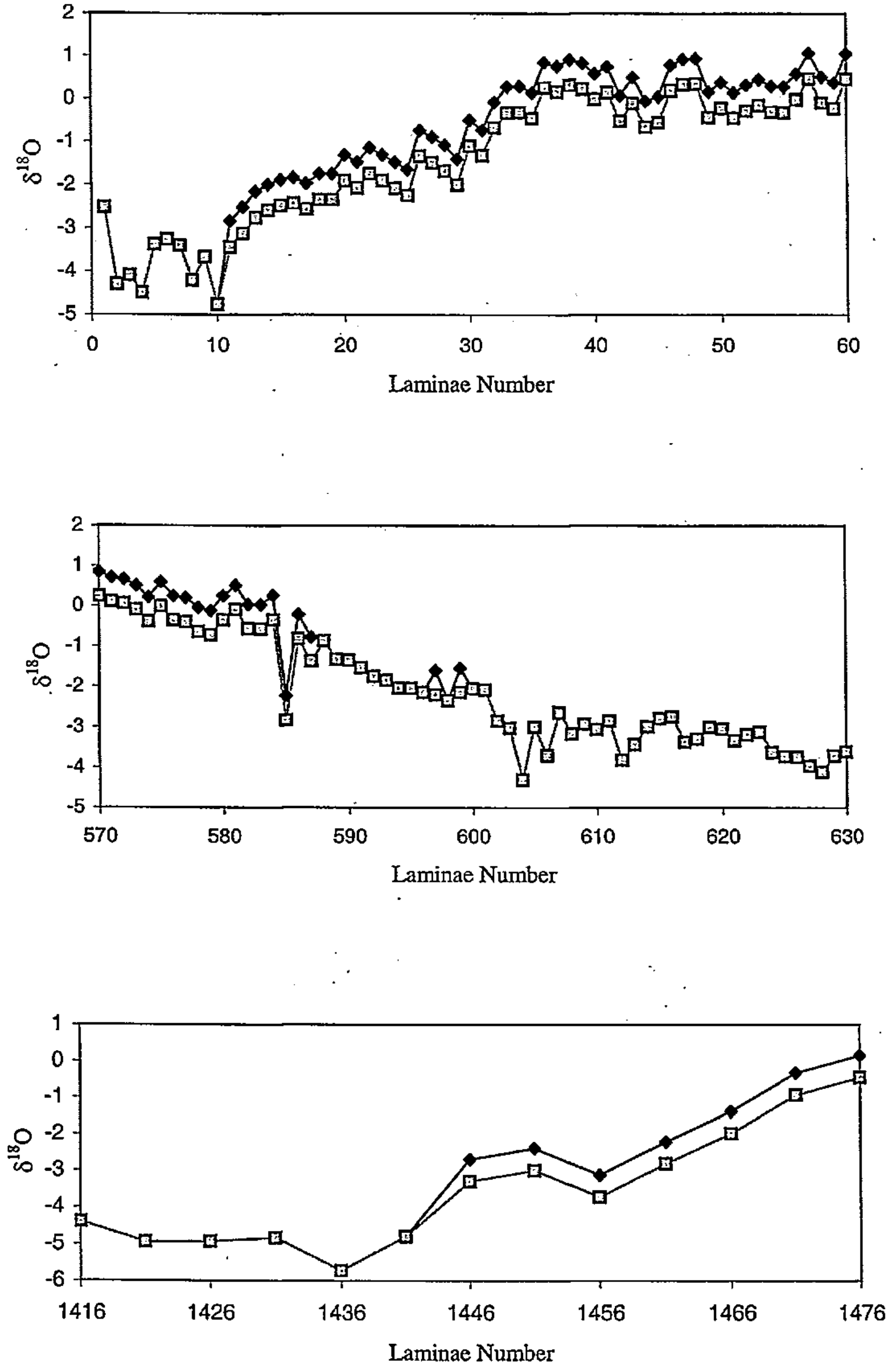

Fig 6.8b $\delta^{18}O$ values through major changes in mineralogy. Showing the raw isotope data (black lines) and values corrected to calcite values (grey lines).

Oxygen isotope values are 0.6 ‰ higher in aragonite in comparison to calcite (Grossman and Ku, 1986). A shift in the isotope record of this amount at times of changing mineralogy (Fig.6.8b) explains some of the variation in the isotope record. However, the changes in $\delta^{18}O$ values are much more gradual than in the $\delta^{13}C$ record and generally much larger than 0.6 ‰. The dominant control on the oxygen isotope values through these times is therefore not the carbonate mineralogy.

Although the shift in $\delta^{18}O$ values is generally more gradual than the change in $\delta^{13}C$ there is still a shift in $\delta^{18}O$, associated with the change in mineralogy between laminae 10 and 11 and between samples 1441-1445 and 1446-1450, that is larger than other change through the time frames plotted in Fig. 6.8. There is no equivalent shift associated with the change in mineralogy between laminae 587 and 588 although there is a similar shift in the $\delta^{18}O$ values earlier in the record, between laminae 603 and 604. All these large shifts occur as the isotope values change between values of ~-2.9‰ and ~-4.7‰. This suggests there may be a hydrological threshold at Nar that is crossed at these points causing a rapid change in $\delta^{18}O$ values.

In general calcite laminae tend to be associated with more negative isotope values (-1.6‰ to -4.8%, mean -3.3‰; for those samples which underwent XRD analysis, Table 1) and aragonite laminae, which are probably formed in more evaporated waters, are associated with more positive values (-2.7‰ to 0.6‰, mean -0.7%; Table 1). Laminae which were a mixture of both calcite and aragonite had a range of between -1.8‰ and 0.3‰ with a mean value of -1.8 ‰. This suggests that there is at least some evaporative control on the isotope values of calcium carbonate in Nar Gölü.

$\delta^{18}O$: $\delta^{13}C$ *co-variation*

The co-variation of oxygen and stable carbon isotope ratios has been used to interpret the hydrological setting of lakes back through time (Talbot, 1990). At Nar the two records co-vary ($r^2 = 0.74$; Fig. 6.9), and this relationship holds throughout the record (Fig. 6.10). Co-varying records tend to be indicative of closed lake systems (Talbot, 1990) where lake water residence time, and the amount of evaporation, often has a key role to play in controlling both oxygen and stable carbon isotope records. Evaporation preferentially removes ^{16}O from the lake waters whereas the increase in $\delta^{13}C$ values during evaporation may be due to three effects (Li and Ku, 1997). Firstly, a reduction of relatively negative

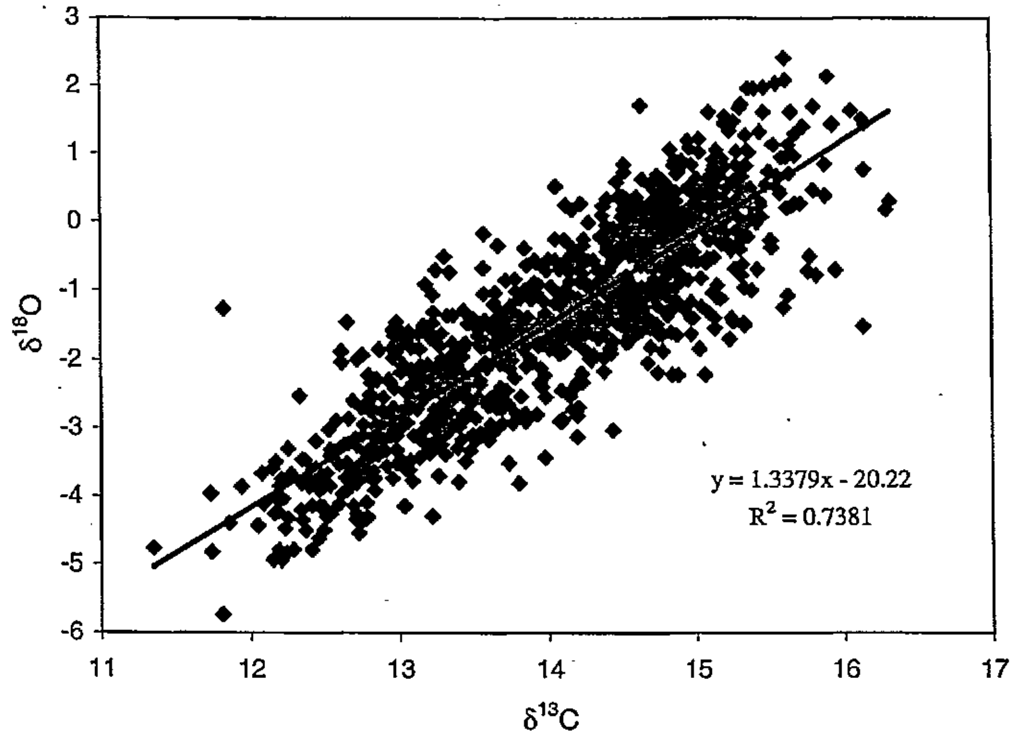

Fig.6.9 $\delta^{18}O$ v. $\delta^{13}C$ for all the Nar carbonate results.

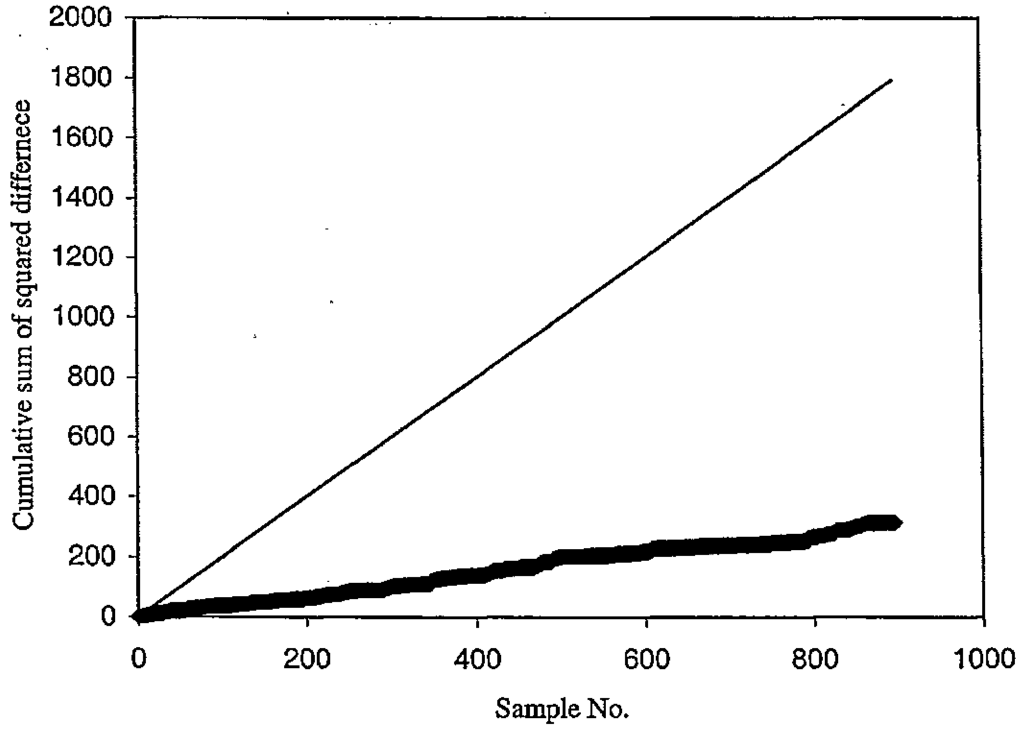

Fig 6.10 Cumulative sum of the square difference for carbonate $\delta^{18}O$ and $\delta^{13}C$ from the annually sampled section of the Nar sequence (thick line). The thin line represents a gradient of two, below which the cumulative sum will fall if the two data sets are positively correlated. Gradient of the Nar data; 0.36; $r^2 = 0.82$; $p=0.000$.

$\delta^{13}C$ groundwaters compared to evaporation will increase $\delta^{13}C$ values of the DIC pool as organic production preferentially removes ^{12}C from the system. Secondly, strong evaporation increases the CO_2 content of the lake causing a net loss of preferentially ^{12}C enriched CO_2, to the atmosphere. Thirdly, a drop in lake levels associated with increased evaporation may lead to mixing of the water column which would increase productivity and remove ^{12}C from the carbon pool. This third process is unlikely to have been as significant at Nar as the laminated sediments suggest the lake has been stratified throughout the sequence.

These processes typically lead to large ranges in $\delta^{18}O$ and $\delta^{13}C$ values, as found at Nar and are typical of small closed lake systems that isotopically respond to changes in the precipitation: evaporation ratio (Leng and Marshall, in press.).

Contemporary waters

Modern lake waters from Nar are enriched in heavy isotopes compared to rainfall (Fig. 5.9). This suggests that evaporation is an important driver of lake water isotope ratios (δ_l) in this lake. Values are more enriched in summer months than they are in spring (Table 5.1) again suggesting that evaporation: precipitation (E: P) ratios are the dominant control on δ_l as E: P is greater during the summer compared to the relatively wet winter and spring.

Lake hydrological and isotope mass balance calculations from the contemporary lake waters and recent meteorological data (Chapter 5) show that evaporation is responsible for 40-60 % of the flux of water through the lake. This again would suggest evaporation plays an important role in lake hydrology and therefore in controlling δ_l.

Comparison with meteorological records

Tables 6.6 to 6.9 highlight the significant ($p<0.05$) relationships from regression analyses between the Nar $\delta^{18}O$ data and climate variables since 1926 (1927 for winter values, and only between 1965 and 1990 for precipitation values). Tables 6.7 and 6.9 compare smoothed climate variable with the isotope data. Smoothing was done using an 8 year weighted average, where the most recent year has a weighting of eight and the oldest year a weighting of 1 etc., as the hydrological budget indicates that the lake residence time is around 8 years and the most recent years are likely to have a larger influence on the system. All climate data, apart from precipitation, are taken from the Ankara records as they are much longer than those from Derinkuyu, and there is a strong relationship between most of the data sets from the two stations:

Min Temperature	$y = 0.9572x - 29.847$	$R^2 = 0.9023$
Average Temperature	$y = 1.0096x - 2.5511$	$R^2 = 0.9867$
Maximum Temperature	$y = 0.9703x - 10.654$	$R^2 = 0.9823$
Relative Humidity	$y = 0.9563x - 8.1119$	$R^2 = 0.8028$
Precipitation	$y = 0.3385x + 178.26$	$R^2 = 0.1745$

where y = Derinkuyu and x = Ankara.

Prior to regression analysis the oxygen isotope values were corrected to remove shifts in the isotope record due to changes in mineralogy i.e. 0.6‰ was taken off the values from laminae below ten to give them a calcite equivalent isotope value.

Tables 6.6 and 6.7 show the data from regressions using the full $\delta^{18}O$ record. The age model established from the ^{137}Cs-corrected ^{210}Pb dates, where lamina no.6 is taken as 1991 is used. Laminae numbers 1 to 5 are taken to represent 2001, 1999, 1997, 1995 and 1993. Tables 6.8 and 6.9 show the results of regression between the laminae data and meteorological variables between 1926 and 1986, removing any effect of the large shift in the isotope record between laminae 10 and 11 that may not be fully explained by a 0.6‰ correction due to mineralogy. This also allows comparison of calibrations over different time periods to see if any relationships found are constant with time.

The full isotope record calibrated with the raw meteorological data (Table 6.6) shows only one significant relationship, with summer relative humidity ($r^2 = 0.15$). Winter precipitation also shows a significant relationship, although the direction of this relationship suggests that it is an artefact of the data as increased precipitation would lead to more negative isotope values and therefore this relationship, although statistically significant, is theoretically incorrect. In this, and the other calibrations, significant relationships are only highlighted where the relationships make theoretical sense.

For the full record calibrated with the smoothed meteorological variables (Table 6.7) summer relative humidity again shows the strongest relationship with the isotope data ($r^2 = 0.54$). Summer average and maximum temperatures also have significant relationships

Table 6.6 Regression relationships between the Nar $\delta^{18}O$ record (corrected for mineralogy) and Ankara annually and seasonally averaged meteorological variables between 1926 and 2001 (Precipitation relationships are with Derenkuyu values beteen 1966 and 1990). Table shows p-value, the direction of the relationship, and the r^2 value. Significant ($p<0.05$) relationships shaded.

	Annual	Spring	Summer	Autumn	Winter
Min. Temp.	0.020 - 6.3	0.240 - 0.6	0.267 - 1.9	0.762 - 0.0	0.301 - 0.1
Av. Temp	0.838 - 0.0	0.803 - 0.0	0.269 + 0.3	0.116 + 2.2	0.232 - 0.7
Max. Temp	0.429 + 0.0	0.725 + 0.0	0.139 + 1.7	0.041 + 4.6	0.347 - 0.0
Precip.	0.284 + 0.8	0.041 + 13.3	0.738 - 0.0	0.457 - 0.0	0.944 + 0.0
R.H.	0.362 - 0.7	0.674 - 0.0	0.000 [illegible] 15.5	0.071 - 3.3	0.000 + 24.2

Table 6.7 Regression relationships between the Nar $\delta^{18}O$ record (corrected for mineralogy) and smoothed (8 year weighted forward running mean) Ankara annually and seasonally averaged meteorological variables between 1933 and 2001 (Precipitation relationships are with Derenkuyu values beteen 1973 and 1990). Values as in Table 6.5.

	Annual	Spring	Summer	Autumn	Winter
Min. Temp.	0.002 - 13.0	0.001 - 15.2	0.340 - 0.0	0.375 + 0.0	0.021 - 6.9
Av. Temp	0.461 + 0.0	0.177 - 1.3	0.000 + 25.3	0.004 + 11.3	0.068 - 3.8
Max. Temp	0.005 + 10.4	0.484 + 0.0	0.000 + 28.1	0.008 + 9.4	0.466 - 0.0
Precip.	0.010 [illegible] 29.0	0.099 - 10.2	0.264 + 1.8	0.738 + 0.0	0.1000 + 10.1
R.H.	0.289 - 0.2	0.35 - 2.0	0.000 [illegible] 53.7	0.719 - 0.0	0.000 + 24.1

Table 6.8 Regression relationships between the Nar $\delta^{18}O$ record (corrected for mineralogy) and Ankara annually and seasonally averaged meteorological variables between 1926 and 1986 (Precipitation relationships are with Derenkuyu values beteen 1966 and 1986). Values as in Table 6.5.

	Annual	Spring	Summer	Autumn	Winter
Min. Temp.	0.522 - 0.0	0.560 - 0.0	0.384 + 0.0	0.952 + 0.0	0.640 - 0.0
Av. Temp	0.470 + 0.0	0.927 + 0.0	0.022 + 7.0	0.331 + 0.0	0.565 - 0.0
Max. Temp	0.439 + 0.0	0.790 + 0.0	0.104 + 2.8	0.425 + 0.0	0.715 - 0.0
Precip.	0.218 + 3.0	0.476 + 0.0	0.769 + 0.0	0.211 - 3.3	0.060 + 13.0
R.H.	0.933 - 0.0	0.870 - 0.0	0.210 - 1.0	0.461 - 0.0	0.001 + 15.9

Table 6.9 Regression relationships between the Nar $\delta^{18}O$ record (corrected for mineralogy) and smoothed (8 year weighted forward running mean) Ankara annually and seasonally averaged meteorological variables between 1933 and 1986 (Precipitation relationships are with Derenkuyu values beteen 1973 and 1986). Values as in Table 6.5.

	Annual	Spring	Summer	Autumn	Winter
Min. Temp.	0.174 - 1.7	0.004 - 13.0	0.011 + 10.2	0.032 + 6.8	0.146 - 2.2
Av. Temp	0.069 + 4.4	0.374 - 0.0	0.000 + 56.5	0.007 + 17.1	0.260 - 0.6
Max. Temp	0.005 + 12.7	0.278 + 0.4	0.000 + 49.2	0.002 [illegible] 15.1	0.650 + 0.0
Precip.	0.068 - 17.5	0.905 - 0.0	0.020 [illegible] 30.0	0.005 + 42.9	0.025 + 27.8
R.H.	0.707 + 0.0	0.299 - 0.2	0.000 [illegible] 29.3	0.060 + 4.9	0.001 + 17.6

although not as strong ($r^2 = 0.25$ and 0.28 respectively). There are also significant, but weak, relationships with autumn average temperatures ($r^2 = 0.11$) and annual rainfall ($r^2 = 0.29$).

For the data between 1926 and 1986 (Tables 6.8 and 6.9) only summer average temperatures show any significant relationship when calibrated with the raw meteorological data, although it is very weak ($r^2 = 0.07$). With the smoothed climate data all summer variables show significant relationships, although precipitation relationships here are made with very few variables (n=14). The strongest relationships are with average and maximum summer temperatures ($r^2 = 0.57$ and 0.49 respectively).

Table 6.10 shows the corrected $\delta^{13}C_{carbonate}$ regression relationships with the smoothed meteorological data between 1933 and 2001; there are no significant relationships with the raw meteorological data. The only significant relationships are with summer average ($r^2 = 0.24$) and summer maximum temperatures ($r^2 = 0.16$).

Tables 6.11 shows the relationships between $\delta^{13}C_{carbonate}$ and the meteorological data between 1933 and 1986, prior to the shift in mineralogy and the large jump in $\delta^{13}C_{carbonate}$ values. Again there are no significant relationships between the isotope data and the raw meteorological data. Significant relationships with summer average ($r^2 = 0.29$) and summer maximum temperatures ($r^2 = 0.21$) are found as with the 1933 to 2001 record. The relationships with $\delta^{13}C_{carbonate}$ are with similar meteorological variables but not as strong as those with $\delta^{18}O$.

The strongest relationships between the carbonate isotope data and the meteorological variables are therefore with summer temperatures and summer relative humidity (Fig. 6. 11). There is a strong negative relationship between temperature and relative humidity through the whole instrumental record (e.g. $RH = 77.209-1.2414T_{max}$; $r^2 = 0.81$). Due to this relationship if either temperature or relative humidity has a strong correlation with the Nar isotope records then the other will have the opposite relationship. It is unclear which of these factors may be controlling the isotope record, as the relationship between the isotope data and one of these variables could be an artefact of the negative relationship between the two.

Table 6.10 Regression relationships between the Nar $\delta^{13}C$ record (corrected for mineralogy) and smoothed (8 year weighted forward running mean) Ankara annually and seasonally averaged meteorological variables between 1933 and 2001 (Precipitation relationships are with Derenkuyu values beteen 1973 and 1990). Values as in Table 6.5.

	Annual	Spring	Summer	Autumn	Winter
Min. Temp.	0.272 - 0.4	0.189 - 1.2	0.445 + 0.0	0.378 + 0.0	0.234 - 0.7
Av. Temp	0.250 + 0.6	0.914 - 0.0	0.000 + 23.6	0.124 + 2.2	0.218 - 0.9
Max. Temp	0.215 + 0.9	0.757 + 0.0	0.001 + 16.4	0.302 + 0.1	0.331 - 0.0
Precip.	0.147 - 6.8	0.602 - 0.0	0.878 - 0.0	0.172 + 5.4	0.205 + 3.9
R.H.	0.099 + 2.8	0.403 + 0.0	0.034 - 5.6	0.259 + 0.5	0.000 + 33.6

Table 6.11 Regression relationships between the Nar $\delta^{13}C$ record (corrected for mineralogy) and smoothed (8 year weighted forward running mean) Ankara annually and seasonally averaged meteorological variables between 1933 and 1986 (Precipitation relationships are with Derenkuyu values beteen 1973 and 1986). Values as in Table 6.5.

	Annual	Spring	Summer	Autumn	Winter
Min. Temp.	0.787 - 0.0	0.196 - 1.3	0.055 + 5.1	0.210 + 1.1	0.886 - 0.0
Av. Temp	0.171 + 1.7	0.661 - 0.0	0.000 + 28.6	0.134 + 2.4	0.823 - 0.0
Max. Temp	0.138 + 2.3	0.924 + 0.0	0.000 + 21.1	0.250 + 0.7	0.865 + 0.0
Precip.	0.211 - 5.0	0.655 - 0.0	0.199 - 5.6	0.156 + 8.3	0.176 + 7.0
R.H.	0.024 + 7.7	0.142 + 2.2	0.066 - 4.8	0.050 + 5.4	0.000 + 33.4

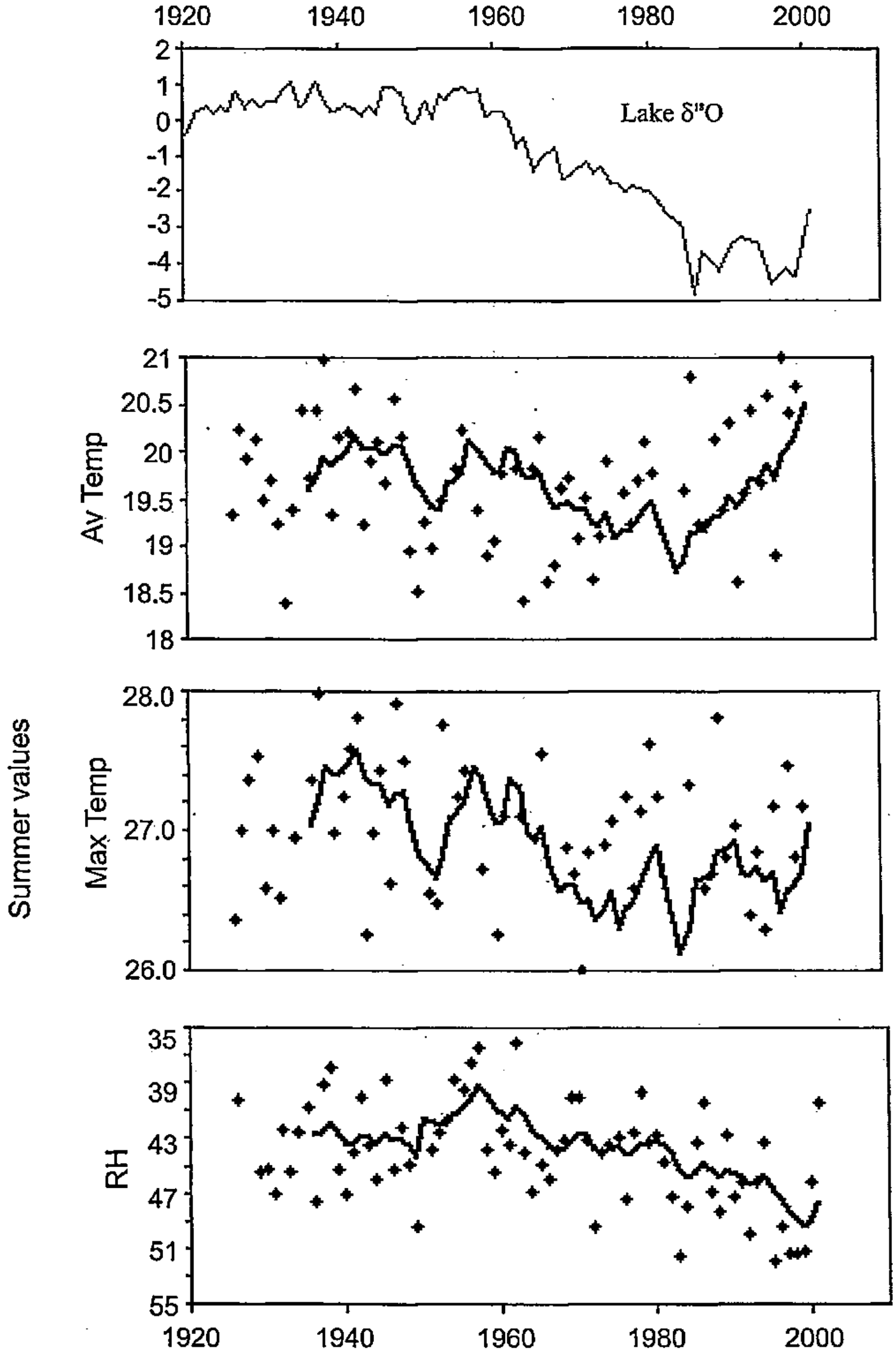

Fig. 6.11 The corrected Nar $\delta^{18}O$ record plotted with summer maximum temperature, summer average temperature and summer relative humidity (both raw (points) and 8 year smoothed (line) meteorological variables are plotted).

Testing the relationships

Possible errors in the chronology or a lag in lake response to climate change may affect the relationships observed above. Regression analyses were therefore carried out with the 8 year smoothed summer average and summer maximum temperatures between 1933 and 1986 and the $\delta^{18}O$ record from Nar, shifting the Nar record by 1 or two years either side of the direct comparison (where laminae 11 is taken to be 1986) to see if this made any difference to the regression relationships (Table 6.12).

The strongest relationships are found when laminae no. 11 is taken to be 1985 rather than 1986 ($r^2 = 0.49$ compared to $r^2 = 0.55$ for summer maximum temperature). It is impossible to know whether this is due to errors in the chronology or because the lake is responding to the previous 8 years' climate rather than the previous 7 years' and the current year's climate.

Looking at the regression equations there is little difference between the relationships from the two different scenarios. When laminae 11 is taken to be 1986 $\delta^{18}O$ = (2.06 x sum. av. temp.) – 45.5, when it is taken to be 1985 $\delta^{18}O$ = (2.11 x sum. av. temp.) – 47.1. $\delta^{18}O$ therefore becomes enriched by ~2‰ for each degree of temperature change based on this correlation.

Additionally, the ^{137}Cs age model may be wrong. Regression analyses run between 8 year weighted average summer meteorological variables and the Nar $\delta^{18}O$ data between 1933 and 2001, taking the laminae counts as the only dating control with laminae number 1 representing 2001 and laminae number 2 representing 2000 etc., shows different strength relationships than the relationships found with the ^{137}Cs corrected varve chronology (Table 6.13). Relative humidity and maximum temperature show strong and significant relationships with the Nar $\delta^{18}O$ record using both chronologies although the relationship with relative humidity shows a stronger relationship with the varve chronology ($r^2 = 0.61$) compared to the ^{137}Cs corrected chronology ($r^2 = 0.54$).

Summer climatic conditions have been shown to have the strongest and most significant relationships with the Nar isotope records. Comparisons were therefore made with the different monthly values to see if one particular month had the most influence on this relationship. The $\delta^{18}O$ record was therefore compared to 8-year weighted average values of monthly data for summer average temperature and summer relative humidity (Table 6.14).

Table 6.12 Regression analyses with changing chronology for the Nar $\delta^{18}O$ data. Values as in Table 6.5.

Lamina 11 =	1988	1987	1986	1985	1984
Summer Average Temperature	0.000	0.000	0.000	0.000	0.000
	+	+	+	+	+
	53.3	5.1	56.5	**57.9**	55.2
Summer Maximum temperature	0.000	0.000	0.000	0.000	0.000
	+	+	+	+	+
	43.3	54.6	49.2	**55.0**	53.4

Table 6.13 Regression analysis between 8 year weighted average summer meteorological variables and Nar $\delta^{18}O$ record between 1933 and 2001 with no ^{137}Cs correction to varve chronology. Values as in Table 6.5.

Relative Humidity	Min. Temperature	Av. Temperature	Max Temperature
0.000	0.004	0.098	0.000
-	-	+	+
61.1	12.5	2.0	22.9

Table 6.14 Regression analyses with monthly meteorological values and the Nar $\delta^{18}O$ record. Values as in Table 6.5.

(a) Monthly with smoothed met data (1926 –2001)

	May	June	July	August	September
Summer RH	0.864	0.075	0.002	**0.000**	0.343
	+	-	-	-	-
	0.0	3.5	12.4	**31.3**	0.0
Summer Av. Temp.	0.078	0.057	0.037	**0.016**	0.745
	+	+	+	+	+
	3.4	4.2	5.3	**7.5**	0.0

(b) Monthly with smoothed met data (1926 –1986)

	May	June	July	August	September
Summer RH	0.032	0.032	0.678	**0.003**	0.546
	+	+	+	-	+
	6.8	6.8	0.0	**14.3**	.0
Summer Av. Temp.	0.0001	0.0001	0.000	**0.000**	0.013
	+	+	+	+	+
	19.1	19.1	30.6	**35.7**	9.6

For both meteorological variables, and in both the 1926 –2001 and 1926 –1986 cases, August values were shown to have the strongest relationships with the isotope records. As with the seasonal analyses, for the full record summer relative humidity shows the strongest relationships, and for the shorter time frame summer average temperature shows the strongest relationships.

Different smoothing of the meteorological data were also used, to see if the isotope relationships were stronger with more smoothed records, which may be the case if the lake has a longer residence time than estimated in Chapter 5. For the 1926 to 2001 record the strongest relationship between summer relative humidity and the $\delta^{18}O$ record is when a 14 yr. weighted average is used ($r^2 = 0.62$). For the average summer temperature record and the $\delta^{18}O$ record between 1926 and 1986, r^2 values are 0.75 with a 14 year weighted average, and increase further with longer smoothing. However, from the calculated water balance the maximum residence time of the lake, with the current hydrological conditions, is limited by the amount of evaporation, as this is the minimum possible flux through the lake. For the lake in 2001 the residence time must be less than 13.5 years. With a 13 year weighted average the r^2 values for the two relationships are 0.61 and 0.74 respectively.

Summary of meteorological comparisons

From comparisons with meteorological data it can be shown that the Nar Gölü $\delta^{18}O$ and $\delta^{13}C$ records have strong and significant relationships with summer temperature and summer relative humidity. These relationships are strongest when the meteorological data are smoothed. The relationships are stronger with longer smoothing of the meteorological record suggesting the lake may be responding to more than the 8 years suggested as the residence time by the mass balance models in Chapter 5.

Temperature and relative humidity influence both the amount, and isotope composition, of evaporation and these relationships would again suggest that the amount of evaporation is the dominant control on the lake $\delta^{18}O$ record.

Non-climatic factors

As well as the climatic factors discussed above it is possible that there are non-climatic factors controlling these two records. In particular changes in the groundwater regime may bring more or less water into the system. An increase in groundwater input would lead to more negative $\delta^{18}O$ and $\delta^{13}C$ values, and vice versa. This would be most likely to lead to rapid shifts in the lake system, such as the rapid shift recorded between laminae 587 and 588. However, it has been shown that the shift in $\delta^{13}C$ values here can be explained entirely by the change in mineralogy, suggesting that changes in groundwater input may not be the cause of these shifts.

6.3.2 Additional controls on $\delta^{13}C_{carbonate}$

Apart from the strong co-variation with the $\delta^{18}O$ record the most notable thing about the $\delta^{13}C$ record is the extremely positive overall values, between +11.3 ‰ and +16.3‰. Most lake water $\delta^{13}C$ values range between values similar to rivers and groundwaters, ~ -10‰, to values associated with equilibration with atmospheric CO_2, ~ +2‰ (Valero-Garces *et al.*, 1999). Groundwaters in the Nar catchment have $\delta^{13}C$ values between -14.3 and -10.7‰, suggesting there are in-lake processes leading to the extremely ^{13}C-enriched $\delta^{13}C$ values of the lake waters.

There are several possible controls which would lead to extremely positive values for $\delta^{13}C_{carbonate}$ and these are discussed here in the context of the Nar lake system.

Physical processes: Preferential degassing of ^{12}C enriched CO_2 from the hot springs may lead to a source of heavy $\delta^{13}C$. However, the $\delta^{13}C$ values of the hot springs are similar to the normal springs in the catchment (Table 5.1), around –13‰, and this would suggest this is not the source of heavy $\delta^{13}C$. Heating of the lake waters by the hot springs would also lead to increased CO_2 degassing from the lake waters, again leading to a ^{13}C enrichment of lake water CO_2. This would also lead to variations in the $\delta^{18}O$: δD relationship as observed in other volcanic lakes (Fig. 2.6). If Nar is compared to the other lakes in the region (Fig. 6.12) there is no evidence that there is significant impact of the hot spring waters on the lake's evaporation regime.

Additional to the above effects on the lake's carbon budget, the radiocarbon ages from the sediments suggest that there is a source of old carbon entering the lake. It is unlikely that this is due to old carbonate rocks as there are no carbonate rocks in the lake catchment or in the surrounding area, which is dominantly volcanic. It is possible that old groundwaters enter the lake, leading to this old carbon effect. Alternatively, volcanic CO_2 can be ^{14}C-free and may therefore lead to an ageing effect for the radiocarbon dates (Olsson, 1986).

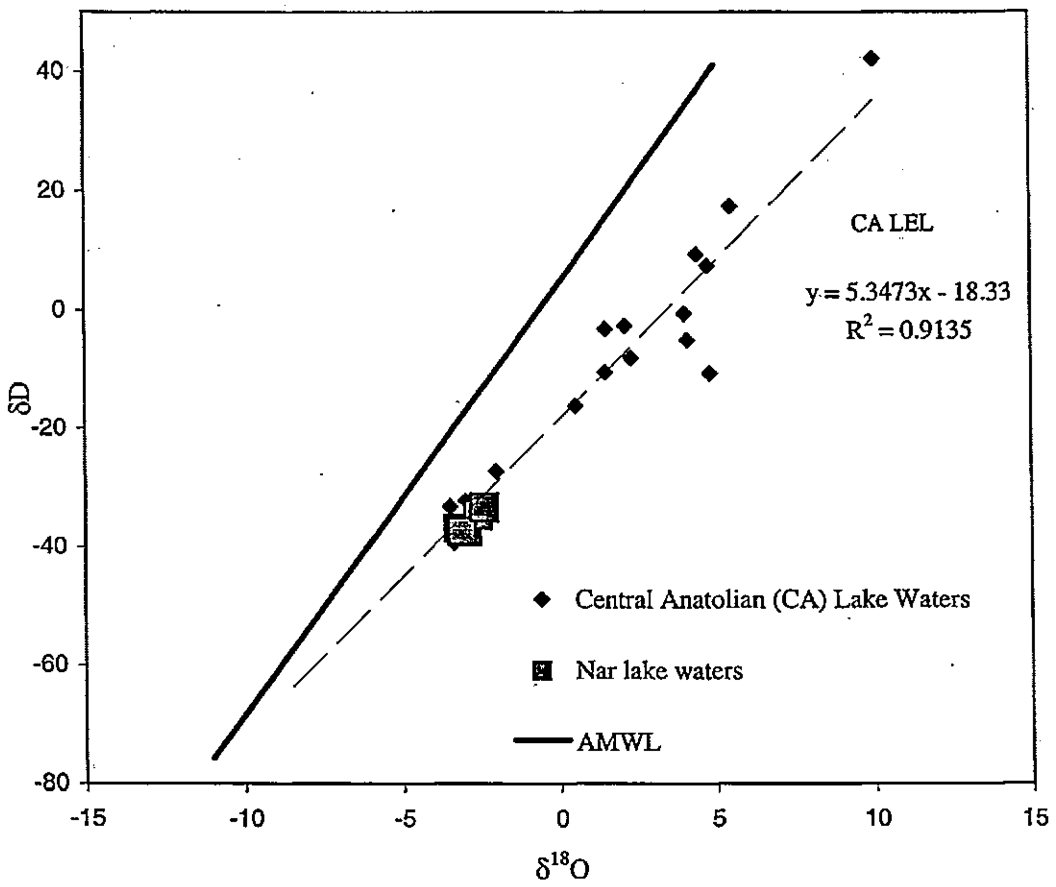

Fig. 6.12 Comparison of Nar waters to other lakes in the region (within the same rainfall regime as described by Türkeş, 1995, Fig. 3.4). There is no evidence of extreme deviation from the Local Evaporation Line of the Nar waters due to geothermal heating.

Old groundwaters would not account for the positive $\delta^{13}C$ values unless they had undergone the processes described above and were a constant factor through the analysed time period. Current groundwaters do not have the strongly positive $\delta^{13}C$ values of the lake waters, suggesting in lake processes are responsible for these positive values. ^{14}C-free volcanic CO_2 is probably the best explanation for the old radiocarbon ages, however as discussed above does not account for the enriched $\delta^{13}C$ values through increased degassing in the lake system.

Biological processes: Diagenesis of organic matter from organic rich marine or lacustrine rocks produces CO_2 enriched in ^{13}C and is commonly associated with carbonate precipitation (Valero-Garces *et al.*, 1999). However there are no organic rich geological units in the Nar region, which is dominated by volcanics, and the carbonates have been observed to be precipitated within the lake.

High productivity can also lead to increased $\delta^{13}C$ values, as ^{12}C is preferentially removed from DIC by organic matter. However the highest values recorded due to this process are around 6‰ (Stiller and Kaufman, 1985), not enough to explain all the enrichment in the Nar system. Where this does occur, it has been explained as a result of mixing following a fall in lake level (Li and Ku, 1997) causing increased nutrient supply to the surface waters. At Nar the sediment sequence is laminated throughout, even in cores taken at a current water depth of 15m. It is therefore likely that the lake has been stratified through the entire time frame analysed and therefore this would not lead to a sudden change in productivity. Values are also heavy throughout the record suggesting that whichever process is causing these values has occurred through all this time. However, the organic laminae at Nar are primarily composed of aquatic algae (see discussion below) which is incorporated into the lake sediments, thus causing removal of ^{12}C and leading to a ^{13}C enriched carbon pool.

Methanogenesis can occur when anoxic conditions occur at the sediment-water interface. Methane has very light $\delta^{13}C$ values, between –50‰ and –100‰ (Talbot, 1990), and as it is removed form the lake system leads to considerable ^{13}C enrichment of the DIC pool (Bridgwater *et al*, 1999). At Nar the lake bottom waters are probably anoxic (see discussion in Chapter 5), and so this is a possible cause of the enriched $\delta^{13}C$ values in this lake. As the lake sediments are laminated throughout the sequence anoxic bottom waters are likely to have been a constant feature of this lake through the last 2000 years, methanogenesis is therefore a plausible mechanism for the high $\delta^{13}C$ values in this lake.

6.4 Organic laminae results

Due to the amount of material it was not possible to analyse every dark laminae for $\delta^{13}C$ and C/N values, and in some cases there was only sufficient material to measure one of the two variables since they were measured separately.

$\delta^{13}C_{organic}$

Organic matter over the 900 years analysed (Fig. 6.13) had an average $\delta^{13}C_{organic}$ value of –22.4 ‰. Values between 1097 and 1375 AD were more or less constant with a mean value of –23.0 ‰. Values then increased until 1434 AD (-20.0 ‰) before becoming more negative until 1538 AD (-24.9 ‰). Between 1434 and 1960 AD there is a long term trend to more positive values, with a large shift to higher values between 1560 and 1620 AD.. Between 1960 and 2001 AD there is a trend to more negative values.

C/N

From 900 to 200 laminae (1097 to 1797 AD) the C/N ratio of the organic matter in the dark laminae fluctuate between values of 9 and 14 (with a mean value of 11.6; Fig. 6.13) with occasional spikes to high values of around 20. Between 1797 and 1895 AD laminae values steadily increase from around 10 to 17 and then return to values of 9 from 1895 to 2001 AD.

6.4.1 Interpretation of organic results

The C/N ratio depends on the composition of the organic matter. Lake algae have C/N ratios between 7 and 9 (Meyers and Teranes, 2001) whereas terrestrial plants generally have much higher values, with mean values above 17 for C3 plants and above 40 for C4 plants (Fig. 2.8).

The C/N data from Nar suggests that the majority of organic matter in the lake sediments is made up of algal matter and examination of thin sections under the microscope also show the organic laminae to contain many diatom frustules. Trends in the record, such as the increase in values between 1797 and 1895 AD, or the occasional spikes of higher values, could therefore be due to increased inwash from the catchment, an increase in catchment vegetation or macrophyte growth, or a combination of the two. However for most of the record the majority of the organic mater in the lake sediments is from lake algae.

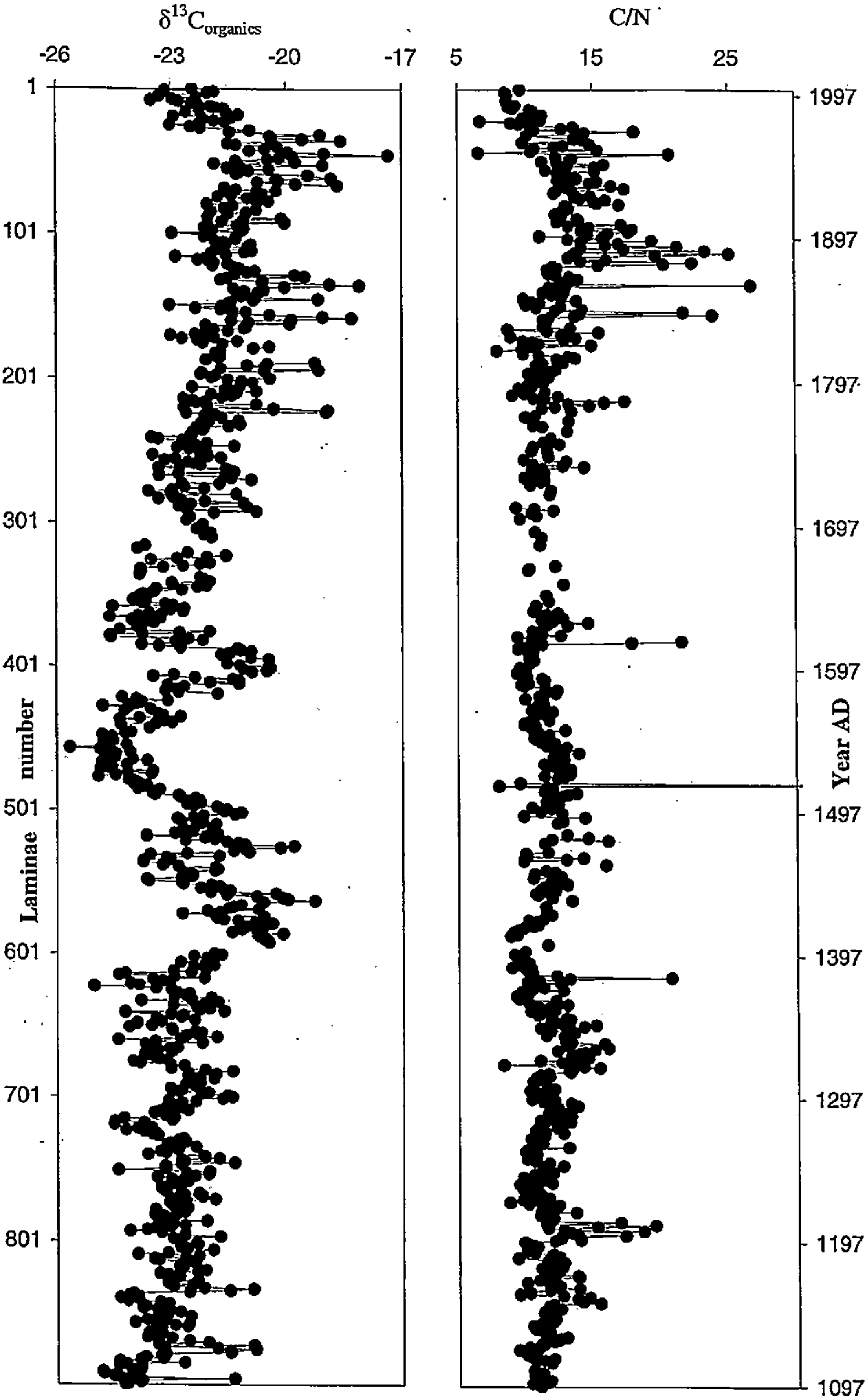

Fig. 6.13 δ^{13}Corganic and C/N results for the top 900 laminae from Nar Gölü (data in appendix 2).

$\delta^{13}C$ values also depend on the make up of the organic matter, C4 plants have values between –10 and –15 ‰, compared to values between –23 and –42 ‰ for C3 plants and lake algae (Meyers and Teranes, 2001; Boutton, 1991). Lake algae $\delta^{13}C$ values depend on the $\delta^{13}C$ of the DIC pool in the lake waters, which vary with changes in productivity or the degree of CO_2 equilibrium (section 2.4).

Plotting $\delta^{13}C$ against C: N ratios (Fig. 6.14), compared to ranges of these values described in other studies, suggests that the organic matter at Nar is a mixture of algae and C3 plants; it is also likely that there is some input from macrophytes. The majority of the data lie closer to the range for algae. $\delta^{13}C$ values appear to be more positive than those found elsewhere, however from the modern lake waters and $\delta^{13}C_{carbonate}$ values, the DIC pool in this lake has been shown to have high $\delta^{13}C$ values and this would account of the more positive values in the $\delta^{13}C_{organic}$ values. Although controls on $\delta^{13}C$ at Nar may have a large non-climatic component it appears that the entire data set has been shifted and that the $\delta^{13}C$ record may therefore still be interpreted as changes in productivity rather than changes in methane production.

If the C: N curve is a proxy of in-wash driven by changes in precipitation it would suggest that there have only been large changes in the precipitation regime at Nar during the last 200 years. In-wash of terrestrial vegetation requires catchment vegetation to be present; it may be therefore that only during the last 200 years has there been a significantly large amount of catchment vegetation, probably as the result of anthropogenic management, to make an impact on the make up of the lake's organic matter.

As the majority of the organic matter at Nar is made up of algae, the $\delta^{13}C$ curve can therefore be interpreted largely as a proxy of palaeoproductivity (Leng and Marshall, in press) with more positive values representing higher productivity and more negative values representing periods of lower productivity.

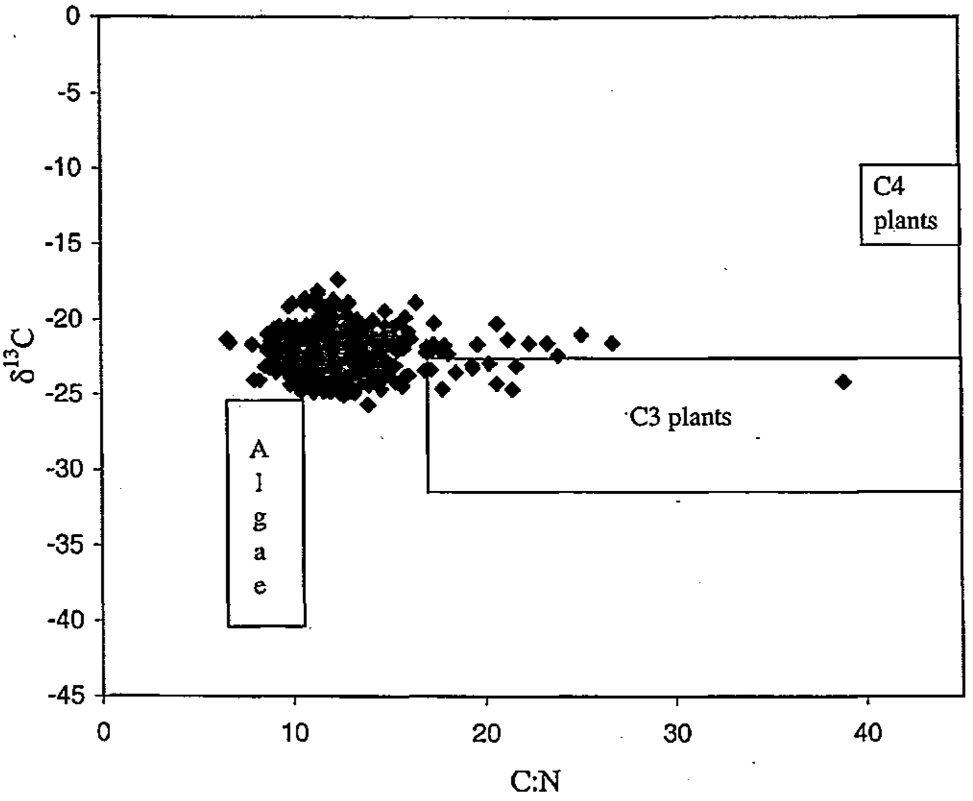

Fig. 6.14 $\delta^{13}C_{organic}$ against C: N ratios from Nar, compared to ranges of plant types from previous studies (Meyers and Teranes, 2001; Leng and Marshall, in press; Fig. 2.8). Values from Nar lie above the normal ranges for algae and C3 plants due to the ^{13}C enriched DIC pool at Nar. Samples between algal or terrestrial plant values are a mix of these two sources, or possibly from lake macrophytes.

Comparison with meteorological records

Tables 6.15 to 6.18 show the significant ($p<0.05$) relationships between meteorological variables and the C: N and $\delta^{13}C_{organic}$ records over the last 75 years.

The strongest relationship for $\delta^{13}C_{organic}$ are with minimum temperatures, particularly with the 8 year smoothed annual ($r^2 = 0.21$) and spring ($r^2 = 0.20$) minimum temperatures (Table 6.16). The relationship is negative; increasing temperatures lead to more negative $\delta^{13}C$ values. As increasing minimum temperatures would tend to be associated with increased productivity this suggests that as productivity increases $\delta^{13}C_{organic}$ values decrease. Although increasing productivity will leave the DIC pool depleted in ^{12}C, leading to more positive values, more organic matter will be produced and fall to the lake bed where if degraded will release ^{12}C back into the lake. For values to become more negative with increased productivity more ^{12}C must be released from the sediments than is taken out of the carbon pool by lake algae, therefore additional terrestrial organic matter would be required. At Nar the organic matter is also known to be preserved in the sediment and C/N ratios suggest input of terrestrial organic matter has reduced over the last 100 years. The relationship found with the meteorological data therefore does not seem theoretically possible.

The strongest significant relationships with the C: N ratios is with spring precipitation with the unsmoothed meteorological data ($r^2 = 0.16$), showing that increases in precipitation lead to higher C: N values, probably due to increased in-wash of catchment organic matter. As the strongest relationship is with the unsmoothed meteorological data it suggests that the C/N record is more sensitive to annual climate variability than the stable isotope proxies. As in-wash is also dependent on the amount of plant material in the catchment and catchment stability there are many non-climatic factors also influencing this record.

Table 6.15 Regression relationships between the Nar $\delta^{13}C_{organic}$ record and Ankara annually and seasonally averaged meteorological variables between 1926 and 2001 (Precipitation relationships are with Derenkuyu values beteen 1966 and 1990). Table shows p-value, the direction of the relationship, and the r^2 value. Significant relationships are highlighted.

	Annual	Spring	Summer	Autumn	Winter
Min. Temp.	0.001 [illegible] 16.3	0.052 - 4.4	0.001 [illegible] 13.6	0.703 - 0.0	0.018 [illegible] 7.5
Av. Temp	0.039 [illegible] 5.1	0.235 - 0.5	0.271 - 0.4	0.221 + 0.8	0.022 [illegible] 6.7
Max. Temp	0.293 - 0.2	0.552 - 0.0	0.443 - 0.0	0.067 + 3.8	0.051 - 4.6
Precip.	0.872 - 0.0	0.576 + 0.0	0.915 + 0.0	0.889 + 0.0	0.467 - 0.0
R.H.	0.787 + 0.0	0.891 + 0.0	0.213 - 0.9	0.230 - 0.7	0.001 + 16.1

Table 6.16 Regression relationships between the Nar $\delta^{13}C_{organic}$ record and smoothed (8 year weighted forward running mean) Ankara annually and seasonally averaged meteorological variables between 1933 and 2001 (Precipitation relationships are with Derenkuyu values beteen 1973 and 1990). Values as in Table 6.5.

	Annual	Spring	Summer	Autumn	Winter
Min. Temp.	0.000 [illegible] 21.2	0.000 [illegible] 19.6	0.088 - 3.4	0.838 + 0.0	0.007 [illegible] 16.9
Av. Temp	0.272 - 0.4	0.054 - 4.5	0.027 + 6.7	0.025 + 6.9	0.003 [illegible] 13.5
Max. Temp	0.745 + 0.0	0.678 - 0.0	0.035 + 6.0	0.019 + 7.6	0.103 - 3.0
Precip.	0.250 - 2.3	0.418 - 0.0	0.204 + 4.0	0.847 - 0.0	0.751 + 0.0
R.H.	0.577 + 0.0	0.878 - 0.0	0.002 [illegible] 15.4	0.623 + 0.0	0.003 + 12.9

Table 6.17 Regression relationships between the Nar C: N record and Ankara annually and seasonally averaged meteorological variables between 1926 and 1986 (Precipitation relationships are with Derenkuyu values beteen 1966 and 1986). Values as in Table 6.5.

	Annual	Spring	Summer	Autumn	Winter
Min. Temp.	0.012 [illegible] 8.1	0.224 - 0.8	0.155 - 1.6	0.613 - 0.0	0.164 - 1.6
Av. Temp	0.273 - 0.3	0.607 - 0.0	0.952 + 0.0	0.781 + 0.0	0.104 - 2.7
Max. Temp	0.490 - 0.0	0.913 + 0.0	0.740 + 0.0	0.374 + 0.0	0.058 - 4.2
Precip.	0.277 + 1.0	0.029 + 16.3	0.815 + 0.0	0.509 - 0.0	0.685 - 0.0
R.H.	0.187 - 1.2	0.226 - 0.8	0.323 - 0.0	0.070 - 3.7	0.001 + 16.3

Table 6.18 Regression relationships between the Nar C: N record and smoothed (8 year weighted forward running mean) Ankara annually and seasonally averaged meteorological variables between 1933 and 1986 (Precipitation relationships are with Derenkuyu values beteen 1973 and 1986). Values as in Table 6.5.

	Annual	Spring	Summer	Autumn	Winter
Min. Temp.	0.064 [illegible] 4.3	0.137 - 2.2	0.270 - 0.4	0.481 + 0.0	0.391 - 0.0
Av. Temp	0.757 + 0.0	0.787 - 0.0	0.108 + 2.8	0.036 + 5.9	0.537 - 0.0
Max. Temp	0.185 + 1.4	0.499 + 0.0	0.085 + 3.5	0.052 + 4.9	0.882 - 0.0
Precip.	0.000 [illegible] 53.8	0.933 + 0.0	0.835 - 0.0	0.635 + 0.0	0.112 + 9.1
R.H.	0.594 - 0.0	0.221 - 0.9	0.005 [illegible] 12.2	0.994 + 0.0	0.052 + 5.0

6.5 Summary and comparison

From the discussion above it can be shown that the $\delta^{18}O$ and $\delta^{13}C_{carbonate}$ records from Nar are controlled predominantly by evaporation during the summer months.

The organic laminae, which are either deposited in spring or autumn, are made up largely of algae and the $\delta^{13}C_{organic}$ record is therefore likely to be a record of changing productivity, although the exact controls on this system are unknown.

For the top 900 laminae in the record relationships between the five proxy records can be compared (Fig. 6.15; Table 6.19). The $\delta^{18}O$ and $\delta^{13}C_{carbonate}$ records co-vary and the controls on these records are discussed in detail above. The $\delta^{13}C_{organic}$ record also appears to co-vary with these other two isotope records ($r^2 = 0.30$ for comparison with $\delta^{18}O$). Although the $\delta^{13}C_{organic}$ record is a lot noisier than the carbonate records the long-term trends are generally the same. This relationship suggests that when the lake is more evaporated and conditions are warmer $\delta^{13}C_{organic}$ values are more positive. The opposite of the relationship found with the meteorological data, suggesting that high productivity is removing ^{12}C from the lake DIC pool rather than adding to it.

The C: N ratios, as discussed above remain more or less constant through the record, apart from during the last 200 years where there is an increase in catchment vegetation washed into the lake probably as a result of anthropogenic management. This suggests that through the last 900 years anthropogenic influences in the catchment have had little impact on the lake system, although this may have to be taken into account when interpreting the record of the last 200 years. This may account for the different relationships found between the $\delta^{13}C_{organic}$ record and meteorological records, during a time where catchment vegetation may have had a non climatic control, and during the longer term record where anthropogenic influence was limited prior to 1800 AD.

The grey-scale record also shows strong relationships with the $\delta^{18}O$ and $\delta^{13}C$ records ($r^2 =$ 0.50 and 0.45 respectively; Table 6.19). Some of this relationship is due to changing mineralogy of the carbonate laminae especially at times of rapid isotope change. The co-variation through the rest of the record is not fully explained although is also partly due to the calcite: aragonite ratio in each lamina.

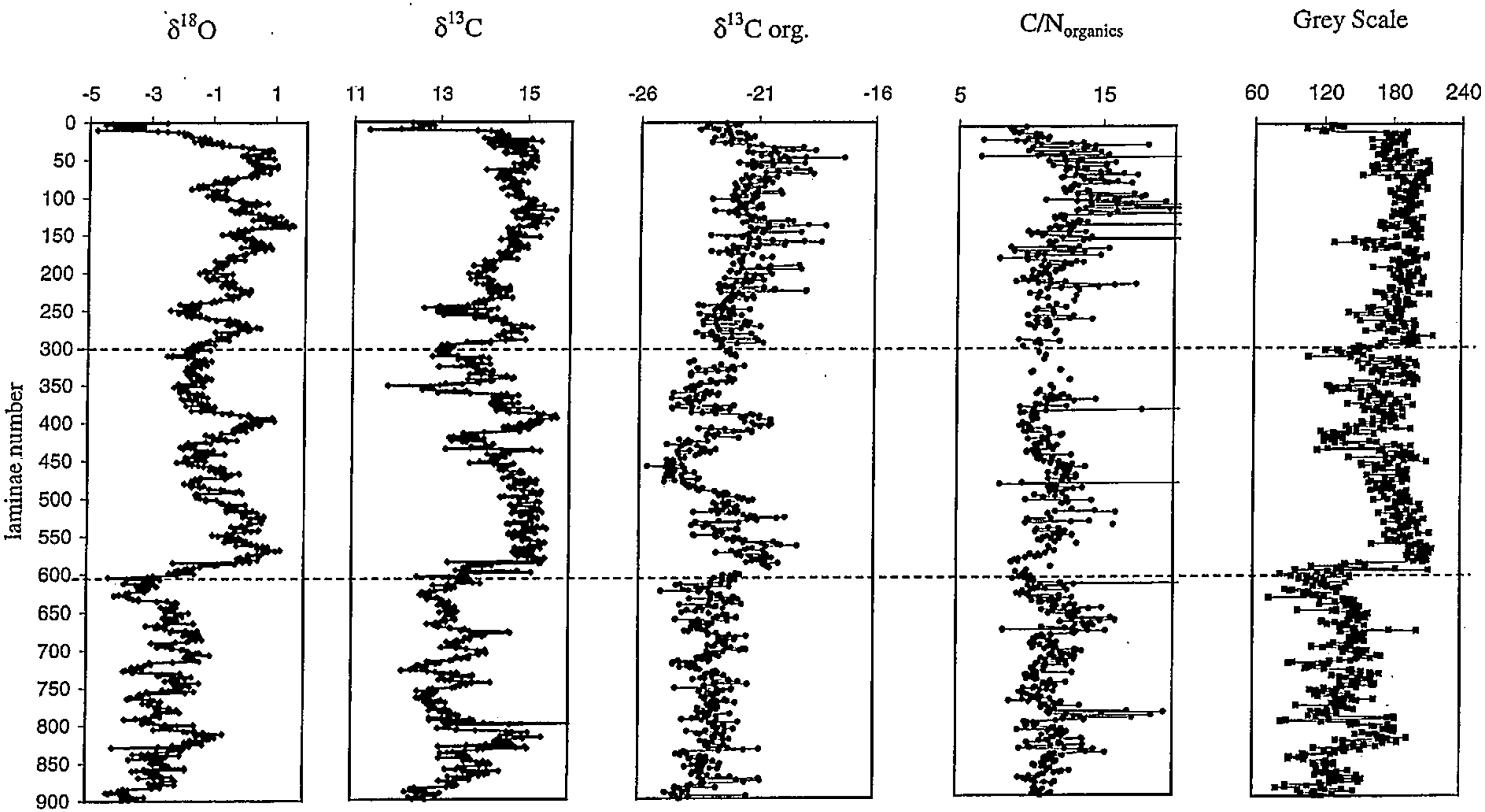

Fig. 6.15 Comparison of 5 proxy records from the top 900 lamiane from Nar Gölü.

Table 6.19 Regression relationships between proxy data sets from the top 900 lamiane from Nar Gölü. p-values, the direction of the relationship, and r^2 values are shown.

		X values			
		$\delta^{13}C_{carbonate}$	$\delta^{13}C_{organic}$	C/N	Grey scale
Y values	$\delta^{18}O$	0.000 + 68.4	0.000 + 30.4	0.000 + 4.5	0.000 + 50.3
	$\delta^{13}C_{carbonate}$		0.000 + 16.5	0.000 + 5.4	0.000 + 45.0
	$\delta^{13}C_{organic}$			0.617 - 0.0	0.000 + 12.8
	C/N				0.000 + 3.5

Chapter 7

BURDUR GÖLÜ – CONTEMPORARY AND PALAEOLIMNOLOGY

7.1 Location and general site description

Lake Burdur is a large (approximately 30km long), deep, non-outlet lake in a northeast to southwest trending graben-like basin in the Taurus mountain zone of southwest Turkey (Fig. 7.1a). The basin is tectonically active, with the last major earthquake in 1971. In 1970 the lake was 77m deep at its deepest point with a lake area of 237 km^2. In 2002 the maximum lake depth was 65m and lake area had reduced by 27% (182.5 km^2), most likely due to the abstraction of in-flowing waters for irrigation (Fig.7.1b; Roberts *et al.*, 2003). Lake volume in 2002 was approximately 3.77×10^9 m^3.

7.2 Catchment Geology

The lake is surrounded by Quaternary deposits (Fig. 7.2) that are particularly well exposed on the southwest lake shore. Most of these deposits are sands and gravels formed in tombolos, beach ridges and Gilbert-type deltas. Debris-flow deposits and subaqeous slump structures are also evident. OSL and radiocarbon dating of these sediments, between 62 and 14 ka BP, suggests that the lake was up to 80m higher than current lake levels at different episodes during this time (Roberts *et al.*, 2003).

On the southeast shore Pliocene lacustrine sediments, including marls, outcrop along most of the length of the lake. At the north east end of the lake the pre-Quaternary geology is composed of upper Palaeocene to Eocene sandstones, conglomerates and limestones (Fig. 7.2). On the northwest shore the northern part if the catchment is composed of Oligocene conglomerates and sandstones with a Mesozoic ophiolite complex outcropping to the south. The pre-Quaternary geology, as well as the Quaternary sediments, suggests a long history of lacustrine activity in the Burdur basin.

The basin is controlled by a series of normal faults (Fig. 7.2) running parallel to each side of the current lake (Price and Scott, 1991 and 1994). Sequence stratigraphic analysis of

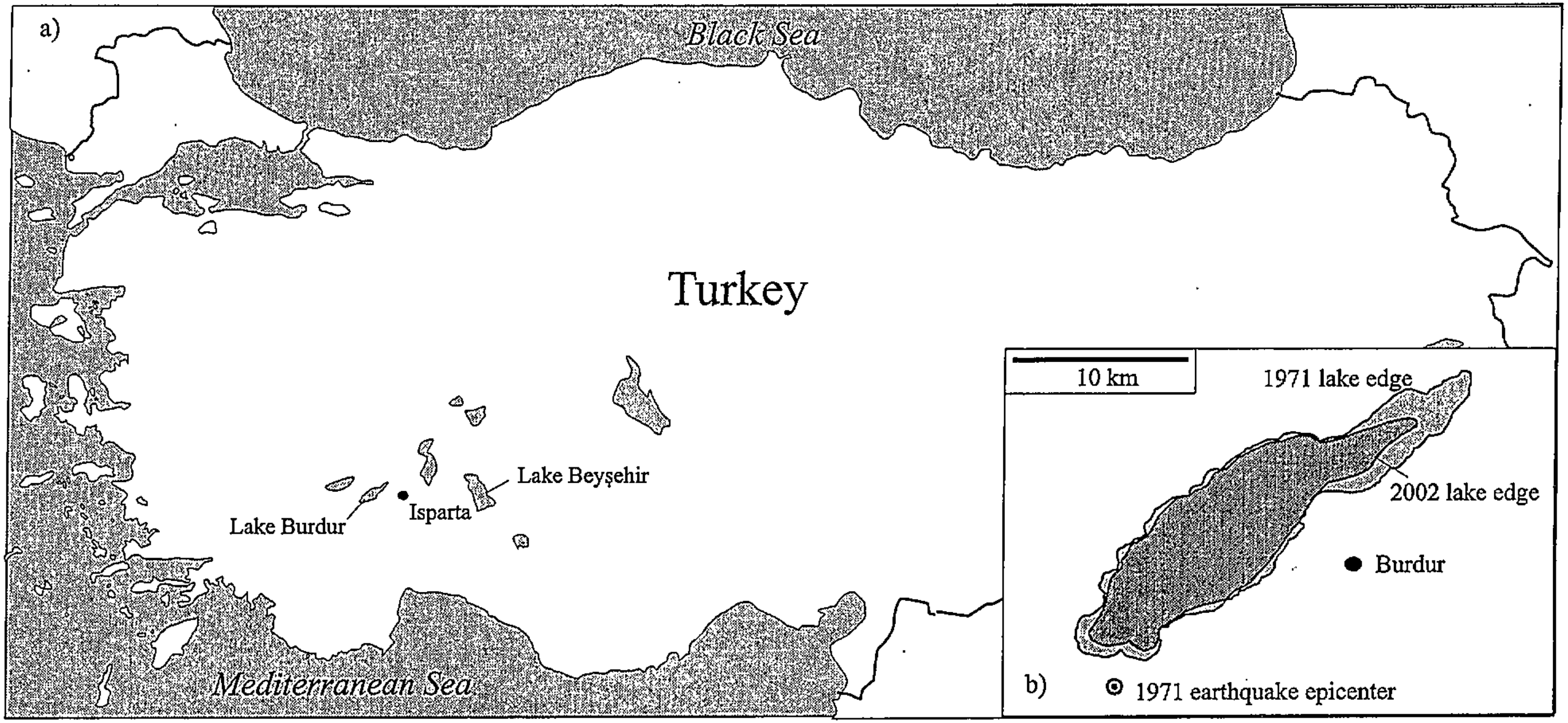
a)
Black Sea
Turkey
Lake Beyşehir
Isparta
Lake Burdur
Mediterranean Sea
10 km
1971 lake edge
2002 lake edge
Burdur
b)
1971 earthquake epicenter

Fig. 7.1 a) Location of Burdur Gölü and other locations mentioned in the text. b) Burdur lake area in 1970 and 2002.

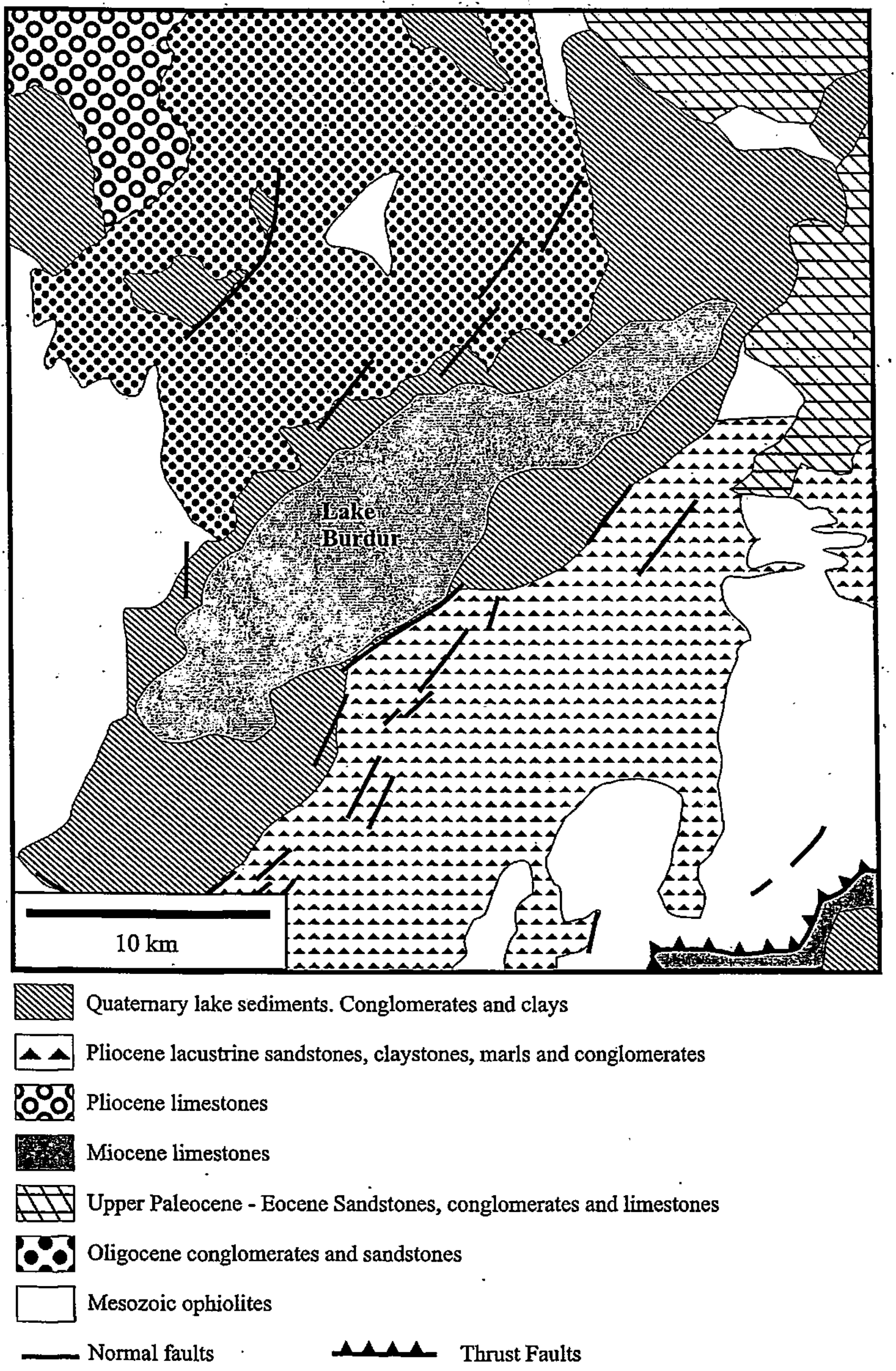
Lake Burdur
10 km
▨ Quaternary lake sediments. Conglomerates and clays
▲▲ Pliocene lacustrine sandstones, claystones, marls and conglomerates
Pliocene limestones
Miocene limestones
Upper Paleocene - Eocene Sandstones, conglomerates and limestones
Oligocene conglomerates and sandstones
Mesozoic ophiolites
Normal faults
Thrust Faults

Fig. 7.2 Geology map of the region around Lake Burdur showing major geological units and major faults (after Price and Scott, 1994; Şenel, 1997).

sub-lacustrine facies, via shallow seismic investigations, suggest movement of the eastern fault at, or towards, the end of the Pleistocene followed by a shift to movement of the western fault. This shift in tectonic activity led to a change in the zones of active sedimentation within the lake (Roberts *et al.*, 2003).

7.3 Climate

Meteorological data are available from Burdur, the major town on the southeast shore of the lake (Fig. 7.1b), between 1929 and 1932 and from 1939 to the present day. For the recent period (1980 to 2001) the warmest months of the year are July and August (average temperatures are 24 to 25 °C), with January and February (average temperatures 2 to 4 °C) the coldest (Fig. 7.3). There is greater variability in winter temperatures compared with summer values. The standard deviation of the maximum monthly temperatures for January and February are 2.5°C and 2.0°C respectively compared to 1.1°C and 1.0°C for July and August.

Total annual precipitation averages 412 ± 78 mm (mean value ± 1σ). January and December are the wettest months, accounting for 28 % of the annual total precipitation, with the driest two months, August and September, accounting for only 6 % of the annual total. However, there is considerable variability in the monthly values (Fig. 7.4), especially in the December and January values.

Evaporation was measured at Burdur, where the average value between 1935 and 1970 was 1072.2 mm yr.$^{-1}$ (Meteoroloji Bülteni, 1974). The value recorded at nearby Beysehir was 987.5 mm yr^{-1}.

These values give an aridity index (P/E) of 0.38.

7.4 Lake Chemistry

The pH and conductivity values suggest the lake is alkaline (pH ~ = 9) and saline, becoming more alkaline and more saline between 1999 and 2002 (conductivity was 32.2 mS in September 1999 and 40.0 mS in July 2002; Table 7.1). Stable isotope values have remained very similar throughout the 4 years where measurements have been taken, although they were significantly lower during April 2002 probably due to spring recharge.

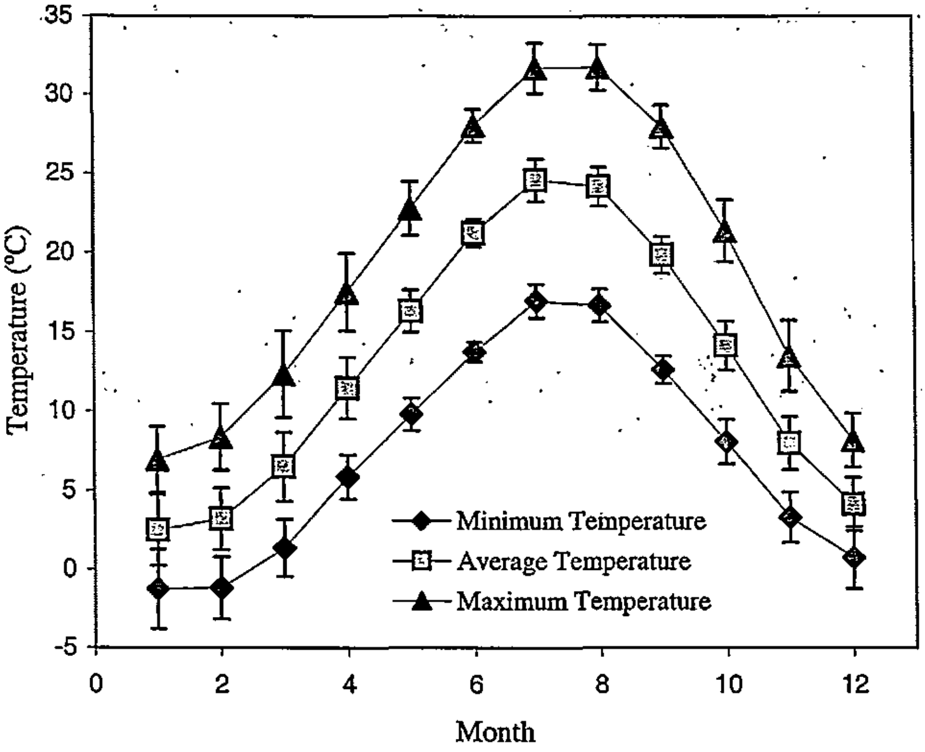

Fig. 7.3 Average monthly temperatures at Burdur between 1980 and 2001. Error bars show standard deviations from the mean through this time period (data from Turkish State Meteorological Service).

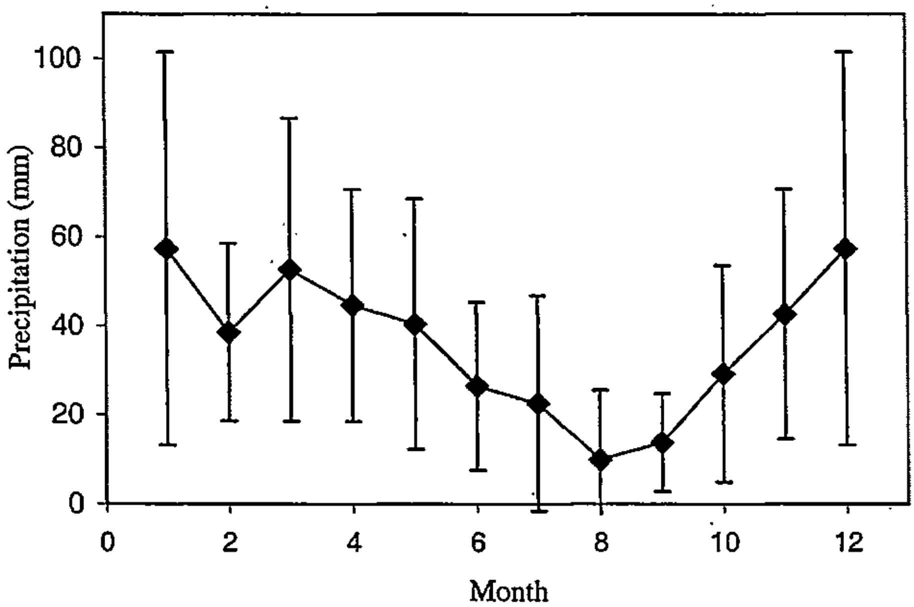

Fig. 7.4 Average monthly values of precipitation at Burdur between 1980 and 2001. Error bars show standard deviations from the mean through this time period (data from Turkish State Meteorological Service).

Table 7.1 Lake Burdur water chemistry measurements.

Sample		Temperature (°C)	Conductivity (mS)	pH	$\delta^{18}O$	δD	$\delta^{13}C$
Location	Depth (m)						
September 1999							
Lake edge		25.0	28.0	8.85			
Lake centre	Surface	23.0	32.2	8.86	3.96	12.1	/
	15m	22.0	31.9	8.85			
July 2000							
Lake edge		28.5	29.52	8.88	4.1	12.1	0.0
July 2001							
Lake centre	Surface	27.5	34.7	9.00	4.2	12.2	2.4
	10	24.6	33.6	8.82			
	15	23.4	33.3	8.89			
	20	19.4	32.9	8.86	4.0	10.5	1.3
	30	18.7	33.7	8.88			
	40	16.4	32.3	8.88			
	50	13.9	28.0	8.83	4.0	9.0	1.1
April 2002							
Lake edge		6.4	/	/	3.6	9.2	-4.5
July 2002							
Lake centre	0	27.6	40.0	9.09	3.9	10.5	-0.1
	10	23.3	39.8	9.03			
	15	13.4	38.9	9.10			
	20	10.0	37.7	9.11	3.8	10.3	-0.3
	30	8.8	38.1	9.16			
	40	8.2	38.0	9.08			
	50	7.4	38.0	9.07	3.8	10.3	/
	55	8.7	38.0	9.14			
Half way between centre and edge		29.2	38.9	8.96	3.8	10.8	-0.2
Lake edge		29.4	39.7	8.95	3.9	12.1	-0.5

Table 7.2 Burdur Gölü major ion water chemistry (g/l) (Roberts, 1980).

Cl^-	SO_4^{2-}	CO_3^-	Mg^{2+}/Ca^{2+}	Na^+	K^+
3.43	6.94	0.32	0.10	4.72	0.04

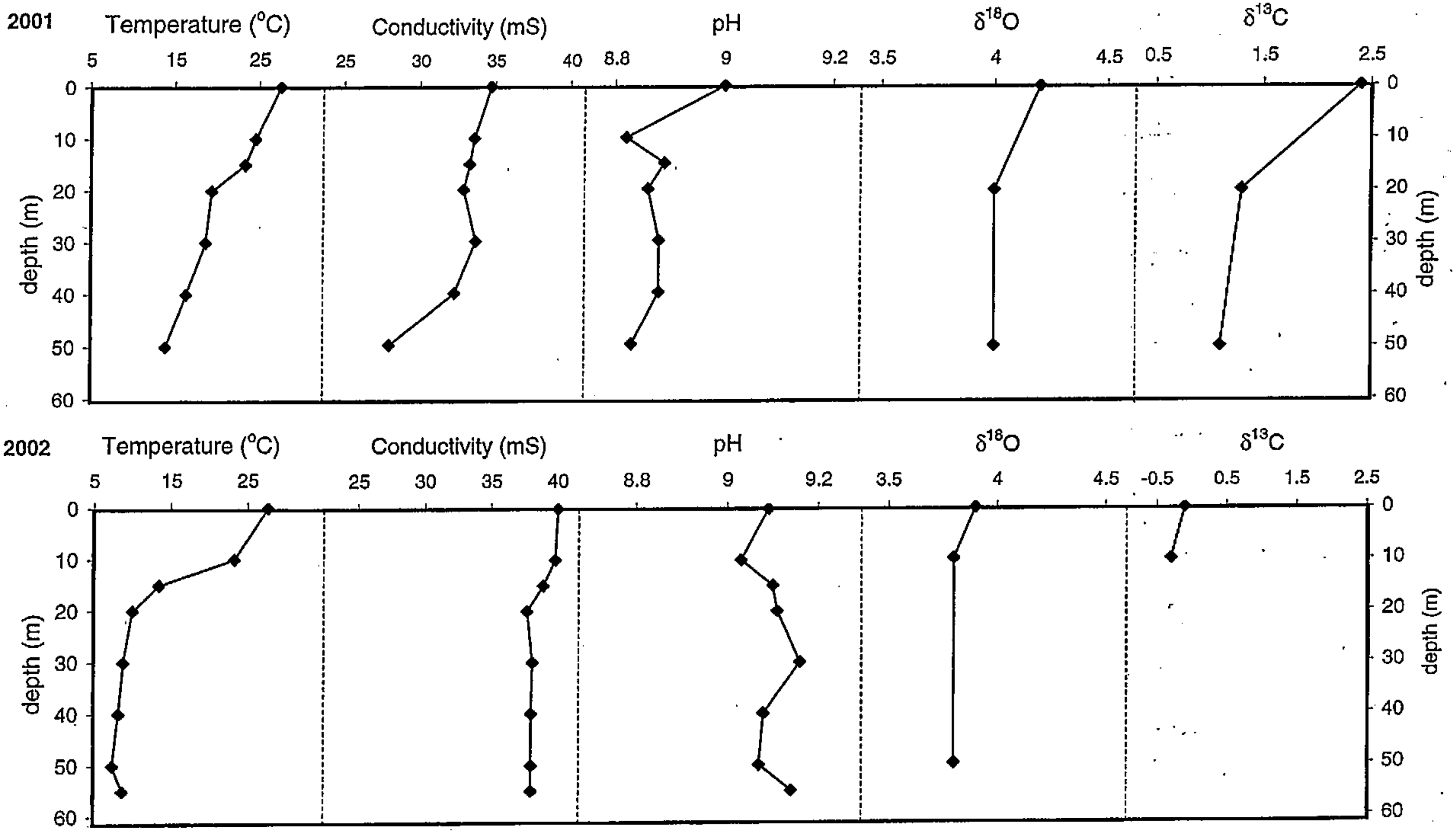

Fig. 7.5 Lake chemistry depth profiles for Burdur Gölü.

Previously published isotope values of Burdur lake waters (Dinçer, 1968) show that the lake has become enriched in ^{18}O between 1964 ($\delta^{18}O = +2.2‰$) and 2002 (+ 3.9 ‰). There is a clear change in depth of temperature and conductivity (Fig. 7.5). However pH and stable isotope values do not show any significant changes through the water column. Na^+ and SO_4^{2-} were the dominant major ions in the alke waters during the late 1970's (Roberts, 1980).

The lake bottom waters appear to be anoxic. There is no evidence of benthic life from Glew cores recovered with the sediment water interface intact, and sediments change colour from black to pale yellow and grey on contact with the air due to oxidation.

7.5 Hydrology

As for Nar Gölü (Section 5.6) two methods for calculating water balance for Lake Burdur will be used, a water balance model and a stable isotope mass balance model.

7.5.1 Water balance model

For the steady state equation

$$P + S_i + Gi = E + S_o + G_o. \tag{7.1}$$

the following values are known for Lake Burdur:

P: 75,190,000 m^3 of rainfall enters the lake directly from precipitation each year (lake area x mean annual rainfall).

E: 195,676,500 m^3 of water is lost from the lake each year through evaporation (annual evaporation x lake area).

S_o: there is no surface runoff from the lake.

From these figures it can be shown that

$$S_i + G_i - G_o = 120,486,500 \text{ m}^3 \tag{7.2}$$

7.5.2 Isotope mass balance modelling.

As well as the water balance model discussed above the stable isotope values of the lake must also balance such that

$$dV\delta_l/dt = P\delta_P + S_i\delta_{Si} + G_i\delta_{Gi} - E\delta_E - S_o\delta_{So} - G_o\delta_{Go} \tag{7.3}$$

where the values δ_l, δ_p, δ_{Si}, δ_{Gi}, δ_E, δ_{So}, δ_{Go} are the isotope values, either $\delta^{18}O$ or δD, of the lake waters, precipitation, surface inflow, groundwater inflow, evaporation, surface outflow and groundwater outflow respectively.

Lake Burdur has no surface outflow, lake waters leaving the lake through ground water are assumed to be the same value as all other waters within the lake such that $\delta_{Go} = \delta_l$. As precipitation will be the dominant control on river and runoff inflow, as well as groundwater inflow it is assumed that $\delta_{Gi} = \delta_{Si} = \delta_P$.

Therefore for Lake Burdur

$$dV\delta_l/dt = P\delta_P + S_i\delta_P + G_i\delta_P - E\delta_E - G_o\delta_l \tag{7.4}$$

For the water balance estimates it is assumed that the lake is in a steady state such that $dV\delta_l/dt = 0$.

Therefore,

$$P\delta_P + S_i\delta_P + G_i\delta_P = E\delta_E + G_o\delta_l \tag{7.5}$$

P and E are already known from measurements and the discussion above.

δ_l: lake surface waters between 1999 and 2002 have $\delta^{18}O$ values of +4.0 ± 0.2 ‰ (Table 7.1)

δ_p: in a given year the average isotope ratio of waters entering the lake will be a weighted average of the values for each month. Isotope values from precipitation were recorded at

Koçbeyli (near Isparta), 25 km east of Lake Burdur (Fig. 7.1), between October 1989 and July 1992 (IAEA/WMO, 2001). The weighted average through this time is –9.4 ‰. This compares to a value of –8.8 ‰ at Ankara from 1996, 1997, 2000 and 2001 monthly values (IAEA/WMO, 2001, 2002; A. Dirican, pers. com., 2002).

Estimates of the isotope values of in-flowing waters to a lake system can also be obtained from the intercept of the local evaporation line with the meteoric water line in δD v. $\delta^{18}O$ space. For lakes in the same precipitation regime as Lake Burdur the LEL crosses the Isparta meteoric water line at $\delta^{18}O = -8.5$ ‰ (Fig. 7.6). The intercept with the Ankara meteoric water line is at $\delta^{18}O = -8.4$ ‰.

These values are more positive than the weighted average of precipitation calculated for Burdur, -8.5 ‰ compared to -9.4 ‰. The intercept of the LEL and MWL represents the total inflow of waters into the lake. As Burdur has a large catchment, river waters have time to evaporate before entering the lake and this may account for most of the differences between these values.

A value of –8.5 ‰ for δ_p will be initially used for the mass balance equation as it incorporates all waters entering the lake.

δ_E: as for Nar Gölü values of δ_E can be calculated from two different equations.

For

$$\delta_E = ((\alpha^*\delta_l) - h\delta_A - \epsilon)/ (1 - h + \epsilon_k) \quad \text{(Kebede \textit{et al.}, 2002)} \tag{7.6}$$

α*: the equilibrium fractionation factor can be calculated

$$1/\alpha^* = \alpha_{eq} = \exp(1137\,T^{-2} - 0.4156\,T^{-1} - 2.0667 \times 10^{-3}) \tag{7.7}$$

where T is the temperature of the lake surface water in degrees Kelvin (Majoube, 1971).

T: as at Nar lake surface temperatures measured over a number of field seasons (Table 7.1) lie between the average and maximum monthly temperatures (Fig. 7.3). Lake surface

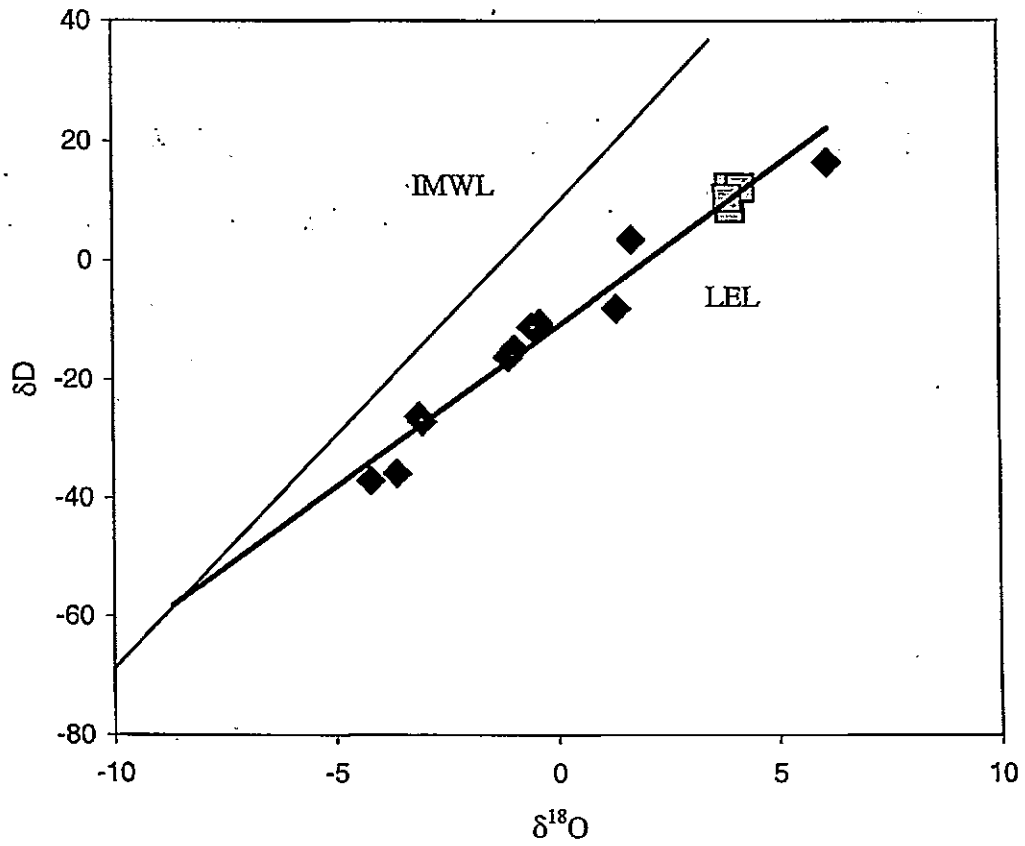

Fig. 7.6 Position of Burdur Gölü (grey squares) on the local evaporation line (LEL), of other lakes (black diamonds) within the same precipitation regime of Türkeş (1996), compared to the Isparta meteoric water line (IMWL).

temperatures will therefore be taken to be the mean of the average and maximum air temperatures. This gives a value of 16.1°C for the mean annual lake surface temperature.

h: for a relative humidity of 0.60 at an average air temperature of 13.0°C, the normalised value of h at 16.1°C is 0.49.

ϵ^*: can be calculated from α^*.

ϵ_k: for $\delta^{18}O$ has been shown to approximate 14.2(1-h) (Gonfiantini, 1986).

δ_A: from $\delta_A = \delta_P - \epsilon^*$ (Gibson *et al.*, 1999), $\delta A = -18.7$ ‰.

Therefore, from equation 7.10, $\delta_E = -8.3$ ‰.

From the Benson and White (1994) equation

$$\mathbf{R}_{evap} = [(\mathbf{R}_{lake}/\alpha_{eq})-(RH f_{ad}\mathbf{R}_{ad})]/\ [(1-RH)/\alpha_{kin}) + RH\ (1-f_{ad})] \qquad (7.8)$$

values of δ_E range between –8.5 ‰ (for $f_{ad} = 0$) to +6.7 ‰ ($f_{ad} = 1$).

Values from both equations give values for δ_E close to those for the in-flowing waters (δ_{in}). It has been shown that for a terminal lake with inflows equalling evaporative loss, the isotopic composition of the lake waters approach a steady state, such that

$$\delta_E = \delta_{in} \qquad \text{(Kebede } et\ al.\text{, 2002).} \qquad (7.9)$$

$\delta^{18}O$ values recorded through 4 years have shown very little variation suggesting that the lake has reached an isotopic steady state. However, very saline lakes, such as Burdur, have additional controls on the evaporative system.

Dissolved salts decrease the thermodynamic activity of the water and also its evaporation rate. However, this effect is small and can be neglected in most cases (Gonfiantini, 1986). Experiments comparing the evaporation of distilled and salt waters show the salt waters to have a much shallower slope in δD v. $\delta^{18}O$ space (Gonfiantini, 1986). Looking at the local evaporation line (Fig. 7.6), Lake Burdur lies on a straight line with other lakes in the region suggesting that there is no dissolved salt effect on the evaporation of this lake.

δ_E can therefore be taken to equal the isotopic composition of the input waters i.e. – 8.5 ‰.

Equation 7.4 can then be solved and from the result, simultaneously solved with equation 7.2, it can be shown that:

$$G_o = 0\ m^3 \qquad S_i + G_i = 120{,}486{,}500\ m^3$$

7.5.3 Summary of hydrological budget

Based on the water and isotope mass balance models above, a summary of the physical characteristics of the Burdur hydrological system and the water flux through Lake Burdur at the present time (assuming a lake in steady state) is given below.

Lake Area	182,500,000 m^2	**Precipitation**	0.412 myr^{-1}
Lake Volume	3,768,289,067m^3	**Evaporation**	1.072 myr^{-1}

Table 7.3 Summary of Lake Burdur hydrological budget.

	Amount	Percentage
Inputs		
Precipitation (m^3)	7.5 x 10^7	38
Surface inflow and Groundwater (m^3)	12.0 x 10^7	62
Outputs		
Evaporation (m^3)	19.6 x 10^7	100
Groundwater (m^3)	0	0
Total Flux (m^3)	19.6 x 10^7	
Residence Time (years)	19.3	

Residence time was calculated from the volume divided by the total flux through the lake (Telford and Lamb, 1999).

7.6 Sediment lithology

A number of Mackereth cores, up to 2m long, were obtained from Lake Burdur in the summer of 2002 (Fig. 7.7). After visual inspection of the stratigraphy in each core BUR02MAI was chosen for analysis as it was the least disturbed and, based on laminae counts, extended the furthest back in time. Through the rest of the chapter core BUR02MAI is the source of the results unless otherwise stated.

The sediment from the Burdur cores is composed of laminated clays (Fig. 7.8) and loss on ignition (Fig. 7.9) shows there is very little variation in the sediment composition through the core. Based on LOI the sediments are composed of approximately 12 % organic matter and 20 % calcium carbonate. The remaining material, i.e. non-carbonate, mainly clay minerals and quartz, accounts for the remaining 68 % of the sediment. The peaks in the carbonate curve correspond to the non-laminated parts of the record (Fig. 7.9), which may be turbidite, or mass flow, structures bringing material from the lake edge to the lake bed. These may also be the result of increased in-wash events bringing large amounts of catchment material, including limestones, into the lake.

XRD of the Burdur sediments shows three types of carbonate present throughout the sequence. Dolomite accounts for approximately 20 % of the carbonate in the sediment, with calcite and aragonite accounting for the remainder. It is likely that the dolomite is allochthonous in origin, as dolomitic limestones are found in the catchment. The amount of dolomite is also higher in samples from the non-laminated sections of the core, thought to be associated with increased catchment in-wash (Fig. 7.9). Assuming that dolomite is not precipitating within the lake, the XRD results indicate that there are catchment-sourced carbonates throughout the sequence.

It is unclear if the calcite and aragonite are precipitating in the lake waters or also being washed into the lake. SEM photographs of the sediment show no visible differences between the different layers creating the laminated appearance of the sediments. The sediments are composed of small (≤5 μm) particles (Fig. 7.10) with no clear morphology. This may suggest that most of the sediments has been reworked from the catchment and there is limited, or no, calcium carbonate precipitation within the lake.

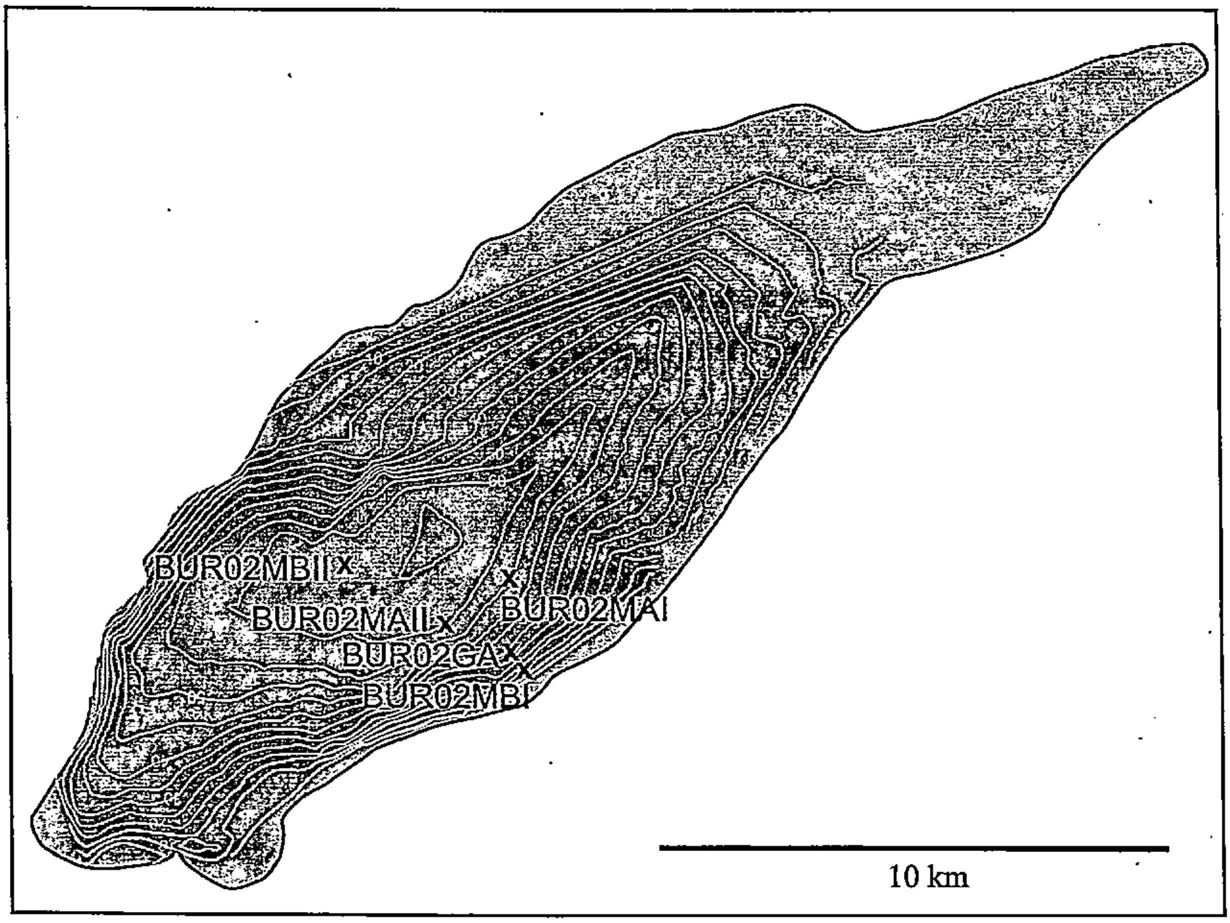
BUR02MBII
BUR02MAII
BUR02MAI
BUR02GA
BUR02MBI
10 km

Fig. 7.7 Location of core sites in Lake Burdur. White lines show water depth (m).

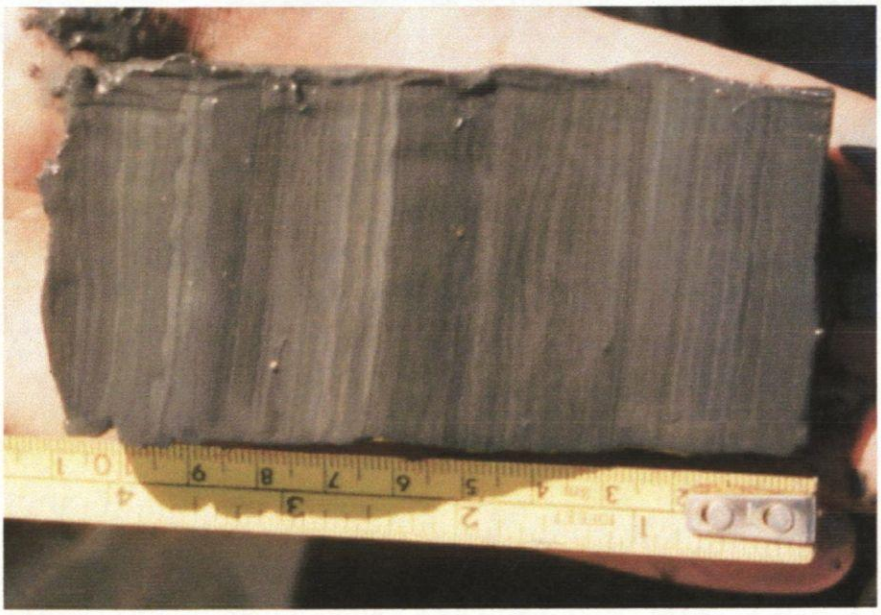

Fig. 7.8 Photo of laminated clays from Lake Burdur.

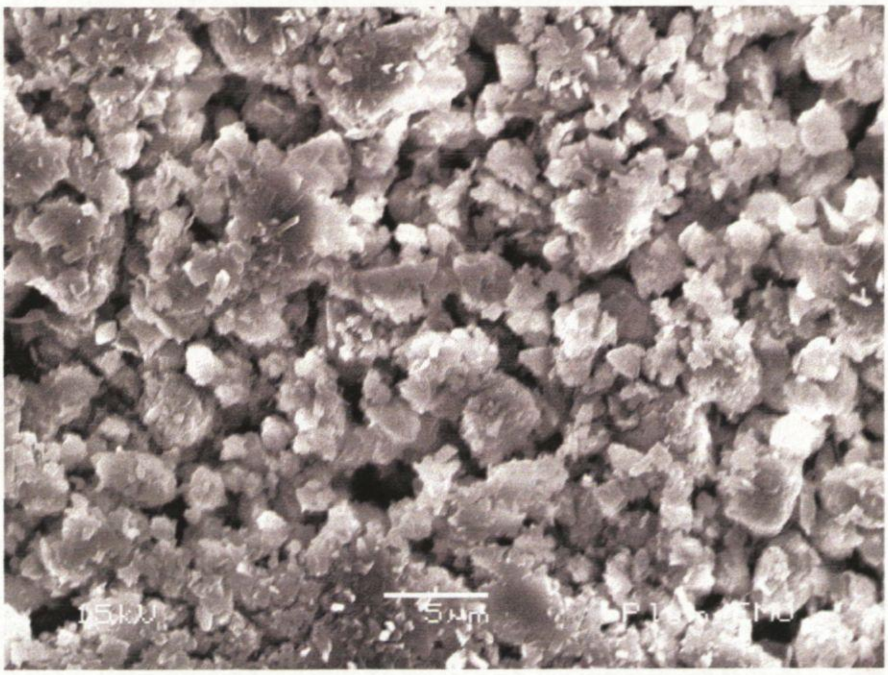

Fig. 7.10 SEM photograph of Lake Burdur sediments.

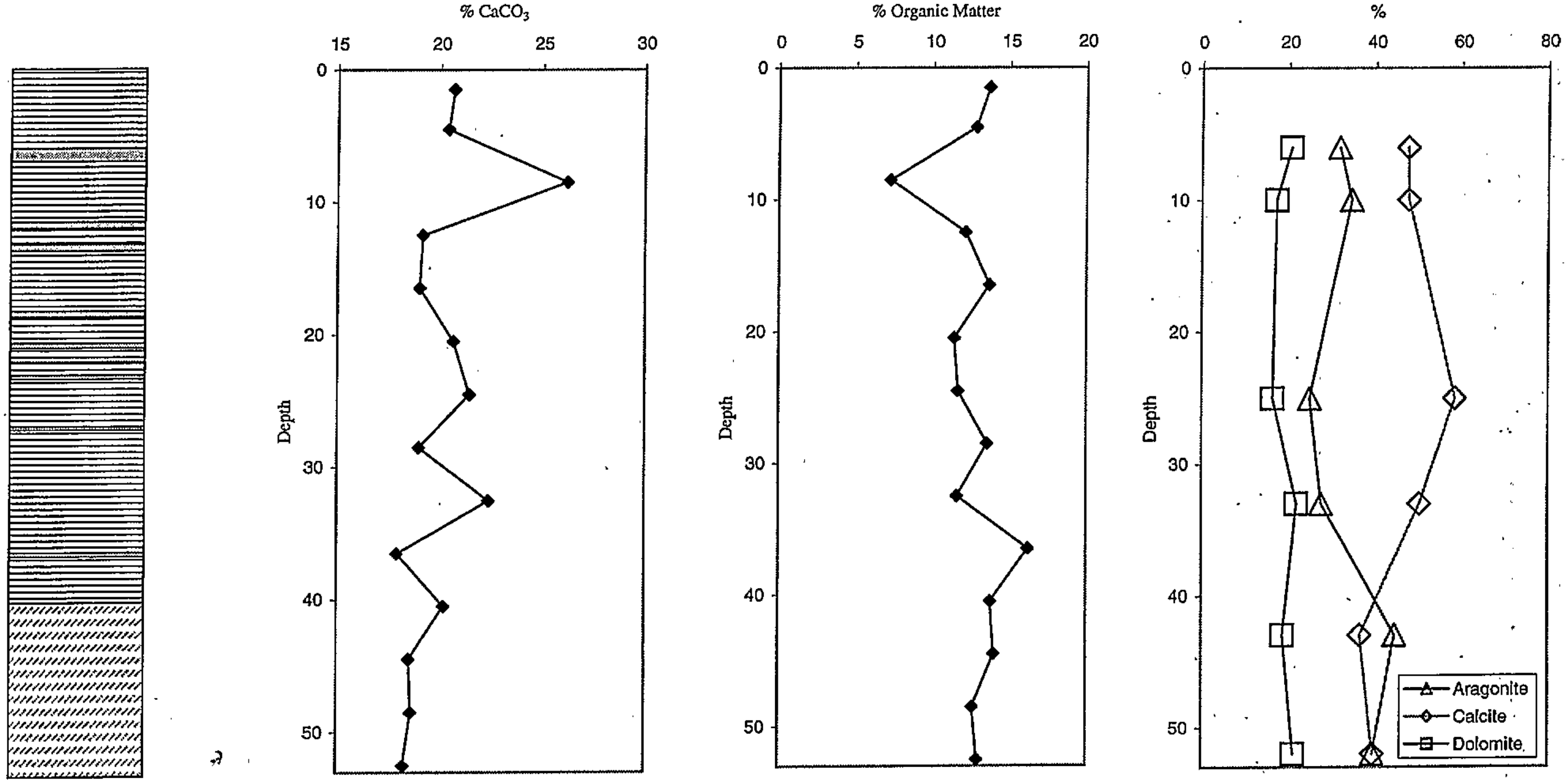

Fig. 7.9 Core BUR02MA1 lithology, LOI and carbonate mineralogy.
Lithology Key: ▤ Laminated sediments ▩ Non laminated sediments ▨ Unclear laminations

7.7 Chronology

^{210}Pb, ^{137}Cs, and ^{241}Am were measured through the top 26 cm of the core to provide an age depth model. ^{137}Cs has three relatively well resolved peaks, at 1.5 cm, 4.5 cm and 9.5 cm (Fig. 7.11). Traces of ^{241}Am at 9.5 cm suggest that this peak records the 1963 fallout maximum from the atmospheric testing of nuclear weapons. The more recent peaks probably record fallout from the 1986 Chernobyl reactor accident.

Total ^{210}Pb activity apparently reaches equilibrium with the supporting ^{226}Ra at a depth of around 10 cm (Table 7.4). Unsupported ^{210}Pb activities, calculated by subtracting ^{226}Ra activity from total ^{210}Pb activity, decline more or less exponentially with depth, suggesting relatively uniform sedimentation in this section of the core (Appleby, 2003 pers. com.).

^{210}Pb dates calculated using the CRS dating model (Appleby *et al.* 1978) place 1986 at a depth of 2 cm, and 1963 at a depth of about 4 cm (Table 7.5), significantly different from the depths suggested by the ^{137}Cs/^{241}Am record. Revised CRS model calculations (Table 7.5) using the 1963 ^{137}Cs date as a reference point (Appleby, 2001) suggest that the apparent total ^{210}Pb / ^{226}Ra equilibrium at ~10 cm may be due to a massive influx of sediment in the early 1960s that diluted the atmospheric flux virtually to zero. A smaller such event in the late 1980s may explain the ^{137}Cs double peak between 1.5 and 4.5 cm. The absence of any unsupported ^{210}Pb below the 1960s event suggests this influx of material may have destroyed the earlier part of the record. Since the surface concentrations place the ^{210}Pb dating horizon at about 1915, at normal rates of sedimentation, this would suggest the loss of ~7 cm (Appleby, 2003 pers. com.). However, there is no sedimentary evidence in any of the cores of removal of material due to a mass flow movement below 9.5 cm and the stratigraphy in these cores can be traced across the basin.

Additionally to the ^{137}Cs ages and ^{210}Pb age model a radiocarbon date was obtained from wood fragments found in core BUR02MB2 (Table 7.6). Correlation of this core with BUR02MAI via visible inspection of the stratigraphy and magnetic susceptibility (Fig. 7.12) allows the date, of 340 ± 40 radiocarbon years BP, to be placed at a depth of 36 cm in core BUR02MAI.

Table 7.4 Fallout radionuclide concentrations in Burdur Lake core BUR02MA1

				^{210}Pb							
Depth		Total		Unsupported		Supported		^{137}Cs		^{241}Am	
cm	g cm^{-2}	Bq kg^{-1}	±	Bq kg^{-1}	±	Bq kg^{-1}	±	Bq kg^{-1}	±	Bq kg^{-1}	±
0.5	0.3	148	13.8	108.6	14.2	39.4	3.5	57.9	2.8	0	0
1.5	0.8	124	11.8	86	11.9	38.1	2.1	260.8	4	0	0
2.5	1.3	95.3	7.7	55.5	7.9	39.8	2	153.9	2.9	0	0
3.5	1.9	106.2	7	74.1	7.3	32.6	1.7	76.8	2.4	0	0
4.5	2.5	94.6	7.4	63.4	7.6	31.2	1.8	137.5	2.7	0	0
5.5	3	70.5	7.3	28.6	7.6	42	2	44.4	1.9	0	0
7.5	4.4	43.6	5.4	13.7	5.5	29.9	1.1	20.8	1	0	0
8.5	5.1	26	6	1.8	6.2	24.2	1.5	71	1.8	0	0
9.5	5.8	42.9	4.4	10.9	4.6	31.9	1.1	87.5	1.6	1.3	0.5
10.5	6.4	33.9	9.4	2.6	9.5	31.3	1.7	50.9	1.8	0	0
11.5	7	40.4	5.6	3	5.8	37.4	1.4	10.1	1	0	0
13.5	8	43.3	5.4	8.3	5.6	34.9	1.5	1.4	0.8	0	0
15.5	9	25.6	6.2	-9	6.3	34.5	1.5	0	0	0	0
17.5	10.1	29.1	4.1	-5.8	4.2	34.9	1.2	0	0	0	0
19.5	11.2	24.5	4.7	-11.1	4.9	35.6	1.3	0.7	0.8	0	0
21.5	12.5	31.6	4.6	-3.5	4.8	35.1	1.3	0	0	0	0
23.5	13.9	20.3	3.8	-10.1	3.9	30.3	1	0	0	0	0
25.5	15.2	16.8	4.2	-15.5	4.3	32.3	1.1	0	0	0	0

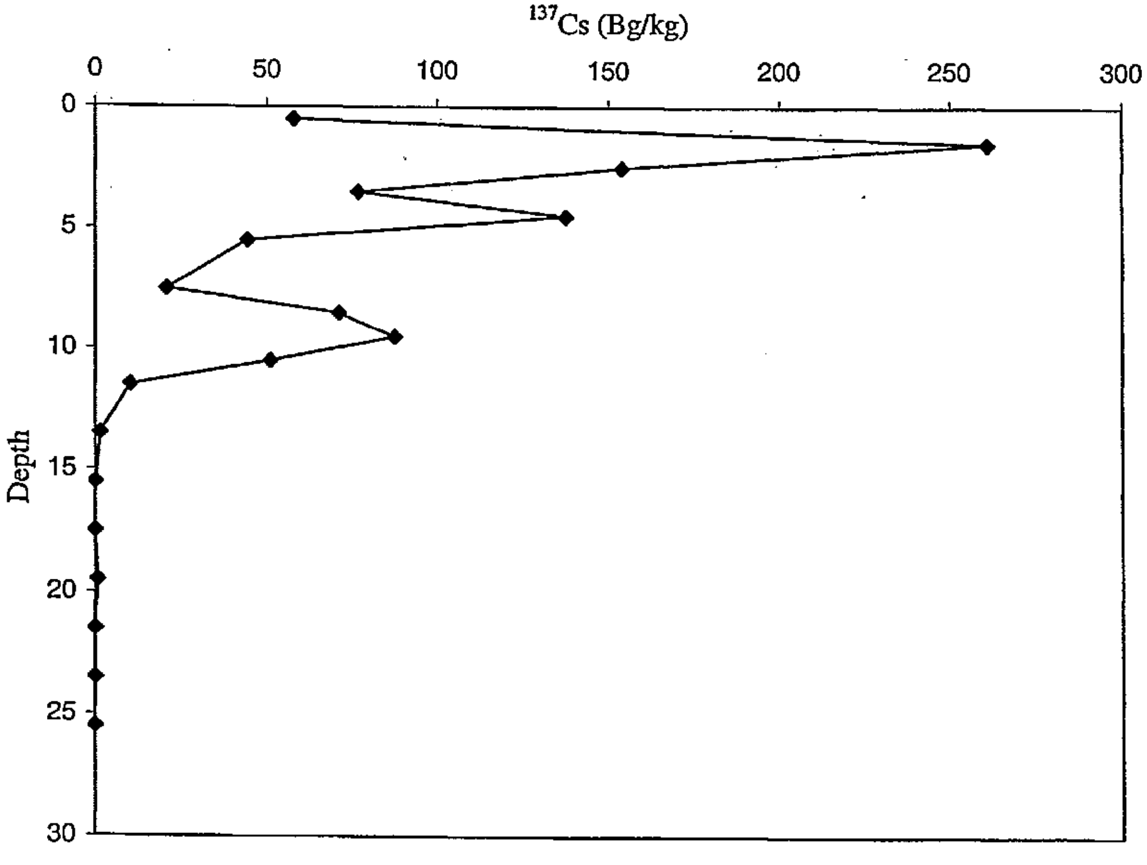

Fig. 7.11 ^{137}Cs profile through core BUR02MAI

Table 7.5 ^{210}Pb chronology of Burdur Gölü (core BUR02MA1)

(a) Raw CRS model dates

Depth		Chronology			Sedimentation Rate		
cm	g cm^{-2}	Date AD	Age y	±	g cm^{-2} y^{-1}	cm y^{-1}	± (%)
0.0	0.00	2002	0				
0.5	0.26	1998	4	2	0.067	0.13	16.1
1.5	0.78	1991	11	2	0.067	0.12	17.9
2.5	1.34	1983	19	3	0.081	0.14	20.0
3.5	1.91	1974	28	4	0.046	0.08	20.8
4.5	2.47	1959	43	8	0.034	0.06	30.3
5.5	3.05	1945	57	12	0.049	0.08	48.8
7.5	4.35	1917	85	29	0.042	0.06	101.0
8.5	5.12	1904	98	36	0.062	0.09	127.1
9.5	5.76	1899	103	44	0.030	0.05	150.8

(b) Corrected CRS model dates

Depth		Chronology			Sedimentation Rate		
cm	g cm^{-2}	Date AD	Age y	±	g cm^{-2} y^{-1}	cm y^{-1}	± (%)
0.0	0.00	2002	0	0			
0.5	0.26	1999	3	1	0.09	0.18	15.0
1.5	0.78	1994	8	2	0.10	0.19	16.2
2.5	1.34	1989	13	2	0.14	0.24	17.1
3.5	1.91	1984	18	2	0.09	0.15	14.8
4.5	2.47	1977	25	3	0.08	0.14	17.9
5.5	3.05	1972	30	4	0.15	0.25	30.3
7.5	4.35	1965	37	5	0.26	0.38	44.0
8.5	5.12	1964	38	5	0.80	1.14	53.6
9.5	5.76	1963	39	5	0.30	0.50	45.4
10.5	6.35	1962	40	5	0.54	0.91	49.4
11.5	6.95	1961	41	6	0.67	1.20	50.3
13.5	8.02	1960	42	6	0.36	0.69	49.1

Table 7.6 AMS Radiocarbon date from wood fragments in core BUR02MB2 (140cm depth). Calibration with INTCAL98 (Stuiver *et al.*, 1998).

Lab Code	**Conventional Radiocarbon Age**	**2 σ calibrated result**
Beta – 17876	340 ± 40 BP	1450 - 1650 AD

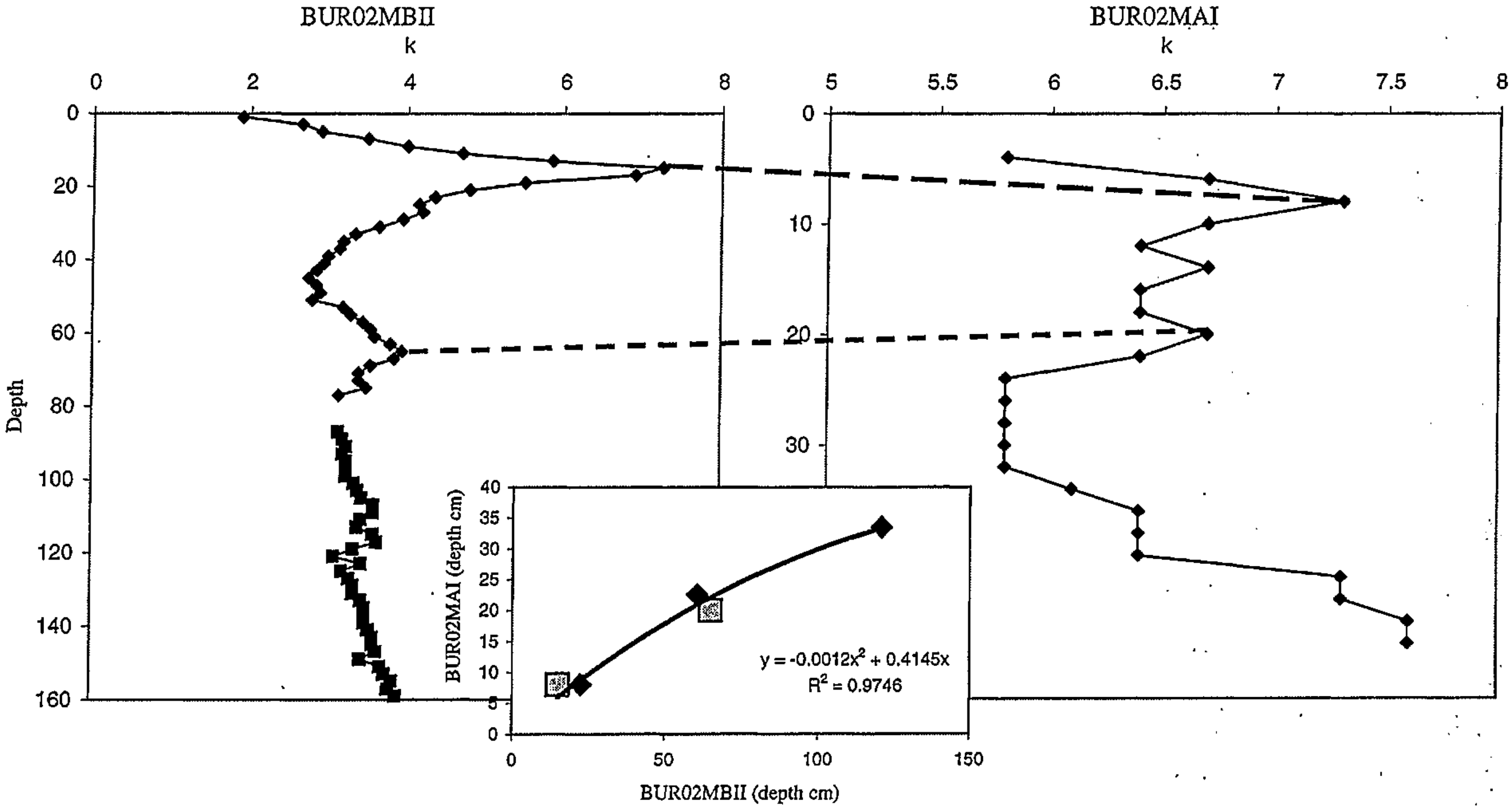

Fig. 7.12 Comparison of magnetic susceptibility profiles from core BUR02MB2 and BUR02MAI. Tie points from magnetic susceptibility (squares) and visual inspection of the cores (diamonds) are shown in inset.

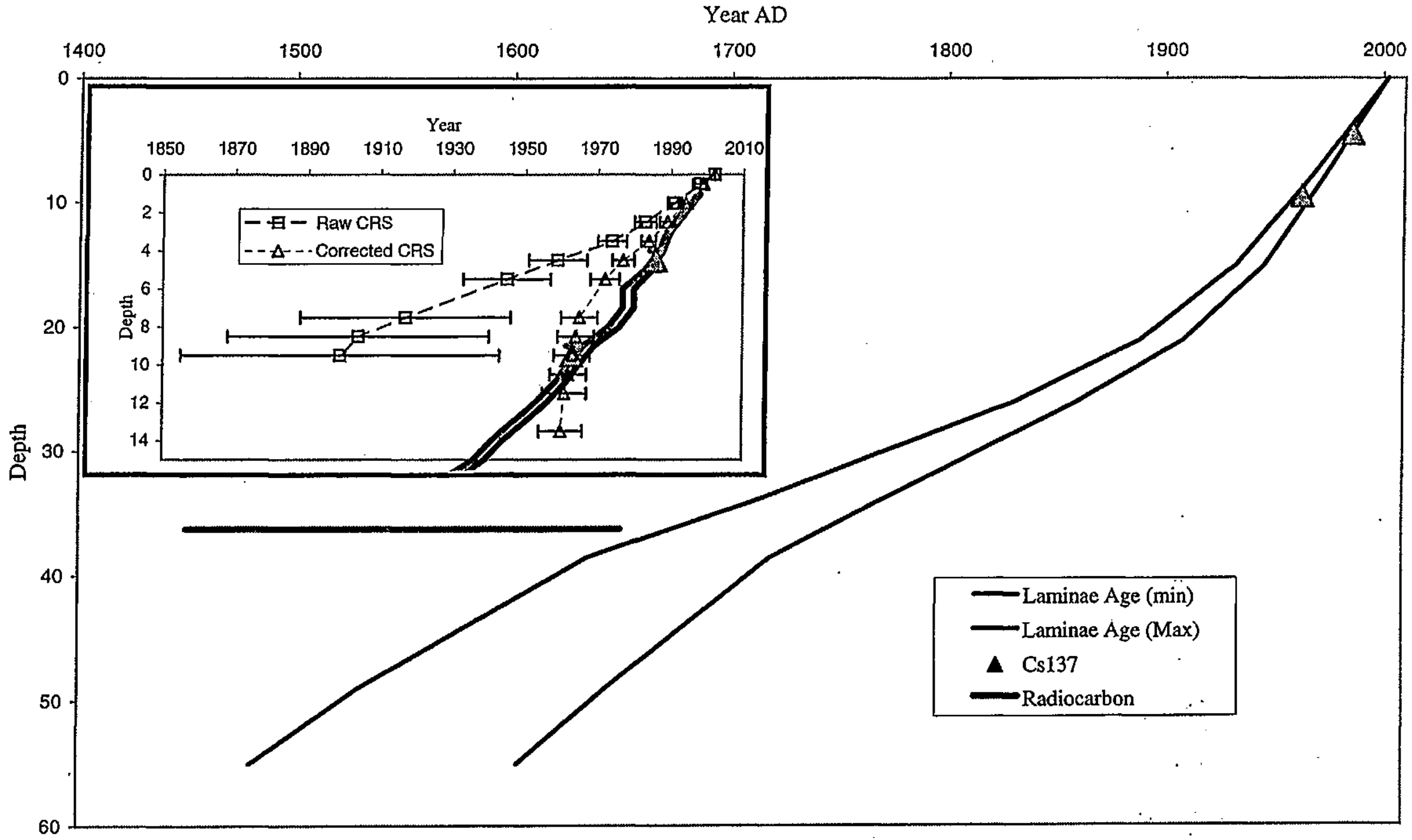

Fig. 7.13 Comparison of ^{137}Cs and radiocarbon dates with laminae counts. a) Detail of recent sediments with ^{210}Pb chronology and ^{137}Cs ages.

The laminations in the core were also counted. If the laminae are plotted against depth and compared to the ^{210}Pb chronology and ^{137}Cs ages it appears that the laminations are annual in nature (Fig. 7.13a). The radiocarbon date is older than the laminae counts at 36 cm depth (Fig. 7.13) and has a large 2σ range (1450 to 1650 AD), as it falls on a radiocarbon plateau. However as this age is taken from a wood fragment that will have been washed in to the lake, and may have taken tens of years to reach the lake bed, it should be taken as a minimum age only.

Although there are some uncertainties with the dates obtained from this core there is no sedimentological evidence of any hiatus in the core, and the laminae (varve) chronology fits with the ^{137}Cs and, more approximately, with the radiocarbon ages. The varve chronology will therefore be used as an age model through the remainder of this study.

7.8 Carbonate Stable Isotope Results

δ^{18}O

δ^{18}O values vary between –0.6 and 0.9 ‰ through the core (Fig. 7.14). There is a trend to more positive values between the base of the core (0.1 ‰) and 32 cm depth (0.9 ‰), from around 1500 to 1730 AD. There is then a long-term trend to more negative values to the top of the core reaching -0.4 ‰ at 0-1 cm, with occasional rapid excursions to more positive values e.g. at 7 and 23 cm.

δ^{13}C

Trends are less evident in the δ^{13}C record (Fig. 7.14), which has a range of 2 ‰, between 0.1 and 2.1 ‰. Again there are occasional rapid shifts towards more positive values at 6, 18, 23 and 32 cm depth. In general there is a trend to more negative values from 1.2 ‰ at 44 cm, approximately 1570 AD, to 0.2 ‰ at 2 cm depth.

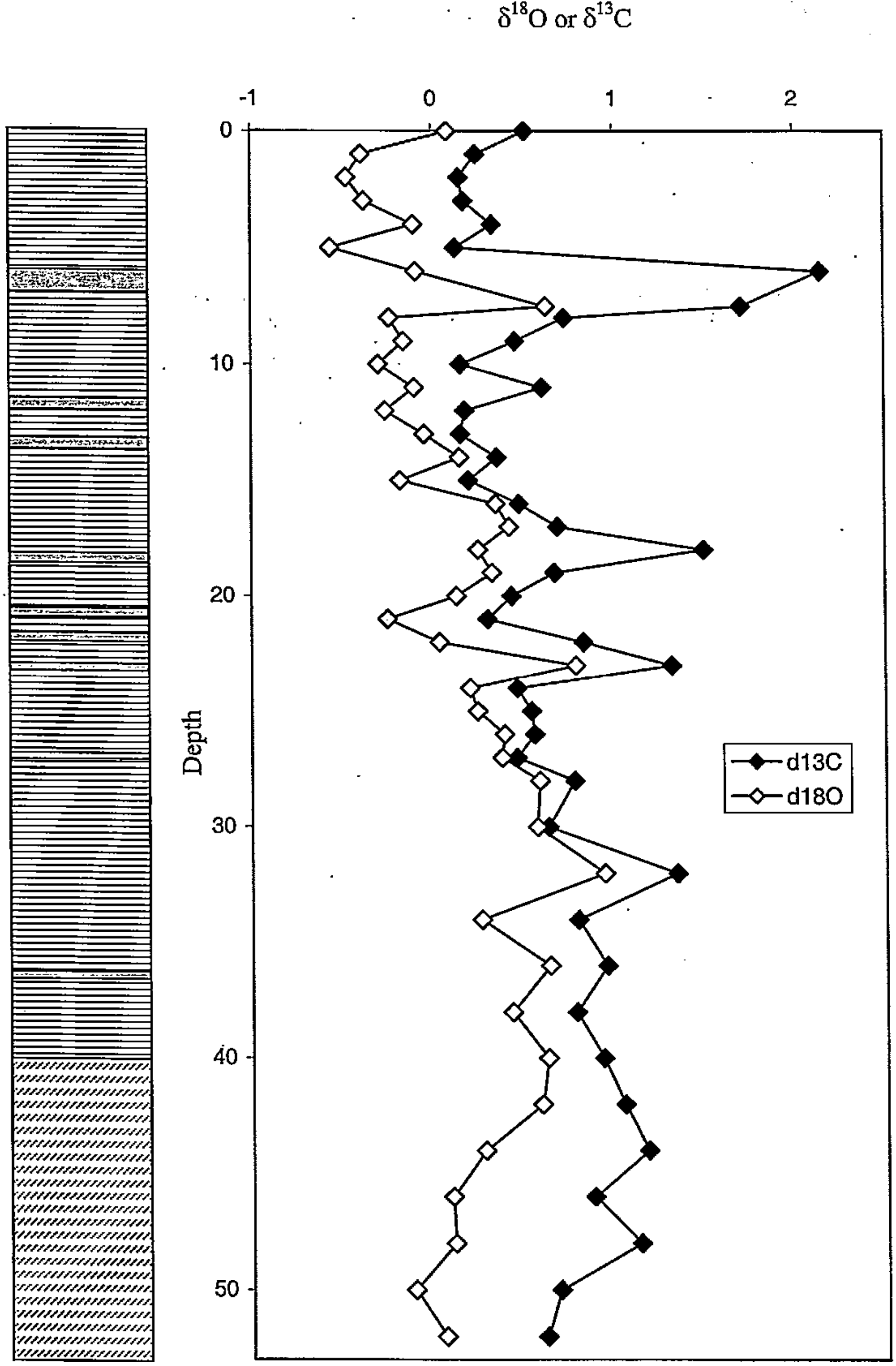

Fig. 7.14 δ^{18}O and δ^{13}C results from BUR02MAI. Lithology key the same as in Fig. 7.9 (data in appendix 2).

7.8.1 Interpretation of carbonate results

Allochthonous Carbonate

The carbonate mineralogy and sediment morphology suggest most of the carbonates in the Burdur sediments may have been reworked from outside the lake and the composition of the total carbonate in a given sample may therefore control the isotope value recorded. Comparing the 6 samples where the amount of each carbonate fraction could be estimated from the XRD analysis with the samples isotope values it would suggest that there is some control from the amount of dolomite in the sample, but the amount of calcite or aragonite does not affect the isotope value (Table 7.7).

The rapid peaks in the carbonate isotope records at 6 cm and 32 cm correspond to peaks in the $CaCO_3$ curve from loss on ignition (Fig. 7.9). This suggests that these positive excursions are associated with sudden increases in carbonate reaching the lake floor. These also correlate to the non-laminated parts of the stratigraphy, which are probably mass flow events from the lake edge or times of rapid in-wash from the catchment. These may be caused by heavy rainfall events, however in Burdur they could also be due to tectonic events leading to mass flow movements or turbidite events.

Dolomite is enriched in ^{18}O by 3-4‰ with respect to coexisting calcite (Land, 1980) and increases in isotopically positive catchment dolomite would therefore explain the positive isotope excursions related to the non-laminated sections of the Burdur sediments. In addition, the samples were prepared for mass spectrometry using standard techniques for calcium carbonate i.e. calcite and aragonite. Magnesium carbonates, such as dolomite, may partially react during this process and differentially fractionate in each sample. The effect of dolomite on the recorded isotope value is therefore difficult to quantify. It has been suggested (Al-Asam *et al.*, 1990) that the effect of the dolomite can be removed by limiting the reaction times of the sample in acid, prior to CO_2 extraction, although this is difficult with fine grained sediments such as those from Burdur.

From lake water isotope values and lake temperature data the value of calcite that would be precipitated in the lake waters can be calculated from the equation of Leng and Marshall (in press):

Table 7.7 Strength of regression relationships between the amounts of calcium carbonate minerals and stable isotope values (n = 6).

Relationship	r^2	p
% Aragonite v. $\delta^{13}C$	0.0056	0.917
% Calcite v. $\delta^{13}C$	0.0080	0.853
% Dolomite v. $\delta^{13}C$	0.3545	0.246
% Aragonite v. $\delta^{18}O$	0.0026	0.978
% Calcite v. $\delta^{18}O$	0.0028	0.866
% Dolomite v. $\delta^{18}O$	0.1437	0.443

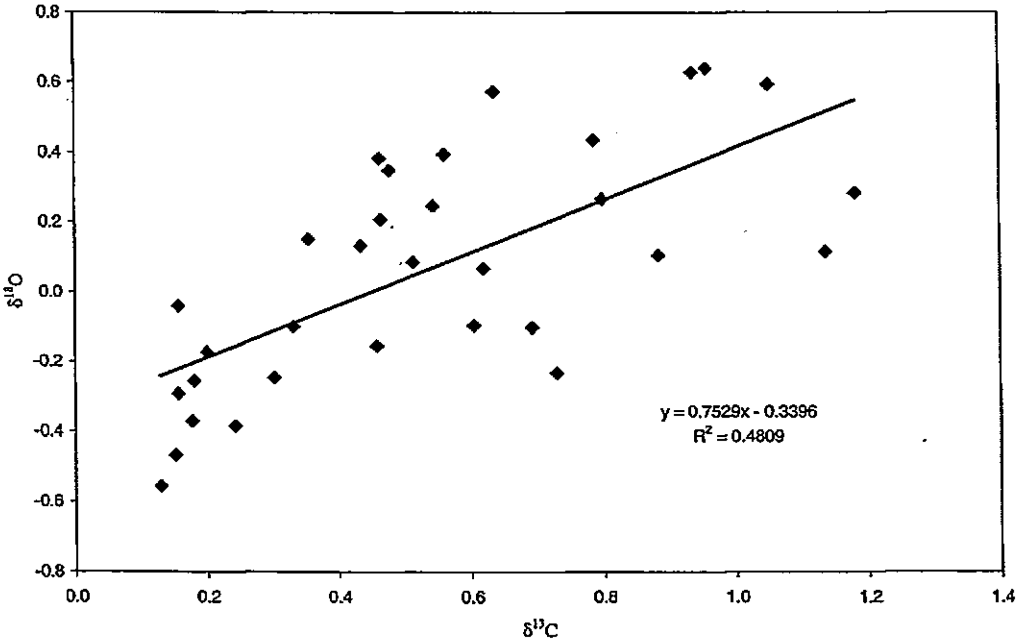

Fig. 7.15 $\delta^{18}O$ v. $\delta^{13}C$ for BUR02MA1 (with sample 8 removed).

$$T(°C) = 13.8 - 4.48(\delta c-\delta w) + 0.08(\delta c-\delta w)^2 \quad (7.10)$$

Based on the values recorded from the surface waters in 2002 (Table 7.1) precipitated calcite would have a value of +1.0 ‰, this compares to a value of + 0.1 % for the surface sediments from Burdur. This suggests that there may be some degree of non-authigenic carbonate in the sample. If calcite was precipitated earlier in the year, at cooler lake water temperatures, or if aragonite was precipitated, the values would become more positive, moving away from the measured surface sediment samples. Additionally the surface sample contain dolomite which would tend to make the sample more positive.

From the previously published values of lake water isotope values (Dinçer, 1968) and the measurements taken in this study (Table 7.1) lake waters are approximately 2‰ more positive in the period 1999 – 2002, compared to 1964 – 1966. However, the surface sediment sample is only 0.12 ‰ heavier than the sample representing 1964-1966.

The sediments do not represent present day lake water isotope conditions or changes in the lake water isotope composition through time. It is most likely, therefore, that the isotope record from Burdur reflects changing amounts of catchment in-wash, due to different amounts of dolomite being present in the core

δ^{18}O: δ^{13}C *co-variation*

With the raw isotope results there is a clear co-varying trend between the δ^{18}O and δ^{13}C records although the relationship is fairly weak ($r^2 = 0.32$). If some of the rapid excursions caused by the non-lacustrine dolomite are removed from the record the co-varying relationship becomes stronger (Fig. 7.15). Strong co-variation often occurs due to the climatic influences on the δ^{18}O and δ^{13}C records in closed lake basins (Talbot, 1990). As, from the discussion above, the isotope record is unlikely to reflect water balance but rather the amount of inwash into the lake, the co-variation here is most likely due to the samples with higher dolomite content having more positive δ^{18}O and δ^{13}C values and vice versa.

Comparison with meteorological records

Although the source of carbonate in the Burdur sediments is mixed, and much of it may be sourced in the catchment, isotope profiles may still show relationships with meteorological variables, particularly if the isotope profiles are controlled by the amount of in-wash.

For comparisons between meteorological records and the $\delta^{18}O$ record, the meteorological record was averaged for the periods of time represented by each sediment sample. Direct comparisons of the two records showed no relationships at a 95% confidence limit (Table 7.8). The strongest relationship was with spring minimum temperature which explained 22.1 % of the isotope variability with a 94 % confidence limit.

Isotope sample 8, representing 1973 – 1976, was removed from the dataset as it shows a strong positive shift thought to be due to non-authigenic carbonate. With this sample removed the only significant relationship is still with spring minimum temperature which in turn explains nearly 30 % of the isotope variability (Table 7.9).

Plots of the spring and autumn minimum temperatures, the two strongest relationships between $\delta^{18}O$ and meteorological variables (Fig. 7.16), compared to the recent isotope record suggest there is not a strong relationship and the relationship found may just be due to similar long term trends in the data set particularly between 1960 and 1990, where the minimum temperatures show a cooling trend. There are no patterns in the meteorological variables that would fit with the isotope profiles if they were shifted to account for a lag in the lake response to climatic changes. This suggests the isotope values of the carbonate analysed are not climatically controlled.

Comparison with lake level records

Lake levels at Burdur have fallen dramatically during recent times, since the early 1970's lake level has fallen by 11.75 m in 30 years (0.39 m/year; Fig. 7.17), possibly due to removal of water for irrigation in the catchment (Roberts *et al.*, 2003). This anthropogenic influence may mask any relationship between the isotope record and meteorological records.

At Burdur the lake level should be a function of precipitation and evaporation, as there is no surface outflow from the lake and inflows from rivers and groundwaters will vary with the amount of precipitation.

From equation 5.1 ($E = [0.015 + 4 \times 10^{-4} T + 10^{-6} z] \times [480 (T + 0.006z)/(84 - A) - 40 + 2.3 u (T - T_d)]$) changes in evaporation can be shown to follow temperatures. Fig. 7.18 shows the rise in lake levels between 1960 and 1970 correspond to a decrease in summer temperature. Temperatures start to rise steadily from the early 1970s, however from 1980

Table 7.8 Regression relationships between the Burdur $\delta^{18}O$ record and averaged meteorological variables between 1941 and 2002. Table shows p-value, the direction of the relationship, and the r^2 value.

	Annual	Spring	Summer	Autumn	Winter
Min. Temp.	0.184	0.060	0.663	0.127	0.288
	+	+	+	+	+
	7.8	22.1	0.0	12.5	2.0
Av. Temp	0.528	0.341	0.496	0.475	0.669
	+	+	+	+	+
	0.0	0.0	0.0	0.0	0.0
Max. Temp	0.847	0.587	0.496	0.857	0.857
	+	+	-	+	+
	0.0	0.0	0.0	0.0	0.0
Precip.	0.653	0.700	0.305	0.736	0.385
	+	+	+	-	+
	0.0	0.0	1.4	0.0	0.0
R.H.	0.793	0.932	0.980	0.705	0.363
	+	+	-	+	+
	0.0	0.0	0.0	0.0	0..0

Table 7.9 Regression relationships between the Burdur $\delta^{18}O$ record and averaged meteorological variables between 1941 and 2002, with sample 8 removed. Values as in Table 8.3.

	Annual	Spring	Summer	Autumn	Winter
Min. Temp.	0.115	0.039	0.711	0.110	0.231
	+	+	+	+	+
	15.3	29.6	0.0	15.9	5.4
Av. Temp	0.435	0.325	0.464	0.492	0.497
	+	+	-	+	+
	0.0	0.6	0.0	0.0	0.0
Max. Temp	0.828	0.658	0.418	0.554	0.668
	+	+	-	+	+
	0.0	0.0	0.0	0.0	0.0
Precip.	0.624	0.974	0.181	0.964	0.201
	+	+	-	-	+
	0.0	0.0	8.8	0.0	7.4
R.H.	0.848	0.998	0.825	0.727	0.241
	+	-	-	+	+
	0.0	0.0	0.0	0.0	4.8

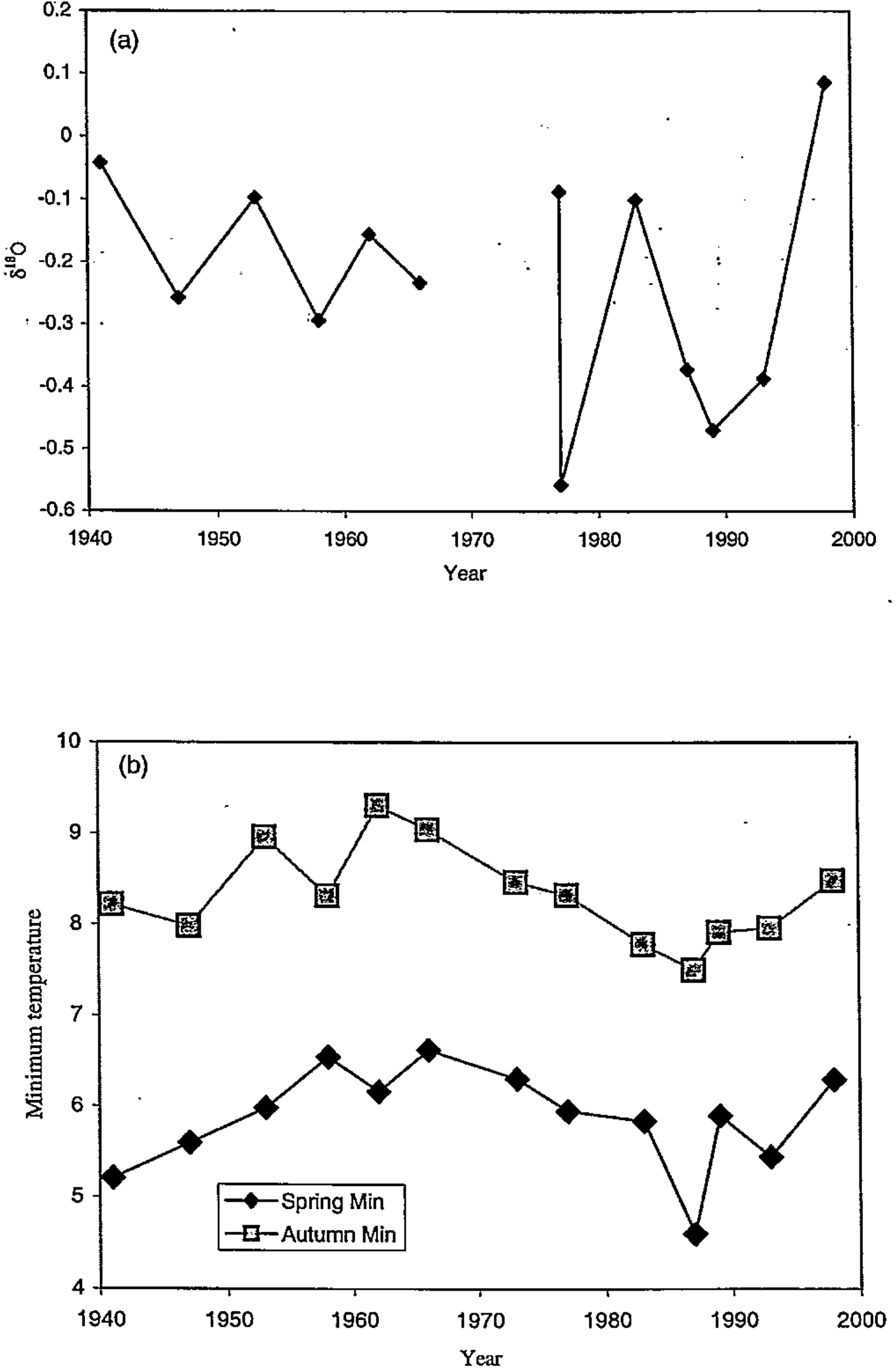

Fig. 7.16 Sediment $\delta^{18}O$ (a) and spring and autumn minimum temperatures (b) (the two strongest relationships for $\delta^{18}O$ v. climate data) between 1940 and 2000 AD.

onwards lake levels fall at a much larger rate than would be expected from the relationship between temperature and lake level in the earlier part of the record.

Fig. 7.19 shows values of normalised precipitation – normalised temperature (as a proxy of P-E) compared to lake levels. There is a lag of 5 years between these two curves, suggesting a lag in lake response to climate change. Taking this lag into account the first 20 years of the two records appear to show a strong relationship but this breaks down from 1970. There are no rises in lake level associated with the increase in P-E during the late 1970's and late 1990's.

Both the above relationships, between temperature or P-E and lake levels, suggest that prior to 1970 lake levels can be related to climate change at Burdur. After 1970 the earlier relationships break down with lake levels becoming considerably lower than would be expected from the climate data. This suggests that since 1970 additional controls, most probably removal of inflowing waters for irrigation, other than climate have been influencing lake level, and possibly, therefore, the stable isotope record at Burdur. However prior to 1970, although it was probably still occurring, irrigation was not a large enough factor to have a significant effect on lake level changes.

Since the early 1970's lake level has fallen at an average of 0.39 m/year, although between 1989 and 1997 the lake fell faster at 0.67 m/year, which is very close to the value for E – P (0.66 m/year) suggesting there may have been no surface inflow into the lake during this time period. This is unlikely, even due to increased irrigation, as there are many rivers and steams that enter the lake. Lake levels therefore seem to have been falling faster than would be suggested by the hydrology. There may be additional non-climatic, non-anthropogenic, controls on lake level, particularly tectonics. The basin is known to be heavily faulted and tectonically active and basin subsidence may therefore account for some of the recorded lake level change.

A decrease in lake level could be caused by a relative increase in evaporation or decrease in input to the lake. From the isotope results above a decrease in in-wash would lead to more negative isotope values as increases in in-wash are marked by shifts to more positive values.

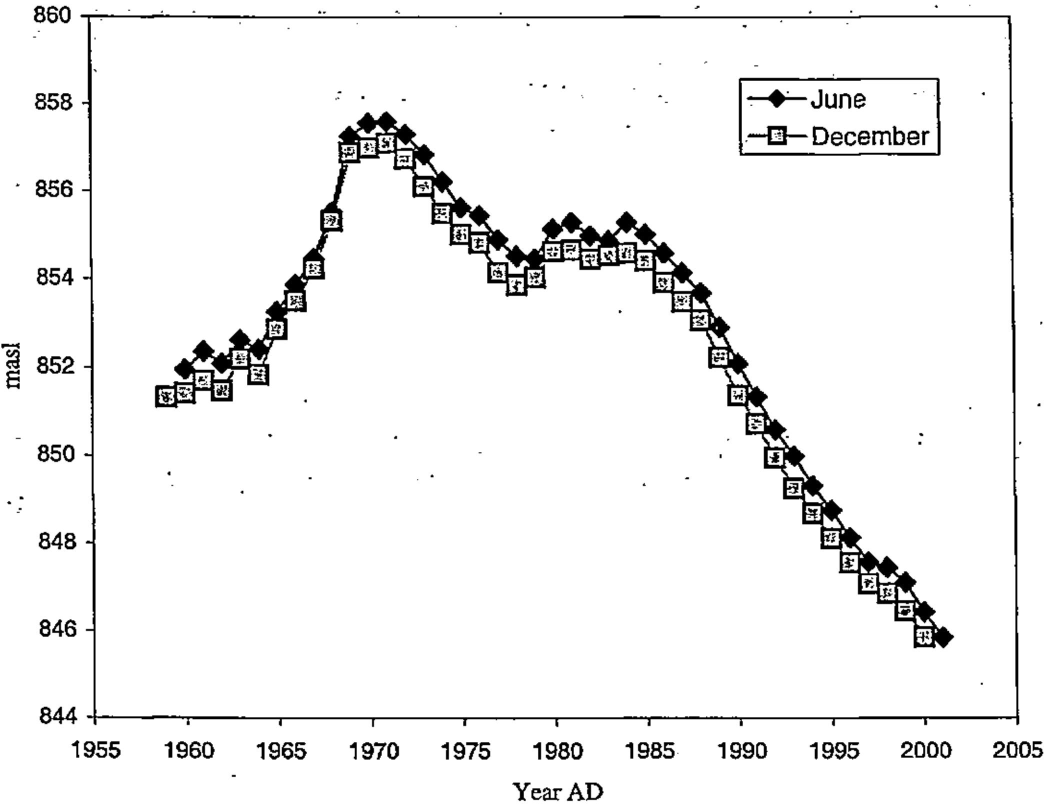

Fig. 7.17 Burdur lake levels between 1940 and 2001.

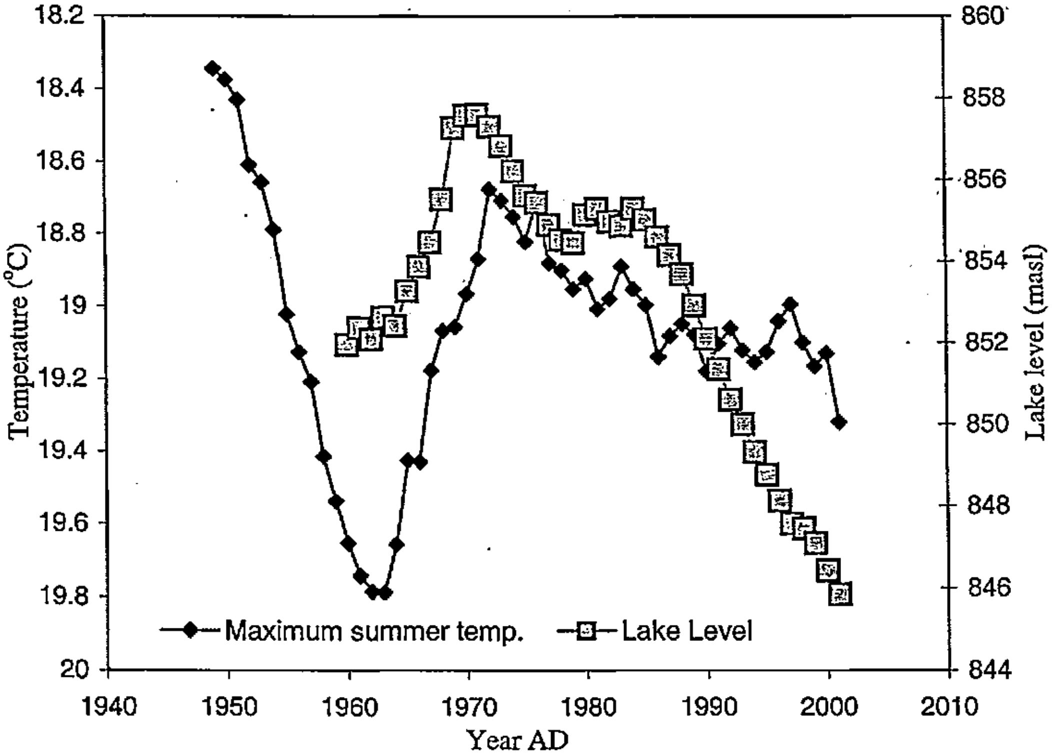

Fig. 7.18 Lake level and maximum summer temperature curves from Lake Burdur. Temperature curve, smoothed with a ten year running mean, is inverted as higher temperatures (increased evaporation) would lead to lower lake levels.

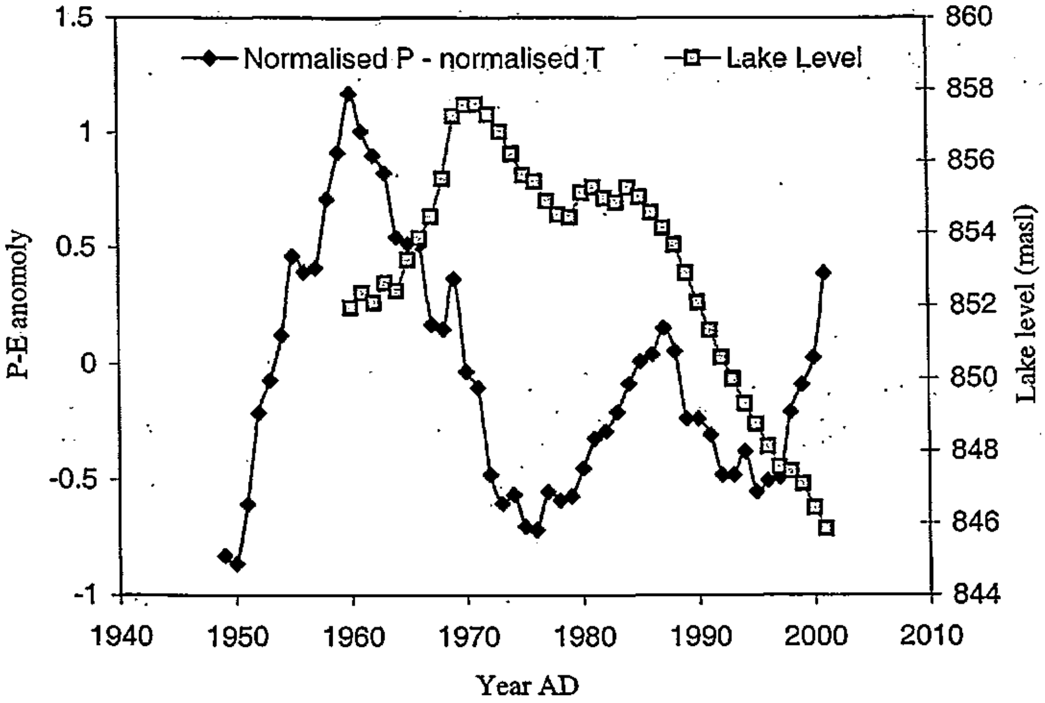

Fig. 7.19 Comparison of normalised P-E (normalised precipitation – normalised temperature) and lake level curves from Lake Burdur.

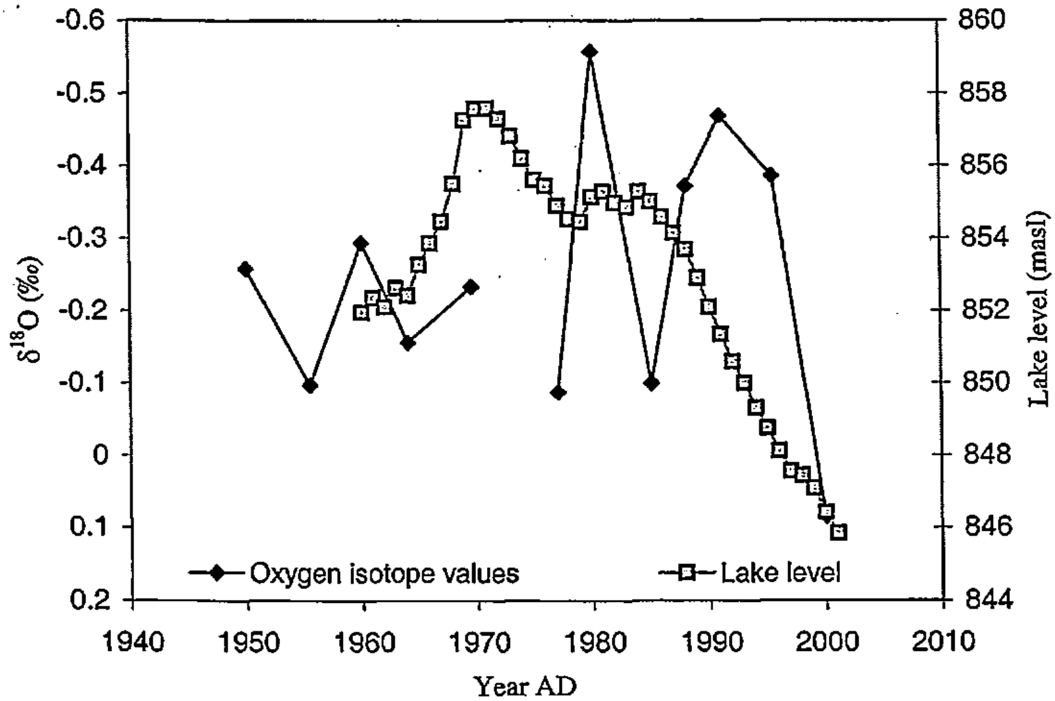

Fig. 7.20 Comparison of oxygen isotope values and lake level curve from Lake Burdur

Comparison of the isotope and lake level time series (Fig. 7.20 suggests there is no clear relationship between lake levels and isotope values recorded in the sediment.

7.9 Summary

The complexity of the carbonate mineralogy in the lake sediments makes the isotope record very difficult to interpret. Increases in carbonate, and slight increases in the amount of dolomite, during the non-laminated sections of the core are marked by distinct shifts in isotope values. These may mark extreme climatic episodes, or tectonic events, but do not tell a story of climatically controlled lake hydrology. The lake sediments do not record the isotope variability recorded by changes in the lake waters and this suggests a large proportion of the lake carbonates are not precipitated within the lake.

The work at Burdur highlights the complexity of lake stable isotope systems and the importance in fully understanding a lake system before interpretations of isotope palaeorecords can be made. Although the Burdur sediments contain carbonate, and show variation through the record it is unlikely that this variability is due to climate. The work at Burdur suggests that using bulk sedimentary carbonate is not a robust methodology if the source of the carbonate can not be pinpointed. Biogenic carbonate, from ostracods or molluscs, would be a better isotope archive in this environment, and although no fossils were found in the cores for this study they are present in the older sediments around the lake edge.

Chapter 8

QUANTIFYING CLIMATE CHANGE

For records of palaeoclimatic change to be useful to other scientific communities, such as climate modellers, or to put the recorded climate variability through the last century into context, it is necessary to quantify records of past change. This requires understanding of the modern processes controlling the palaeoarchive and the assumption that these controls have not changed significantly through time or, if they have, that changes can be sufficiently accounted for. This is particularly important when trying to quantify changes in climate from lake oxygen isotope records as there are many factors which control lake stable-isotope values (chapter 2). Even a single climate variable can have many effects on the lake isotope system. Temperature, for example, not only controls the fractionation between lake waters and precipitated carbonates but also affects the stable isotope value of precipitation entering the lake. Temperature also plays a large role in controlling the amount of evaporation and this may be the dominant effect in some lake systems, such as Nar and Burdur. It is therefore important that in quantifying climate change from these records all assumptions are stated, errors are carefully calculated, and the reconstructed climate variable can be shown to have a strong control on the isotope records through the instrumental time period.

Many quantified reconstructions are based on calibration of the palaeoarchive with recorded instrumental data either directly (e.g. tree ring precipitation reconstructions; e.g. D'Arrigo and Cullen, 2001) or via transfer functions (e.g. diatom salinity reconstructions; e.g. Reed *et al.*, 1999), taking the assumption that these modern relationships hold through time. Alternatively, systems can be modelled (e.g. Benson and Paillet (2002) for lake isotope records) to show how climate must vary to force the archive system into the observed response. With the data from this study both climate calibration and modelling can be employed to try to quantify changes in Turkish climate through the last two millennia from the isotope record from Nar Gölü. The record from Burdur is not understood sufficiently to be used for quantification.

8.1 Calibration with meteorological variables

The Nar stable isotope record shows strong relationships with summer relative humidity and summer temperatures (chapter 6) between 1926 and 2001, the time period for which instrumental data are available. For the oxygen isotope record, corrected for changes in mineralogy, compared to the 8 year smoothed meteorological variables between 1933 and 2001 (Table 6.6) the relationships are:

$$\text{Summer RH} = 45.23 - 0.98\ \delta^{18}\text{O} \qquad r^2 = 53.7\ \% \tag{9.1}$$

$$\text{Summer av. temp.} = 0.13\ \delta^{18}\text{O} + 22.11 \qquad r^2 = 25.0\ \% \tag{9.2}$$

$$\text{Summer max. temp.} = 0.16\ \delta^{18}\text{O} + 29.01 \qquad r^2 = 28.1\ \% \tag{9.3}$$

For the data between 1933 and 1986, prior to the change in mineralogy and therefore removing any possible errors caused by this correction (Table 6.8), the relationships are:

$$\text{Summer RH} = 45.78 - 0.76\ \delta^{18}\text{O} \qquad r^2 = 29.3\% \tag{9.4}$$

$$\text{Summer av. temp.} = 0.28\ \delta^{18}\text{O} + 22.01 \qquad r^2 = 56.5\% \tag{9.5}$$

$$\text{Summer max. temp.} = 0.16\ \delta^{18}\text{O} + 28.90 \qquad r^2 = 49.2\% \tag{9.6}$$

For the remainder of the chapter only the strongest two relationships, with summer relative humidity for the full record and average summer temperature for the pre-1986 record, will be discussed in terms of quantification of the isotope record.

It has been shown (chapter 6) that stronger relationships are found with these two meteorological variables if they are smoothed with a 13 year weighted average, the maximum lake residence time (chapter 5), compared to the 8 year smoothing in the above relationships. The following relationships result:

$$\text{Summer RH} = 45.12 - 0.96\ \delta^{18}\text{O} \qquad r^2 = 60.0\% \tag{9.7}$$

$$\text{Summer av. temp.} = 0.27\ \delta^{18}\text{O} + 22.06 \qquad r^2 = 73.3\% \tag{9.8}$$

Assuming uniformatarianism, these relationships, particularly 9.1, 9.5, 9.7 and 9.8, can therefore be used to reconstruct climatic variability in the past.

Errors

Although r^2 values give some idea of how much of the relationship is explained it is also necessary to quantify any errors. Standard deviations of the residuals from the regression relationships, between the recorded meteorological variables and stable isotope values, give an idea of the errors on the reconstructions. Most of the recorded temperature and relative humidity values lie within the 2 standard deviation (2 σ) error envelope (Fig 8.1, 8.2), although extreme values in the meteorological records are not recorded by the lake sediment isotopes.

Although the error range is smaller than the range of the recorded variables, for the summer relative humidity reconstruction (Fig. 8.1a) the error range is 5.38 % (4 σ) compared to a range of 10.51 % for the recorded relative humidity, and for the temperature reconstruction (Fig. 8.2a) the 4 σ range is 1.05 °C compared to a recorded range of 1.77 °C, the reconstructions have a much smaller range. The range of the temperature reconstruction is still just larger than the error range, 1.08 °C compared to 1.05 °C, however for the relative humidity reconstruction the range is less than that of the errors, 5.20 % compared to 5.38 %. For this reconstruction a flat line, indicating no change, could therefore be drawn through the error window, even though there is a change of over 10 % in the recorded relative humidity through this time period.

With the relationships from the 13 yr smoothed meteorological variables the errors are much smaller and in both cases are smaller than the range in the reconstruction, for the summer relative humidity reconstruction the error range is 4.54 % compared to a range of 4.90 % in the reconstruction (Fig. 8.1b). For the temperature relationship, the error range is 0.7 °C compared to a range in the reconstruction of 1.04 °C (Fig. 8.2b).

8.2 Modelling

Modelling the lake response to climatic changes can help interpretation of isotopic changes through the sediment record (e.g. Benson and Paillet, 2001; Ricketts and Johnson, 1996). The simplest form of lake isotope model takes a well mixed lake system in equilibrium and

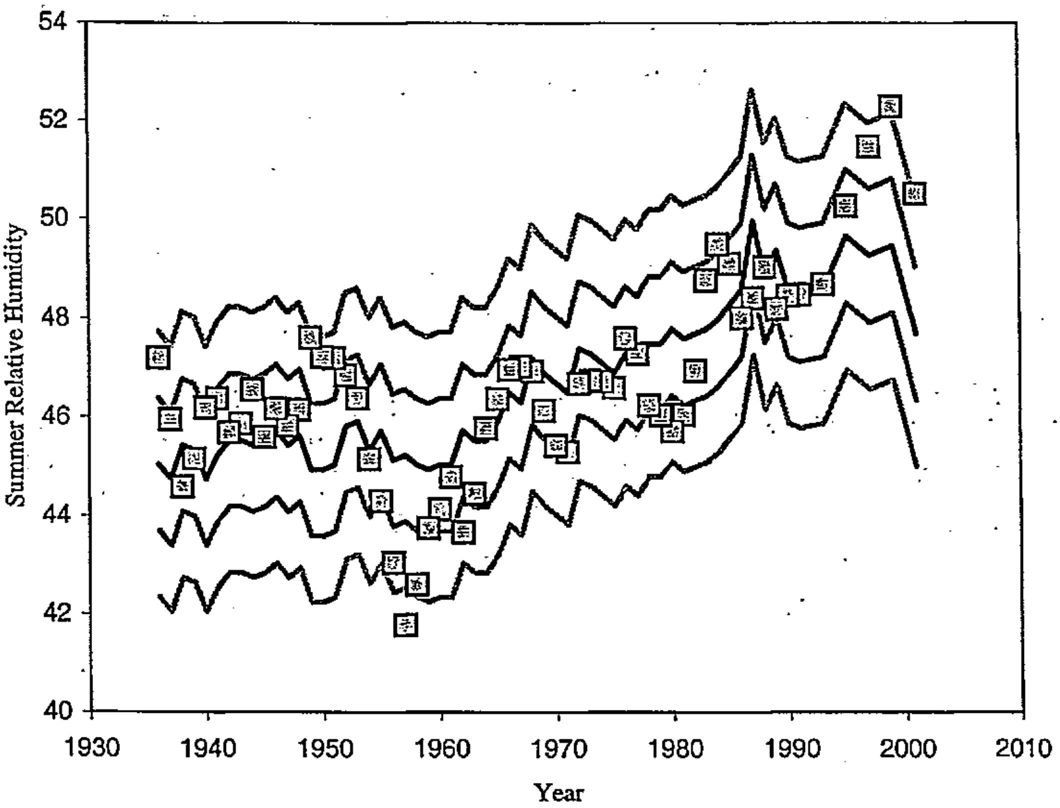

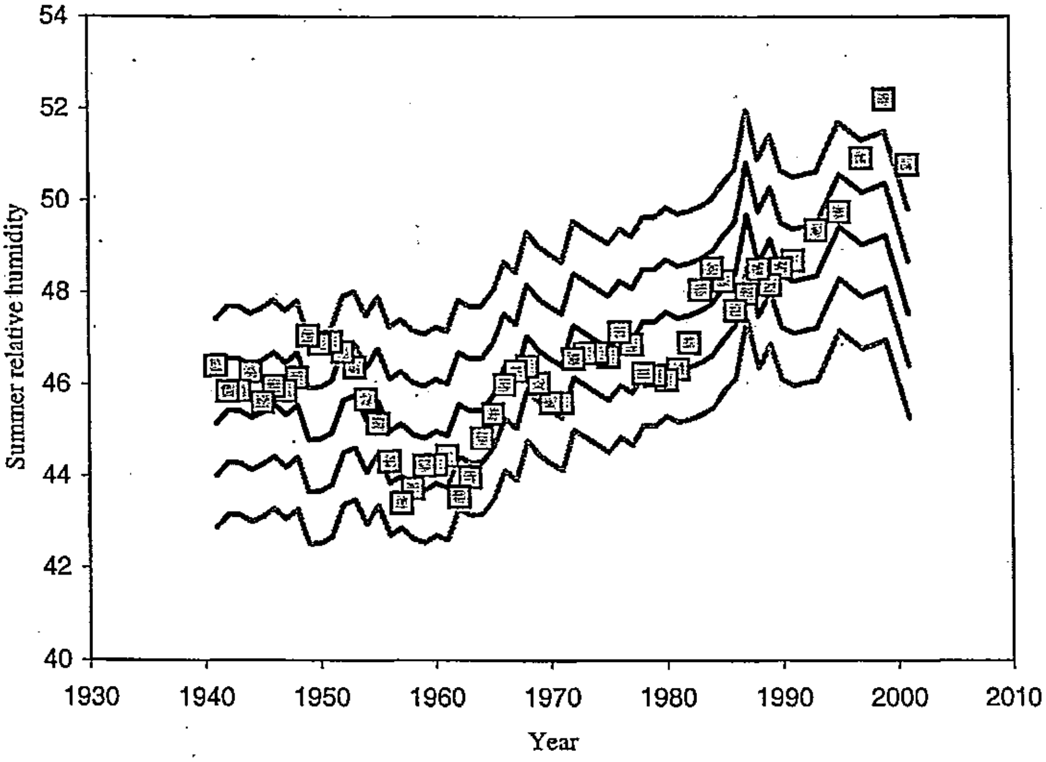

Fig. 8.1 Reconstructed summer relative humidity through the instrumental time period with 1 σ (dark grey lines) and 2 σ (light grey lines) errors from relationships with 8 year (a) and 13 year (b) smoothed meteorological variables. Grey squares show recorded summer relative humidity.

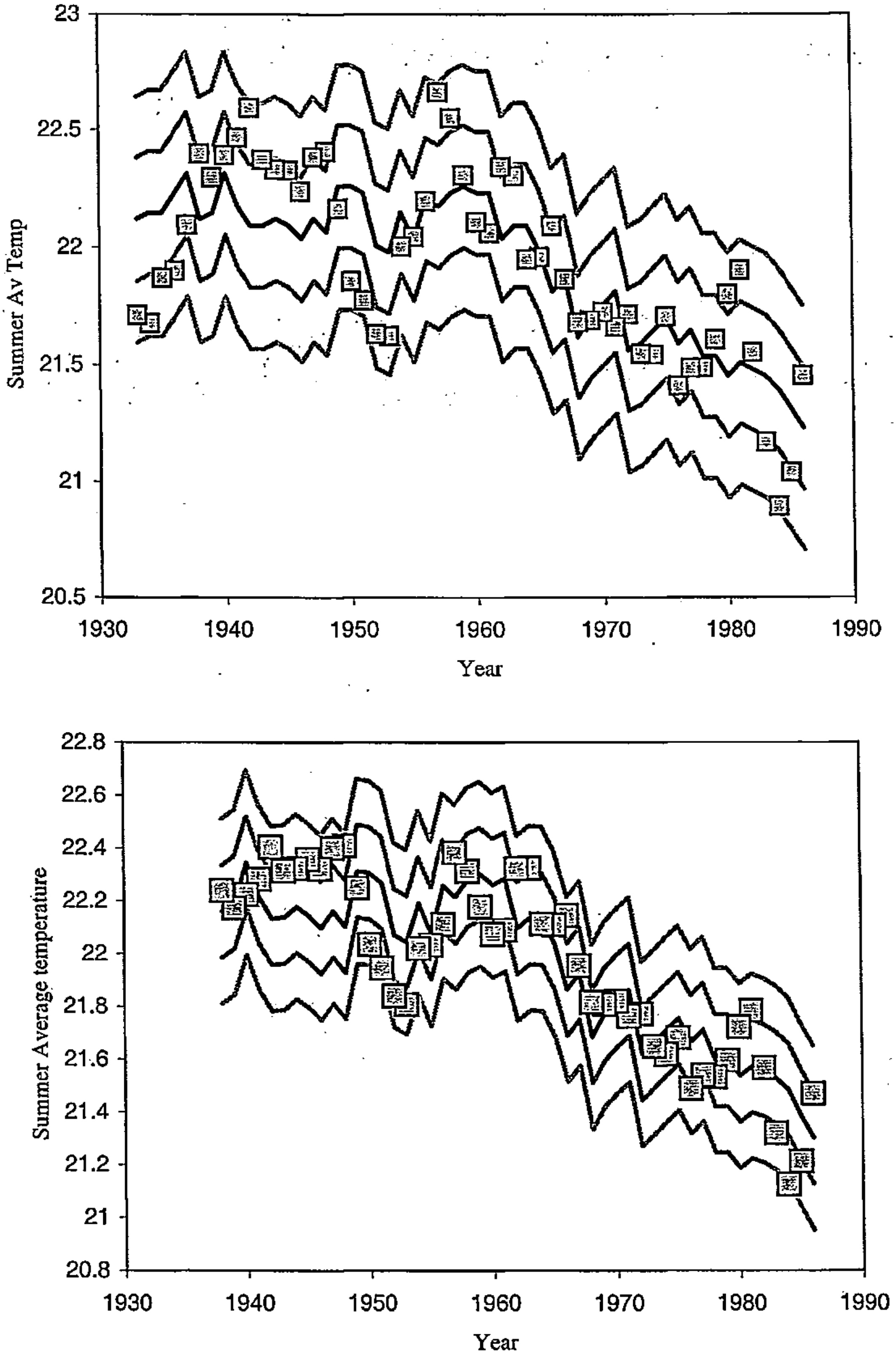

Fig. 8.2 Reconstructed summer average temperature through the instrumental time period with 1 σ (dark grey lines) and 2 σ (light grey lines) errors from relationships with 8 year (a) and 13 year (b) smoothed meteorological variables. Grey squares show recorded summer average temperature.

then forces one of the variables, keeping all others constant, to observe the lake system response. A steady state model for Nar can be built from the initial hydrological variables calculated and estimated in Chapter 5.

It has already been shown (equation 5.7) that at Nar

$$dV\delta_l/dt = P\delta_P + S_i\delta_P + G_i\delta_{Gi} - E\delta_E - G_o\delta_l \qquad (9.9)$$

which can also be written

$$d\delta_l/dt = [(P\delta_P + S_i\delta_P + G_i\delta_{Gi} - E\delta_E - G_o\delta_l) - \delta_l\, dV/dt]/V \qquad (9.10)$$

Values of all these variables are known from the mass balance models used to estimate the lake hydrological budget (Chapter 5) and can therefore be used as the initial values for the steady state model. As the model records changes in δ_l all values for calculating δ_E must also be known as δ_E is a function of δ_l.

Model assumptions

As the model also results in changes in volume the lake area will also change, thus changing the amount of evaporation and rainfall directly from and into the lake respectively. It is also assumed that G_o is proportional to the surface area of the lake bed in contact with the lake water, which will also therefore depend on volume. A relationship between volume, lake area and lake bed surface area is therefore required. From the bathymetry values all these measurements can be calculated for different lake depths. However, there is no simple relationship between these values that can be transferred to the model, especially at values when the lake is deeper than currently observed, and at shallow depths. Lake areas and volumes calculated at different depths, compared with calculated surface areas show strong quadratic relationships (Fig. 8.3), however these curves would predict reductions in lake area at high volumes and do not intercept at (0, 0). Log curves through the data points are probably a more realistic model of reality but do not fit the data well (Fig. 8.3).

In the model the lake basin is therefore taken to be an oblate ellipsoid ($a = b > c$), as this is the nearest regular shape to the real lake basin. Changes in lake volume can then be used to calculate changes in lake area and lake bed surface area.

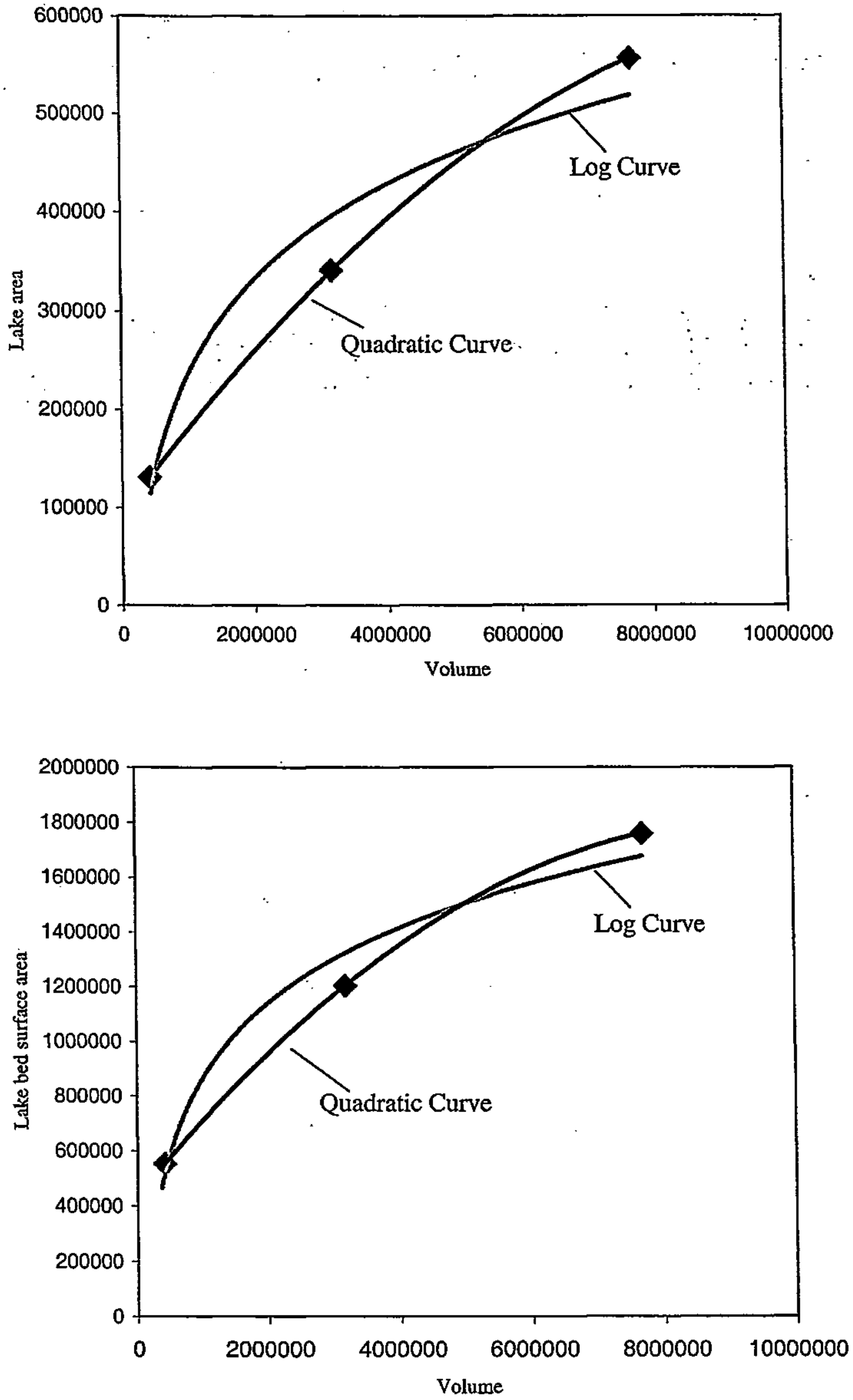

Fig. 8.3 Relationships between lake volume and lake area (a) and lake volume and lake bed surface area (b) from Nar.

As groundwater inflow is largely meteoric water (see discussion in chapter 5), δ_{Gi} is taken to equal δ_P. Groundwater inflow to a lake tends to be concentrated at the lake margin (Almendinger, 1990) and the amount of inflow is therefore also dependent on the area of the lake. G_i is therefore taken to be a function of lake area and the amount of precipitation. In the model δ_P and RH are both taken to be proportional to temperature as the relationships between these variables and temperature are known to be strong (Fig. 5.11; section 6.3.1). The amount of evaporation is also dependent on temperature (equation 5.2).

Two steady state models are used, using the two different calculations of δ_E from Chapter 5, Model 1 using the Benson and White (1994) equation 5.12, and Model 2 using equation 5.10. Table 8.1 shows the initial calculated values for the contemporary lake compared to initial values of the models. To set up a model in equilibrium with values as close as possible to the modern lake system, slight adjustments had to be made to the temperature values. The values shown here represent the model having run to an equilibrium state i.e. there is no change in lake volume or δ_l with a residence time and other values very close to those estimated or measured from the modern lake.

Model Results

Using these initial values it is then possible to force the system to observe changes in δ_L. As RH, E and δ_P are functions of temperature, temperature and precipitation are the major two variables in the model. By shifting these values and running the model to equilibrium, new values for δ_l are observed (e.g. Fig. 8.4). During changes in temperature minimum, average and maximum temperatures are all shifted by the same amount.

Values do not go straight to equilibrium (Fig. 8.4). δ_l values first shift to a maximum value before decreasing again to a new equilibrium state. In reality the lake is unlikely to reach its new equilibrium state as each year values of P and T change.

For changes to new values of T or P the initial value, after one year of change, the maximum value and the new equilibrium value can be compared. As a strong relationship with relative humidity was found between the isotope data and instrumental climate records, the relationship between lake water $\delta^{18}O$ and relative humidity was also observed in the models.

Table 8.1 Comparison of initial model values and recorded values from Nar Gölü. Values in LH column are described in Chapter 5.

	Reality	Model 1	% difference	Reality	Model 2	% difference
Volume	7692360.0	7862813.4	-2.2		7811372.7	-1.5
δ_l	-2.8	-2.4	15.5		-2.2	20.2
Lake area	556500.0	564690.8	-1.5		562225.2	-1.0
P	0.3	0.3	0.0		0.3	0.0
P amount	178080.0	180701.1	-1.5		179912.1	-1.0
δ_P	-10.6	-9.8	7.6		-9.8	7.6
k	0.3	0.3	0.0		0.3	0.0
Catchment area	2408000.0	2408000.0	0.0		2408000.0	0.0
S_i	148120.0	147464.7	0.4		147662.0	0.3
G_i	651677.0	651677.0	0.0	1010012.0	1010012.0	0.0
δ_{Gi}	-10.6	-9.8	7.6		-9.8	7.6
E calculated	1140.4	1124.1	1.4		1124.1	1.4
E measured	1.0	1.0	2.1		1.0	2.1
E amount	570412.0	566380.5	0.7		563907.5	1.1
δ_E	-15.7	-15.2	3.0	-20.6	-20.2	2.1
R_E	1.0	1.0	0.0			
Aeq		1.0			1.0	
δ_A	-21.0	-20.3			-20.3	3.5
R_A		1.0				
e*		10.5			10.5	
Ek					7.7	
sat vp lake					14.4	
sat vp air					11.4	
vp air					6.6	
h					0.5	
G_o	407465.0	413462.3	-1.5	765800.0	773678.5	-1.0
δ_{Go}	-2.8	-2.4	15.5		-2.2	20.2
a		424.0			423.0	
b	26.0	20.9	19.7		20.8	19.8
e		1.0			1.0	
Surface Area		1139544.0			1134568.4	
T_{lake}	285.8	285.5	0.1		285.5	0.1
f_{ad}	0.0	0.0				
RH	0.6	0.6	-1.9		0.6	-1.9
T average	9.2	8.9	3.5		8.9	3.5
z	1363.0	1363.0	0.0		1363.0	0.0
A	38.0	38.0	0.0		38.0	0.0
u	3.2	3.2	0.0		3.2	0.0
Td	6.9	6.5	5.8		6.5	5.8
T min.	2.7	2.5	7.1		2.5	7.1
T max.	16.0	15.8	1.4		15.8	1.4
Inflow	977877.0	979842.8	-0.2	1336212.0	1337586.1	-0.1
Outflow	977877.0	979842.8	-0.2	1336212.0	1337586.1	-0.1
Residence Time	7.9	8.0	-2.0	5.8	5.8	-1.4

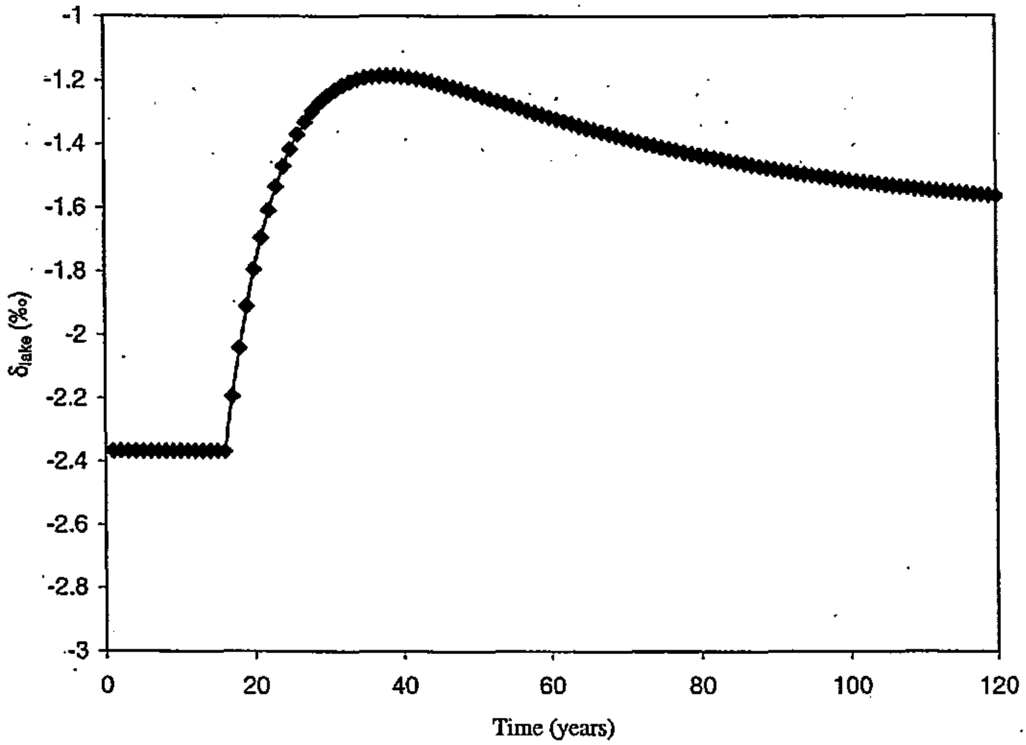

Fig. 8.4 Change in lake water oxygen isotope value with a change in average annual temperature from 8.85 to 9.85 °C in Model 1.

From the initial steady state (Table 8.1) the model was shifted to new values of T, holding P constant. The resulting numbers recorded (Table 8.2) led to the following relationships between lake water isotope values and meteorological variables.

For Model 1:

For equilibrium values:

$$T = 1.2234(\delta^{18}O) + 11.853 \tag{9.11}$$

$$RH = -1.7494(\delta^{18}O) + 53.792 \tag{9.12}$$

For initial shifts:

$$T = 5.7449(\delta^{18}O) + 22.424 \tag{9.13}$$

$$RH = -8.2152(\delta^{18}O) + 38.675 \tag{9.14}$$

For Maximum shifts:

$$T = 0.8463(\delta^{18}O) + 10.859 \tag{9.15}$$

$$RH = -1.2102(\delta^{18}O) + 55.213 \tag{9.16}$$

For Model 2:

For equilibrium values:

$$T = 1.1571(\delta^{18}O) + 11.497 \tag{9.17}$$

$$RH = -1.6546(\delta^{18}O) + 54.301 \tag{9.18}$$

For initial shifts:

$$T = 3.6112(\delta^{18}O) + 16.882 \tag{9.19}$$

$$RH = -5.464(\delta^{18}O) + 46.6 \tag{9.20}$$

For Maximum shifts:

$$T = 1.9106(\delta^{18}O) + 10.893 \tag{9.21}$$

$$RH = -1.3022(\delta^{18}O) + 55.165 \tag{9.22}$$

Although the relationships for the initial shifts in isotope values differ, the two models produce very similar relationships for changes in equilibrium state and especially for the maximum change in δ_l during any change.

The model was then run holding temperatures constant and changing the amount of precipitation, again initial, maximum and changes in equilibrium state were recorded.

Table 8.2 Values of initial and maximum shifts and new equilibrium states for temperature changes to steady state models.

Model 1

RH	T_{max}	T_{av}	Equilibrium	Max. during change	Initial change
59.516	14.80	7.85	-3.34	-3.56	-2.54
58.086	15.80	8.85	-2.36		
56.656	16.80	9.85	-1.57	-1.19	-2.19
55.226	17.80	10.85	-0.90	-0.02	-2.01

Model 2

RH	T_{max}	T_{av}	Equilibrium	Max. during change	Initial change
59.516	14.80	7.85	-3.20	-3.34	-2.50
58.086	15.80	8.85	-2.23		
56.656	16.80	9.85	-1.38	-1.14	-1.96
55.226	17.80	10.85	-0.61	-0.05	-1.66

For Model 1:

For Initial shifts $$P = -0.3459(\delta^{18}O) - 0.4987 \quad (9.23)$$

For Maximum shifts $$P = -0.0538(\delta^{18}O) + 0.2069 \quad (9.24)$$

For Model 2:

For Initial shifts $$P = -0.2473(\delta^{18}O) - 0.2326 \quad (9.25)$$

For Maximum shifts $$P = -0.686(\delta^{18}O) + 0.0177 \quad (9.26)$$

In both models there is no simple relationship between changes in precipitation and new lake equilibrium values (Fig. 8.5). Increase in precipitation lead to more negative isotope values, however decreases in precipitation do not lead to any major change in the lake equilibrium values. This may be due to there being no change in the net flux through the lake with a decrease in precipitation i.e. the decrease in input = decrease in output due to reduction in lake volume, whereas with an increase in precipitation input becomes greater than output therefore leading to more negative isotope values.

Isotopic values of lake waters respond in the model as suggested in chapter 6 for the controls on the Nar isotope record. Increasing temperatures, and the associated fall in relative humidity, lead to more positive isotope values, as does a decrease in the amount of rainfall. Decreasing temperatures and increasing relative humidity lead to more negative isotope values.

Testing the models

These relationships are based on changes from one initial steady state. Starting the model in different steady states, with different starting temperatures, the same exercise as above can be carried out to observe if the model behaves differently (Table 8.3). Whatever the starting value, equilibrium values for a given temperature are the same in all cases. However the initial values, and maximum values, and the differences between the starting values and initial and maximum values, do change with differing starting temperatures. As conditions gets warmer, and less humid, the values of the initial shifts in the system get smaller and the maximum values during changes get larger, although at a much lower

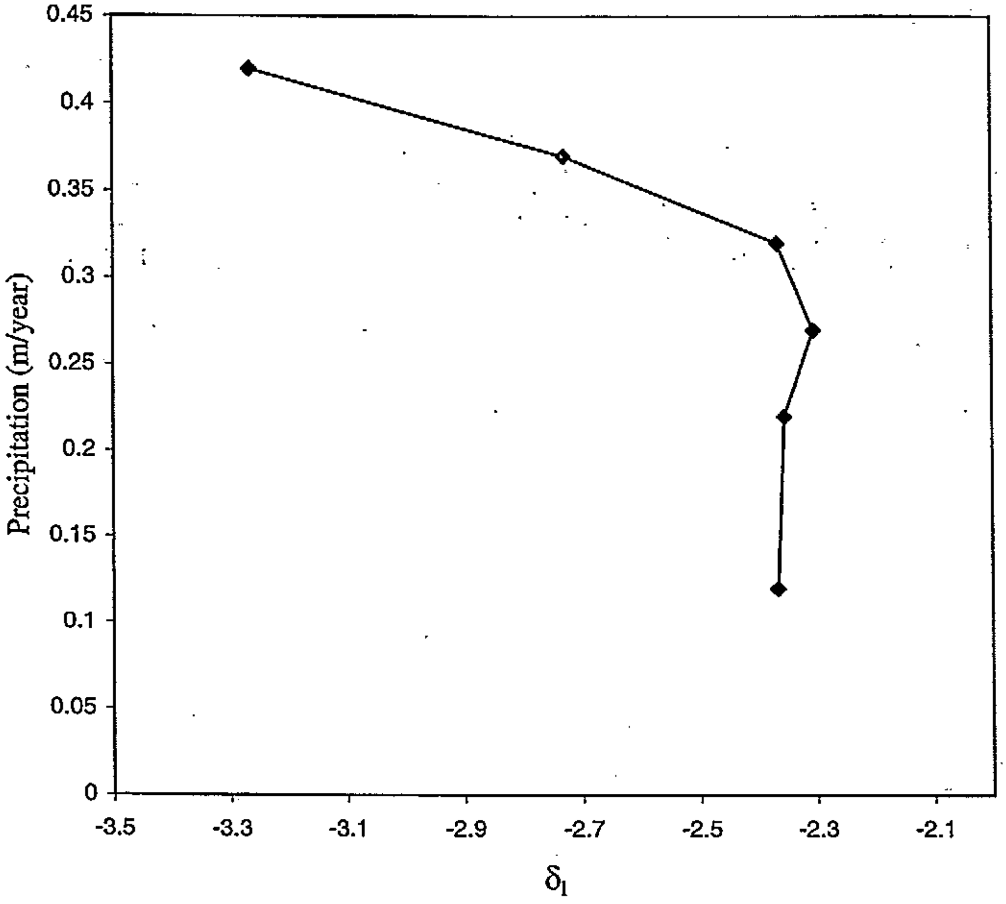

Fig. 8.5 Equilibrium δ_l values with changing values of precipitation in Model 1.

Table 8.3 Changes in initial and maximum shifts and equilibrium oxygen isotope values (‰) from different initial states of Model 1.

Tav	Equilibrium	Max change	Initial Change	Original - initial	Original - max
Start at 8.85					
6.85	-4.47	-4.76	-2.70	0.24	2.29
7.85	-3.34	-3.56	-2.54	0.07	1.09
8.85	-2.46				
9.85	-1.57	-1.19	-2.19	-0.27	-1.28
10.85	-0.90	-0.02	-2.01	-0.45	-2.45
Start at 9.35					
7.35	-3.92	-4.30	-2.37	0.38	1.93
8.35	-2.87	-3.14	-2.18	0.19	1.15
9.35	-1.99				
10.35	-1.26	-0.85	-1.79	-0.20	-1.14
11.35	-0.60	0.28	-1.59	-0.40	-2.27
Start at 9.85					
7.85	-3.41	-3.87	-2.05	0.42	2.24
8.85	-2.44	-2.74	-1.84	0.21	1.12
9.85	-1.63				
10.85	-0.93	-0.52	-1.41	-0.22	-1.10
11.85	-0.28	0.57	-1.18	-0.45	-2.20

Table 8.4 Comparison of model relationships, for maximum shifts for a given climate change, and climate calibration relationships for the range of values in the Nar record.

	Relative Humidity			Average Temperature		
$\delta^{18}O$	**Climate Calibration**	**Model 1**	**Model 2**	**Climate Calibration**	**Model 1**	**Model 2**
-5.7	50.8	62.1	62.6	20.4	6.0	5.7
-2	47.2	57.6	57.8	21.5	9.2	9.1
-1	46.2	56.4	56.5	21.7	10.0	10.0
0	45.2	55.2	55.2	22.0	10.9	10.9
1	44.3	54.0	53.9	22.3	11.7	11.8
2	43.3	52.8	52.6	22.6	12.6	12.7
2.4	42.9	52.5	52.0	22.7	12.9	13.1
Range	7.9	9.8	10.5	2.3	6.9	7.4

rate than the change in the initial shift. Similar patterns to those initially observed are found for changes in amounts of precipitation when the model has a lower initial precipitation value. As in Fig. 8.5 a reduction in precipitation makes no difference to the equilibrium lake water isotope value whereas increasing amounts of precipitation lead to more negative equilibrium isotope values.

The relationships in the model can be compared to the relationships found from the isotope record climate calibration. Compared to the calibration relationships with summer relative humidity (9.1) and summer average temperature (9.5) the closest relationships from the models are with the maximum shifts in δ_l (Equations 9.15, 9.16, 9.21 and 9.22). Taking these relationships over the full range of the $\delta^{18}O$ record from Nar (-5.7 ‰ to 2.4 ‰) the model relationships result in larger ranges of reconstructed temperature, 6.9 °C compared to 2.3 °C for the climate calibration relationship, and relative humidity values, 9.8% compared to 7.9%, and the values are colder and more humid (Table 8.4). The relationships from the model and the climate calibration are closer for relative humidity values than for temperature.

The difference in values between the model and the climate calibration relationships may be due to the different time periods represented by the model and the climate calibration. The model is run on yearly time steps, with annual average values, whereas the climate calibrations are based on summer climate variables.

Monthly steady state model

To try and understand the effect of different seasons on the lake isotope system the models can be run on monthly time steps using the average annual values of temperature and precipitation (Figs. 5.5 and 5.6). The models change to new equilibrium states where they change monthly, with the most negative values in May and the most positive in October (Fig. 8.6). The annual range in Model 1 is 0.75 ‰ compared to 1.14 ‰ in Model 2, the average values are more negative in Model 1, -1.48 ‰, compared to -0.55 ‰ in Model 2.

Both models predict annual changes similar in range those observed in the field. A sine curve fitted to the recorded water isotope values from 2001 and 2002, with the most positive values in October and the most negative values in April and May, has a range of 0.97 % (Fig. 8.7). However both models predict values more positive than those recorded.

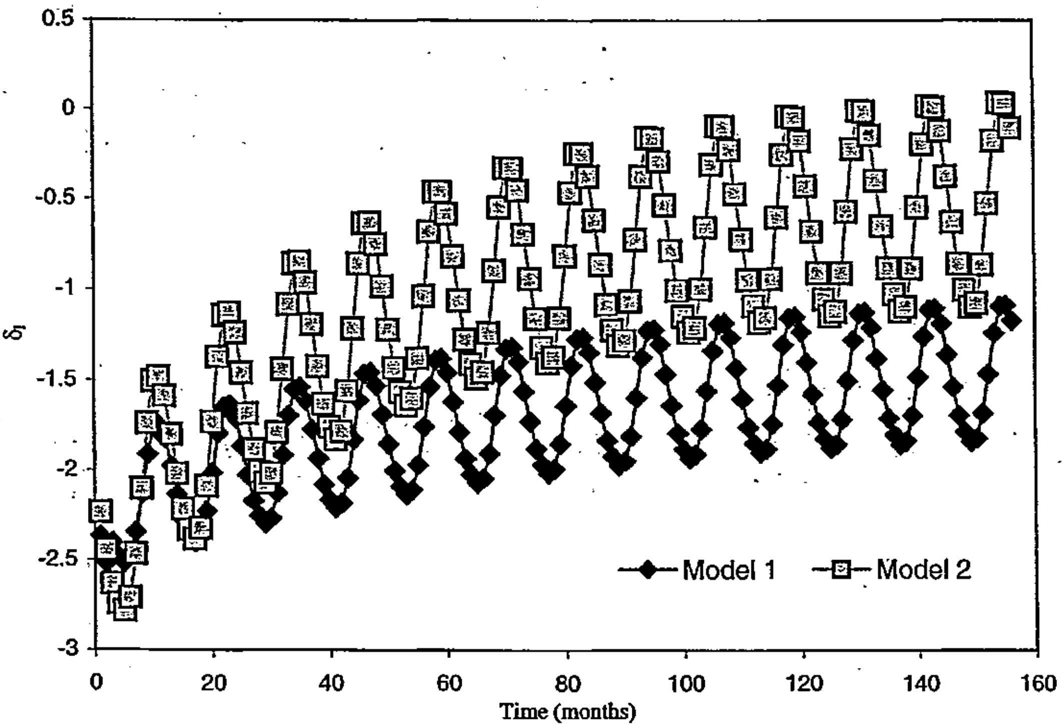

Fig. 8.6 Shifts from annual steady state model to monthly steady state model using average precipitation and temperature values from Derinkuyu.

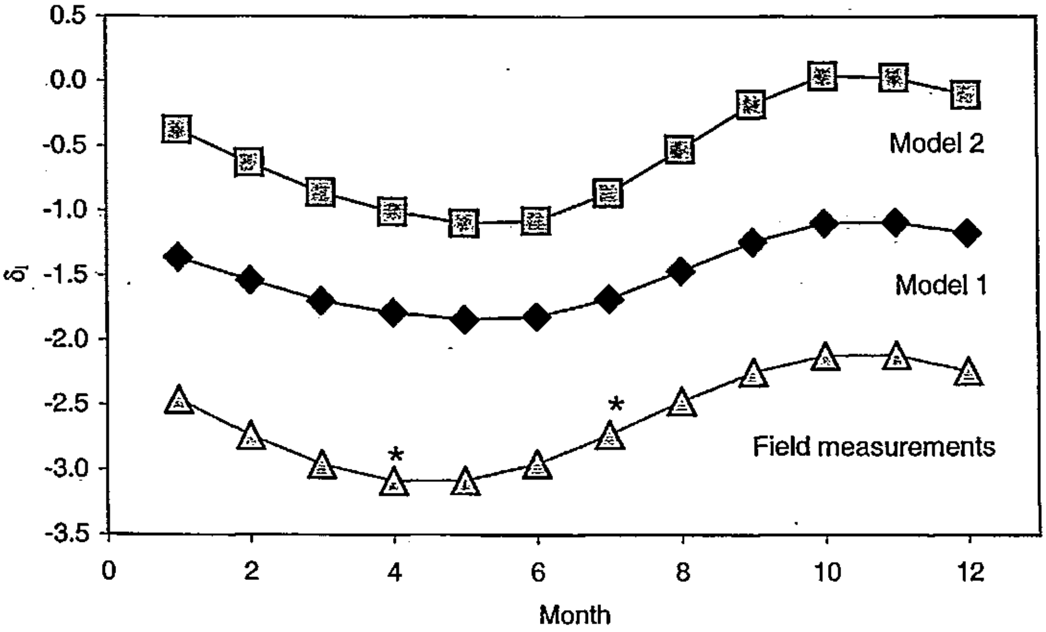

Fig. 8.7 Modelled annual variability in lake water isotope values. Compared to estimated values from recorded isotope values (*).

Dynamic Models

The sensitivity of the models can be further tested by modelling variability through the instrumental time period, using the recorded instrumental data, and comparing the model output with the recorded isotope data. Lake water isotope values predicted by the model must be converted to values of carbonate, based on temperature and the predicted isotope value of the lake water (equation 5.15), for comparison with the measured isotope values from the sediments. The models are run on annual or monthly time steps, and the carbonates measured represent lake waters and temperatures at only a particular time of the year, probably the early summer. These factors must be taken into account when comparing the models to the recorded isotope variability. Summer temperatures are therefore used for the carbonate calculations, whereas annual average temperatures are used for calculating changes in δ_l.

Initial conditions for the model are generally unknown. Temperatures and recorded carbonate isotope values are known, and initial values of δ_l can therefore be estimated. The initial volume of the lake is unknown and therefore can be changed until the model fits the data.

Meteorological data is only available from Derinkuyu between 1965 and 1990, and the full data required for the model only between 1966 and 1989. Using this data Model 1 output only represents 38 % of the variability in the Nar isotope record through this time period, although the direction and magnitude of the change are correct.

The models will only be useful for climatic reconstruction if one variable can be changed in the model and produce the measured response in the isotope values. If precipitation values are held constant between 1966 and 1990 in the model the relationship between the predicted and observed isotope values is stronger (Fig. 8.8; $r^2 = 0.55$). In Model 2 $r^2 = 0.36$ for the predicted versus observed isotope values suggesting that Model 1 is a better representation of the Nar system and will therefore be used from this point on.

The better fit with the constant precipitation suggests that there is limited variability in input to the lake. In the model the amount of precipitation controls the amount of surface inflow and the amount of groundwater inflow. If the model lake responds better to a constant input, of the average values of precipitation through the time period, this suggests that variability in precipitation may be buffered by movement through the catchment such

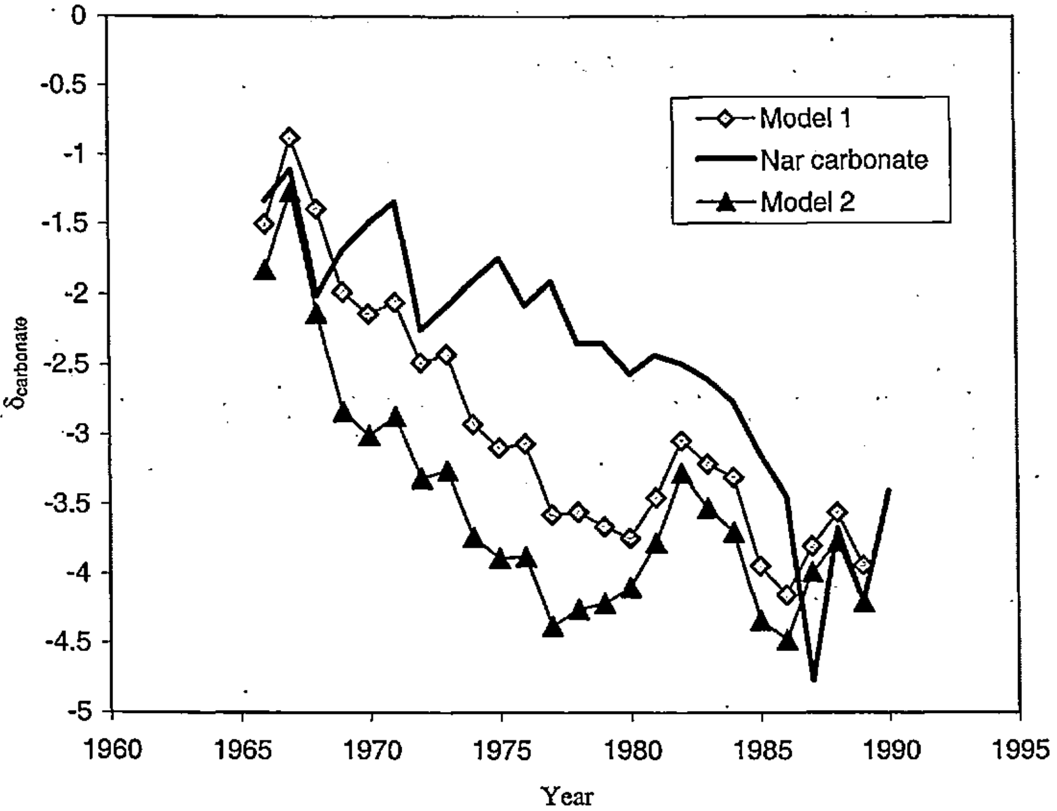

Fig. 8.8 Modelled and recorded carbonate isotope values between 1966 and 1990 with constant precipitation.

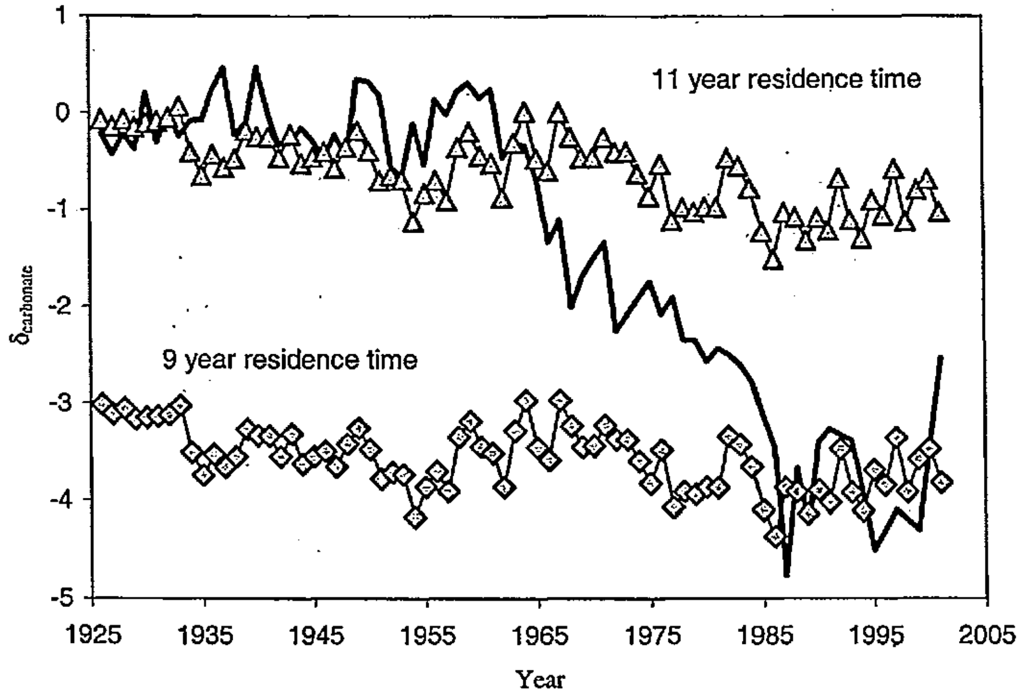

Fig. 8.9 Modelled and recorded carbonate isotope values between 1926 and 2001 with constant precipitation, models run with varying residence times compared to carbonate isotope values (black line).

that the resulting lake inflow is more or less constant. This also suggests that evaporation, and other temperature-related factors are the dominant control on the lake water isotopes as no variance in precipitation is required for the system to change as recorded.

However, this model represents a very short time period and it is important that the model can also predict isotope values over longer time periods. Temperature data are available from Ankara between 1926 and 2001 and these values can be adjusted to values for Derinkuyu based on the relationships between the two data sets between 1965 and 1990 (Table 6.9). For this period the model predicts only 22 % of the recorded variability when precipitation is kept constant (Fig. 8.9).

Possible errors in the model

Although the major shift in the isotope record between 1960 and the late 1980s is recorded by the model, the model does not account for the magnitude of the recorded isotope variability, with a shift of only -1.4 ‰ compared to a shift of -3.5 ‰ recorded in the sediments. Part of this difference may be explained by the possible hydrological threshold in the Nar lake system, as discussed in chapter 6, although this would only account for ~1‰ of the difference.

There are errors in the estimates of the hydrological conditions in Chapter 5, especially in the estimates of the amount of groundwater inflow and outflow. Changes in these values would alter the residence time of the lake.

Changing the residence time makes little difference to the range of oxygen isotope variability in the model. A new model, with a residence time of 11 years compared to approximately 8 years in the original model has a range of 1.5‰ compared to a range of 1.4‰ for the original model between 1967 and 1986. The major difference between the models is the absolute values, with the longer residence time resulting in more positive carbonate isotope values. The 11 year residence time model predicts the recorded values of $\delta^{18}O$ prior to the shift at 1960 whereas the 8 year residence time model predicts values post 1990. This suggests that residence times may have shifted from 1960 to 1990 due to changes in the flux through the system.

Annual precipitation at Derinkuyu has a long term decrease in values between 1966 and 1990 suggesting there may have been an additional change in the lake hydrology during this time resulting in increased groundwater inflow, or surface runoff leading to an increase in flux into the lake. However rainfall trends are very localised in this region, the relationship with Derinkuyu and Ankara precipitation values has an r^2 value of only 0.1745, and the relationship between Derinkuyu and Nevşehir, only 25 km to the north has an r^2 value of 0.51. As Nar is a similar distance from Derinkuyu as Derinkuyu is from Nevşehir it may be that there are significant differences between precipitation at Nar and Derinkuyu. It may be therefore that there was a localised increase in precipitation at Nar between 1960 and 1990 causing the reduction in residence time of the lake..

The flux for the 11 year residence time model is 714801 m^3yr^{-1} compared to 97877 m^3yr^{-1} for the original, 8 year residence time, model. If inflow into the lake was controlled only by precipitation, and not lake area, precipitation would have to change from 0.32myr^{-1}, pre-1960, to 0.44 myr^{-1}, post 1980, for the required change in flux to change the residence times and the associated isotope values. Alternatively values could change from 0.23 myr^{-1} to 0.32 myr^{-1}, depending if 0.32myr^{-1} is taken to be the initial or final value of precipitation. In the dynamic model, where changes in influx are also dependent on changing lake volume, precipitation in the 11 yr residence time model has to change to a maximum value of 0.48 myr^{-1}, and a steady state of 0.40 myr^{-1} to achieve the recorded shift in lake water isotope values (Fig. 8.10). The maximum precipitation at Derinkuyu between 1966 and 1990 was 0.42 myr^{-1} and the values of predicted precipitation change from the models are therefore in the order of the natural variability in precipitation in the Nar region.

8.3 Reconstructions

The models respond differently than the climate calibration relationships; specifically the model cannot reproduce the range in the recorded isotope values by changing only one variable. However, while the models do not predict changes of the same magnitude they do generate changes at the same time and in the same direction as the isotope record. This suggests that there may be a response in the lake system that amplifies the trends in isotope values picked out in the models.

The relationships found with the meteorological data describe a more sensitive system than those explained by the model, although the relationships are in the same direction. There

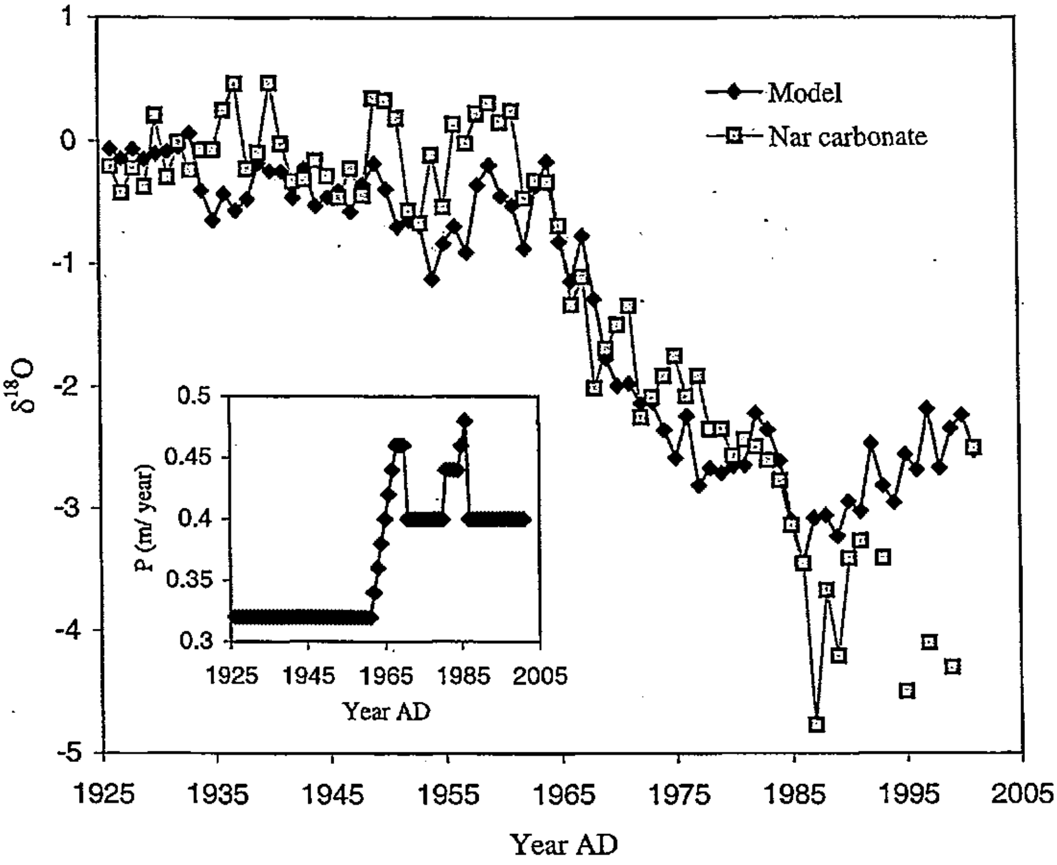

Fig. 8.10 11 year residence time model with required change in precipitation (inset) to force observed change in Nar Gölü carbonate $\delta^{18}O$. See discussion of differences, post 1985, in text.

are sufficient unknowns in the model that it is not possible to understand fully the lake isotope system and how it shifts at the magnitude observed in the carbonate record. Therefore, the sensitivity of the system as suggested by the climate calibrations may be broadly correct. The climate-isotope relationships can therefore be used to reconstruct how climate may have varied in central Turkey through the last 2000 years.

The summer average temperature - isotope relationship is based only on calibration with the isotope record prior to 1986, when the mineralogy changed from aragonite to calcite. It would therefore be invalid to use this relationship to reconstruct climate beyond the point in the record where the carbonate laminae shift from calcite to aragonite (c. 1400 AD). The summer relative humidity calibration can be used through the whole record. For reconstructions the calibrations with the 13 year smoothed meteorological variables will be used as these are the strongest relationships with the smallest errors. However this means that the reconstructed climate record will also be similarly smoothed.

The temperature reconstruction between 1410 and 1986 AD (Fig. 8.11) shows 1986 to be the coolest summer (21.3 °C) through the record, 1.2 °C colder than the warmest summer, 1860 (22.5 °C). With the error envelope of 0.7 °C, 1860 could have been only 0.5 °C warmer and may have been up to 1.9 °C warmer. As well as these being the extreme years in the record the 1980s is the coldest decade (although only 6 years data are available), with an average temperature of 21.5 °C, and the 1860s is the warmest decade, 22.3 °C. The next two warmest decades are the 1420's, 22.2 °C, and the 1930's, 22.2 °C, and these are the only three decades averaging over 22.2 °C. The second and third coldest decades are the 1640's, 21.6 °C, and the 1740's, 21.6 °C. There are only 3 decades averaging below 21.6 °C.

The summer relative humidity calibration was based on the $\delta^{18}O$ record corrected for change in mineralogy. The rest of the record must also therefore be corrected before this calibration is applied for the climate reconstruction. Based on XRD of the carbonate laminae (table 6.1) a correction of -0.6‰ is applied to the aragonite laminae between 1410 and 1986 AD, 1398 and1400 AD, 856 and 861 AD, and from 551 to the base of the record, 276 AD.

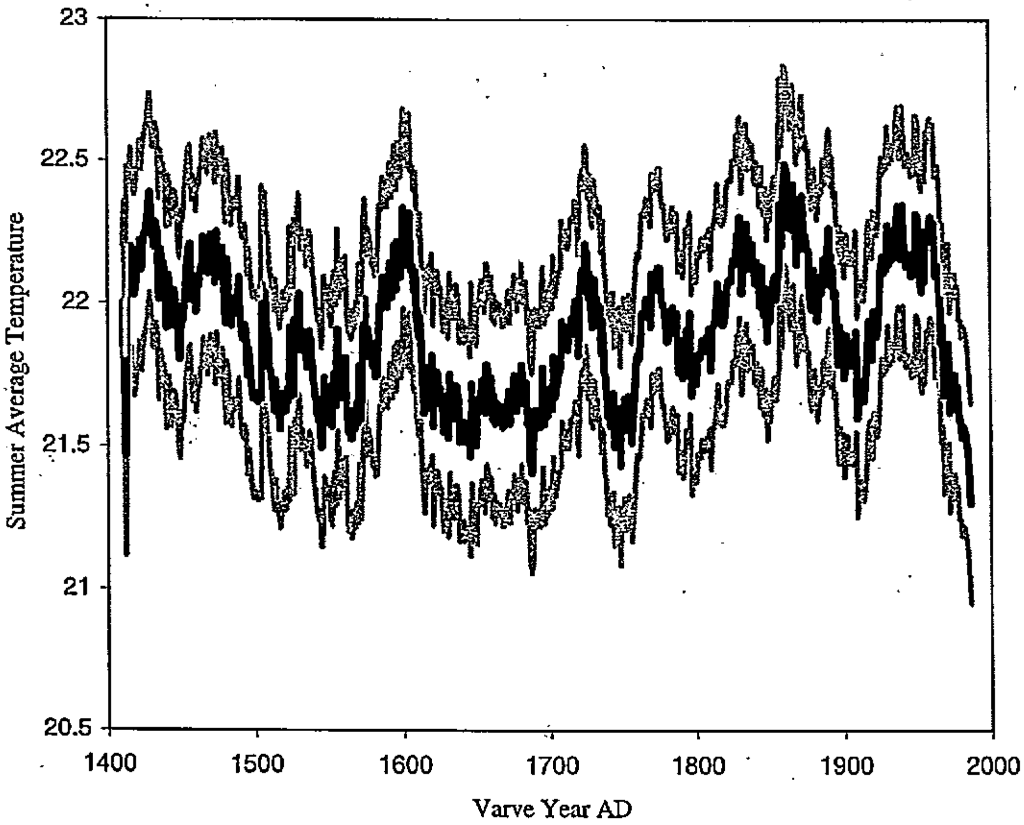

Fig. 8.11 Temperature reconstruction between 1410 and 1986 AD.

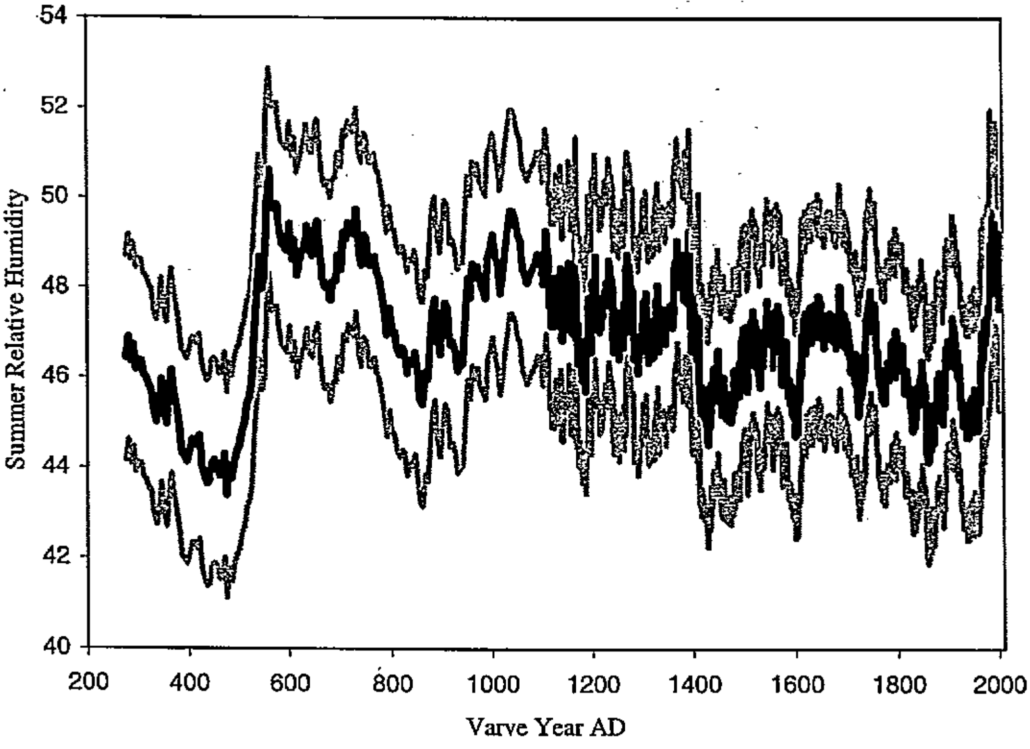

Fig. 8.12 Relative humidity reconstruction between 276 and 2001 AD

The reconstruction (Fig. 8.12) suggests that the sample representing 470 to 476 AD was the least humid period (43.4 %) in the record with 561 to 565 AD the most humid (50.6 %). Including the errors, this suggests a shift in summer relative humidity of between 2.8 % and 11.8 % in the space of 90 years. The 560's were the most humid decade in the record, averaging 50.2 %, with the 430's the least humid decade, averaging 43.7 %. During the last millennium 1860 was the least humid year, 44.2 %, and the period 1041 to 1045 AD was the most humid.

8.4 Summary

The oxygen isotope record from Nar Gölü shows strong and significant relationships with summer relative humidity and temperature suggesting that the isotope record is a proxy for evaporation largely driven by these meteorological variables. The relationships found from the climate calibrations can be used for the quantification of the palaeorecord if it is assumed that the relationships observed during the 20th century hold through time.

The validity of these observed climate-proxy relationships can be checked by modelling the lake isotopic system and observing modelled changes during the instrumental time period. The models produce shifts in the isotope record in the same direction and at the same time as those recorded from the sedimentary carbonate although the model system is not as sensitive as the real lake. By manipulating the models it can be shown that the model underestimates the change in flux associated with climatic change, or else requires changes in more than one variable to force the system into the recorded state.

Due to the complex nature of lake isotope systems, and the number of potential errors in the equations on which the models are based, it is assumed that the relationships observed from the calibration of the oxygen isotope records against climate variables are broadly correct and that these can be used to quantify past climatic change.

Chapter 9

LATE HOLOCENE CLIMATE TRENDS

The evidence from Nar Gölü suggests that the $\delta^{18}O$ carbonate record is a record of summer lake water isotope values driven largely by changes in evaporation due to variation in relative humidity and/ or temperature. The record suggests that there have been wide variations in the amount of evaporation through the last 2000 years with periods of increased evaporation prior to 530 AD and between 1400 and 1970 which were probably associated with times of increased summer temperatures and reduced relative humidity. The period between 530 and 1400 AD was a period of relatively less evaporation probably associated with lower summer temperatures and higher summer relative humidity.

9.1 Comparison with other records

There is some evidence, from the modelling and sudden shifts in the $\delta^{18}O$ values (chapter 8), that there may be some non-climatic factors influencing the hydrology at Nar through the instrumental time period. This may have also been the case through the rest of the record. Comparison with other palaeorecords may show if the shifts recorded in the Nar record occur at the same time, and at the same magnitude, as climate changes suggested by other proxy records, or if events are unique to Nar and, therefore, possibly non-climatic.

During the summer, the season represented by the Nar $\delta^{18}O$ record, Turkish climate is linked to Hadley cell circulation and variation in the African and Indian summer monsoons (chapter 3). The records from Nar are therefore most likely to follow patterns observed in nearby sites and in other regions controlled by Hadley cell and monsoon variations during the summer months, and these will therefore be used in the comparative analysis that follows.

9.2.1 Turkey and the Near East

There are no other lake isotope records that span the last two millennia from Turkey or the Eastern Mediterranean region at a high resolution. Some records do include the late

Holocene but at a low resolution and with generally poor dating control, with none of the sites discussed below having any radiocarbon dates younger than 2000 years BP.

The records from Zeribar (Stevens *et al.*, 2001) and Gölhisar (Eastwood *et al.*, submitted) show a positive trend in isotope values through the last 2000 years, as observed in the Nar record between 500 and 1960 AD, but do not show the major negative shift observed in the Nar record at around 500 AD (Fig. 9.1). The record from Lake Van (Lemke and Sturm, 1997) shows positive peaks at 600 and 1300 AD which may correspond to positive peaks in the Nar record at 476 and 1428. In this case the lower peak in the Van record at 1000 AD would correspond to the smaller peak at Nar at 856 AD. The comparison of the Nar and Van records is of interest as both chronologies are based on varve counting, although the coarseness of the Van sampling intervals may account for some of the difference between the two records.

The record from Eski Acıgöl (Roberts *et al.*, 2001) appears to show the opposite trends to Nar and Van, with negative peaks, at 469, 748 and 1117 AD, that may correspond to the events discussed above. Alternatively the negative peaks in the Eski Acıgöl record could correspond to the negative points in the Nar record at 561 and 1358 AD. This ambiguity highlights the difficulties in comparing records from sites with coarse sampling resolution and poor chronological control.

The Nar record shows a much larger range in $\delta^{18}O$ values compared to the other lake sites (Fig. 9.1). Lakes under different hydrological conditions do show differences in the range of values, with large closed lakes and open lakes tending to show smaller ranges compared to small closed lakes (Leng and Marshall, in press). In addition open lakes will show more negative values than closed lake systems. For the lakes discussed here, lakes with more positive mean isotope values generally have slightly larger ranges (Fig. 9.2), although the Nar record has a range approximately 5‰ higher than any of the other lakes suggesting there are additional controls on this lake system (see below for further discussion).

There are further late-Holocene isotope records, from non-lake archives, in the eastern Mediterranean region. A $\delta^{18}O$ record from planktonic foraminifera found in deep-sea cores off the Israeli coast (Schilman *et al.*, 2001) has been interpreted as a record of changes in the evaporation/ precipitation ratio for the eastern Mediterranean basin. Large-scale trends in the record are similar to those at Nar (Fig. 9.3) with the MWP showing a time of

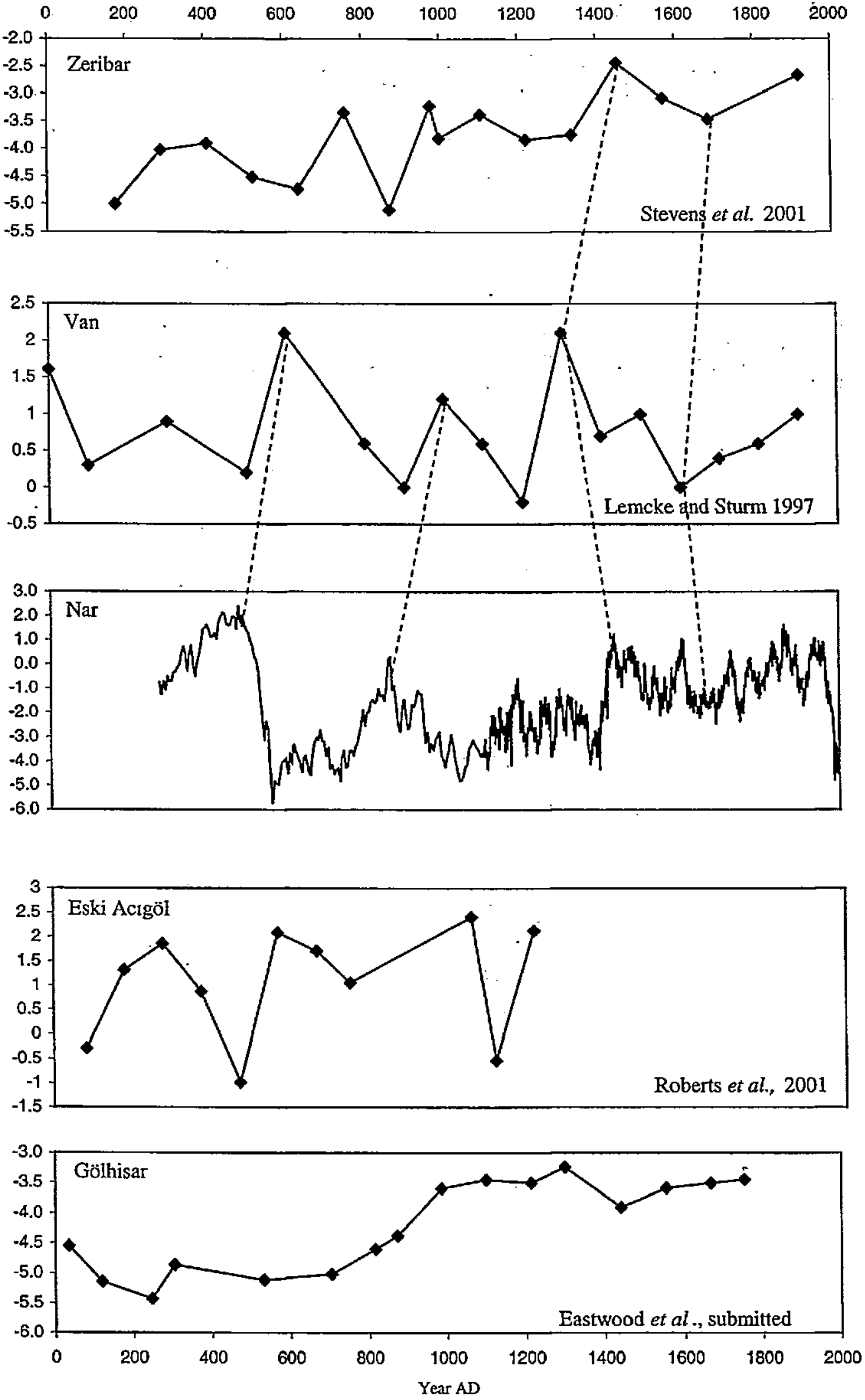

Fig. 9.1 Comparison of Nar $\delta^{18}O$ record with other Turkish and Near East lake isotope records (all y-axis values are $\delta^{18}O$ ‰), with possible correlations shown with dashed lines.

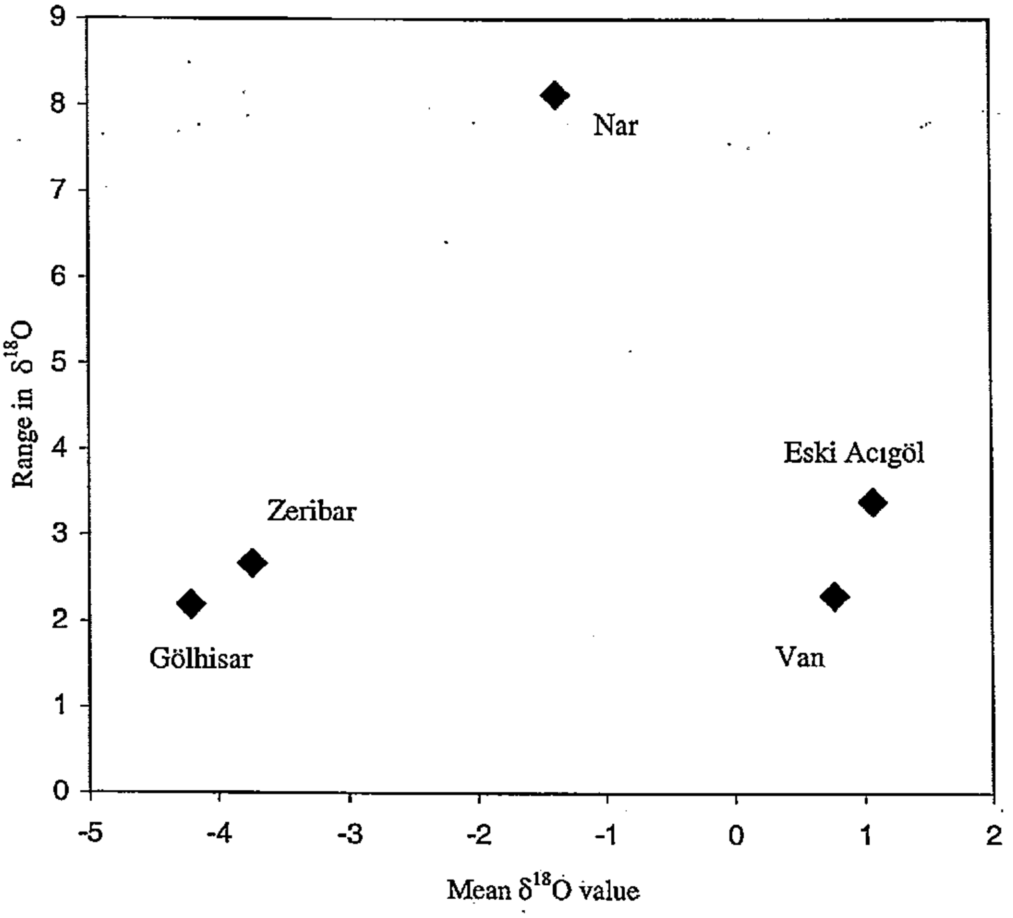

Fig.9.2 Range and mean value relationship for $\delta^{18}O$ values from lakes in Fig. 9.1.

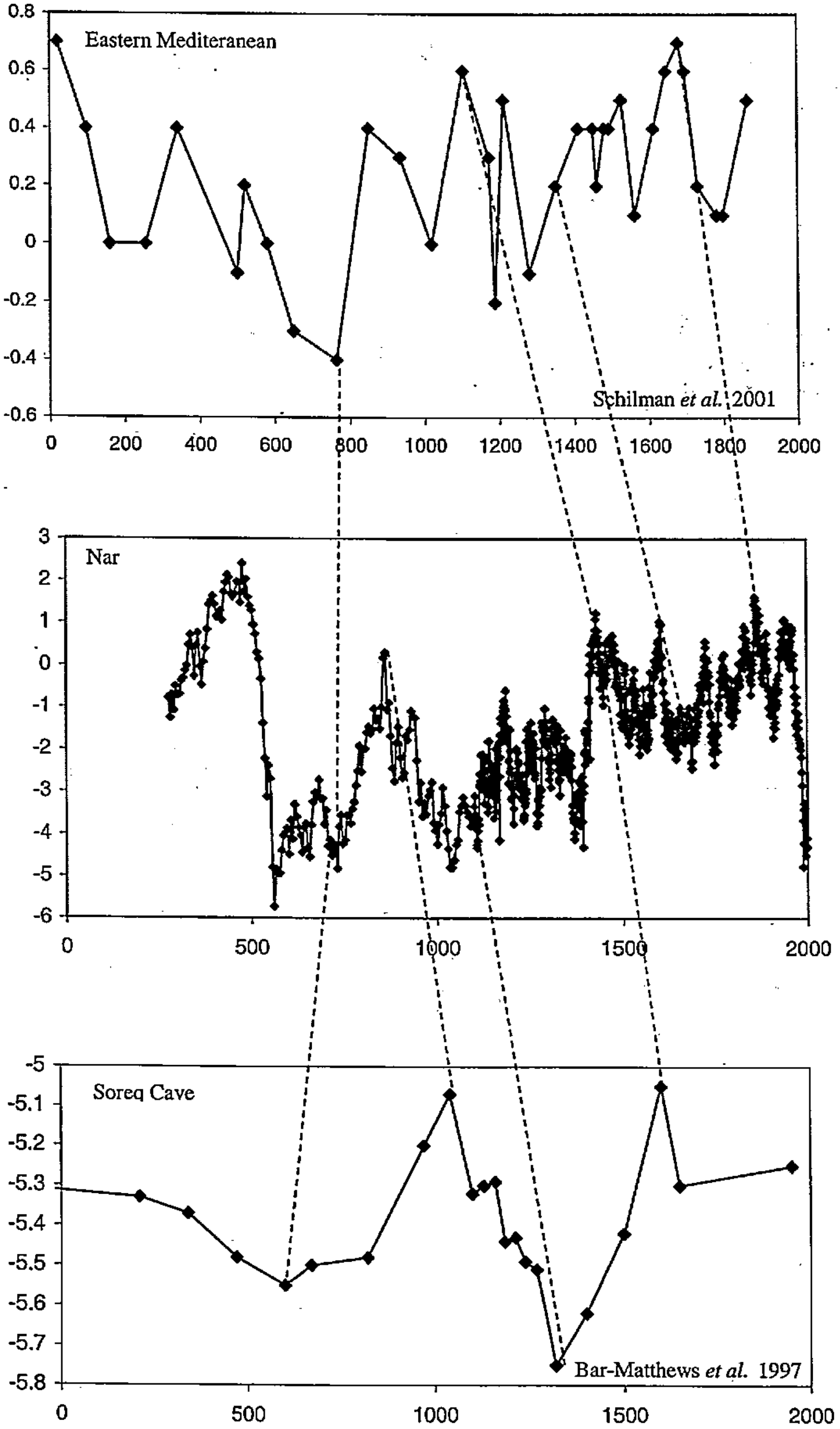

Fig. 9.3 Comparison of Nar $\delta^{18}O$ record with $\delta^{18}O$ records from the Eastern Mediterranean Sea and Soreq cave, Israel, with possible correlations shown by dashed lines.

decreased E/P and showing more negative isotope values. A record of $\delta^{18}O$ from a speleothem from Israel also spans the past 2000 years (Bar-Mathews *et al.*, 1997). The largest shift in this record is to more negative values, interpreted as an increase in precipitation, around 1320 AD with periods of relatively lower rainfall either side of this wet period. This dry-wet-dry sequence may correspond to the decrease then increase in isotope values at Nar between 1429 and 1937 AD, a pattern that is also evident in the planktonic foraminifera curve. As with the lake records differences in sampling resolution and low numbers of dates through this time period make comparisons with the Nar record difficult.

For comparison with these other low-resolution records the Nar sequence can be aggregated into samples representing 1cm slices of the core and then "sampled" at different resolutions to observe how differing sampling resolutions might affect inter-record comparisons. In this exercise the core counts and depths from each counted section through the core are used to give a laminae v. age relationship; it is assumed that the laminae between two depths are of equal width. Average $\delta^{18}O$ values for each cm of the Nar sequence can then be calculated. Using this record it is possible to look at how the isotope variability from the original record would be represented at different sampling resolutions. The total amount of the original record explained by the records at different sampling resolutions can be estimated by giving values to equivalent depths in the original record to points lying between two samples in the re-sampled records. The new estimated values therefore lie along a straight line between two sample points and there are the same number of observations in the original and new records. Regression analysis can then be used to give r^2 values, explaining the variability in the original data set explained by the new constructed data sets.

For the full length record 81 % of the range from the original records is explained by a 16cm sampling resolution record, there is some small variation in the mean value and the standard deviation of the record increases as the sampling resolution is increased (Table 9.1). The 1 cm resolution record explains 95% of the variability in the original record, and the 16cm resolution record explains 68%. However, the full record is biased by the lower parts of the core where sampling resolution was at 5 laminae resolution and each sample represented approximately 1 cm of core already.

Table 9.1 Comparison of Nar record sampled at different resolutions compared to the original $\delta^{18}O$ data set.

		Original	Every cm	Every 2 cm	Every 4 cm	Every 8cm	Every 16 cm
Data	**Min**	-5.73	-5.73	-5.73	-4.93	-4.93	-4.93
	Max	2.40	2.40	2.40	2.40	2.40	1.72
	Range	8.13	8.13	8.13	7.33	7.33	6.66
	Mean	-1.38	-1.51	-1.50	-1.47	-1.48	-1.32
	SD	1.45	1.70	1.74	1.72	1.82	1.93
Compared to Original	**Min (difference)**		0.00	0.00	-0.80	-0.80	-0.80
	Max (difference)		0.00	0.00	0.00	0.00	-0.68
	Range (percentage)		100.00	100.00	90.20	90.20	81.86
	Mean (difference)		0.13	0.12	0.09	0.10	-0.06
	SD (percentage)		117.52	120.49	119.17	125.77	133.76
	Variability Explained (R^2)		0.946	0.926	0.886	0.833	0.680

Table 9.2 Comparison of Nar record sampled at different resolutions compared to the annual part of the original $\delta^{18}O$ data set.

		Original	Every cm	Every 2 cm	Every 4 cm	Every 8cm	Every 16 cm
Data	**Min**	-4.77	-4.77	-4.09	-3.67	-3.67	-2.95
	Max	1.61	1.40	1.40	0.91	0.90	0.90
	Range	6.38	6.16	5.49	4.57	4.56	3.85
	Mean	-1.28	-1.20	-1.19	-1.18	-1.15	-0.97
	SD	1.26	1.31	1.29	1.25	1.38	1.47
Compared to Original	**Min (difference)**		0.00	-0.68	-1.10	-1.10	-1.82
	Max (difference)		-0.22	-0.22	-0.70	-0.71	-0.71
	Range (percentage)		96.63	86.04	71.71	71.56	60.32
	Mean (difference)		-0.08	-0.09	-0.10	-0.13	-0.31
	SD (percentage)		103.69	102.24	99.28	109.49	116.44
	Variability Explained (R^2)		0.919	0.895	0.845	0.777	0.577

Looking at only the annually resolved part of the record (i.e. the last 900 years) the range is shown to reduce significantly with increased sampling resolution. Only 60 % of the range is explained by the 16cm resolution record (Table 9.2), although most of the range is reproduced at 1cm sampling resolution (97 %). In this case the mean value of the record also becomes more negative, reaching 0.3 ‰ more negative at 16cm resolution, with increased sampling resolution and the standard deviation of the record also generally increases (Table 9.2). In this case the 1cm record explains 92 % of the variability in the original, annual resolution, record with the 16cm resolution record explaining only 58 % (Fig. 9.4).

The sampling resolution of the Nar sequence therefore accounts for some of the difference in the range of the Nar record compared to the other eastern Mediterranean lakes (Fig. 9.1). The 16cm resolution record has a range of 6.7 %, compared to 8.1 ‰ for the full record. In addition the Nar record is known to include changes in carbonate mineralogy from calcite to aragonite, and vice versa, which would cause a 0.6 ‰ shift in the isotope values. This reduces the range to 6.1 %. This is still, however, over twice the range of most of the other lakes. Additionally to the change in mineralogy, threshold shifts seem to appear in the Nar $\delta^{18}O$ record during the most rapid shifts in the isotope system (chapter 6), and these account for another 1‰ in the total range.

As well as differences in the range of $\delta^{18}O$ values due to the sampling resolution, differences in the timing of events may be due to differences between radiocarbon and varve age models. The 1cm resolution record from Nar can be put against a theoretical radiocarbon chronology and compared to the annual record and varve chronology to observe how much difference these differences may make to event timings.

Varve ages from 6 arbitrary depths through the core were compared to the radiocarbon calibration curve and radiocarbon ages given to these depths. As radiocarbon ages are associated with an error, an error of ± 40 years was arbitarily given to each of these radiocarbon ages. These ages, plus errors, were then calibrated, using the OxCal calibration programme, and the resulting ages and errors (Table 9.3) recorded and used to create an age-depth model along with the ^{137}Cs dates from the top of the core (Fig. 9.5).

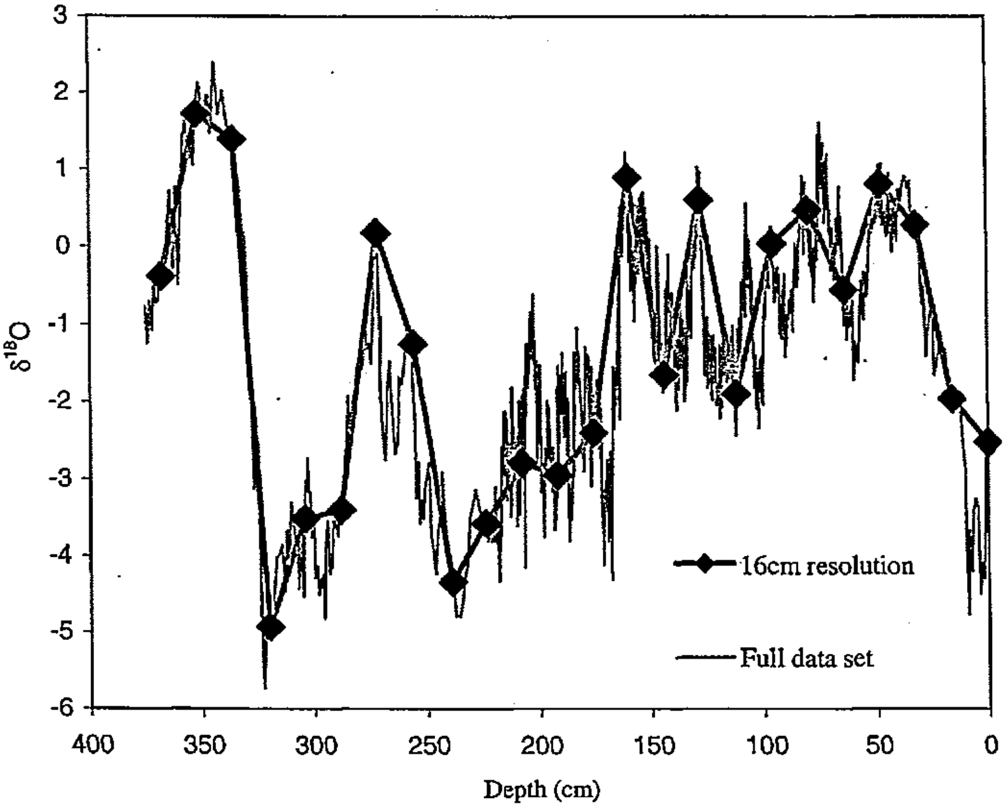

Fig. 9.4 Comparison of Nar record with hypothetical record at a 16cm sampling resolution.

Table 9.3 Hypothetical radiocarbon dates for the Nar record.

Depth (cm)	**Varve Age AD**	**Equivalent Radiocarbon Age (BP)**	**Calibrated Radiocarbon Age AD (2 σ range)**		
107	1733	153 ± 40	1660	-1805	1960
149	1498	353 ± 40	450	-1505	1640
199.5	1204	867 ± 40	1030	-1190	1260
250.5	985	1066 ± 40	890	-990	1030
303	692	1262 ± 40	660	-730	880
356	412	1639 ± 40	260	-390	540

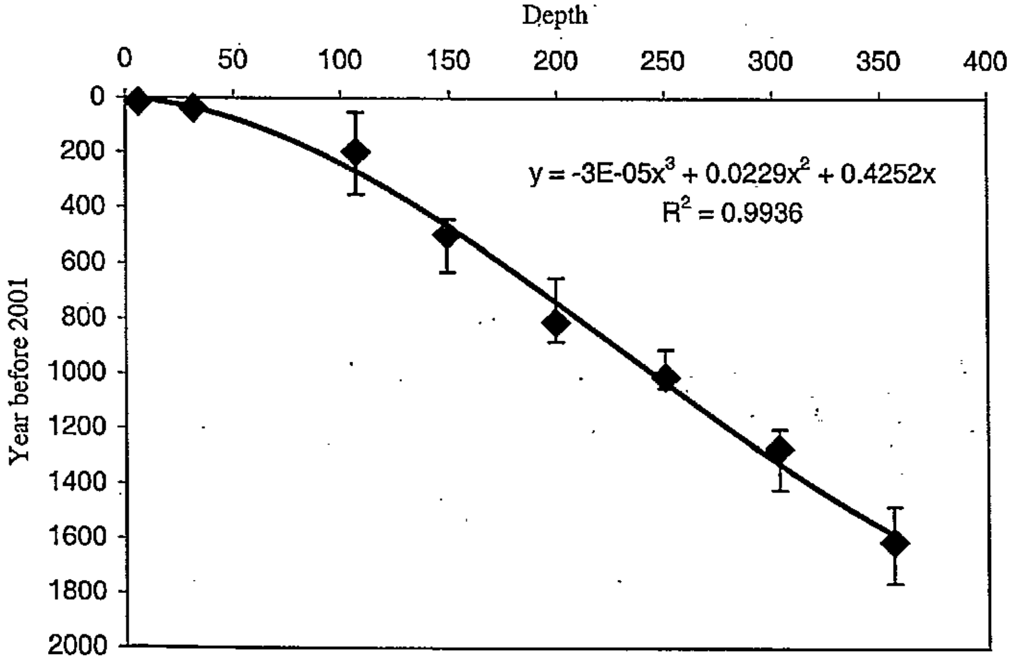

Fig. 9.5 Hypothetical age depth model for Nar.

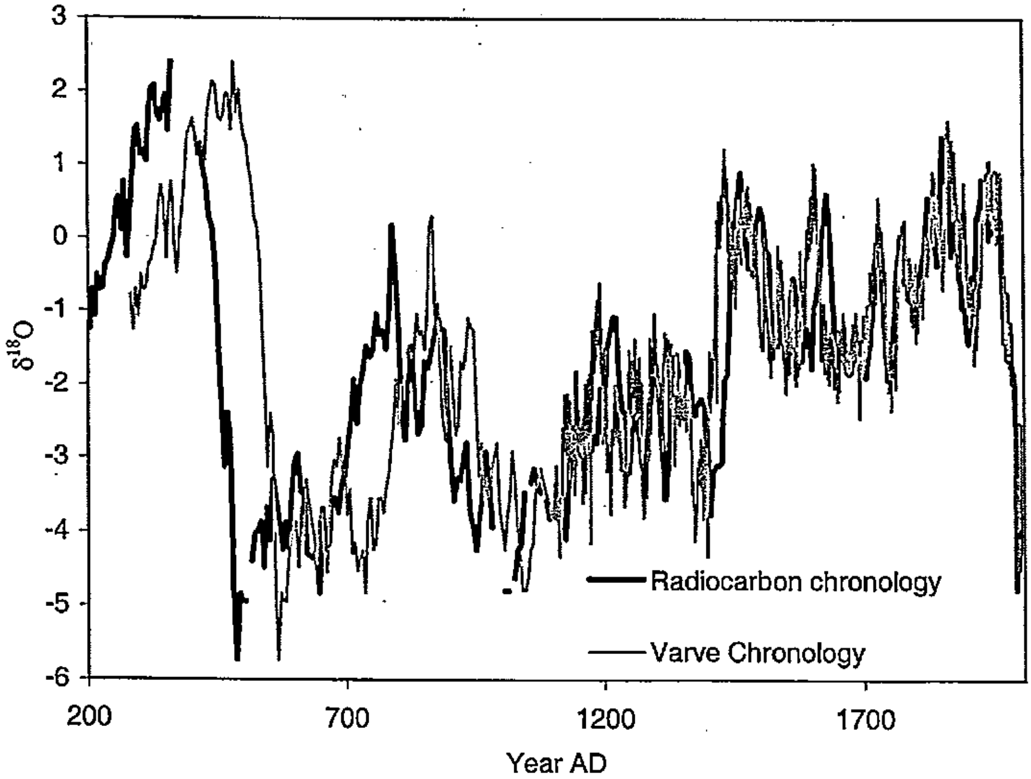

Fig. 9.6 Comparison of $\delta^{18}O$ record from Nar plotted with varve chronology and hypothetical radiocarbon chronology.

Comparison of the isotope curves based on the two chronologies shows that there are significant differences between the timing of events through the record (Fig. 9.6), although these differences in the two chronologies vary through the core. This is particularly true during the early part of the record where differences between the two records are approximately 100 years. These differences are a result of the polynomial age model drawn between the arbitrary dates, rather than large differences between the ages at the points where radiocarbon ages were taken. Comparisons of the different Turkish and Near East isotope records (Fig. 9.1) showed differences between equivalent events in the isotope stratigraphies in the order of 100 years, differences that may therefore be due to errors in core chronologies, particularly in age model reconstruction, rather than differences in the timing of the events. There may also be additional errors in some of the dates from the other lake sites due to the incorporation of old carbonate from the catchment or volcanic processes (e.g. at Eski Acıgöl; Roberts *et al.*, 2001).

9.1.2 African Monsoon

Comparison of the Nar oxygen isotope data with rainfall from the Sahel region of Africa (Hulme, 2003), which is under the influence of the African Monsoon, shows a strong correlation through the instrumental time period (Fig. 9.7). There is an opposite relationship, with the Nar record becoming more negative, suggesting less evaporation, as the Sahel region becomes drier.

Relatively high resolution records of lacustrine isotopic change through the late Holocene exist from North and East Africa (Vershuren *et al.*, 2001; Holmes *et al.*, 1997; Street-Perrott *et al.*, 2000) and, based on the relationship observed through the instrumental time period, may be expected to show climatic shifts at the same time as the Nar record. The Kajemarum Oasis isotope record from Nigeria (Fig. 9.8) shows significant variability throughout the last 2000 years particularly c. 500 AD, where there is a rapid shift to more positive values. In general the isotope record from Kajemarum is interpreted by the authors as a water-balance proxy, and therefore a reflection of salinity (Holmes *et al.*, 1997). However the shift at 500 AD does not match other salinity proxies in the core, suggesting there may be other reasons for this shift in isotope values. It was suggested that this shift may be due to changes in the $\delta^{18}O$ of precipitation, or the amount of precipitation due to a decrease in the westward transport of water vapour or a reduction in the intensity of convection (Street-Perrott *et al.*, 2000).

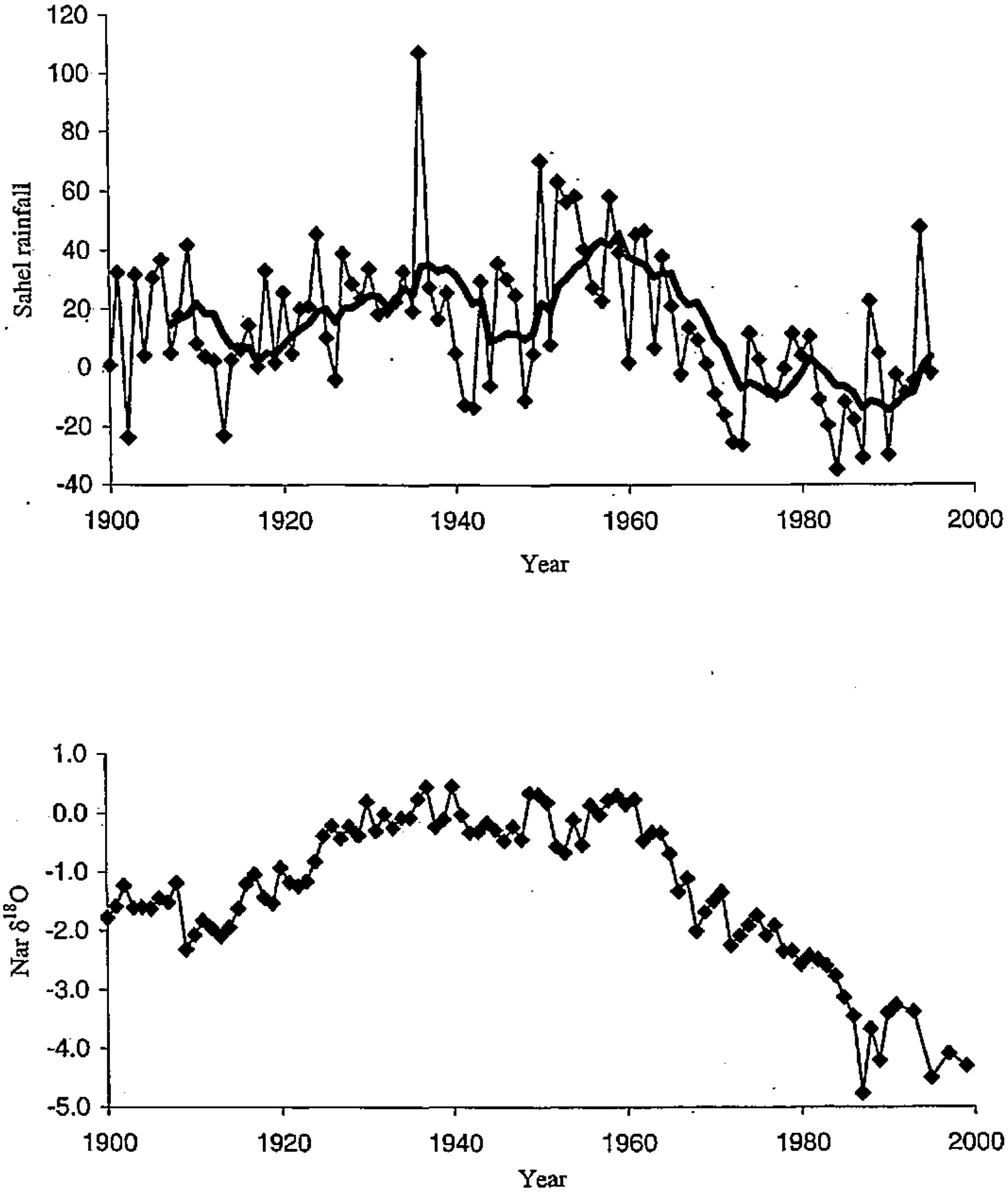

Fig. 9.7 Relationship between the Nar $\delta^{18}O$ record and Sahel rainfall (Hulme, 2003) through the instrumental time period.

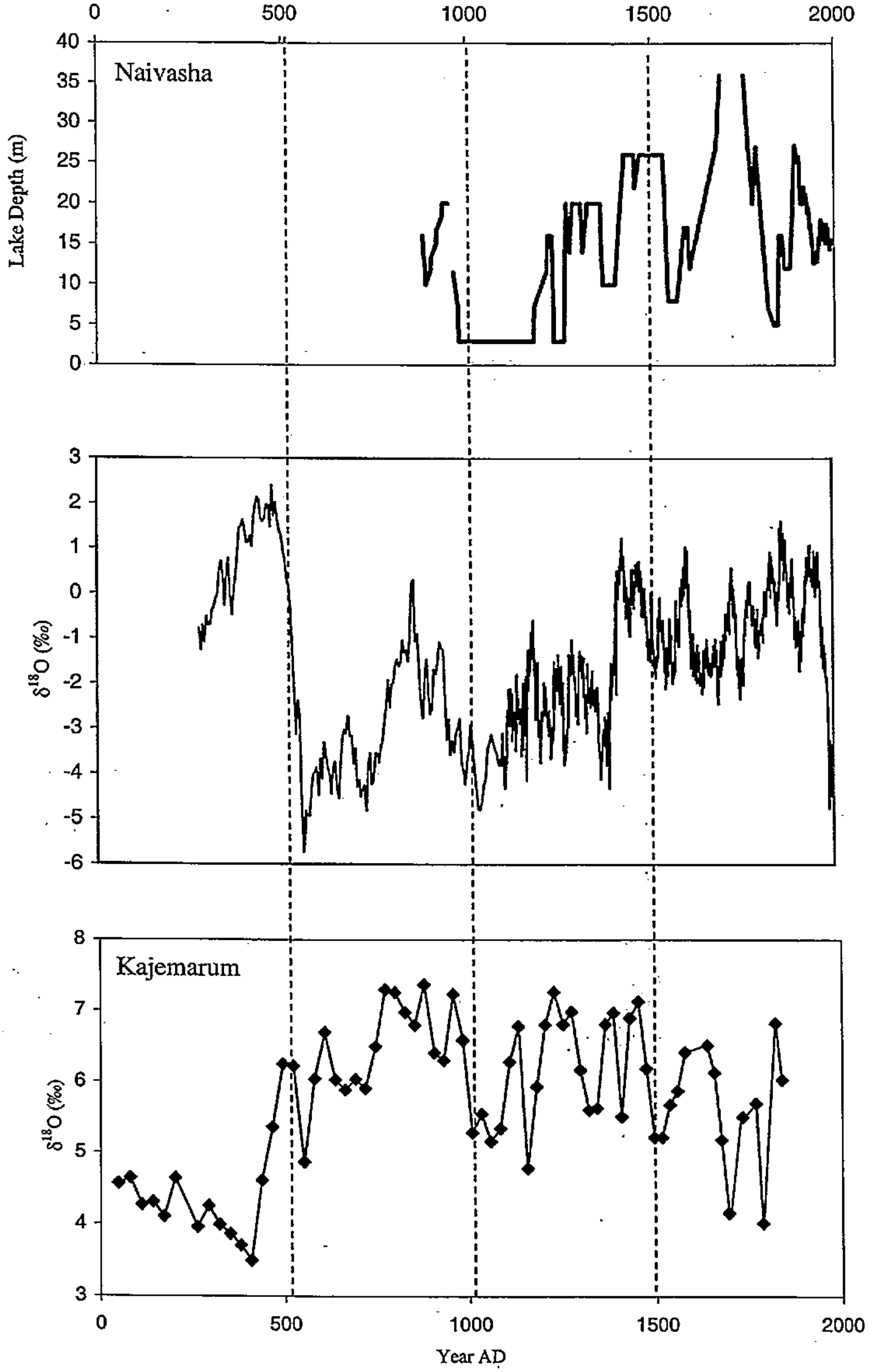

Fig. 9.8 Comparison of Nar $\delta^{18}O$ record with African late Holocene lake records from Naivasha (Verschuren *et al*., 2001) and Kajemarum Oasis (Street-Perrott *et al*., 2002).

This positive isotope shift occurs at the same time as the largest shift in the Nar record, where values become more negative. The shift at Nar appears to be associated with a reduction in lake salinity as there is a shift from aragonite to calcite production at the same time in the core. Even if the Kajemarum record is not controlled by changes in water balance at this time, and the shift is enhanced by changes in values of precipitation, it does suggest that important climate shifts occurred at both sites during the 6th century AD. Looking at the remainder of the two records there again seem to be opposite trends with the Kajemarum record becoming more negative between 750 and 1700 AD (the LIA), a time during which the Nar record becomes more positive (Fig. 9.8).

During this period conditions also became wetter at Naivasha in Kenya (Fig. 9.8). The lake low-stand between 1000 and 1200 AD corresponds to a time of more negative isotope values in the Nar record. The lake-level fall prior to 1000 AD corresponds to a reduction in evaporation at Nar, and from 1200 to 1600 AD there is generally an increase in evaporation at Nar as lake levels at Naivasha rise. There is further evidence of increased monsoon rainfall in Africa during the LIA from records of Nile river discharge which was at its highest during the LIA compared to any other time during the last 1400 years (Kutzbach, 1987).

9.2.3 Indian Monsoon

Comparison of the Nar oxygen isotope record with Indian summer monsoon rainfall through the instrumental time period (Parathasarathy *et al.*, 1995) shows periods of reduced rainfall during Indian summers in years of more negative isotope values at Nar, representing wetter or reduced evaporation conditions (Fig. 9.9), although between 1850 and 1900 the trends in the records describe the opposite relationship.

An annual proxy record of Indian monsoon variability through the past two millennia has been produced from varved marine sediments from the oxygen minimum zone in the northeastern Arabian Sea off Pakistan (von Rad *et al.*, 1999). Varve thickness and turbidite events were measured (Fig. 9.10). Periods of increased varve thickness and large numbers of turbidite events are recorded between 1600 and 1900 AD (the LIA), 1000 and 1300 AD, and 100 and 900 AD and interpreted as times of increased summer monsoon precipitation and/or increased river run off. In general these periods correspond to times of more positive isotope values, increased evaporation conditions, in the Nar isotope record. Varve thickness minima and reduced numbers of turbidite events recorded between 1300 and

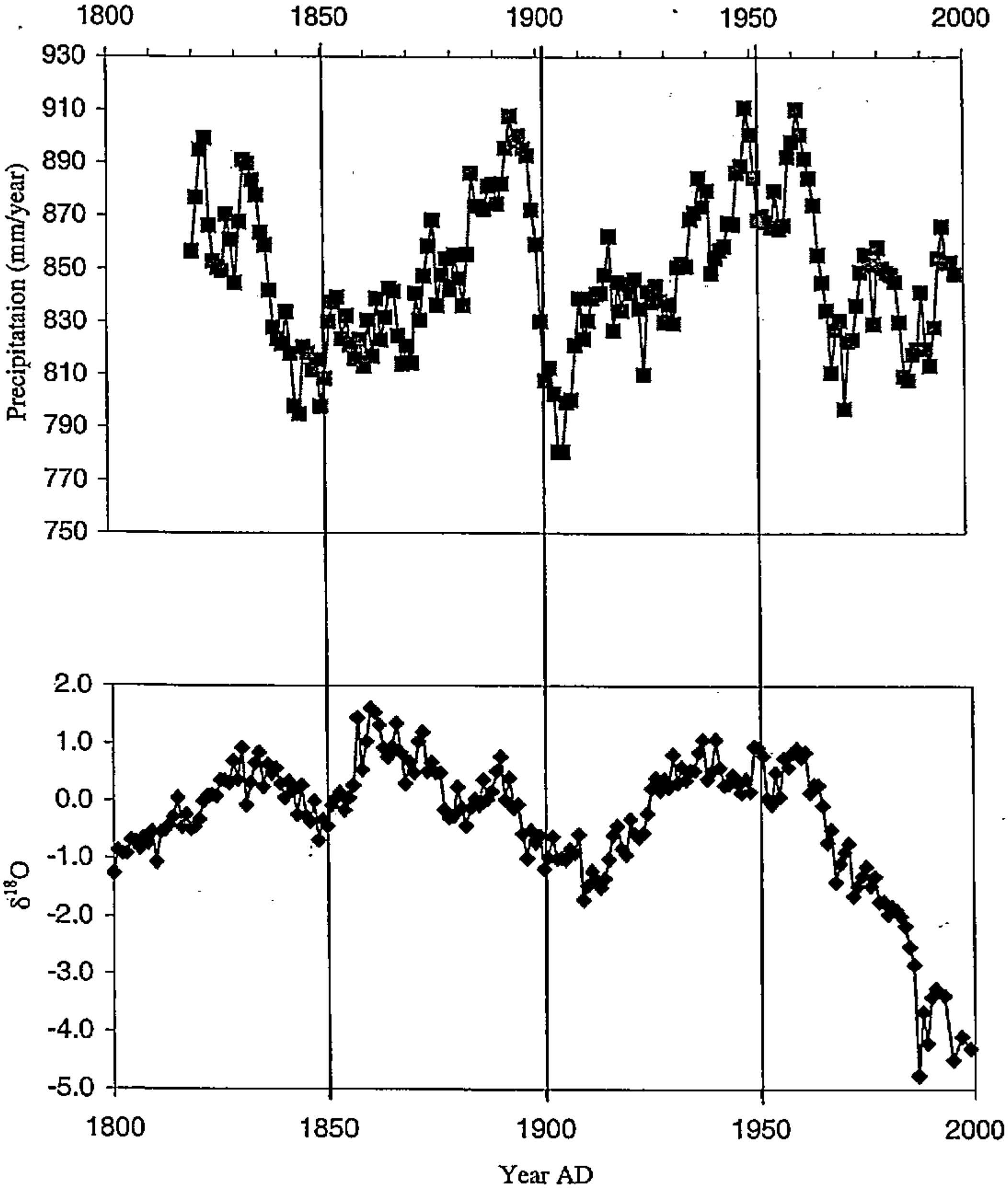

Fig. 9.9 Comparison of Nar record with Indian monsoon rainfall index (Parthasarathy *et al*., 1995) through the instrumental time period (1820-1998).

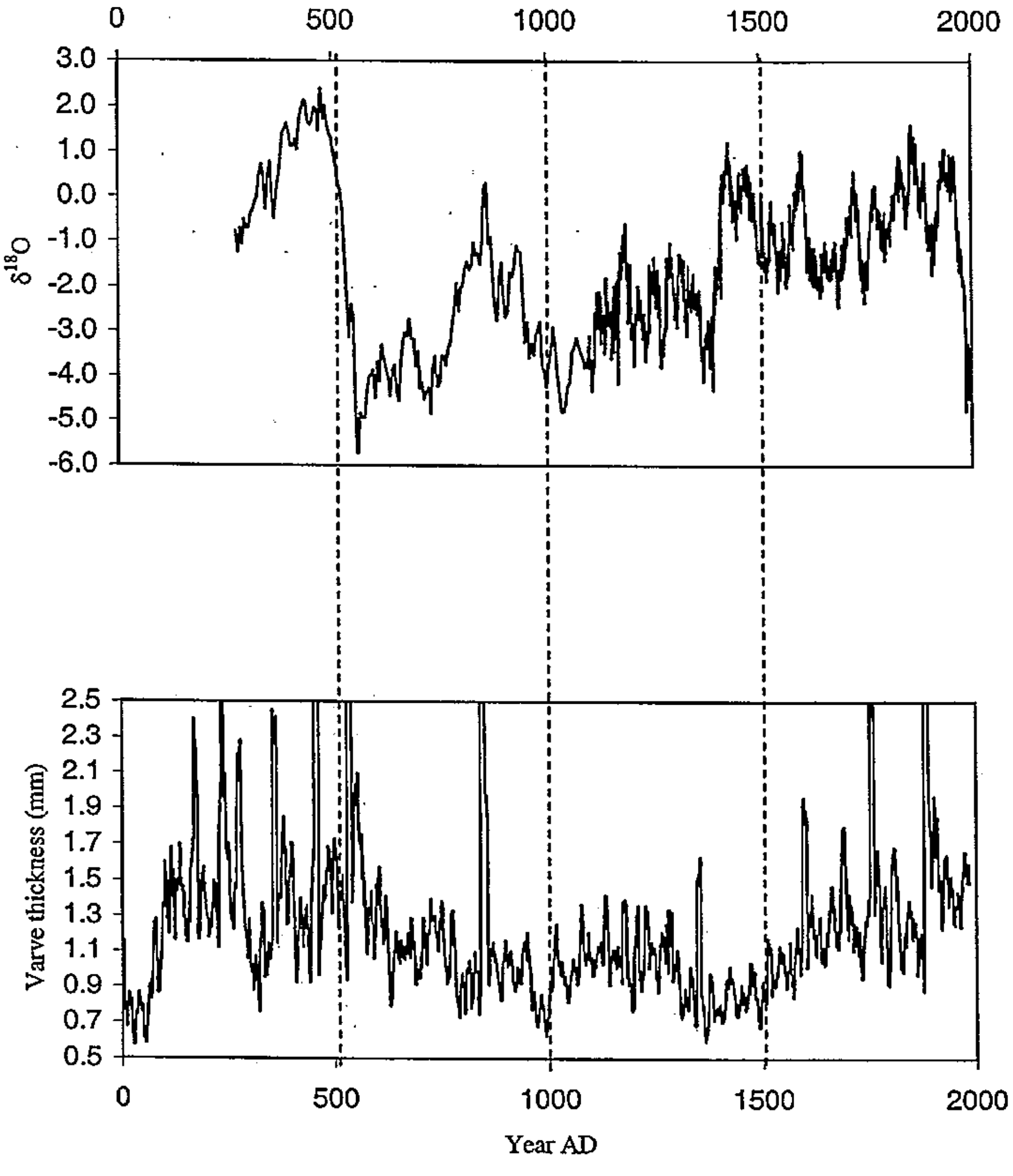

Fig. 9.10 Record of varve thickness from offshore Pakistan as a proxy record of the Indian monsoon (von Rad *et al.*, 1999) compared to $\delta^{18}O$ record from Nar Gölü.

1600 AD and at 1000 AD are interpreted as periods of low precipitation and/or decreased river runoff. These times generally correspond to periods of more negative isotope values, or reduced evaporation conditions, in the Nar isotope record (Fig. 9.10).

Denniston *et al.* (2000) record changes in the summer Indian monsoon from changes in mineralogy of a speleothem from central Nepal. They note the largest change in mineralogy during the last 2300 years at around 500 AD recorded by a change in speleothem mineralogy from aragonite, precipitated during times of reduced monsoon precipitation and cave aridity, to alternating calcite and aragonite laminae, suggesting times of elevated summer monsoon precipitation and increased cave humidity. This corresponds to the largest shift in the Nar isotope record from positive to negative values, suggesting a shift to more humid conditions, and in the Kajemarum Oasis record where there is a shift to more positive isotope values.

The varved marine sediments and Nepal speleothem therefore show opposite trends to each other for Indian summer monsoon conditions around 500 AD. The speleothem record has been interpreted as a shift to more humid conditions, and the marine varve record suggests a decrease in precipitation at this time. However changes in the East Asian Monsoon occur at the same time and show shifts to wetter conditions (Morrill *et al.*, 2003). As the Nepal cave site sits close to the boundary between Southwest and East Asian Monsoon influence it is possible that it has been influenced more by changes in the eastern monsoon.

9.2 Climate Cycles

Further evidence of climatic links between different proxy records, and with instrumental data, can be obtained from observing cycles in the records. Records showing variability at the same periodicities may be under the influence of the same forcing mechanisms. The annual $\delta^{18}O$ record from Nar, between 1096 and 1991 AD, shows dominant cycles at 60, 85 and ~135 years (Fig. 9.11; Table 9.4). The full record, with the annual part of the record averaged at 5 year intervals to give consistent time steps, shows dominant cycles at 60, 85, ~170, 365, and 512 years (Fig. 9.11; Table 9.4). The $\delta^{13}C$ annual record shows cycles at the same periodicities, at ~ 60 and ~ 138 years (Table 9.4) and the annual grey scale record through the whole of the Nar record shows cycles at ~60, ~80, ~140, 341, and 512 years (Table 9.1).

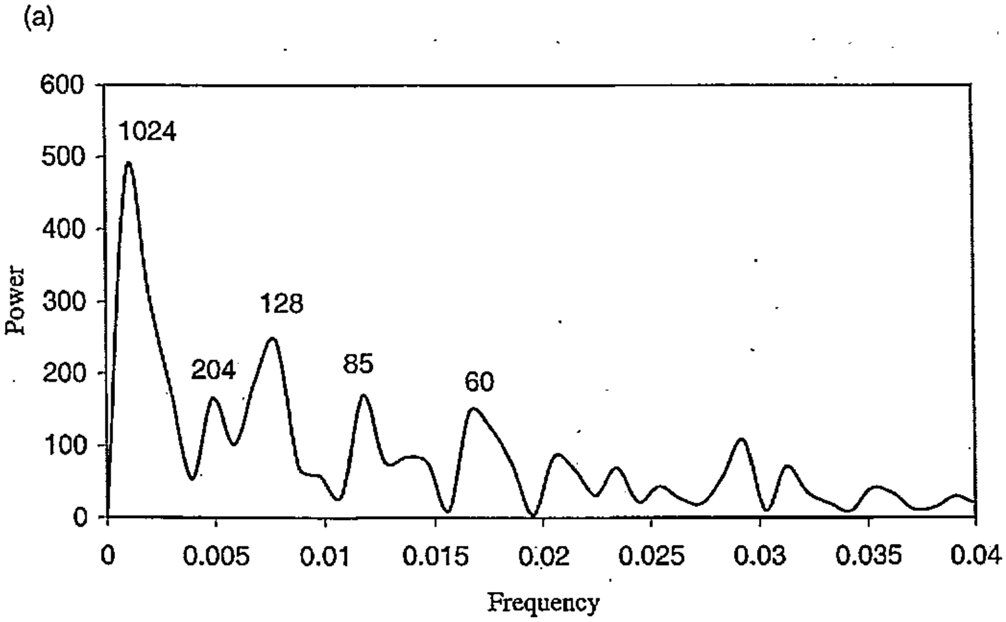

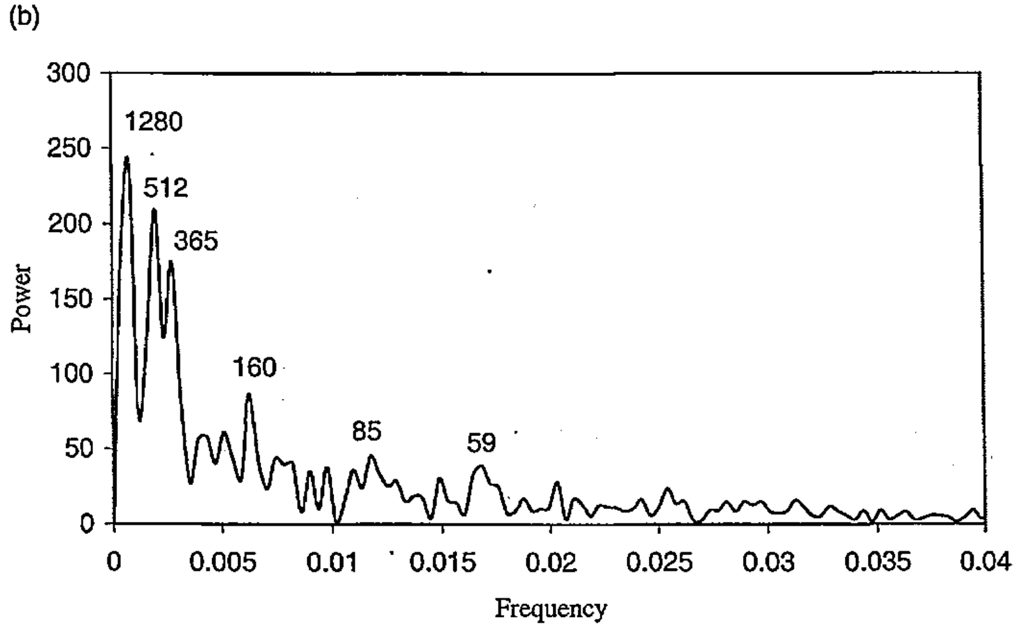

Fig. 9.11 Raw periodograms (Fourier Transform) from Nar Gölü $\delta^{18}O$ data for annual record (a) and 5 year mean record (b), major peaks are labled with length of cycle in years. From cycles observed in 1000 perturbations of the data cycles below ~60 years are not significant.

Table 9.4 Dominant cycles observed in Nar Gölü proxy data from spectral analysis.

Proxy	Cycles from Fourier Transform	Cycles from Blackman-Tuckey method
$\delta^{18}O$ annual (1096-1991)	128.0, 85.3, 60.2	143.4, 58.8
$\delta^{18}O$ 5 year mean record (276 -2001)	512.0, 365.7, 160, 85.3, 59.5	188.7, 85.4, 59.8
$\delta^{13}C$ annual (1096-1991)	512.0, 146.3, 60.2	132.8, 57.8
Grey scale annual (1096-1991)	204.8, 146.3, 93.1, 78.8, 60.2	58.8
Grey scale annual (276-2001)	512.0, 341.0, 227.5, 146.3, 60.2	137.9, 83.4, 60.8

Table 9.5 Cycles found in Nar $\delta^{18}O$ records at different sampling resolutions.

Sampling Resolution (cm)	Cycles from Fourier Transform	Cycles from Blackman-Tuckey method
1	512, 160, 142	715, 162
2	510, 255, 159, 141	719, 163
4	427, 160, 135	719, 163
8	527, 158	/
16	527	/

Table 9.6 Cycles observed in Indian monsoon rainfall index and Indian monsoon proxy records from spectral analysis using the same techniques as the Nar data.

Data	Cycles from Fourier Transform	Cycles from Blackman-Tuckey method
Indian Monsoon rainfall	64.0	65.2
Marine varve thickness (1096-1991)	102.4, 68.3, 60.2	112.0, 65.2
Marine varve thickness (276-1993)	341.3, 102.4	99.6

The annual nature of the Nar record gives strength to interpretations made from cycles found by spectral analysis. Using the same techniques as for the annual record, spectral analysis carried out on the hypothetical lower resolution Nar records show how the cycles that are found vary with different sampling resolution (Table 9.5). The cores were assumed to have undergone uniform sedimentation throughout the time period analysed, and only the data below 91 cm were used, as sedimentation rates have changed at the top of the core (Fig. 9.5). As the sampling resolution is increased the higher frequency spectra are not picked up, as would be expected, the lower frequency periodicities however do vary with changing sampling resolution and many are not picked up at all in the smoothed periodogram from the Blackman-Tuckey method.

Cycles at the frequencies observed in the Nar record have also been observed in other records (O'Sullivan *et al.*, 2002). For comparison with Nar, again it is important to compare records from the same region or those that may be influenced by the same climate patterns. Cycles have been observed in the proxy records of the Indian monsoon that relate to the cycles observed at Nar. Agnihotri *et al.* (2002) report cycles of ~188, ~120 and ~54 years and a weaker cycle at ~89 years from Indian monsoon proxies records from the Arabian sea, the latter two cycles are similar to the 85 and 60 year periodicities observed in the Nar data set although the Arabian sea data sets are not annually resolved. von Rad *et al.* (1999) report cycles at 750, 250, 125, 96 and 56 years, as well as some cycles at lower frequencies, from the varved marine sediments off Pakistan. The 56 and 125 year cycles broadly correspond to cycles found in the Nar record. Additionally, the Indian monsoon rainfall index has cycles of around 60 years that correlate to changes in the Nar record (Fig. 9.8).

For comparison of the cycles in these data sets the data were re-analysed using the same methods as for the Nar record, so direct comparisons could be made (Table 9.6). The marine varve thickness record was analysed between 1096 and 1991 for direct comparison with the annual record from Nar, and then between 276 and 1993 AD for comparison with the whole record. Differences in the periodicities observed here and in the published record are due to the manipulation of the data set by von Rad *et al.* (2002) to remove the effects of turbidite events; here the raw data were used for the analysis. From the re-analysis of the data a clear ~60 year cycle is observed in the Indian monsoon series, the marine varve thickness record and in the Nar isotope record.

The 60 year cycles run in phase through both the marine varve record and the Nar record although there seems to be a shift in the periodicities in the more recent parts of the record (Fig. 9.12). Looking at cycles in different time windows of 250 years in the two data sets through the last 900 years, i.e. long enough for 60 year cycles to be significant and during which time the Nar isotope data is at an annual resolution, it can be shown that the dominant cycles vary with time (Table 9.7). Although 64 year cycles are not present in all of the time windows analysed, where they are not, cycles are often found at multiples of 64, at 16, 32 and 128 years. In the latest 250 year window, 1700 to 1950 AD, there is a 51 year cycle in the Nar $\delta^{18}O$ record and no dominant 64 year cycle. This 51 year cycle is also observed in the Indian monsoon proxy record between 1600 and 1850 AD and between 1100 and 1350 AD suggesting there may be periods of time where the 64 year cycle is replaced by a cycle of shorter wavelength.

9.3 Controls on climate change

9.3.1 Temperature change

From the Mann and Jones (2003) temperature reconstruction the period 800 to 1400 AD, the Medieval Warm Period (MWP), is observed to be warmer than the periods preceding and following it. This is a time of more negative $\delta^{18}O$ values, suggesting reduced evaporation and cooler summers, in the Nar record (Fig. 9.13). The coldest periods in the Mann and Jones (2003) temperature reconstruction are the 6th, and 15th, 17th, and 19th centuries (LIA), and correspond to the periods of the most positive isotope values in the Nar record, times of enhanced evaporation and warmer and less humid summers.

This would suggest that at times of generally colder Northern Hemisphere climate, summer evaporation was enhanced at Nar Gölü, and during periods of relatively warm Northern Hemisphere climate summer evaporation was reduced. If the relationships from the climate calibrations are valid through time this suggests that summer conditions at Nar behave in an opposite manner to Northern Hemisphere average temperatures. Over glacial-interglacial time scales previous studies have suggested changes between cold and dry and warm and wet conditions (e.g. Roberts *et al.*, 2001; chapter 3), rather than the warm and dry conditions suggested here. It may be the case, therefore, that in central Turkey the LIA was relatively dry and cold, thus resulting in increased evaporation and more positive isotope values, and conditions were relatively warm and wet, resulting in more negative isotope values, during the MWP.

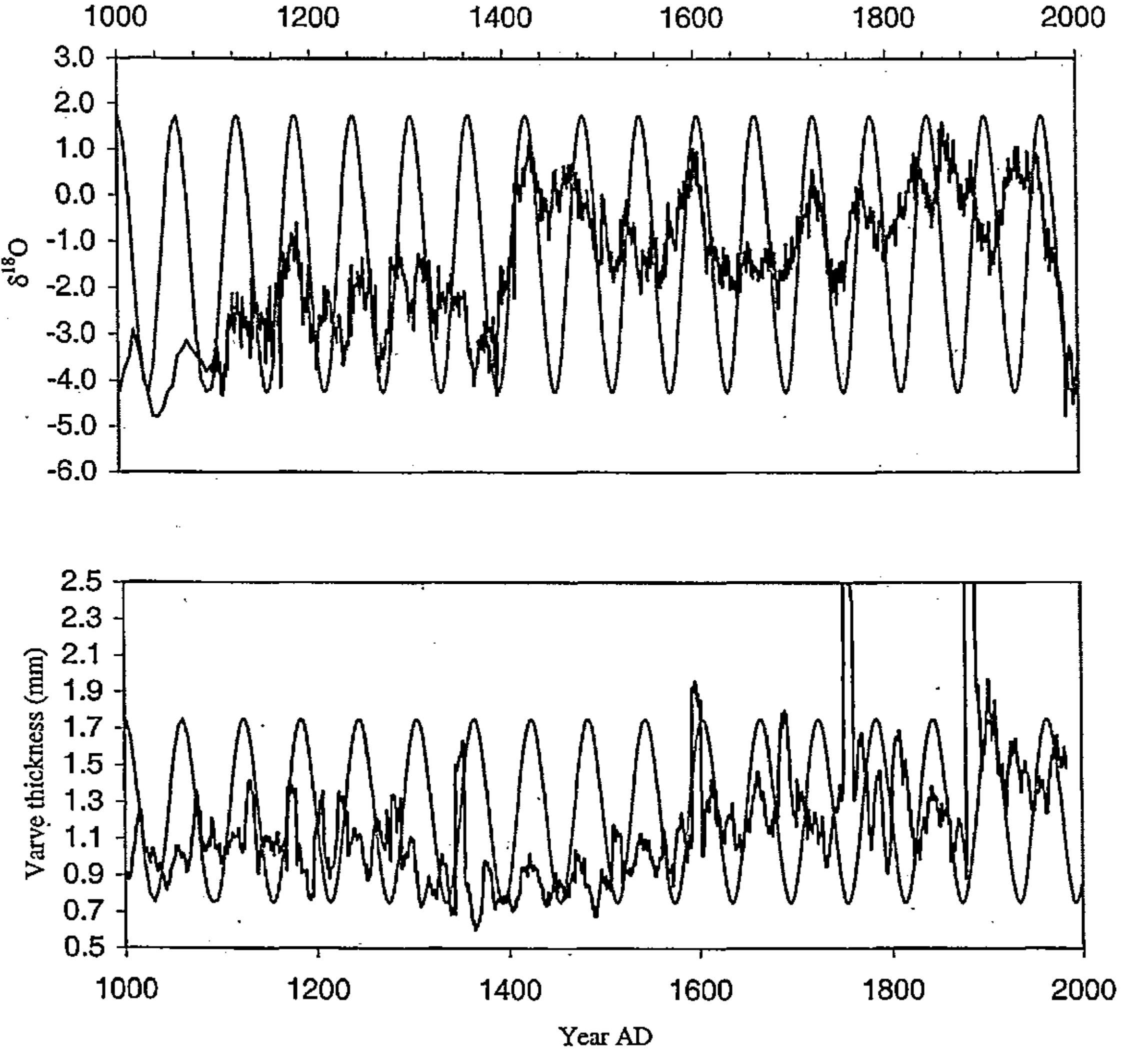

Fig. 9.12 60 year cycles in Nar and Indian monsoon (von Rad *et al.,* 1999) proxy records.

Table 9.7 Dominant decadal scale cycles, of approximately 60 years, from the Nar δ^{18}O record and the varved marine record of von Rad et al. (1998) during different time windows. 64 year cycles are highlighted in bold.

Time Window (years AD)	Cycles in Nar δ^{18}O record (years)	Cycles in varved marine record (years)
1100-1950	128, 85, 57	68, 60, 24
1100-1350	128, **64**, 32	128, 51
1200-1450	128, 32	**64**, 36.6
1300-1550	**64**	85.3, **64**, 32
1400-1650	128, 23, 16	42.6
1500-1750	128, **64**, 42, 32	85.3
1600-1850	**64**	85, 51, 32, 16
1700-1950	51	**64**, 16

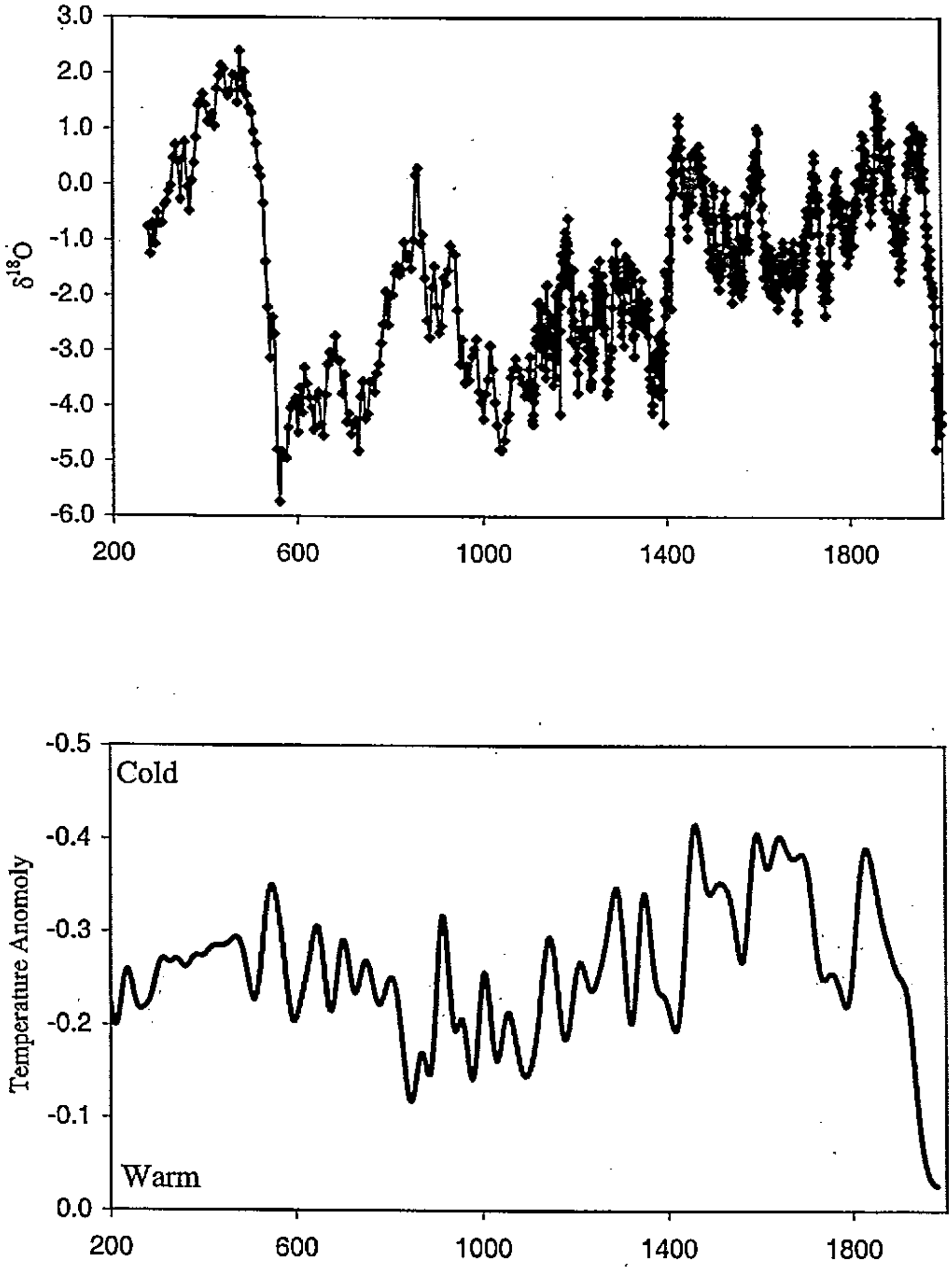

Fig. 9.13 Nar $\delta^{18}O$ record compared to temperature reconstruction through the past 2000 years (Mann and Jones, 2003).

Care must be taken when comparing records based on different seasonal and spatial sampling intervals (Jones *et al.*, 1998). The record from Nar is a record of summer conditions from a single site, although reconstructed temperature trends are likely to be valid for the rest of central Anatolia. The temperature reconstruction of Mann and Jones (2003) is an average for the entire hemisphere, based on average annual temperatures. It is possible that central Anatolia behaved opposite to the majority of the Northern Hemisphere during the past two millennia and that at Nar the summer conditions were reflecting average annual temperature trends. Alternatively, average temperatures may still have been cooler during the LIA in Turkey if winter conditions cooled more than summer conditions warmed, and vice versa during the MWP. This would suggest a change in seasonality in Turkey associated with these global climate shifts.

The major shifts in the Nar record, at c. 500 and c. 1400 AD, correspond, respectively, to changes from relatively cold to relatively warm, or warm to cold, periods of northern hemisphere annual average temperatures. This suggests that these temperature shifts are causing changes in global circulation patterns which in turn affect hydrology in Turkey, India and Africa. However, the largest shifts in the Nar record, and the other summer monsoon proxies is at 500 AD, whereas the largest shift in the Mann and Jones (2003) temperature record in the last two millennia was c. 1400 AD.

Over the last century variations in Sahel rainfall are highly correlated with the degree of contrast in seas surface temperatures (SSTs) between the northern and southern oceans. Cold northern oceans and warm southern oceans are associated with dry years in the Sahel and vice versa (Street-Perrott *et al.*, 2000). A recent drought in the Sahel region (Fig. 9.6) has also be linked to freshening of the North Atlantic over the same time period (Street-Perrott and Perrott, 1990). Disruption of the North Atlantic thermohaline circulation, that would occur if these waters were freshened, and reduced northern Atlantic SSTs would lead to enhanced dominance of the Hadley cell over the Sahel and would be associated with a decrease in both monsoonal and cyclonic moisture (Swezey *et al.*, 1999).

How these processes are linked to changes in Turkish and Indian monsoon climate is unclear. Raicich *et al.* (2003) show clear links between African and Indian summer monsoon rainfall and sea level pressure (SLP) in the Mediterranean basin through the instrumental time period. However the data suggest that increased monsoon precipitation in India and Africa is associated with lower SLP in the eastern Mediterranean and enhanced SLP in the western basin. The data from Nar suggest that increased monsoon rainfall is linked to drier conditions in Turkey which would be associated with a dominance of high, not low pressure systems. The stations used for the comparisons by Raicich *et al.* (2003) are all coastal stations and the high Turkish plateau may behave differently to the Turkish coast. Enhanced low pressure systems over Tibet, associated with increased monsoonal rainfall, may lead to stronger, north-easterly summer airflow over Turkey, sourced in relatively warm continental Eurasia (Kutzbach, 1987). This may explain the increased evaporation at Nar during times of increased Indian monsoon rainfall.

9.3.2 Solar variability

Cycles with periodicities similar to those found in the Nar and Indian monsoon records have also been observed in $\Delta^{14}C$ records, a proxy of solar activity (Stuiver and Braziunas, 1993, 1995). $\Delta^{14}C$ represents the ^{14}C activity in the atmosphere, recorded by tree rings, and corrected back through time for ^{14}C decay. Although some variability in the record may be due to variability in the Earth's magnetic field, influencing the amount of ^{14}C produced in the atmosphere, centennial and sub-centennial, scale variability in ^{14}C production can be attributed to solar variability (Stuiver and Braziunas, 1995).

Cycles have been found in the global $\Delta^{14}C$ record at 512, 356, 143-149, 85-88 and 57-63 years (Stuiver and Braziunas, 1995), which correspond to cycles observed in the Nar and Indian monsoon records (Table 9.1 and 9.3). This suggests that there may be some forcing influence from solar variability on decadal changes in the India – Mediterranean –African summer climate system. There is no clear century scale relationship between the $\Delta^{14}C$ record and the Nar $\delta^{18}O$ record (Fig. 9.14). The 512 year cycle is clear in the Nar sequence but less clear through the last two millennia in the $\Delta^{14}C$ record. The decadal scale cycles are also unclear in the $\Delta^{14}C$ record as they are probably hidden in the longer scale variability and at a smaller scale. Re-analysis of the $\Delta^{14}C$ data using the same spectral analysis techniques as for the Nar record (Table 9.8) show that the decadal scale cycles at ~ 88 and ~60 years also exist in the $\Delta^{14}C$ data. Cycles from all the records analysed in this chapter (Table 9.9) suggest there is a solar forcing mechanism behind at least the decadal variability in the Nar $\delta^{18}O$ record and Indian monsoon climate system.

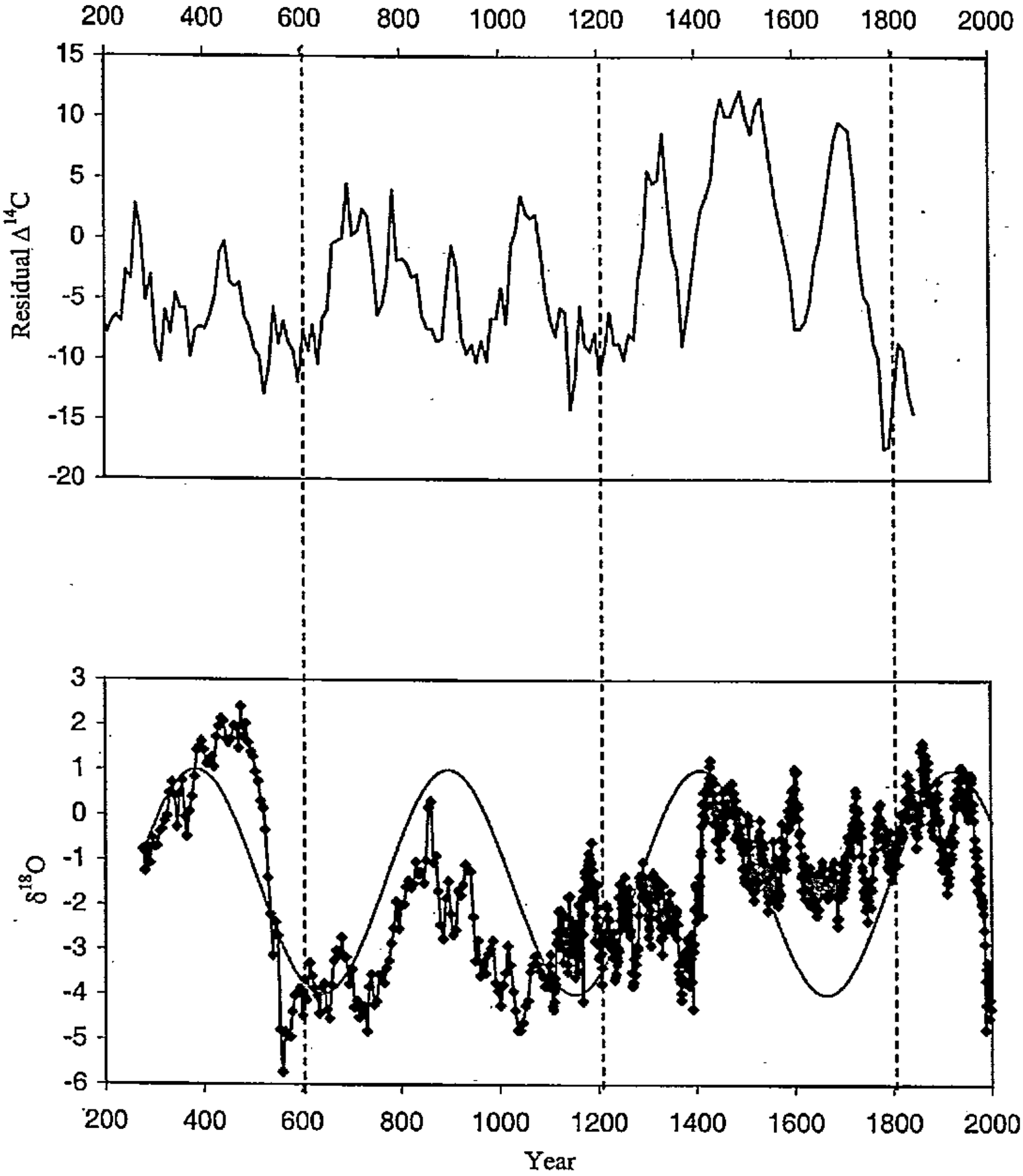

Fig. 9.14 Nar $\delta^{18}O$ record compared to $\Delta^{14}C$ residual plot (Stuiver and Braziunas, 1995), showing sine curve with a 512 year periodicity.

Table 9.8 Cycles observed in Δ^{14}C data sets from spectral analysis techniques used for the Nar data sets.

Data	**Cycles from Fourier Transform**	**Cycles from Blackman-Tuckey method**
Δ^{14}C annual	170.7, 73.14, 51.2	/
Δ^{14}C decadal	320.0, 196.9, 128, 106.7, 91.4, 61.0	/
Δ^{14}C decadal residuals	640.0, 320.0, 213.3, 128.0, 106.7, 56.9	211.8, 128.6, 57.1

Table 9.9 Comparisons of the cycles discussed in this chapter. Bold cycles are those published but not found when using the same techniques as were used for the Nar data.

Nar δ^{18}O	**Nar δ^{13}C**	**Nar Grey Scale**	**Indian Monsoon Rainfall**	**Indian Monsoon proxy**	**Δ^{14}C**
					640
512	512	512		**500**	**512**
365.7	341		341	**375**	**356**
					320
		227.5			213.2
		204.8			196.9
160					
143.4	146.3	146.3			**147**
128		132.8		**125**	128
				102.4	106.7
		93.1		**96**	91.4
85.3		78.8			**85**
			64	66	
60	60	60		60.2	57-61

9.4 Summary

There is a clear link between summer climate variability in Africa, India and the Eastern Mediterranean basin through the last two millennia. Increased monsoon rainfall in Africa and India occur at times of increased evaporation in the Cappadocian region of central Turkey. Major shifts in this system are associated with changes between relatively warm and cold states of Northern Hemisphere temperatures whereas decadal variability in the system, particularly cycles at ~ 60 year periodicity, may be controlled by solar variability.

Chapter 10

CONCLUSIONS

This study aimed to obtain high-resolution proxy records of climate change through the last 2,000 years from the Eastern Mediterranean region via records of lacustrine chemical variability, particularly changes in oxygen-isotope values, by:

- obtaining lake cores with precise temporal control i.e. varves.
- high-resolution sampling and analysis of these lake sediments.

To further interpretation of the stable isotope records other geochemical proxies, including mineralogy and colour analysis, were also measured from the lake sediments.

The thesis aimed to calibrate high-resolution lacustrine stable isotope records with instrumental climate data, and study contemporary lake isotope systems, to increase understanding of the controls on lake isotope dynamics in the Mediterranean region.

Through the climate calibration and from modelling lake oxygen isotope variability the thesis aimed to quantify proxy records of past climate variability. Comparison of the data obtained during this study was compared to previous work from the Eastern Mediterranean region and beyond to better understand changes in climate through the last two millennia.

10.1 High resolution records of stable isotopes from authigenic carbonate.

Two varved lakes from Turkey were investigated to obtain high resolution records of climate change through the last two millennia. An annually resolved record for the last 900 years was obtained from Nar Gölü, a crater lake in the Cappadocian region of central Turkey, the longest annually resolved proxy climate record from the Near East region (chapter 6). Records of $\delta^{18}O$, $\delta^{13}C_{carbonate}$, $\delta^{13}C_{organic}$, C/N ratios and changes in colour were measured. The $\delta^{18}O$ and $\delta^{13}C_{carbonate}$ record were extended for a further 825 years, at a 5 year bulk sample resolution, grey scale values were also recorded at an annual resolution through this time period. Authigenic carbonates from a second varved lake sediment sequence, Lake Burdur, were also measured, at approximately a 5 year bulk sample resolution, through the last 500 years.

Both lakes showed changes in carbonate mineralogy through the bulk carbonate record. The mineralogy of the Burdur lake carbonates suggest that many of these sediments are sourced in the catchment and therefore do not reflect changing values of lake water isotope ratios (chapter 7). By contrast, the carbonates in Nar Gölü have been shown to precipitate in the lake and this record can therefore be taken to reflect changing lake water isotope values.

This difference between the sites demonstrates the importance of fully understanding the sedimentary environment within a given lake before climatic inferences can be drawn from lake stable isotope values. Sedimentary carbonates are not always suitable for stable isotope analysis and in lakes such as Burdur other archives, such as biogenic carbonate, need to be investigated, if available, to understand the isotope hydrology of the system.

10.2 Controls on $\delta^{18}O$ values in Mediterranean lakes

The annual nature of the Nar Gölü sediments allowed the $\delta^{18}O$ record to be calibrated against observational climate variables between 1926 and 2001 to observe what the major driver behind the lake $\delta^{18}O$ record was. Strong correlations were found with summer temperature and relative humidity, particularly when the meteorological data were smoothed (chapter 6). This suggests that the carbonate isotope record from this lake is primarily a record of summer evaporation. The strongest relationships were found with smoothed meteorological data suggesting that the residence time of the lake controls how responsive the proxy records are to annual climate variability. In addition, hypothetical re-sampling of the Nar record at lower resolutions (chapter 9) demonstrated the amount of natural variability that may be lost in proxy records sampled at low resolution from non-laminated sediments. At Nar only 58% of the full variability in the record was explained at a sampling resolution similar to previous records from the region.

Collection of sediment from traps and the sediment – water interface, and measurements of lake waters during different seasons of the year allowed the timing of carbonate precipitation to be established (chapter 5). Carbonates appear to precipitate in Nar during the early summer, which confirms that the $\delta^{18}O$ record from Nar is likely to relate to summer climate conditions, although conditions through the rest of the year will still influence the value of δ_l. These relationships are likely to be important for other lake stable-isotope systems in the region, although individual lakes should be investigated carefully to understand the principle driver behind isotope change in each system.

10.3 Quantifying climate change

The relationships for the climate calibrations can be used to quantify past change in climate if the assumption is made that the controls on the lake have been constant through time and that there are no significant non-climatic factors that influence the lake isotope system.

Modelling of the lake system (chapter 8) suggests that a change in water flux through the lake is associated with the shift in isotope values between 1960 and 1980 AD. The increase in flux required for this shift may be associated with an increase in precipitation during a period of cooling and increased relative humidity. This suggests that the P/E ratio and resultant changes in lake hydrological flux may be the most important drivers of lake $\delta^{18}O$ values. Quantifying lake isotope records is problematic as often more than one variable, in this case both precipitation and evaporation, need to change to fully explain shifts in the isotope record. Models are also based calculations containing errors and unknown variables.

10.4 Late Holocene climate change

The Nar record shows the largest shifts in the system c. 530 and c. 1400 AD and during the 1960's to 1990's. The former two shifts are associated with changes in Northern Hemisphere temperatures between relatively warm and cold states and also correspond to the major shifts in proxy records of the Indian and African monsoon systems during the past two millennia (chapter 9). This suggests that climate is the dominant control on the Nar lake system, with changes in global temperature patterns causing shifts in summer atmospheric circulation over India, African and the Eastern Mediterranean. Between 276 and ~530 AD, and between ~1400 and ~1960 AD, summer evaporation was relatively enhanced at Nar Gölü. 530 to 1400 AD was a period of reduced summer evaporation.

At lower temporal resolution, decadal and century-scale cycles observed in the Nar record correspond to cycles found in proxy records of solar activity suggesting there is a solar forcing component to the Late Holocene climate patterns observed both at Nar and in the Indian monsoon region.

10.5 Future work

The composition and seasonal resolution of the Nar sediment record make it an important resource for further palaeoclimatic study. Further isotope studies could be carried out on other constituents in the core, e.g. $\delta^{18}O$ from diatom silica or organic cellulose (chapter 2), and this would lead to further understanding of lake isotope systems and the differences recorded by different isotope proxies.

There is a relationship between the carbonate mineralogy and isotope values at Nar, which is reflected in the grey scale record of the carbonate laminae. Further investigation of these issues may enable a more detailed statistical relationship between isotope values and carbonate mineralogy to be established. Analysis of the digital core images, including laminae thickness, may also help in understanding this relationship and provide a further proxy for lake system change.

A more in-depth study of the Burdur isotope-mineralogy relationship, including sampling of all the catchment carbonates, may lead to better understanding of $\delta^{18}O$ shifts in the Burdur sediments. Re-analysis of the carbonate stable-isotopes, after trying to remove the effect of dolomite (chapter 7), may produce a climate proxy from these sediments although it is more likely to be a proxy for changes in in-wash than changes in catchment P: E change.

Identification of diatom species and changes in floral composition through the cores from both lakes would make an interesting comparison with the isotope records as an alternative indicator of salinity. There are older sediments below those analysed in this study and there is, therefore, the potential to increase the length of the proxy records from Nar and Burdur further back into the Holocene.

APPENDIX I

XRD RESULTS

Standard XRD traces for calcite, aragonite, dolomite, and quartz Page II

XRD traces for Nar carbonate laminae Page III

XRD traces for Burdur samples Page VII

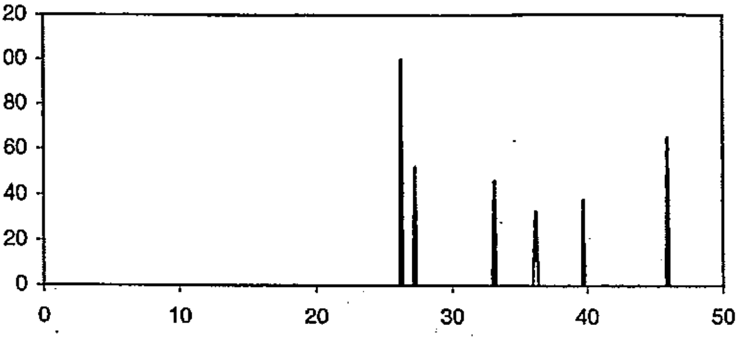
Aragonite

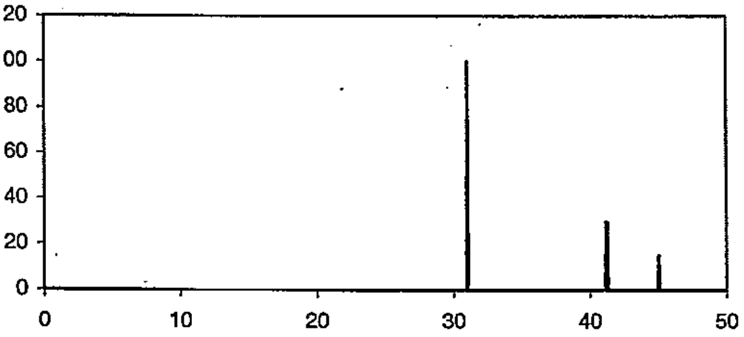
Dolomite

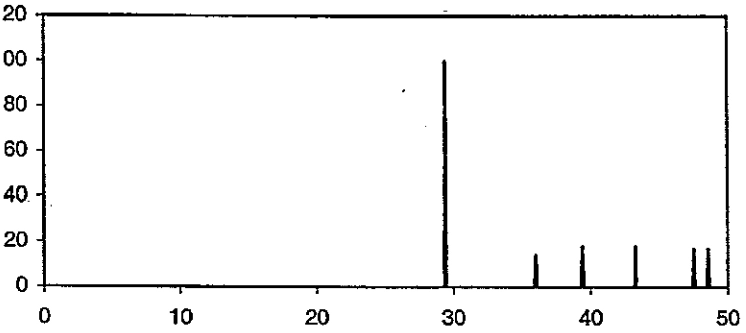
Calcite

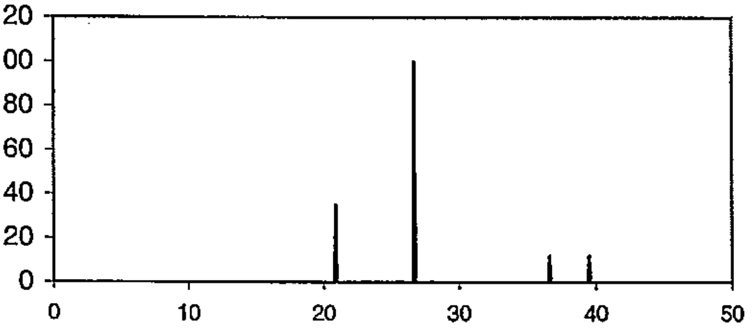
Quartz

Nar

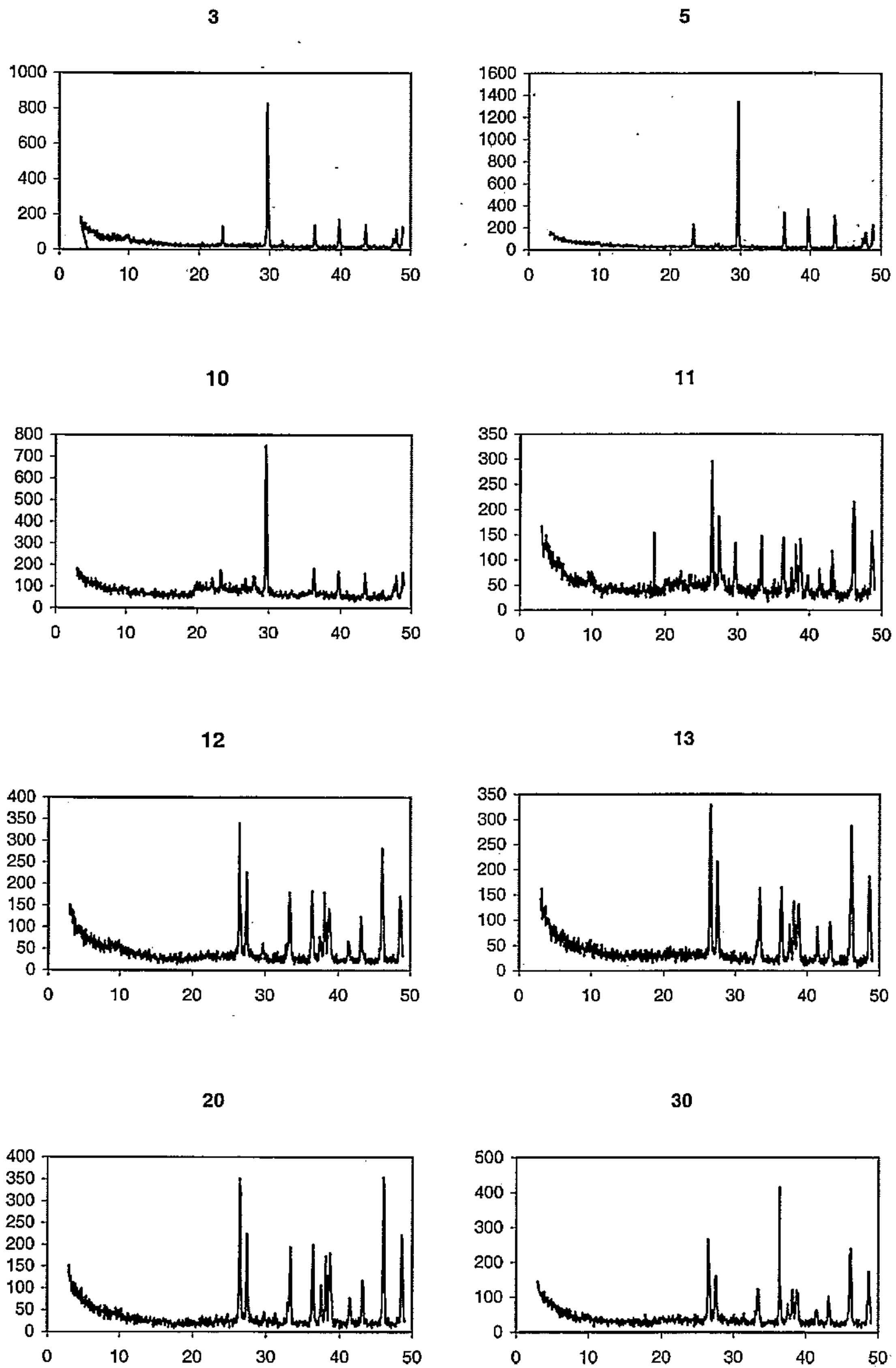
3
1000
800
600
400
200
0
0
10
20
30
40
50
5
1600
1400
1200
1000
800
600
400
200
0
0
10
20
30
40
50
10
800
700
600
500
400
300
200
100
0
0
10
20
30
40
50
11
350
300
250
200
150
100
50
0
0
10
20
30
40
50
12
400
350
300
250
200
150
100
50
0
0
10
20
30
40
50
13
350
300
250
200
150
100
50
0
0
10
20
30
40
50
20
400
350
300
250
200
150
100
50
0
0
10
20
30
40
50
30
500
400
300
200
100
0
0
10
20
30
40
50

33

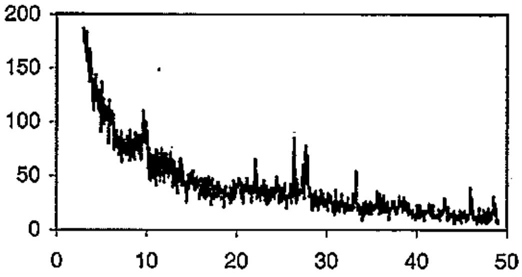

40

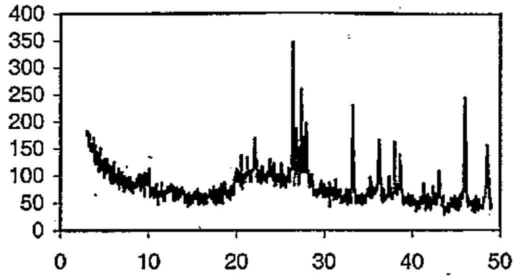

55

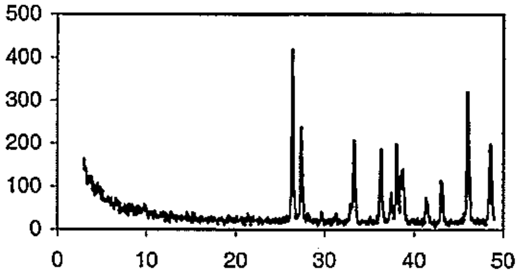

142

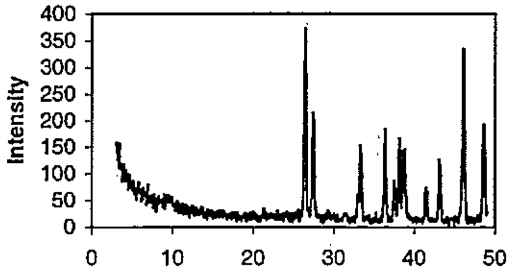

328

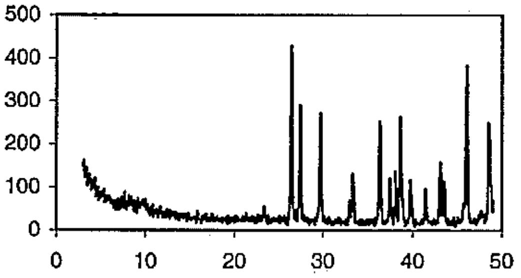

584

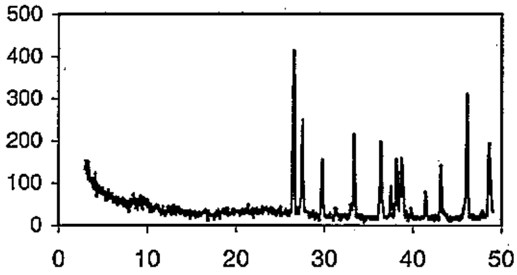

585

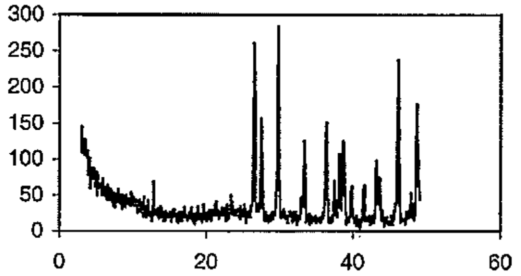

586

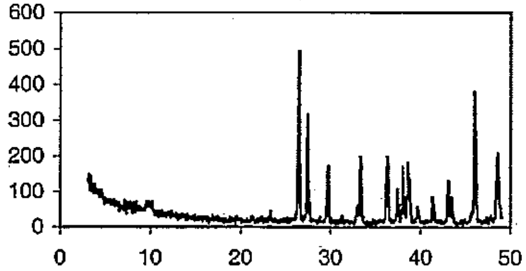

596

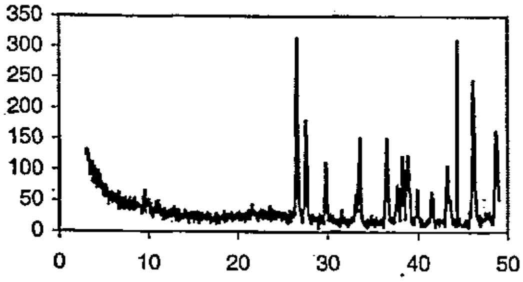

597

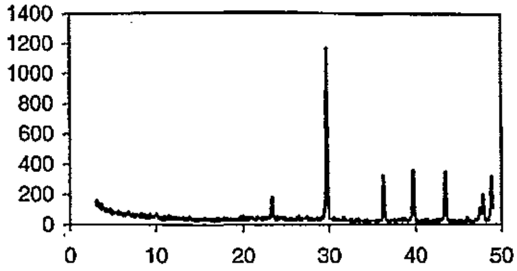

598

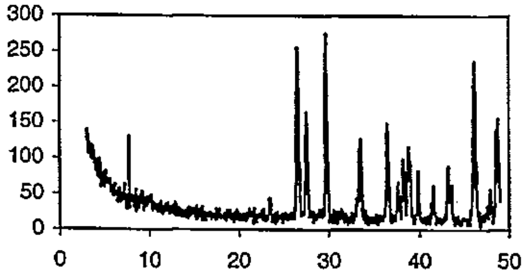

807

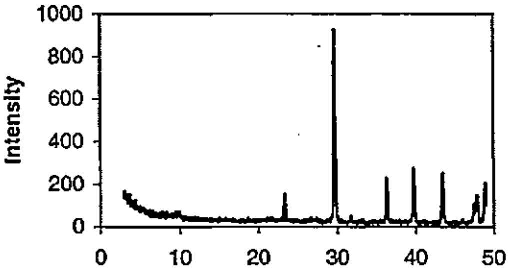

896

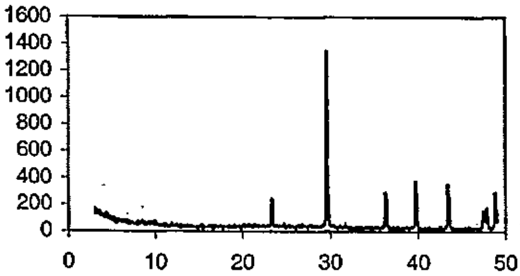

921

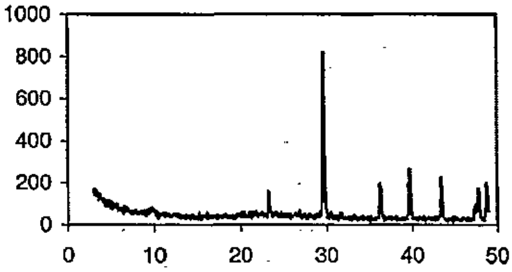

1141

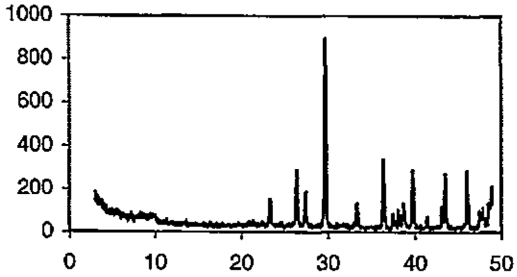

1196

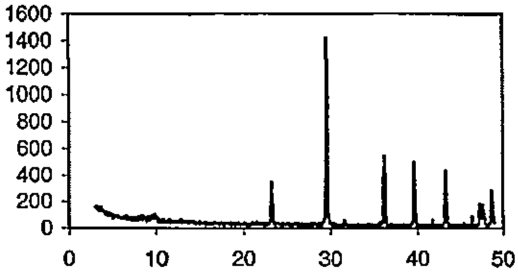

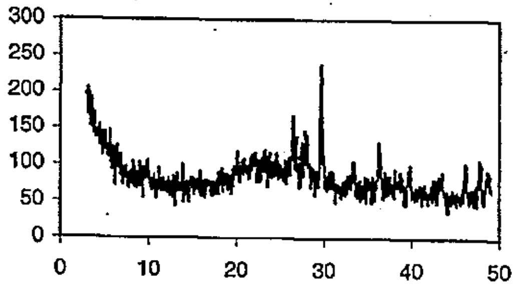

1441

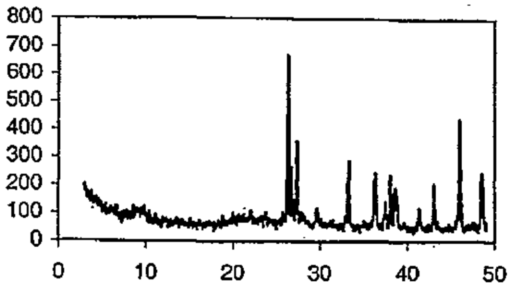

1446

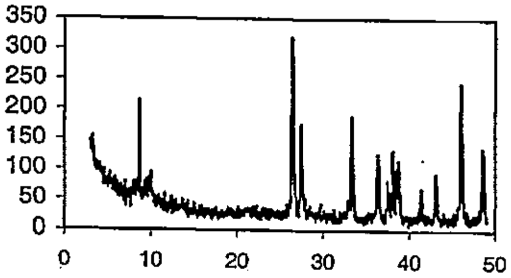

1631

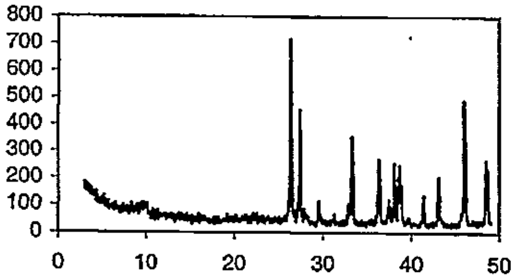

1711

Burdur

3 to 4 cm

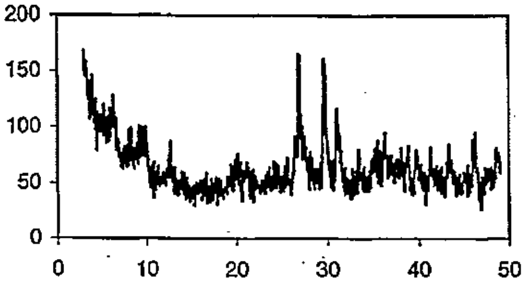

6 to 7

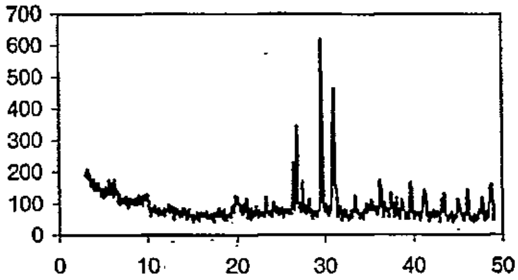

9 to 10

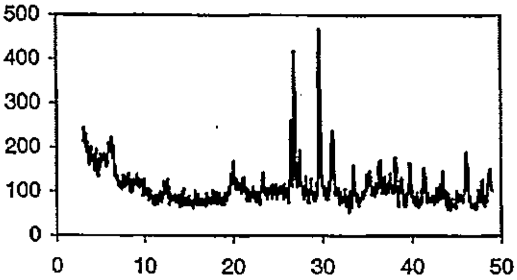

24 to 25

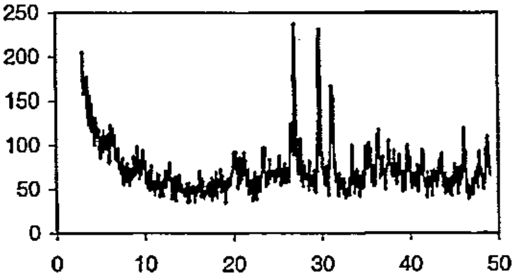

32 to 33

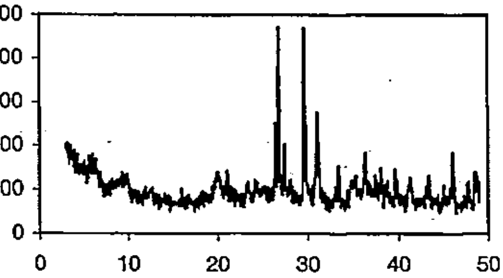

42 to 43

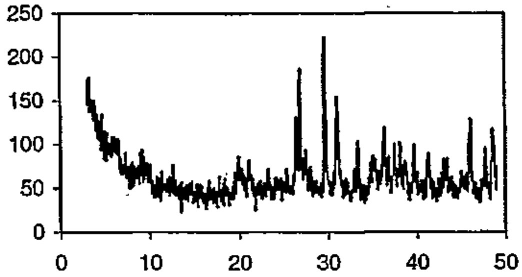

52 to 53

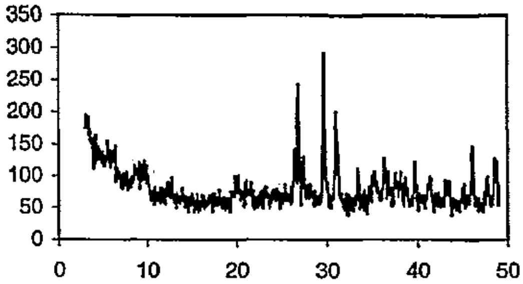

Appendix 2

OTHER RESULTS

CD includes:	Nar Gölü	Carbonate laminae grey scale (Fig. 6.3)
	Nar Gölü	Age - depth model (Fig. 6.6)
	Nar Gölü	Carbonate $\delta^{18}O$ (Fig.6.7)
	Nar Gölü	Carbonate $\delta^{13}C$ (Fig. 6.7)
	Nar Gölü	Organic $\delta^{13}C$ (Fig. 6.13)
	Nar Gölü	Organic C/N ratio (Fig. 6.13)
	Burdur Gölü	Carbonate $\delta^{18}O$ (Fig. 7.14)
	Burdur Gölü	Carbonate $\delta^{13}C$ (Fig. 7.14)

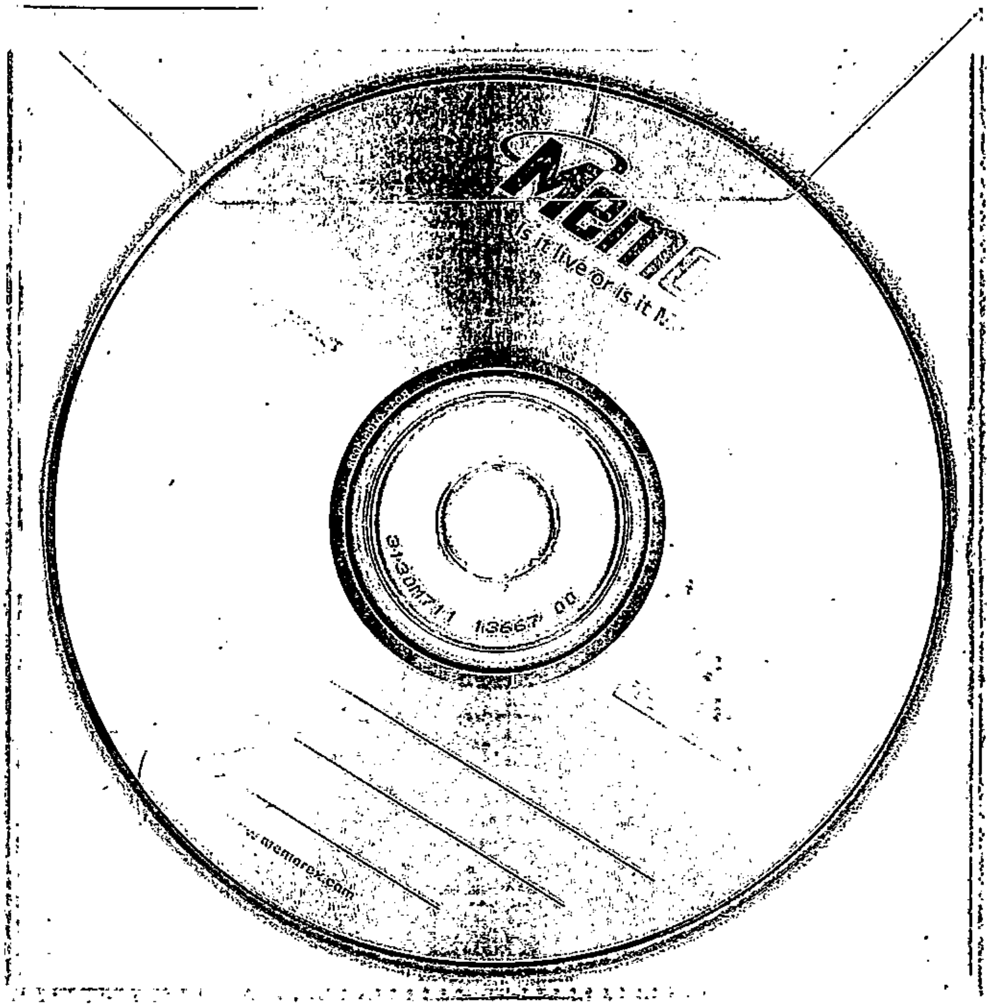
Memo
Is it live or is it M
313DM741 13667 00
www.memorex.com

REFERENCES

Abbott, M.B, Wolfe, B.B, Aravena, R, Wolfe, A.P. and Seltzer, G.O. 2000. Holocene hydrological reconstructions from stable isotopes and paleolimnology, Cordillera Real, Bolivia. *Quaternary Science Reviews* **19**, 1801-1820.

Agnihotri, R., Dutta, K., Bhushan, R. and Somayajulu, B. L. K. 2002. Evidence for solar forcing on the Indian Monson during the last millennium. *Earth and Planetary Science Letters* **198**, 521-527.

Al-Asam, I.S., Taylor, B.E. and South, B. 1990. Satble isotope analysis of multiple carbonate samples using selective acid extraction. *Chemical Geology* **80**, 119-125.

Almendinger, J.E. 1990. Groundwater control of closed-basin lake levels under steady-state conditions. *Journal of Hydrology* **112** (3-4), 293-318.

Anderson, R.Y. 1993. The varve Chronometer in Elk Lake: Record of climatic variability and evidence for solar/geomagnetic-14C-climate connection. In Bradbury, J.P and Dean, W.E (eds.) *Elk Lake, Minnesota: Evidence for Rapid climate changes in the North-Central United State,* , Geological Society of America Special Paper 276.

Appleby P G, 2001. Chronostratigraphic techniques in recent sediments. In W M Last & J P Smol (eds.) *Tracking Environmental Change Using Lake Sediments Volume 1: Basin Analysis, Coring, and Chronological Techniques*, Kluwer Academic, pp171-203.

Appleby, P G & F Oldfield, 1978. The calculation of ^{210}Pb dates assuming a constant rate of supply of unsupported ^{210}Pb to the sediment. *Catena* **5**, 1-8

Appleby P G, P J Nolan, D W Gifford, M J Godfrey, F Oldfield, N J Anderson & R W Battarbee, 1986. ^{210}Pb dating by low background gamma counting. *Hydrobiologia*, **141**, 21-27.

Appleby, P G, N Richardson, & P J Nolan, 1991. ^{241}Am dating of lake sediments. *Hydrobiologia*, **214**, 35-42.

Appleby, P G, N Richardson, & P J Nolan, 1992. Self-absorption corrections for well-type germanium detectors. *Nuclear Instrument & Methods B*, **71**, 228-233.

Atkinson, T.C., Briffa, K.R. and Coope, G.R. 1987. Seasonal temperatures in Britain during the past 22 000 years, reconstructed using beetle remains. *Nature*, **325**, 587-92.

Barker, P.A., Street-Perrott, F.A., Leng, M.J., Greenwood, P.B., Swain, D.L., Perrott, R.A., Telford, J. and Ficken, K.J. 2001. A 14 ka oxygen isotope record from diatom silica in two alpine tarns on Mt Kenya. *Science* **292**, 2307-2310.

Bar-Matthews, M., Ayalon, A. and Kaufman, A., 1997. Late Quaternary paleoclimate in the Eastern Mediterranean region from stable isotope analysis of speleothems at Soreq Cave, Israel. *Quaternary Research* **47**, 155-168.

Battarbee, R.W. 2000. Palaeolimnological approaches to climate change, with special regard to the biological record. *Quaternary Science Reviews*, **19**(1-5), 107-124.

Benson, L. V. and White, J. W. C. 1994. Stable isotopes of oxygen and hydrogen in the Truckee River-Pyramid Lake surface-water system. 3. Source of water vapor overlying Pyramid Lake. *Limnology and Oceanography* 39(8), 1954-1958.

Benson, L and Paillet, F. 2002. HIBAL: a hydrologic-isotopic-balance model for application to paleolake systems. *Quaternary Science Reviews* **21**, 1521-1539.

Birks, H.J.B. 1998. Numerical tools in palaeolimnology – Progress, potentialities, and problems. *Journal of Paleolimnology* **20**, 307-322.

Bolle, H.-J. 2003. Climate, Climate Variability, and Impacts in the Mediterranean Area: An Overview. In Bolle, H.-J. (ed.) 2003. *Mediterranean climate – variability and trends*. Springer-Verlag, Berlin.

Bottema, S. and Woldring, H. 1984. Late Quaternary vegetation and climate of southwest Turkey II. *Palaeohistoria* **26**, 123-149.

Boutton, T.W. 1991. Stable Carbon Isotope ratios of Natural Materials: II. Atmospheric, Terrestrial, Marine, and Freshwater Environments. In Coleman, D.C. and Fry, B. 2001 (eds.) *Carbon Isotope Techniques*, Academic Press Limited, London.

Bridgewater, N.D., Heaton, T.H.E. and O'Hara, S.L., 1999. A late Holocene palaeolimnological record from central Mexico, based on faunal and stable-isotope analysis of ostracod shells. *Journal of Paleolimnology*, 22(4): 383-397.

Briffa, K.R., Osborn, T.J., Scweingruber, F.H., Harris, I.C., Jones, P.D., Shiyatov, S.G. and Vaganov, E.A. 2001. Low-frequency temperature variations from a northern tree ring density network. *Journal of Geophysical Research* **106**, 2929-2941.

Briffa, K.R., Osborn, T.J., Scweingruber, F.H., Jones, P.D., Shiyatov, S.G. and Vaganov, E.A. 2002. Tree-ring width and density data around the Northern Hemisphere: Part 1, local and regional climate signals. *The Holocene* 12(6), 737-757.

Campbell, I.D., Campbell, C., Apps, M.J., Rutter, N.W. and Bush, A.B.G. 1998. Late Holocene ~1500 yr climatic periodicities and their implications. *Geology* 26(5), 471-473.

Cole, J.E., Rind, D., Webb, R.S., Jouzel, J. and Healy, R., 1999. Climatic controls on interannual variability of precipitation δ^{18}O: Simulated influence of temperature, precipitation amount, and vapor source region. *Journal of Geophysical Research* 104(D12), 14223-14235.

Coleman, M.L., T.J. Shepherd, J.J. Durham, J.E. Rouse, & G.R. Moore. 1982. Reduction of water with zinc for hydrogen isotope analysis. *Analytical Chemistry* 54, 993-995.

Coplen, T.B., Kendall, C. and Hopple, J. 1983. Comparison of stable isotope reference samples. *Nature* **302**, 236-238.

Craig, H., 1957. Isotopic standards for carbon and oxygen and correction factors for mass-spectrometric analysis of carbon dioxide. *Geochimica et Cosmochimica Acta* **12**, 133-149.

Craig, H., 1961. Isotopic variations in meteoric waters. *Science* **133**, 1702-1703.

Craig, H. and Gordon, L.I., 1965. Deuterium and oxygen-18 variation in the ocean and marine atmosphere. *Stable isotopes in Oceanography Studies and Paleotemperatures.* Laboratory di Geologica Nucleara, Pisa.

Cullen, H.M. and deMenocal, P.B. 2000. North Atlantic Influence on Tigris-Euphrates Streamflow. *International Journal of Climatology* **20**, 853-863.

D'Arrigo, R and Cullen, H.M. 2001. A 350-Year (AD 11628-1980) Reconstruction of Turkish Precipitation. *Dendrochronologia* **19**(2), 169-177.

Dansgaard, W., 1964. Stable Isotopes in Precipitation. *Tellus* **16**, 436-468.

Dean, W.E. 1974. Determination of carbonate and organic matter in calcareous sediments and sedimentary rocks by loss on ignition: comparison with other methods. *Journal of Sedimentary Petrology* **44**, 242-248.

Denniston, R.F., Gonzalez, L.A., Asmerom, Y., Sharma, R.H and Reagan, M.K. 2000. Speleothem evidence for changes in Indian summer monsoon precipitation over the last ~2300 years. *Quaternary Research* **53**, 196-202.

Dillon, P.J., Evans, R.D. and Molot, L.A. 1990. Retention and resuspension of phosphorous, nitrogen, and iron in a Central Ontario lake. *Canadian Journal of Fisheries and Aquatic Science* **4**, 1269-1274.

Dinçer, T. 1968. The use of Oxygen 18 and Deuterium Concentrations in the water balance of lakes. *Water Resources Research* **4**, 1289-1306.

Eastwood, W.J., Roberts, N., Lamb, H.F., and Tibby, J.C. 1999. Holocene environmental change in southwest Turkey: a palaeoecological record of lake and catchment-related changes. *Quaternary Science Reviews* **18**, 671-695.

Eastwood, W.J., Leng, M.J., Roberts, N. and Davis, B. submitted. Holocene climate change in the eastern Mediterranean region: a comparison of stable isotope and pollen data from a lake record in southwest Turkey. *Journal of Quaternary Science.*

Epstein, S. and Mayeda, T. 1953. Variation in ^{18}O content of waters from natural sources. *Geochimica et Cosmochimica Acta* **4**, 213-224.

Esper, J, Cook, E.R. and Schweingruber, F.H. 2002. Low-frequency signals in long tree-ring chronologies for reconstructing past temperature variability. *Science* **295**, 2250-2253.

Fritz, S.C., Ito, E., Yu, Z., Laird, K.R. and Engstrom, D.R. 2000. Hydrologic variation in the northern Greta Plains during the last two millennia. *Quaternary Research* **53**, 175-184.

Gat, J.R., 1996. Oxygen and Hydrogen isotopes in the Hydrological Cycle. *Annual Review of Earth and Planetary Science Letters* 24, 225-262.

Gat, J.R. and Carmi, I., 1970. Evolution of the isotopic composition of atmospheric waters in the Mediterranean Sea area. *Geophysical Research* 75(15), 3039-3048.

Gat, J.R., Mook, W.G and Meijer, H.A.J., 2001. *Environmental Isotopes in the Hydrological Cycle; Principles and Applications. Volume 2: Atmospheric Water.* IAEA, Vienna. Accessible at http://www.iaea.org/programmes/ripc/ih/volumes/volume2.htm.

Gibson, J.J., Edwards, T.W.D. and Prowse, T.D. 1999. Pan-derived isotopic composition of atmospheric water vapor and its variability in northern Canada. *Journal of Hydrology* 217, 55-74.

Glew, J.R. 1991. Miniature gravity corer for recovering short sediment cores. *Journal of Paleolimnology* 5, 285-287.

Gonfiantini, R. 1986. Environmental isotopes in lake studies. In Fritz, P and Fontes, J-C. (eds.) *Handbook of environmental isotope geochemistry volume 2B.* Elsevier, Amsterdam.

Goodfriend, G.A., 1990. Rainfall in the Negev Desert during the middle Holocene, based on ^{13}C of organic matter in land snail shells. *Quaternary Research* 34, 186-197.

Grossman, 1984. Carbon isotopic fractionation in live benthic foraminifera – comparison with inorganic precipitate studies. *Geochimica et Cosmochimica Acta* 48, 1505 - 1512.

Grossman, E.L. and Ku, T-L. 1986. Oxygen and carbon isotope fractionation in biogenic aragonite: temperature effects. *Chemical Geology* 59, 59-74.

Hammarlund, D., Edwards, T.W.D., Bjork, S., Buchardt, B. and Wohlfarth, B., 1999. Climate and environment during the Younger Dryas (GS-1) as reflected by composite stable isotope records of lacustrine carbonates at Torreberga, southern Sweden. *Journal of Quaternary Science* 14, 17-28.

Hardy, R. and Tucker, M. 1988. X-ray powder diffraction of sediments. In Tucker, M. (ed.) *Techniques in Sedimentology* Blackwell, Oxford.

Heaton, T.H.E, Holmes, J.A. and Bridgewater, N.D., 1995. Carbon and oxygen isotope variations among lacustrine ostracods: implications for palaeoclimatic studies. *The Holocene* 5(4), 428-434.

Heaton, T.H.E. and Chenery, C.A. 1990. Use of zinc turnings in the reduction of water to hydrogen for isotopic analysis. NERC Isotope Geosciences Laboratory Report, 24.

Holmes, J. A., 1996. Trace element and stable-isotope geochemistry of non-marine ostracod shells in Quaternary palaeoenvironmental reconstruction. *Journal of Paleolimnology* 15, 223-235.

Holmes, J.A., Street-Perrott, F.A, Allen, M., Fothergill, P., Harkness, D., Kroon, D. and Perrott, R.AA 1997. Holocene palaeolimnology of Kajemarum Oasis, northern Nigeria; an isotopic study of ostracodes, authigenic carbonate and organic carbon. *Journal of the Geological Society* 156, 357-368.

Hulme, M. 2003. Sahel rainfall. Accessible at http://www.cru.uea.ac.uk/tiempo/floor2/data/sahel.htm

Hurrell, J.W. 1995. Decadal trends in the North Atlantic Oscillation, Regional Temperatures and Precipitation. *Science* 269, 676-679.

IAEA/WMO 2001. Global Network of Isotopes in Precipitation. The GNIP Database. Accessible at: http://isohis.iaea.org

Jones, M.D., Leng, M.J., Eastwood, W.J., Keen, D.H. and Turney, C.S.M. 2002. Interpreting stable isotope records from freshwater snail shell carbonate: a Holocene case study from Lake Gölhisar, Turkey. *The Holocene* 12(5), 629-634.

Jones, P.D., Briffa, K.R., Barnett, T.P. and Tett, S.F.B. 1998. High-resolution palaeoclimatic records for the last millennium: interpretation, integration and comparison with General Circulation Model control-run temperatures. *The Holocene* 8(4), 455-471.

Jones, P.D., Osborn, T.J. and Briffa, K.R. 2001. The evolution of climate over the last millennium. *Science* 292, 662- 667.

Jouzel, J., Froehlich, K. and Schotterer, U., 1997. Deuterium and oxygen-18 in present-day precipitation: data and modelling. *Hydrological Sciences Journal* 42(5), 747-763.

Kahya, E. and Karabörk, M.Ç. 2001. The analysis of El Niño and La Niña signal in streamflows in Turkey. *International Journal of Climatology* 21, 1231-1250.

Karaca, M., Deniz, A. And Tayanc, M. 2000. Cyclone track variability over Turkey in association with regional climate. *International Journal of Climatology* 20: 1225-1236.

Kebede, S., Lamb, H., Telford, R., Leng, M. and Mohammed, U. 2002. Lake-groundwater relationships, oxygen isotope balance and climate sensitivity of the Bishoftu crater lakes, Ethiopia. In Odada, E.O and Olago, D.O. (eds.) *The East African Great Lakes: Limnology, Palaeolimnology and Biodiversity, Kluwer.*

Kelts, K and Hsu, J.J., 1978. Freshwater Carbonate Sedimentation. In Lerman, A. (ed.), 1978. *Lakes: geology, chemistry, physics.* Springer Verlag, New York.

Kendrew, W.G. 1961. *Climates of the continents.* Oxford University Press. 608pp

Kim, S-T and O'Neil, J.R. 1997. Equilibrium and nonequilibrium oxygen isotope effects in synthetic carbonates. *Geochimica et Cosmochimica Acta* 61(16), 3461 – 3475.

Kutiel, H. And Benaroch, Y. 2002. North Sea-Caspian Pattern (NCP) – an upper level atmospheric teleconnection affecting the Eastern Mediterranean: Identification and definition. *Theoretical and Applied Climatology* 71, 17-28.

Kutiel, H, Maheras, P, Türkeş, M and Paz, S. 2002. North Sea-Caspian Pattern (NCP) – an upper level atmospheric teleconnection affecting the eastern Mediterranean – implications on the regional climate. *Theoretical and Applied Climatology* 72, 173-192.

Kutzbach, J.E. 1987. The changing pulse of the monsoon. In Fein, J.S. and Stephens, P.L. (eds.) *Monsoons*, John Wiley and Sons.

Lamb, A.L., Leng, M.J., Lamb, H.F., and Mohammed, M.U. 2000. A 9000-ear oxygen and carbon isotope record of hydrological change in a small Ethiopian crater lake. *The Holocene* 10(2), 167-177.

Lamb, H., Kebede, S., Leng, M., Ricketts, D., Telford, R. and Umer, M. 2002. Origin and isotopic composition of aragonite laminae in an Ethiopian crater lake. In Odada, E.O and Olago, D.O. (eds.) *The East African Great Lakes: Limnology, Palaeolimnology and Biodiversity, Kluwer.*

Land, L.S. 1980. The isotopic and trace element geochemistry of dolomite: the state of the art. In Zenger, D.H (ed.), *Concepts and models of dolomitisation.* SEPM Special Publication **28**, 87-110.

Landmann, G., Reimer, A., Lemcke, G. And Kempe, S. 1996. Dating Late Glacial abrupt climate changes in the 14,570 yr long continuous varve record of Lake Van, Turkey. *Palaeogeography, Palaeoclimatology, Palaeoecology* **122**, 107-118.

Lemke, G. And Sturm, M. 1997. $\delta^{18}O$ and trace element Measurements as Proxy fro the Reconstruction of Climate Changes at Lake Van (Turkey): Preliminary Results. In Dalfes, N.D. (ed.) *Third Millennium BC Climate Change and Old World Collapse*, NATO ASI Series. 149.

Leng, M. 2003. Stable-isotopes in lakes and lake sediment archives. In Mackay, A, Battarbee, R, Birks, J and Oldfield, F. (eds.) *Global change in the Holocene*, Hodder Arnold, London.

Leng, M.J., Roberts, N., Reed, J.M. and Sloane, H.J., 1999. Late Quaternary palaeohydrology of the Konya Basin, Turkey, based on isotope studies of modern hydrology and lacustrine carbonates. *Journal of Paleolimnology*, **22**, 187-204.

Leng M.J. and Anderson N.J. 2003. Isotopic variation in modern lake waters from western Greenland. *The Holocene* **13**(4), 605-611.

Leng, M.J. and Marshall, J.D., in press. Palaeoclimate interpretation of stable isotope data from lake sediment archives. *Quaternary Science Reviews.*

Li, H.C. and Ku, T.L., 1997. $\delta^{13}C - \delta^{18}O$ covariance as a paleohydrological indicator for closed-basin lakes. *Palaeogeography Palaeoclimatology Palaeoecology* **133**(1-2), 69-80.

Linacre, E 1992. *Climate Data and Resources: A Reference and Guide.* Routledge, London 366 pp.

Livingstone, D.A. 1955. A lightweight piston sampler for lake deposits. *Ecology* **36**, 137-139.

Lotter, A. F., Renberg, I., Hansson, H., Stöckli, R. And Sturm, M. 1997. A remote controlled freeze corer for sampling unconsolidated surface sediments. *Aquatic Sciences* **59**(4), 295-303.

Mackereth, F.J.H. 1958. A portable core sampler fro lake deposits. *Limnology and Oceanography* **3**, 181-191.

Mackereth, F.J.H. 1969. A short core sampler for subaqueous deposits. *Limnology and Oceanography* 15 145-151.

Majoube, 1971. Fractionnement en oxygène-18 et en deutérium entre l'eau et sa vapeur. *Journal of Chemical Physics* 187, 1423-1436.

Mann, M.E. 2002. Large –Scale Climate Variability and Connections with the Middle East in Past Centuries. *Climatic Change* 55, 287-314.

Mann, M.E., Bradley, R.S. and Hughes, M.K. 1998. Global-scale temperature patterns and climate forcing over the past six centuries. *Nature* 392, 779-787.

Mann, M.E. and Jones, P.D. 2003. Global surface temperatures over the past two millennia. *Geophysical Research Letters* 30(15), 1820-1823.

Merlivat, L. and Jouzel, J., 1979. Global climatic interpretation of the D-^{18}O relationship for precipitation. *Journal of Geophysical Research* 84(C8), 5029-5033.

Meteoroloji Bulteni 1974. Devlet Meteoroloji Işleri Genel Müdürlüğü (State Meteorological Services), Ankara.

Meyers, P.A. and Teranes, J.L. 2001. Sediment Organic Matter. In Last, W.N. and Smol, J.P. (eds.), 2001. *Tracking Environmental Change Using Lake Sediments. Volume 2: Physical and Geochemical Methods.* Kluwer Academic Publishers, Dordrecht, The Netherlands.

Mook, W.G., Bommerson, J.C. and Staverman, W.H., 1974. Carbon isotope fractionation between dissolved bicarbonate and gaseous carbon dioxide. *Earth and Planetary Science Letters* 22, 169-176.

Moore, J.J., Hughen, K.A., Milller, G.H and Overpeck, J.T. 2001. Little Ice Age recorded in summer temperature reconstruction from varved sediments of Donard Lake, Baffin Island, Canada. *Journal of Paleolimnology* 25, 503-517.

Morrill, C., Overpeck, J.T and Cloe, J.E. 2003. A synthesis of abrupt changes in the Asian summer monsoon since the last deglaciation. *The Holocene* 13(4), 465-476.

NOAA, 2003. El Niño theme page. http://www.pmel.noaa.gov/tao/elnino/nino-home.html.

Nuhfe, E.B., Anderson, R.Y., Bradbury, J.P. and Dean, W.E. 1993. Modern sedimentation in Elk Lake, Clearwater County, Minnesota. . In Bradbury, J.P and Dean, W.E (eds.) *Elk Lake, Minnesota: Evidence for Rapid climate changes in the North-Central United State,* Geological Society of America Special Paper 276.

O'Sullivan, P.E., Moyeed, R., Cooper, M.C. and Nicholson, M.J. 2002. Comparison between instrumental, observational and high resolution proxy sedimentary records of Late Holocene climatic change – a discussion of possibilities. *Quaternary International* 88, 27-44.

Olsson, I. 1986. Radiometric Dating. In: Berglund, B.E. (ed.), *Handbook of Holocene Palaeoecology and Palaeohydrology* Wiley, New York.

Paillard, d., Labeyrie, L. and Yiou, P. 1996. Macintosh program performs time-series analysis. *EOS Transactions AGU* 77, 379. An electronic supplement of this reference is available at; http://www.agu.org/eos-elec/96097e.html.

Parathasarathy, B., Munot, A.A and Kothawale, D.R. 1995. Monthly and seasonal rainfall series for all-India homogeneous regions and meteorological sub-divisions: 1871-1994. *Contributions from Indian Institute of Tropical Meteorology* Research report RR-065, Pune. Data from IRI climate library accessible at http://Ingrid.idgo.columbia.edu/SOURCES/Indices/India/rainfall.

Penman, H.L. 1948. Natural evaporation from open water, bare soil and grass. *Proceedings of the Royal Society A.* **193**, 120-145.

Price, S.P. and Scott, B. 1991. Pliocene Burdur basin, SW Turkey: tectonics, seismicity and sedimentation. *Journal of the Geological Society* **148**, 345-354.

Price, S.P. and Scott, B 1994. Fault –block rotations at the edge of a zone of continental extension; southwest Turkey. *Journal of Structural Geology* **16**(3), 381-392.

Raicich, F, Pinardi, N and Navarra, A. 2003. Teleconnections between Indian Monsoon and Sahel Rainfall and the Mediterranean. *International Journal of Climatology* **23**, 173-186.

Reed, J.M., Roberts, N and Leng, M.J. 1999. An evaluation of the diatom response to Late Quaternary environmental change in two lakes in the Konya Basin, Turkey, by comparison with stable isotope data. *Quaternary Science Reviews* **18**, 631-646.

Ricketts, R.D. and Johnson, T.C., 1996. Climate change in the Turkana basin as deduced from a 4000 year long $\delta^{18}O$ record. *Earth and Planetary Science Letters* 142(1-2), 7-17.

Rindsberger, M., Magaritz, M., Carmi, I. and Gilad, D., 1983. The relation between air mass trajectories and the water Isotope Composition of Rain in the Mediterranean Sea Area. *Geophysical Research Letters* 10(1), 43-46.

Roberts, N. 1980. *Late Quaternary geomorphology and palaeoecology of the Konya basin, Turkey*. Ph.D. thesis, London University.

Roberts, N. 2002. Did prehistoric landscape management retard the post-glacial spread of woodland in Southwest Asia? *Antiquity* 76, 1002-1010.

Roberts, N., Reed, J.M., Leng, M.J., Kuzucuoglu, C., Fortugne, M., Bertaux, J., Woldring, H., Bottema, S., Black, S., Hunt, E. and Karabiyikoglu, M. 2001. The tempo of Holocene climatic change in the eastern Mediterranean region: new high-resolution crater-lake sediment data from central Turkey. *The Holocene* 11(6), 721-736.

Roberts, N and Jones, M. 2002. Towards a Regional Synthesis of Mediterranean Climatic Change Using Lake Stable Isotope Records. *PAGES News* 10(2), 13-15.

Roberts, N., Karabıyıkoğlu, M., Jones, M., Mather, A., Jones, G., Rodenberg, I., Eastwood, W.J., Kapan-Yeşilyurt, S, Yiğitbaşıoğlu, H. and Watkinson, M. 2003. Climatic and tectonic controls over Late Quaternary sedimentation in the lake Burdur basin, southwest Turkey. *INQUA congress proceedings.*

Rosenmeir, M.F., Hodell, D.A., Brenner, M Curtis, J.H., Martin, J.B., Anselmetti, F.S., Ariztegui, D., Guilderson, T.P. 2002. Influence of vegetation change on watershed hydrology: implications for palaeoclimatic interpretation of lacustrine $\delta^{18}O$ records. *Journal of Paleolimnology* 27, 117-131.

Rosqvist, G.C., Rietti-Shati, M. and Shemesh, A., 1999. Late glacial to middle Holocene climatic record of lacustrine biogenic silica oxygen isotopes from a Southern Ocean island. *Geology* 27(11), 967-970.

Rozanski, K., 1985. Deuterium and oxygen-18 in European groundwaters - Links to atmospheric circulation in the past. *Chemical Geology* (Isotope Geoscience Section) 52, 349-363.

Rozanski, K., Araguas-Araguas, L. and Gonfiantini, G., 1992. Relation between long-term trends of oxygen-18 isotope composition of precipitation and climate. *Science* **258**, 981-985.

Rozanski, K., Froehlich, K., Mook, W.G and Stichler, W. 2001. Environmental Isotopes in the Hydrological Cycle; Principles and Applications. Volume III: Surface water. Accessible at http://www.iaea.org/programmes/ripc/ih/volumes/volume3.htm.

Saarnisto, M. 1986. Annually laminated sediments, in Berglund, B.E. (ed.) *Handbook of Holocene Palaeoecology and Palaeohydrology* Wiley, Chichester, UK.

Sassan, G. 1964. MTA Dergisi Sheet 63.

Schaaf, M and Thurow, J. 1997. Tracing short cycles in long records: the study of inter-annual to inter-centennial climate change from long sediment records, examples from the Santa Barbara Basin. *Journal of the Geological Society, London.* **154**, 613-622.

Schilman, B., Bar-Matthews, M., Almogi-Labin, A., and Luz, B. 2001. Global climate instability reflected by Eastern Mediterranean marine records during the late Holocene. *Palaeogeography, Palaeoclimatology, Palaeoecology* **176**, 157-176.

Schnurrenberger, D., Russell, J. and Kelts, K. 2003. Classification of lacustrine sediments based on sedimentary components. *Journal of Paleolimnology* **29**, 141-154.

Şenel, M. 1997. Türkiye Jeoloji Haritaları. Isparta Paftası 1:250 000 ölçekli. Jeoloji etütleri dairesi, Ankara

Shemesh, A., Rosqvist, G., Rietti-Shati, M, Rubensdotter, L., Bigler, C., Yam, R and Karlen, W 2001. Holocene climate change in Swedish Lapland inferred from an oxygen isotope record of lacustrine biogenic silica. *The Holocene* **11**, 447-454.

Siegenthaler, U. and Eicher, U., 1986. Stable oxygen and carbon isotope analyses. In: B.E. Berglund (ed.), *Handbook of Holocene Palaeogeography and Palaeohydrology*. John Wiley & Sons Ltd., pp. 407 - 422.

Stevens, L.R., Wright, H.E. and Ito, E. 2001. Proposed changes in seasonality during the late-glacial and Holocene at Lake Zeribar, Iran. *The Holocene* **11(6)**, 747-755.

Stiller, M. and Kaufman, A., 1985. Paleoclimatic trends revealed by the isotopic composition of carbonates in Lake Kinneret. *Zeitschrift fur Gletscherkunde und Glazialgeologie* **21**, 79-87.

Street-Perrott, F.A. and Perrott, R.A. 1990. Abrupt climate fluctuations in the tropics: the influence of Atlantic Ocean circulation. *Nature* **343**, 607-611.

Street-Perrott, F.A., Holmes, J.A., Waller, M.P., Allen, M.J., Barber, N.G.H., Fothergill, P.A., Harknes, D.D., Ivanovich, M., Kroon, D. and Perrott, R.A. 2000. Drought and dust deposition in the West African Sahel: a 5500-year record from Kajemarum Oasis, northeastern Nigeria. *The Holocene* **10** (3), 293-302.

Stuiver, M., 1970. Oxygen and carbon isotope ratios of fresh-water carbonates as climatic indicators. *Journal of Geophysical Research* **75**, 5347-5257.

Stuiver, M. and Braziunas, T.F. 1993. Sun, ocean, climate and atmospheric $^{14}CO_2$: an evaluation of causal and spectral relationships. *The Holocene* 3(4), 289-305.

Stuiver, M. and Braziunas, T.F. 1995.Evidenece of solar activity variations, in Bradley, R.S. and Jones, P.D. (eds.) *Climate since A.D. 1500* Routledge, London, UK.

Stuiver, M., P.M. Grootes, and T.F. Braziunas. 1995. The GISP2 ^{18}O climate record of the past 16,500 years and the role of the sun, ocean and volcanoes. *Quaternary Research* **44**, 341-354.

Stuiver, M., Reimer, P.J., Bard, E., Beck, J.W., Burr, G.S., Hughen, K.A., Kromer, B., McCormac, F.G., v. d. Plicht, J., and Spurk, M., 1998. INTCAL98 Radiocarbon age calibration 24,000 - 0 cal BP. *Radiocarbon* **40**,1041-1083.

Swezey, C., Lancaster, N., Kocurek, G., Deynoux, M., Blum, M., Price, d. and Pion, J.-C. 1999. Response of Aeolian systems to Holocene climatic and hydrological changes on the northern margin of the Sahara: a high-resolution record from the Chot Rharsa basin, Tunisia. *The Holocene* 9(2), 141-147.

Talbot, M.R., 1990. A review of the palaeohydrological interpretation of carbon and oxygen isotopic ratios in primary lacustrine carbonates. *Chemical Geology (Isotope Geosciences Section)* **80**, 261-279.

Tan, E and Unal, Y.S. 2003. Impact of NAO to Winter Precipitation and Temperature Variability over Turkey. *Geophysical Research Abstracts* 5, 00626.

Taylor, A.H., Icarues Allen, J. and Clark. P.A. 2002. Extraction of a weak climatic signal by an ecosystem. *Nature* 416, 629-632.

Telford, R.J and Lamb, H.F. 1999. Groundwater-Mediated Response to Holocene Climatic Change Recorded by the Diatom Stratigraphy of an Ethiopian Crater Lake. *Quaternary Research* **52,** 63–75.

Thompson, L.G., Mosley-Thompson, E., Davis, M.E., Henderson, K.A., Brecher, H.H., Zagorodnov, V.S., Mashiotta, T.A., Lin, P-N., Mikhalenko, V.N., Hardy, D.R. and Beer, J. 2002. Kilimanjaro Ice Core Records: Evidence of Holocene Climate Change in Tropical Africa. *Science* **298**, 589-593.

Touchan, R., Garfin, G.M., Meko, D.M., Funkhouser, G., Erkan, N., Hughes, M.K. and Wallin, B.S. 2003. Preliminary reconstructions of Spring Precipitation in Southwestern Turkey from Tree-Ring Width. *International Journal of Climatology* **23**, 157-171.

Türkeş, M. 1996. Spatial and temporal analysis of annual rainfall variations in Turkey. *International Journal of Climatology* **16**, 1057-1076.

Türkeş, M. 2003. Spatial and Temporal Variations in Precipitation and Aridity Index Series of Turkey. In Bolle, H.-J. 2003. *Mediterranean climate – variability and trends*. Springer-Verlag, Berlin.

Türkeş, M, Sümer, U.M. and Kilic, G. 1995. Variations and trends in annual mean air temperatures in Turkey with respect to climate variability. *International Journal of Climatology* **15**, 557-569.
Türkeş, M., Sümer, U.M. and Kilic, G. 1996. Observed changes in maximum and minimum temperatures in Turkey. *International Journal of Climatology* **16**, 463-477.

Turney, C.S.M., 1999. Lacustrine bulk organic $\delta^{13}C$ in the British Isles during the Last Glacial Holocene Transition (14-9 ka ^{14}C BP). *Arctic, Antarctic and Alpine Research* 31(1), 71-81.

Tzedakis, P.C., Frogley, M.R. and Heaton, T.H.E. 2002. Duration of Last Interglacial conditions in northwestern Greece. *Quaternary Research* **58**, 53-55.

Valero-Garces, B.L., Delgado-Huertas, A., Ratto, N. And Navas, A 1999. Large ^{13}C enrichment in primary carbonates from Andean Altiplano lakes, northwest Argentina. *Earth and Planetary Science Letters* **171**, 253-266.

van Zeist, W., Woldring, H. and Stapert, D. 1975. Late Quaternary vegetation and climate of southwestern Turkey. *Palaeohistoria* 17, 55-143.

Varekamp, J.C. and Kreulen, R., 2000. The stable isotope geochemistry of volcanic lakes, with examples from Indonesia. *Journal of Volcanology and Geothermal Research* 97(1-4), 309-327.

Verschuren, D., Laird, K.R and Cumming, B.F. 2000. Rainfall and drought in equatorial east Africa during the past 1,100 years. *Nature* **403**, 410-414

von Grafenstein, U., Erlenkeusser, H., Brauer, A., Jouzel, J. and Johnson, S., 1999. A mid-European decadal isotope-climate record from 15,500 to 5,000 years ago. *Science* 284, 1754-1757.

von Rad, U., Schaaf, M., Michels, K.H, Schultz, H., Berger, W.H and Siroko, F. 1999. A 5000-yr record of climate change in varved sediments from the oxygen minimum zone off Pakistan, Northeastern Arabian Sea. *Quaternary Research* **51**, 39-53.

Wassenaar, L., Aravena, R., Fritz, P. and Barker, J. 1990. Isotopic composition (^{13}C, ^{14}C, ^{2}H) and geochemistry of aquatic humic substances from groundwater. *Organic Geochemistry* **15**, 383-396.

Wei, K. and Gasse, F., 1999. Oxygen isotopes in lacustrine carbonates of West China revisited: implications for post glacial changes in summer monsoon circulation. *Quaternary Science Reviews* 18(12): 1315-1334.

Wick, L., Lemcke, G. and Sturm, M. 2003. Evidence of Late glacial and Holocene climatic change and human impact in eastern Anatolia: high-resolution pollen, charcoal, isotopic and geochemical records from the laminated sediments of Lake Van, Turkey. *The Holocene* 13(5), 665-675.

Wolfe, B.B., Edwards, T.W.D., Elgood, R.J. and Beuning 2001. Carbon and oxygen isotope analysis of lake sediment cellulose: methods and applications. In Last, W.N. and Smol, J.P. (eds.), 2001. *Tracking Environmental Change Using Lake Sediments. Volume 2: Physical and Geochemical Methods.* Kluwer Academic Publishers, Dordrecht, The Netherlands.

Wright, H.E. 1967. A square rod piston sampler for lake sediments. *Journal of Sedimentary Petrology* 37, 975-976.

Wright, H.E. 1980. Cores of soft lake sediments. *Boreas* **9**, 107-113.

Zanchetta, G., Di Vito, M., Fallick, A.E. and Sulpizio, R., 2000. Stable isotopes of pedogenic carbonates from the Somma-Vesuvius area, southern Italy, over the past 18 kyr: palaeoclimatic implications. *Journal of Quaternary Science* **15**(8), 813-824.